

UC Davis

UC Davis Electronic Theses and Dissertations

Title

Studies of Chemically Modified Oligonucleotides Towards RNA-Binding Proteins

Permalink

<https://escholarship.org/uc/item/6fp3h4zc>

Author

Pham, Kevin

Publication Date

2022

Peer reviewed|Thesis/dissertation

Studies of Chemically Modified Oligonucleotides Towards RNA-Binding Proteins

By

KEVIN MINH PHAM
DISSERTATION

Submitted in partial satisfaction of the requirements for the degree of

DOCTOR OF PHILOSOPHY

in

Chemistry

in the

OFFICE OF GRADUATE STUDIES

of the

UNIVERSITY OF CALIFORNIA

DAVIS

Approved:

Peter A. Beal, Chair

Sheila S. David

Kit S. Lam

Committee in Charge

2022

*To my partner, Joe Salamon, mother, Kim Nguyen, and father, Mitchell Lader:
Thank you for all your love and belief in me to keep pushing forward*

Studies of Chemically Modified Oligonucleotides Towards RNA-Binding Proteins

Abstract

Oligonucleotides are short polymeric chains of nucleic acids that are immensely useful for a plethora of scientific applications. By way of chemical modification, post-transcriptional processes such as RNA interference (RNAi) or RNA editing can be studied at the molecular level using oligonucleotides. More so, oligonucleotides, which typically use the simple mechanism of base pairing to a complementary target nucleic acid sequence of interest, can be exploited to create therapeutics against diseases. Researchers developing oligonucleotide-based therapeutics often face challenges of specificity, off-targeting effects, oligonucleotide trafficking, metabolic stability, cellular uptake, delivery to specific tissues, and more. Therefore, chemical modifications along the oligonucleotide sugar and phosphate backbone and, less commonly, the nucleobase are used to overcome these obstacles.

In Professor Peter Beal's lab, we take particular interest in designing nucleobase modifications that can be incorporated onto oligonucleotides to further understand the structure and function of RNA that can bind to other RNA or RNA-binding proteins in RNAi or RNA editing. This dissertation will describe chemically modified oligonucleotides that were used to study their effects on the catalytically active RNAi protein, Argonaute2 (Ago2), and the adenosine-to-inosine (A-to-I) editing enzyme adenosine deaminase acting on RNA (ADAR).

Chapters 2 and 3 describe a published study in examining the effects of chemically modified antisense oligonucleotides targeting microRNA (anti-miRs) at the 3'-end nucleotide that can interact with a nucleotide-binding pocket in human Ago2 (hAgo2) when loaded with a microRNA strand. First, Chapter 2 describes the earlier stages of this work and goes into detail a molecular docking method to computationally screen 1'-triazole modified nucleotide analogs that can interact with the hAgo2 pocket. Additionally, precursor anti-miRs with a 3'-end, 1'-alkynyl modification were designed and tested in an established cellular based assay to confirm if the anti-miR could be converted into triazoles with various substituents using copper(I)-catalyzed azide/alkyne cycloaddition (CuAAC) reactions. We docked a library of 190 triazole-modified nucleotides, carefully evaluated the scoring of each docked ligand, and picked 17 triazoles that could be modified onto a 2'-O-methylated 15mer anti-miR with 1'-alkynyl 3'-end nucleotide.

Chapter 3 continues to describe the identification of a significantly potent ester triazole-modified anti-miR among the 17 triazoles screened. Numerous investigative experiments were then conducted to determine the mechanism by which the ester modification elicits high potency. Such experiments included structure activity relationships, generalizability to two anti-miR sequences, nuclease resistance, miRNA target de-repression analyses, and a biotinylated anti-miR pulldown assay to determine hAgo2 binding affinity of the ester-modified anti-miR.

Finally, Chapter 4 describes preliminary work to evaluate inhibition of ADAR1 in cultured cells using either an 8-azanebularine-containing RNA duplex inhibitor or ADAR mutant proteins that can impede dimerization needed for A-to-I editing activity.

Table of Contents

Abstract	iii
List of Figures	ix
List of Tables	xii
List of Abbreviations	xiii

Chapter 1: Introduction

1.1 Dissertation overview	1
1.2 Chemical design of therapeutic oligonucleotides	2
1.3 Chemically modified oligonucleotides in RNAi therapeutics	8
1.4 Chemically modified oligonucleotides targeting Adenosine Deaminase Acting on RNA (ADAR)	18
1.5 References	24

Chapter 2: Identification of a precursor anti-microRNA for computationally-screened 3'-end chemical modifications and potency screening in cellular based assays

2.1 Introduction	33
2.2 Methods	
2.2.1 MiR-21 reporter plasmid generation	36
2.2.2 Cell culture	36
2.2.3 Transfection and dual luciferase assay	37
2.2.4 Oligonucleotide synthesis and purification	38
2.2.5 Computational screening of triazole-modified nucleotides docked into the t1A-binding pocket of hAgo2	39
2.2.6 Table of mass spectra for anti-miR21 oligonucleotides	41
2.3 Results	
2.3.1 MiR-21 dual luciferase reporter system for anti-miR potency studies in cells	42
2.3.2 Potency screening of 2'-O-methylated 9mer anti-miR21	44
2.3.3 Potency screening of 2'-O-methylated anti-miR21 at varying sequence lengths	45
2.3.4 Potency screening of 15mer anti-miR21 with 3-end nucleotide substitutions	46
2.3.5 Computational screening of t1 triazole-modified nucleotide library using Fast Rigid Exhaustive Docking (FRED)	48

2.3.6 Design and synthesis of 15mer anti-miR precursor for 3'-end triazole modifications	51
2.4 Discussion	53
2.5 References	58
2.6 Table of primer sequences	60

Chapter 3: Potency and characterization of 3'-end ester-modified anti-microRNA oligonucleotides

3.1 Introduction	61
3.2 Methods	
3.2.1 MiR-122 dual luciferase reporter plasmid generation	61
3.2.2 Cell culture	62
3.2.3 Transfection and dual luciferase assay	62
3.2.4 Oligonucleotide preparation	63
3.2.5 Generation of t1-triazole modified anti-miR via copper(I)-catalyzed azide/alkyne cycloaddition (CuAAC) reaction	64
3.2.6 Snake venom phosphodiesterase (SVPD) assay	65
3.2.7 hAgo2 mammalian and yeast expression vector generation	65
3.2.8 MiR-21 mimic duplex generation	67
3.2.9 hAgo2 pulldown assay	67
3.2.10 Western blotting	68
3.2.11 RT-qPCR	69
3.2.12 Immunofluorescence and fluorescence microscopy	70
3.2.13 Expression of poly-Histidine-tagged full-length hAgo2 protein	71
3.2.14 Tables of mass spectra and sequences for anti-miR oligonucleotides	72
3.3 Results	
3.3.1 Improved potency of anti-miR21 by 3'-end triazole modifications in HeLa cells	75
3.3.2 Structure activity relationships of ester functional group on 3'-end of anti-miR21	79
3.3.3 Improved potency of anti-miR122 by 3'-end triazole modification in HuH-7 cells	81
3.3.4 Exonuclease resistance assay of 3'-end triazole-modified anti-miR21	85
3.3.5 Biotin pulldown of miR-21-loaded hAgo2 using 3'-end modified anti-miR21 to assess binding affinity	86
3.3.6 Analyses of 3'-end modified anti-miR21-induced changes in endogenous miR-21 target gene regulation	88

3.3.7 Transfection efficiency of anti-miR oligonucleotides by fluorescence microscopy	91
3.3.8 Protein expression of poly-Histidine-tagged full-length hAgo2 in <i>Saccharomyces cerevisiae</i> BCY123 cells	92
3.4 Discussion	94
3.5 References	102
3.6 Table of primer sequences	105

Chapter 4: Cellular-based ADAR inhibition assays using 8-azanebularine-containing HER1 oligonucleotides and ADAR deaminase protein mutants

4.1 Introduction	106
4.2 Methods	
4.2.1 Oligonucleotide synthesis and purification	107
4.2.2 Human serum stability assay of 8-azaN-containing HER1 RNAs	109
4.2.3 Cell culture	109
4.2.4 Transfection of cells with HER1 8-azanebularine-containing RNA inhibitors	110
4.2.5 Electroporation of cells with HER1 8-azaN inhibitors	111
4.2.6 Transfection of cells with ADAR deaminase inhibitor plasmid constructs	111
4.2.7 RNA editing analysis from cultured cells	112
4.2.8 Western blotting	113
4.2.9 Table of mass spectra for HER1 oligonucleotides	114
4.3 Results	
4.3.1 Human serum stability of HER1 RNA oligonucleotides containing 8-azanebularine	115
4.3.2 Inhibition profile of endogenous ADAR1 targets in cells by HER1 8-azaN duplex	118
4.3.3 Editing profile of endogenous ADAR1 targets in HEK293T cells treated with HER1 8-azaN 16 bp duplex	121
4.3.4 Quantification of overexpressed ADAR protein at varying concentration of HER1 8-azaN 16 bp duplex in HEK293T cells	124
4.3.5 Endogenous transcript editing profile in cells treated with HER1 8-azaN RNA duplexes	126
4.3.6 Editing profile of ADAR editing targets in cells treated with ADAR deaminase domain (ADARd) protein inhibitors	131
4.4 Discussion	135
4.5 References	144

4.6 Table of Oligonucleotides	149
-------------------------------------	-----

Appendices

Appendix A: Library of 3',5'-bisphosphate, 1'-triazole-modified nucleotides for Fast Rigid Exhaustive Docking (FRED) into the adenosine-binding pocket of hAgo2, from Chapter 2	150
Appendix B: Table of ChemGauss4 scores of docked triazole nucleotide ligands, from Chapter 2	155

List of Figures

Figure

1.1	Panel of chemical modifications applied onto oligonucleotides	4
1.2	RNAi pathway by siRNA or miRNA	9
1.3	The crystal structure of hAgo2	10
1.4	Panel (not exhaustive) listing chemical modifications on siRNA	12
1.5	Chemical modifications of RNAi molecules reported in the Beal lab	15
1.6	The human ADAR family and A-to-I editing reaction scheme	19
1.7	Functional roles of post-transcriptional A-to-I editing by ADAR	20
1.8	Crystal structures or models of ADAR protein bound to dsRNA substrate	23
2.1	The t1-adenosine (t1A) nucleotide-binding pocket in human Argonaute2 (hAgo2)	35
2.2	Anti-miR potency screening using miR-21 dual luciferase reporter assay in HeLa cells	42
2.3	Potency profile of 2'-O-methylated 9mer anti-miR21 in HeLa cells	44
2.4	Potency profile of anti-miR21 at varying lengths	45
2.5	Potency profile of 15mer anti-miR21 with nucleobase substitutions or modifications at the 3'-end	46
2.6	Constraints imposed on t1-adenosine reference ligand in the hAgo2 t1A-binding pocket receptor	49
2.7	Poses of a docked 1'-triazole nucleotide into the hAgo2 receptor	50
2.8	Design and potency profile of 15mer anti-miR21 with 3'-end 2'-deoxy-1'-ethynyl- ribose and C3 spacer modification	52
3.1	Design of 3'-end triazole-modified 15mer anti-miR21	76
3.2	Potency profile of 3'-end triazole-modified anti-miR21 in HeLa cells	79

3.3	Structure activity relationship of 3'-end ester-modification on anti-miR21 in HeLa cells	80
3.4	Potency of 2'-O-methylated anti-miR122 oligonucleotide in HuH-7 cells	82
3.5	Potency profile of 3'-end triazole-modified anti-miR122 in HuH-7 cells	83
3.6	Potency selectivity comparison of anti-miR21 to anti-miR122 in HeLa cells	84
3.7	Decay curve of 3'-end triazole-modified anti-miR21 in snake venom phosphodiesterase (SVPD)	86
3.8	5'-biotin anti-miR21 pulldown of miR-21 guide-loaded hAgo2	87
3.9	Protein expression analysis of PDCD4 from HeLa cells treated with 3'-end modified anti-miR21	89
3.10	RT-qPCR analysis of endogenous miR-21 targets in HeLa cells treated with anti-miR21	90
3.11	Fluorescence microscopy of HeLa cells transfected with Cy3-conjugated anti-miR	92
3.12	Western blotting detection of polyhistidine-tagged human ADAR2 and Ago2	93
3.13	Close up of target RNA nucleotide 16 (t16) interaction in hAgo2 crystal structure complexed with guide-target RNA duplex (PDB: 6N4O)	97
3.14	Highest-scored pose of methyl acetate triazole ligand docked into the t1A-binding hAgo2 receptor	100
4.1	Serum stability of 8-azanebularine- (8-azaN) containing HER1 RNAs	116
4.2	Editing of endogenous ADAR1 targets in HeLa cells upon transfection with HER1 8-azanebularine 16bp duplexes	118
4.3	Percent editing profile of ADAR targets in HEK293T cells	121
4.4	Overexpression of HA-tagged ADAR1 p110 isoform or ADAR2 full length protein in cells with respect to HER1 RNA inhibitor	124
4.5	Editing profile of endogenous NUP43 editing target at various sites in HEK293T cells transfected with siRNA control or HER1 8-azaN inhibitor duplexes	127

4.6	Percent editing profile of endogenous NEIL1 and 5-HT _{2c} R mRNA transcripts in U87 cells treated with HER1 8-azaN duplexes	128
4.7	Editing of endogenous transcripts in HeLa cells treated with overexpression of ADAR1d mutant protein inhibitors	132
4.8	Editing of endogenous ADAR2 target in HEK293T cells co-transfected with ADAR2 full length protein and ADAR2d mutant protein inhibitors	133

List of Tables

Table

2.1 Former docking scores and dissociation constants of t1 nucleotide triazole-modified and control target RNA oligonucleotides (from Dr. Scott Suter's dissertation) ...	55
2.2 Updated docking scores and luciferase activity ratios of t1 triazole-modified and control nucleotides on 15mer anti-miR21	55
3.1 Triazoles tested for potency on 3'-end of 15mer anti-miR21	76
3.2 Endogenous miR-21 targets in HeLa cells for analyses upon anti-miR21 treatment	89

List of Abbreviations

(<i>E</i>)-5'-VP	<i>Trans</i> (<i>E</i>)-5'-vinylphosphonate
1-EdR	1'-ethynyl-2'-deoxyribose
1-EdR C3	1'-ethynyl-2'-deoxyribose with 3 carbon spacer
1-ER	1'-ethynyl-ribose
2-thio dT	2-thio-2'-deoxythymidine
2'-F	2'-fluoro
2'-FANA	2'-fluoro-arabinonucleic acid
2'-MOE	2'-methoxyethyl
2'-OMe	2'-O-methyl
3'-UTR	3'-Untranslated region
5-HT _{2C} R	5-hydroxytryptamine receptor 2C
5'-(<i>R</i>)-Me P	5'-(<i>R</i>)-methylphosphate
5'-CHF P	α -fluoromethylenephosphonate
5'- <i>E</i> -VPu	5'-(<i>E</i>)-vinylphosphonate 2'-O-methyl uridine
5'-VP	5'-vinylphosphonate
7-EAA	7-ethynyl-8-aza-7-deazaadenosine
7-EAG	7-ethynyl-8-aza-7-deazaguanosine
8-alkoxyA	8-alkoxyadenosine
8-azaN or 8N	8-azanebularine
A-to-I	Adenosine-to-Inosine
ADAR	Adenosine deaminase acting on RNA
ADARd	ADAR deaminase domain
Ago2	Argonaute2
AGS	Aicardi-Goutières syndrome
AHP	Acute hepatic porphyria
Anti-Anti	Antibiotic-Antimycotic
anti-miR	Antisense oligonucleotide targeting microRNA
arRNA	ADAR-recruiting RNA
ASGPR	Asialoglycoprotein
ASO	Antisense oligonucleotide
AZIN1	Antizyme inhibitor 1
BCA	Bicinchoninic acid
Bdf2	Bromodomain-containing factor 2
Bi	Biotin
Blcap	Bladder cancer associated protein
bp	Base pair
BPNT1	3' (2'),5'-bisphosphate nucleotidase 1

C	Cytosine
c-ODN	Circle oligodeoxynucleotide
cDNA	Complementary DNA
CDS	Coding sequence
cEt	Constrained ethyl
CM - Ura	Yeast complete media minus uracil
CMV	Cytomegalovirus
Cog3	Conserved oligomeric Golgi complex subunit 3
cPent-AP	N2-cyclopentyl-2-aminopurine
cPent-G	N2-cyclopentyl-guanine
CPG	Controlled pore glass
Cu	Copper
CuAAC	Copper(I)-catalyzed azide/alkyne cycloaddition
CuSO ₄	Copper (II) sulfate
Cy3	Cyanine 3
dA	2'-deoxyadenosine
DAP	2,6-diaminopurine
DAPI	4',6-diamidino-2-phenylindole
DBU	1,8-diazabicyclo(5.4.0)undec-7-ene
dC	2'-deoxycytidine
dDAP	2'-deoxy-2,6-diaminopurine
dG	2'-deoxyguanosine
DGCR8	DiGeorge syndrome critical region 8
DHFR	Dihydrofolate reductase
DMEM	Dulbecco's modified Eagle medium
DMSO	Dimethyl sulfoxide
DNA	Deoxyribonucleic acid
DPBS	Dulbecco's phosphate-buffered saline
DSH	Dyschromatosis symmetrica hereditaria 1
dsRBD	Double-stranded RNA-binding domain
dsRNA	Double-stranded RNA
DTT	Dithiothreitol
dU	2'-deoxyuridine
dUdA	t1 nt as 2'-deoxyadenosine, t2 nt as 2'-deoxyadenosine
dZ	2'-deoxy Benner's base
EDTA	Ethylenediaminetetraacetic acid
Eef2k	Eukaryotic elongation factor 2-kinase
EMSA	Electrophoretic mobility shift assay
ENA	Ethylene-bridged nucleic acid
Et3N·3HF	Triethylamine trihydrofluoride

EtOH	Ethanol
F	Forward
FACS	Fluorescence-activated cell sorting
FAM	Fluorescein
FBS	Fetal bovine serum
FDA	Food and Drug Administration
FHNA	3'-fluorohexitol nucleic acid
FL	Full-length
FRED	Fast rigid exhaustive docking
FRET	Förster resonance energy transfer
g1	Guide RNA nucleotide at position 1
GA	Gibson assembly
GalNAc	<i>N</i> -acetylgalactosamine
GAPDH	Glyceraldehyde 3-phosphate dehydrogenase
GFP	Green fluorescent protein
Gli1	Glioma-associated oncogene homolog 1
GluR-B	Glutamate receptor subunit B
HA	Human influenza hemagglutinin
hAgo2	Human Argonaute2
HEK293T	Human embryonic kidney 293 cells with large SV40 T antigen
HeLa	Henrietta Lacks
HEPES	4-(2-Hydroxyethyl)-1-piperazineethanesulfonic acid
HER1	Human epidermal growth factor receptor 1
HMGA2	High mobility group AT-hook 2
HuH-7	Human hepatoma 7
Idua	Alpha-L-iduronidase
IFN	Interferon
IgG	Immunoglobulin G
IP	Immunoprecipitation
ISG	Interferon-stimulated gene
K _D	Dissociation constant
L1	Linker 1
L2	Linker 2
LARII	Luciferase assay reagent II
LEAPER	Leveraging endogenous ADAR for programmable editing of RNA
LNA	Locked nucleic acid
m ⁷ G	7-Methylguanosine
mA	2'-OMe adenosine
MALDI-TOF	Matrix assisted laser desorption ionization - time of flight
MCF-7	Michigan Cancer Foundation-7

MDA5	Melanoma differentiation-associated protein 5
MID	Middle domain
miRNA	microRNA
mRNA	Messenger RNA
MS	Mass spectrometry
NEIL1	Nei like DNA glycosylase 1
NES	Nuclear export signal
NH ₄ OH	Ammonium hydroxide
nt	Nucleotide
NUP43	Nucleoporin 43
OD ₆₀₀	Optical density measured at 600 nm wavelength
OG	8-oxo-7,8-dihydroguanosine
PAGE	Polyacrylamide gel electrophoresis
PAZ	PIWI-Argonaute-Zwolle
PBS	Phosphate buffer saline
PCR	Polymerase chain reaction
PDB	Protein Data Bank
PDCD4	Programmed cell death 4
PIK3CB	Phosphatidylinositol-4,5-bisphosphate 3-kinase catalytic subunit beta
PIWI	P-element induced wimpy testis
PKR	Protein kinase R
PMO	Phosphorodiamidate morpholino oligomer
PNA	Peptide nucleic acid
Pol III	RNA polymerase III
Pr-AP	N ² -propyl-2-aminopurine
pre-miRNA	pre-microRNA
pri-miRNA	Primary microRNA
PS	Phosphorothioate
pSc	<i>Saccharomyces cerevisiae</i> expression plasmid
PVDF	Polyvinylidene difluoride
R	Reverse
R-domain	Arginine-rich domain
RESTORE	Recruiting endogenous ADAR to specific transcripts for oligonucleotide-mediated RNA editing
RFP	Red fluorescent protein
RISC	RNA-induced silencing complex
RL/FF	Renilla/firefly
RNA	Ribonucleic acid
RNAi	RNA interference
rpm	Revolutions per minute

RT-PCR	Reverse transcription polymerase chain reaction
RTC	Reverse transcriptase control
s.e.m.	Standard error of the mean
S&G	Stop & Glo Reagent
Sat	Saturation mutagenesis
SDRE	Site-directed RNA editing
SELEX	Systematic evolution of ligands by exponential enrichment
Seq	Next generation sequencing
siADAR1 L + S	SiRNA targeting ADAR1 (long + short)
siRNA	Small interfering RNA
SMILES	Simplified molecular-input line-entry system
SNP	Single nucleotide polymorphism
ss-siRNA	Single-stranded siRNA
SVPD	Snake venom phosphodiesterase
T	Thymine
t1	Target RNA nucleotide position 1
t1A	Target RNA adenosine at position 1 nucleotide
TBST	Tris-buffered saline with Tween 20
tcDNA	Tri-cyclo DNA
TCEP	Tris(2-carboxyethyl)phosphine hydrochloride
TENT	Tris, EDTA, NaCl, Triton X-100
TEV	Tobacco etch virus
THF	Tetrahydrofuran
THPTA	Tris(3-hydroxypropyltriazolylmethyl)amine
TLR	Toll like receptor
TMEM63B	Transmembrane protein 63B
TNF α	Tumor necrosis factor alpha
TRBP	Trans-activation response RNA-binding protein
TTR	Transthyretin
U	Uracil
U87	Uppsala 87
UNA	Unlocked nucleic acid
UV	Ultraviolet light
VIDA	Visualization and data analysis
yeAgo2	Yeast expression vector with Ago2 gene
ZEN	N,N-diethyl-4-(4-nitronaphthalen-1-ylazo)-phenylamine

Chapter 1

Introduction

1.1 Dissertation overview

Throughout the years, the Beal lab has made many contributions towards studying RNA and RNA-binding proteins through the design and implementation of chemically modified oligonucleotides. More specifically, we have identified various oligonucleotide modifications that can alter function and recognition in the post-transcriptional processes RNA interference (RNAi) and RNA editing. Now, because of our recently solved crystal structures, we have been able to advance our understanding of the intricate RNA editing enzyme, adenosine deaminase acting on RNA (ADAR), and how it interacts with RNA. Our work continues to answer basic science questions to support research that the scientific community can use for therapeutic-related endeavors.

This dissertation will describe two studies of chemically modified oligonucleotides and their interactions with either Argonaute2 (Ago2), the catalytically active component in RNAi, or ADAR. Chapters 2 and 3 will describe our discovery of a highly potent, 3'-end ester-modified antisense oligonucleotide targeting microRNA (anti-miR) that was published in *Bioorganic and Medicinal Chemistry Letters*.¹ Chapter 2 will first describe the earlier stages of this study that includes computational screening of 3'-end anti-miR nucleotide analogs into the adenosine nucleotide-binding pocket in Ago2, and establishing a cellular-based anti-miR potency assay to identify an alkynyl-modified anti-miR precursor for modifications using copper(I)-catalyzed azide/alkyne cycloaddition (CuAAC, also known as "click) reactions. Chapter 3 will then describe the potency screening of triazole-modified anti-miRs and how we evaluated the characteristics of the

highly potent ester triazole modification by structure activity relationships, its generalizability in two anti-miR sequences, nuclease resistance, and binding affinity to hAgo2 by a biotin pulldown assay. Finally, Chapter 4 will describe my efforts in establishing a cellular-based ADAR1 inhibition assay using a short, 8-azanebularine-containing oligonucleotide as part of an RNA duplex.

1.2 Chemical design of therapeutic oligonucleotides

Oligonucleotides are short polymeric chains of nucleic acid that can be used as therapeutics to treat diseases.² The most common modality by which oligonucleotides interact with a nucleic acid target is complementary base-pairing at the Watson-Crick face, enabling high sequence specificity and rational design if the target sequence is known.^{2,3} To date, oligonucleotides in drug classes such as small interfering RNAs (siRNAs)⁴, anti-microRNAs or microRNA (miRNA) mimics⁵, aptamers⁶, and antisense oligonucleotides (ASOs)⁷ are being developed to target biomolecules that are involved in cellular processes such as RNAi, splicing, gene activation, toll like receptor (TLR) activation, and others.^{8,9}

A crucial feature in developing therapeutic oligonucleotides is designing chemical modifications to improve characteristics such as specificity towards a target sequence, nuclease resistance, cellular uptake, and distribution into certain tissues.⁸ The first major breakthrough in ASO chemical modification strategies was the incorporation of phosphorothioate (PS) linkages, where an oxygen atom in the phosphodiester moiety bridging two nucleotides is replaced with a sulfur atom (**Figure 1.1**).¹⁰ Discovered by chemist Fritz Eckstein, PS linkages remain to be an advantageous modification strategy

for oligonucleotides to improve nuclease resistance and even trafficking and cellular uptake.¹¹⁻¹³ In addition, because the PS linkage introduces a stereocenter at the phosphorous, diastereomeric centers S_p and R_p have been characterized when applied onto oligonucleotides. For example, it was found that the R_p diastereomer can bind to a target strand more tightly and increase RNase H activity over the S_p diastereomer, but is less nuclease resistant.^{14,15} Given this, alternating patterns or precise positioning of the S_p and R_p stereocenters on an oligonucleotide may improve overall potency.

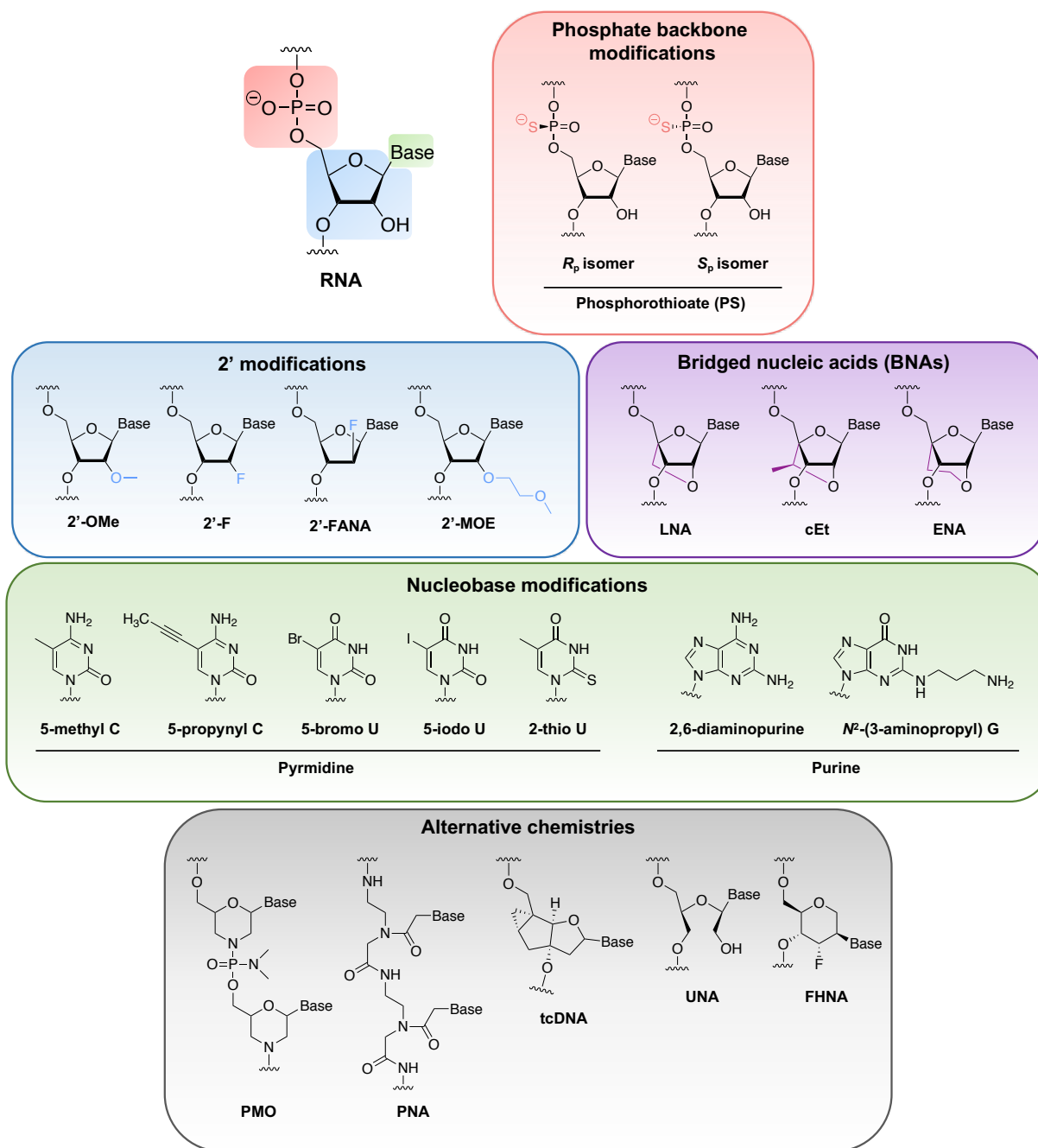


Figure 1.1 Panel of chemical modifications applied onto oligonucleotides. This panel is not exhaustive of all oligonucleotide chemistries. Abbreviations: 2'-OMe = 2'-O-methyl; 2'-F = 2'-fluoro; 2'-FANA = 2'-fluoro-arabinonucleic acid; 2'-MOE = 2'-methoxyethyl; LNA = locked nucleic acid; cEt = constrained ethyl; ENA = ethylene-bridge nucleic acid; C = cytosine; U = uracil; G = guanine; PMO = phosphordiamidate morpholino oligomer; PNA = peptide nucleic acid; tcDNA = tri-cyclo DNA; UNA = unlocked nucleic acid; FHNA = 3'-fluorohexitol nucleic acid.

Not long afterwards, during what is known as the second generation of oligonucleotide chemistry design, modifications at the 2'-position of nucleosides such as 2'-O-methyl (2'-OMe), 2'-fluoro (2'-F), 2'-fluoro-arabinonucleic acid (2'-FANA), and 2'-methoxyethyl (2'-MOE) were discovered and used to improve oligonucleotide properties (**Figure 1.1**). The 2'-OMe modifications are naturally occurring in cells and can increase binding affinity, nuclease resistance, and reduce immune stimulation.^{16,17} The 2'-F modification has similar properties to 2'-OMe and was often used in aptamer design¹⁸ or in an alternating pattern with 2'-OMe on siRNA strands.¹⁹ As an alternative to 2'-F, the 2'-FANA modification causes the nucleotide to adopt a DNA-like conformation (C2'-*endo* sugar pucker) and was found to increase binding affinity and stability when applied in combination with DNA nucleotides on RNase H-compatible ASOs.²⁰⁻²² Furthermore, in a study on 2'-O-alkyl substituted nucleoside analogs, 2'-MOE was found to increase nuclease resistance and binding affinity more effectively than 2'-OMe and thus are used in numerous oligonucleotide designs, including the FDA-approved, RNase-H competent ASO mipomersen (Kynamro) that was previously used to treat homozygous familial hypercholesterolemia.^{23,24}

Bridged nucleic acid modifications such as locked nucleic acid (LNA), constrained ethyl (cEt), and ethylene-bridged nucleic acid (ENA) are also some commonly used modifications in the oligonucleotide therapeutics field (**Figure 1.1**).²⁵⁻²⁷ The main feature amongst these modifications is the bridging of the 2' and 4'-carbon positions on ribose, which pre-organizes the sugar into a thermodynamically favorable, RNA-like C3'-*endo* pucker conformation. As a result, employing bridged nucleic acid-type modifications on oligonucleotides can facilitate A-form helical formation when bound to a complementary

target strand and improve binding recognition and activity by RNA-binding proteins such as RNase H and Ago2.^{28,29} Bridged nucleic acids are reported to have higher binding affinity and potency than 2'-modifications^{30,31}; however, other studies suggest that cytotoxic effects, particularly in the liver, can occur if too many nucleotides in ASOs are modified with these groups.³²

Nucleobase modifications are another approach to alter oligonucleotide properties (**Figure 1.1**).³³ Modifying the 5-position of pyrimidines C, U, and T is a highly explored site for modification or substitution. For example, 5-methyl-C is a naturally occurring epigenetic DNA modification that can enhance duplex thermal stability of RNA-targeting oligonucleotides due to the stacking of the methyl group between nucleobases in the major groove.^{33,34} Other modifications such as 5-propynyl C, 5-bromo-, and 5-iodo-uracil have also been found to improve duplex stability.^{33,35} The Mayers group designed CuAAC-functionalized handles using synthesized C5-ethynyl-2'-deoxyuridine and azides bearing different functional groups to generate an aptamer library, termed "clickmers", to expand the chemical diversity of libraries used for SELEX- (systematic evolution of ligands by exponential enrichment) based applications.^{36,37} An example of a pyrimidine modified at the 2-position is 2-thio-2'-deoxythymidine (2-thio dT), where Østergaard and colleagues found that modifying the DNA gapmer region of an ASO with 2-thio dT can affect allele selectivity and treat Huntington's disease by targeting single nucleotide polymorphisms (SNPs).^{38,39} The 2-thio group was hypothesized to clash with amino acid residues near the catalytic site in RNase H, thus altering cleavage specificity. A comprehensive overview on more post-synthetic nucleobase modifications on RNA oligonucleotides can be found in a review by Bartosik and colleagues.⁴⁰

As for purines, modifications such as 2,6-diaminopurine provide additional hydrogen interactions to a complementary base, and N²-imidazolylpropyl-, and N²-aminopropyl guanine modifications are reported to make electrostatic interactions with the phosphate backbone in the major groove of a duplex (**Figure 1.1**).⁴¹ In our lab, we have made numerous contributions to designing purine analogs onto oligonucleotides for studying recognition by dsRNA binding proteins such as PKR (Protein Kinase R) and ADAR as well as improve siRNA performance using an Ago2 structure-guided rationale. More of our works will be briefly discussed in **1.2** and **1.3**.

Lastly, there are many other alternative oligonucleotide chemistries such as PMO (phosphorodiamidate morpholino oligomer), PNA (peptide nucleic acid), tcDNA (tri-cyclo DNA), UNA (unlocked nucleic acid), and FHNA (3'-fluorohexitol nucleic acid), to name a few, that are being studied in academic and industrial settings (**Figure 1.1**).^{2,3,8,42} Overall, chemically modified oligonucleotide-based therapies have gained an increasing level of success with FDA-approval and are becoming more common for treating a variety of human diseases. From the first FDA-approved 21mer PS-linked DNA ASO, fomivirsen (Vitravene)⁴³, discovered in 1998 by Isis Pharmaceuticals (now called Ionis Pharmaceuticals) to treat cytomegalovirus (CMV) retinitis, to the recent siRNA and ASO drugs givosiran (Givlaari) or viltolarsen (Viltepso) by Alnylam Pharmaceuticals or NS Pharma that are used to treat acute hepatic porphyria (AHP) or Duchenne muscular dystrophy, respectively, it is satisfying to see the promising potential that oligonucleotide therapeutics can provide.⁴⁴ Also, pseudouridine- (ψ) modified mRNA vaccine formulations by Moderna or BioNTech and Pfizer have certainly saved many people's lives around the world by providing dramatically improved immunity against SARS-CoV-

2 during this ongoing pandemic.⁴⁵ Pseudouridine is a naturally occurring modified nucleotide that is found in many types of RNA in all cells and is known to enhance RNA stability and decrease RNA-induced immune responses.^{46,47} Both mRNA vaccines contain modified ψ , namely N1-methyl-pseudouridine, that is made by methylating the N1 position by N1-specific ψ methyltransferase Nep1 and can increase nuclease resistance and immune response evasion even greater than unmodified ψ .⁴⁸ Encoding of the SARS-CoV-2 spike protein is therefore made more efficient and improves SARS-CoV-2 immunity.

1.3 Chemically modified oligonucleotides in RNAi therapeutics

The discovery of RNA interference by Nobel laureates Andrew Fire and Craig Mello revolutionized current methods to develop RNA-based therapeutics.^{49,50} Post-transcriptional gene silencing activity by RNA interference is performed by two small noncoding RNA molecules: microRNAs (miRNAs) or small interfering RNAs (siRNAs) (**Figure 1.2**).⁵¹ MiRNAs differ from siRNAs by being transcribed from the genome within the nucleus before being processed and exported out into the cytoplasm as mature ~20 bp duplexes by the Drosha/DGCR8 complex, Exportin-5, and Dicer/TRBP complex, respectively.⁵² Furthermore, in mammals, miRNAs bind to the 3'-UTR of mRNA strands with partial complementarity, resulting in translational repression and/or mRNA degradation.⁵³ Exogenous siRNAs typically base-pair with full complementary to a mRNA target strand for cleavage when the guide strand is loaded into Ago2.⁵⁴

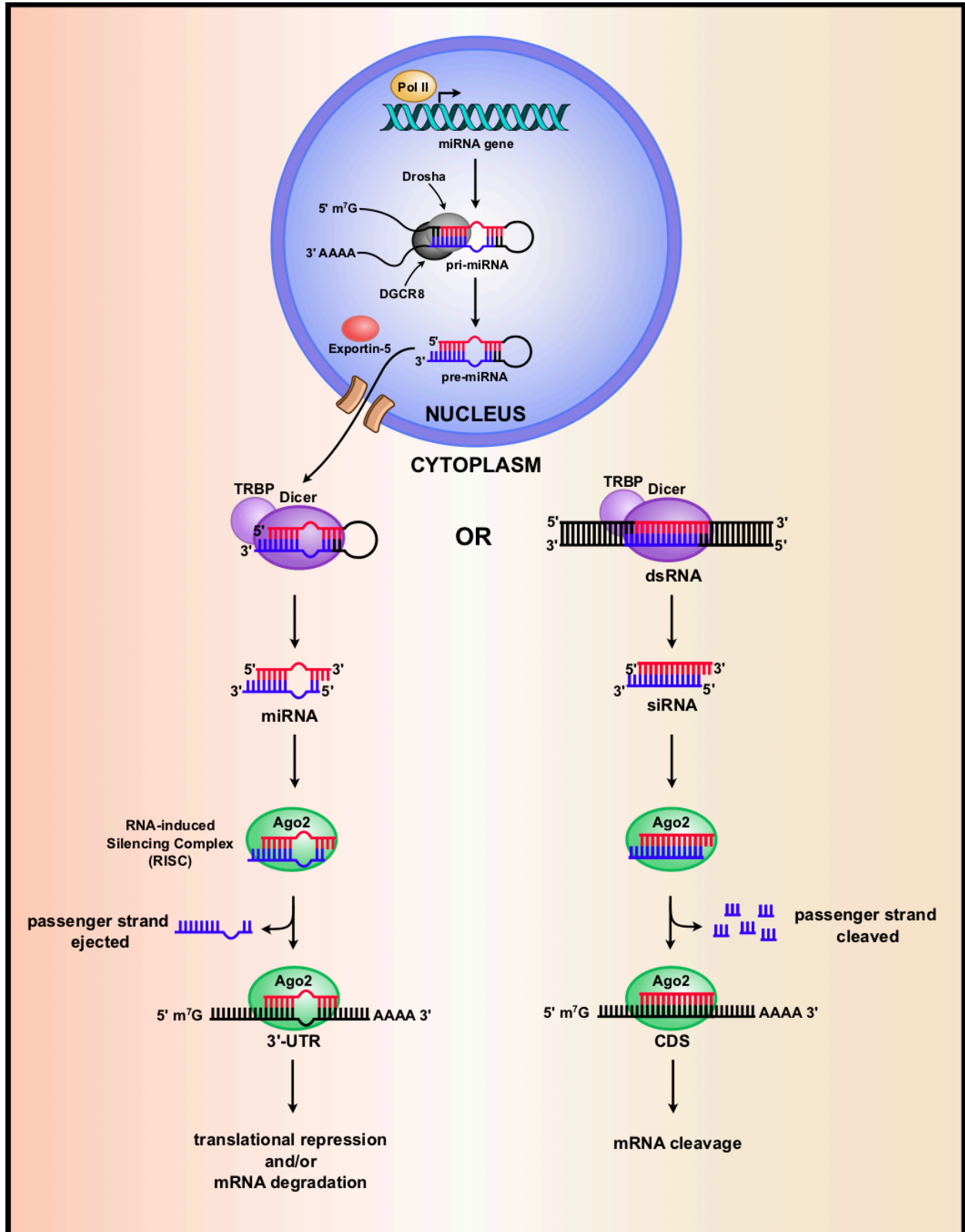


Figure 1.2 RNAi pathway by siRNA or miRNA.

The solved crystal structure of human Ago2 (hAgo2) stimulated efforts to design chemical modifications on RNAi-related oligonucleotides for potential therapeutic effects (**Figure 1.3**).⁵⁵⁻⁵⁷ Briefly, hAgo2 has a bilobed structure and can cradle a target RNA strand when bound to a loaded guide strand. The PAZ domain anchors the 3'-end of a guide miRNA or siRNA strand, whereas a phosphate-binding pocket within the MID domain can bind a phosphorylated 5'-end (**Figure 1.3 C and D**).^{58,59} The PIWI domain contains an RNase H-like active site and is responsible for slicing activity.⁶⁰ Furthermore, a solvated, nucleotide-binding pocket located between the L2 and MID domains was found to have higher binding specificity towards a target RNA strand adenosine at position 1 (t1A) over other canonical and modified bases.⁵⁷ More details about the t1A-binding pocket and our contribution to designing oligonucleotide modifications targeting this site will be described in Chapters 2 and 3.

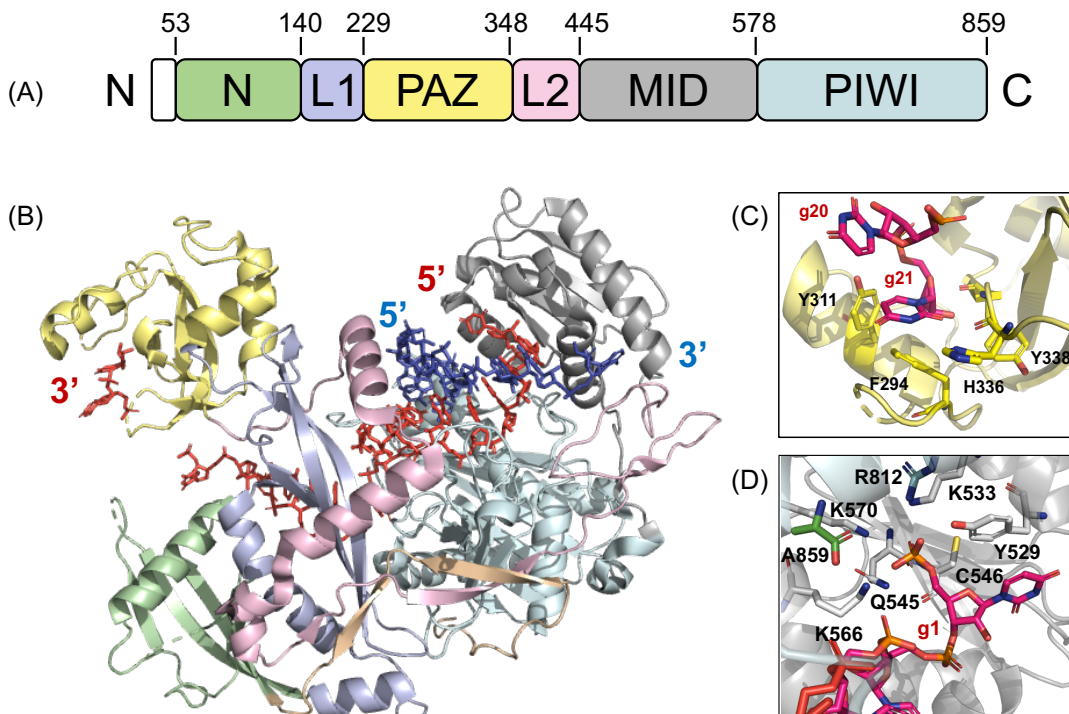


Figure 1.3 The crystal structure of hAgo2. (A) Domain map of full-length hAgo2. (B) Crystal structure of full-length hAgo2 with bound guide-target RNA duplex (PDB: 4W5O). The guide RNA strand is in red, and the target strand is in blue. (B) Close-up of PAZ domain interactions with 3'-end guide RNA nucleotide (guide strand nucleotide 21, g21). (C) Close-up of guide strand 5'-phosphate interactions with the MID domain phosphate-binding pocket. An A859 residue (green) from the N domain and an R812 residue (light blue) from the PIWI domain also make contacts within the pocket. g1 = guide strand nucleotide position 1

Several works to design chemically modified siRNAs guided by the structure of hAgo2 are in literature.⁶¹ One of the most notable structure-guided chemical modifications on siRNAs is the metabolically stable 5'-vinylphosphonate (5'-VP) moiety (**Figure 1.4**), discovered by Ionis Pharmaceuticals, that is used to replace the natural phosphate group at the 5'-end of an siRNA guide strand. Lima et. al. found that the 5'-VP modification on single-stranded siRNA (ss-siRNA) increased mRNA knockdown in mouse liver compared to 5'-phosphorylated control ss-siRNA.⁶² As an extension to this work, Prakash and colleagues used the crystal structure of hAgo2 to design and test analogs of 5'-phosphate by either adding substituents at the 5'-carbon position such as 5'-(*R*)-methylphosphate [5'-(*R*)-Me P] or designing 5'-methylene phosphonate analogs such as mono-fluorinated α -fluoromethylene phosphonate (5'-CHF P) and carried out structure-activity relationship studies of ss-siRNA activity *in vitro* and *in vivo* (**Figure 1.4**).⁶³ In addition, they found that rigidifying the 5'-methylene phosphonate moiety into a *trans* (*E*)-5'-VP analog was more potent than the (*Z*)-isomer as the (*E*)-isomer can better mimic the conformation of 5'-phosphate bound into the hAgo2 MID domain. Overall, the stereoelectronic-altering analogs at the 5'-end of ss-siRNAs could indeed promote gene silencing activity.

In the case of duplex siRNA, Elkayam et al. found that applying the 5'-(*E*)-vinylphosphonate (5'-*E*-VP) modification at the 5'-end of the guide strand of siRNA duplex

targeting transthyretin (TTR) mRNA also enhanced gene silencing activity in primary mouse hepatocytes and mouse liver.⁶⁴ To determine the structural basis for the improvement in siRNA activity, they crystallized hAgo2 loaded with a guide RNA oligonucleotide bearing a 5'-terminal 5'-(*E*)-VP 2'-OMe uridine (5'-(*E*)-VPu) modification using similar methods to crystallize the hAgo2-miR-20a complex.⁶⁵ At the 5'-phosphate-binding pocket in the MID domain, they found that the 5'-(*E*)-VPu moiety causes slight shifts in the pocket and generates an interaction with residues that are not seen with the structure with unmodified RNA, suggesting that the improved RNAi activity by the modified siRNA is strictly due to these altered interactions at the pocket. Overall, the 5'-VP modification strategy has great potential to be applicable on therapeutic siRNAs.

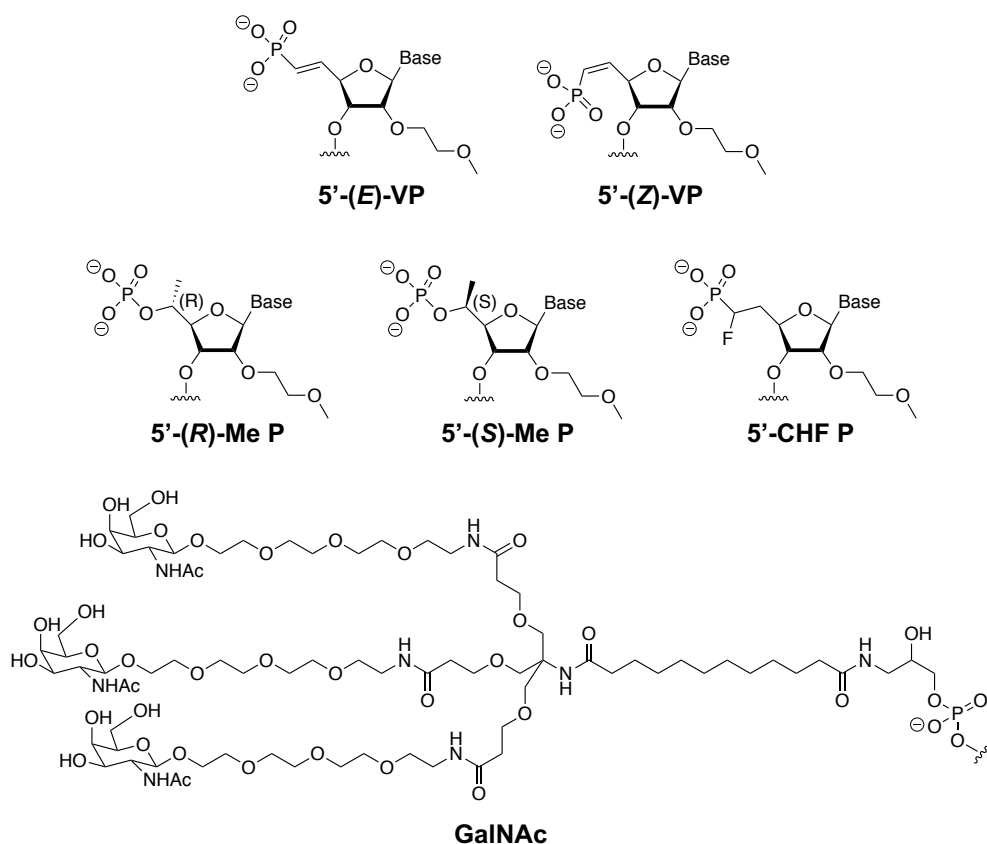


Figure 1.4 Panel (not exhaustive) listing chemical modifications on siRNA. Abbreviations: 5'-(*E*)-VP = 5'-(*E*)-vinylphosphonate; 5'-(*Z*)-VP = 5'-(*Z*)-vinylphosphonate; 5'-(*R*)-Me P = 5'-(*R*)-

methylphosphate; 5'-(S)-Me P = 5'-(S)-methylphosphate; 5'-CHF P = 5'- α -fluoromethylenephosphonate; GalNAc = *N*-acetylgalactosamine. GalNAc is shown as a trivalent structure as is used for siRNA conjugation.

Another major breakthrough in siRNA drug design is the use of GalNAc (*N*-acetylgalactosamine) conjugation to improve delivery into cells (**Figure 1.4**).⁶⁶ The GalNAc moiety serves as a ligand to the asialoglycoprotein receptor (ASGPR) that is highly expressed and abundant on the surface of hepatocytes.⁶⁷ Indeed, FDA-approved siRNAs such as givosiran (GIVLAARI™) and inclisiran (ALN-PCSsc, licensed as Leqvio® by Novartis), both designed by Alnylam Pharmaceuticals, are conjugated with a trivalent GalNAc group at the 3'-end of the sense (passenger) strand and are used to treat acute hepatic porphyria or hypercholesterolemia.^{68,69} Other GalNAc-conjugated siRNAs including Dicerna Pharmaceuticals' nedosiran (DCR-PHXC) to treat primary hyperoxaluria, or Alnylam and Genzyme's fitusiran (ALN-AT3SC) to treat hemophilia, are currently in phase 3 clinical trials.^{66,70}

Our lab has reported many studies that primarily involve using CuAAC "click" chemistry to modify siRNA strands bearing ethynyl-modified nucleobase precursors at specific positions to facilitate interactions with hAgo2. To be succinct, we have made triazole modifications from alkynyl-derived nucleobase analogs such as 7-ethynyl-8-aza-7-deazaadenosine^{71,72}, 1'-ethynyl ribose^{73,74}, and 2-propargylaminopurine⁷⁵ at the 5'-end (g1), 3'-end (g20 or g21), or other nucleotides along the guide strand to probe interactions with either the MID or PAZ domain of hAgo2, or to control miRNA-like off targeting effects (**Figure 1.5A**).^{73,74,76,77} Prior to reported structures of full-length hAgo2, previous graduate student Dr. Hayden Peacock used the same post-synthetic CuAAC strategy to design 2-aminopurine analogs that could project into the minor groove of dsRNA and

perturb double-stranded RNA binding by proteins such as PKR or ADAR that could hinder siRNA performance.^{75,78} Similarly, our lab has also collaborated with Prof. Cynthia Burrows to design and test analogs of *N*²-alkylated 8-oxo-7,8-dihydroguanine or 8-alkoxyadenosine (**Figure 1.5A**) on the guide strand of siRNAs whose substituents can also project into the minor groove and mitigate off-target recognition by PKR or ADAR, yet can retain RNAi activity when the sterically demanding group “switches” out into the major groove upon loading into the RNA-induced silencing complex (RISC).^{79,80}

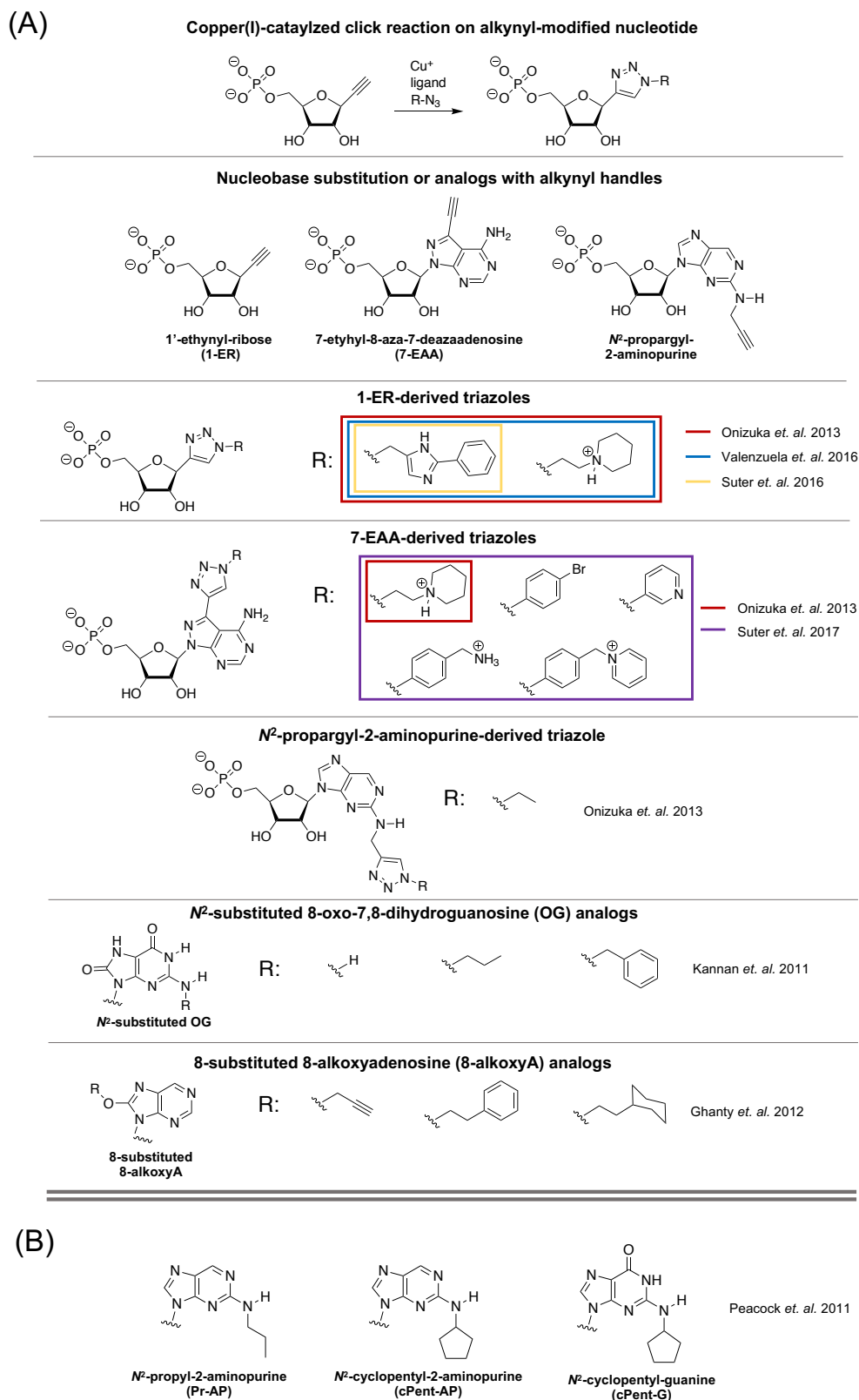


Figure 1.5 Chemical modifications of RNAi molecules reported in the Beal lab. (A) Chemical modifications on siRNAs. (B) Chemical modifications on miRNA-122 mimic.

In the miRNA therapeutics field, synthetic antisense oligonucleotides targeting microRNAs (anti-miRs) or miRNA mimics to treat dysregulated miRNAs correlated with disease are also being developed.⁸¹ Unfortunately, miRNA-based therapies have not been as successful as siRNAs as none have yet reached the market, likely due to difficulties with overcoming off-targeting towards undesired miRNA that share a same seed sequence in a given miRNA family.⁸² In either case, the chemical modification strategies used in anti-miRs or miRNA mimics are similar to what is used for other oligonucleotide-based therapies. To name a few miRNA-based therapeutics currently in clinical trials, anti-miRs such as antimiR-92a (MRG-110) or cobomarsen (antimiR-155, MRG-106) are two LNA-modified oligonucleotides developed by miRagen Therapeutics that are in phase 2 clinical trials.^{83,84} Santaris Pharma (acquired by Roche) developed a 15mer LNA/PS-modified anti-miR targeting miR-122 and is in phase 3 clinical trials for treating hepatitis C virus (HCV) infection.⁸⁵ RGLS4326 (anti-miR17) by Regulus Therapeutics is a 23mer oligonucleotide comprised of cEt, 2'-OMe, and 2'-F modifications in the complementary seed region to miR-17 and is in phase 1b trials for potential treatment of autosomal dominant polycystic kidney disease (ADPKD).⁸⁶ On the other hand, remlarsen (MRG-201), developed by miRagen Therapeutics, is a miR-29b mimic that is modified with a combination of 2'-OMe, 2'-F, RNA, PS linkages, and a cholesterol conjugation and is in phase 2 clinical trials for treating pathological fibrosis.^{87,88}

Reports of chemically-modified miRNA mimics are rather minimal in comparison to siRNA.⁸⁹ However, our group, in collaboration with Sirna Therapeutics (acquired by Merck), reported nucleobase-modified miR-122 mimics to control immune stimulation, a common obstacle to overcome in RNAi therapeutics.⁹⁰ A guanosine analog containing

an N^2 -cyclopentyl group (cPent-G) or 2-aminopurine analogs containing N^2 -propyl (Pr-AP) or N^2 -cyclopentyl (cPent-AP) substituents were employed at various positions along the miR-122 mimic guide strand and, at some positions, were found to be critical for cytokine stimulation (**Figure 1.5B**). Similar to the chemical modification strategy on siRNAs mentioned above, this strategy made use of nucleobase analog substituents that would be directed towards the minor groove of the mimic duplex and block recognition at the double-stranded RNA-binding motif by proteins PKR or ADAR1, thus mitigating TLR-mediated immune stimulation.⁷⁵

There are a handful of reports towards designing unique chemical modifications on anti-miRs that differ from the commonly used chemistries for oligonucleotides. As an example, Lennox et. al. report using N,N-diethyl-4-(4-nitronaphthalen-1-ylazo)-phenylamine (“ZEN”) modifiers at or near the terminal ends of anti-miR21 increased binding affinity and exonuclease resistance, as determined by cell-based, melting temperature, and serum resistance assays.⁹¹ Ariyoshi et. al. used the hAgo2 crystal structure to make amino acid-conjugated anti-miRs that, when bound to miR-loaded hAgo2, would disrupt interactions between the PIWI-box and 5'-end of miRNA strand and promote release, therefore inhibiting RNAi activity.⁹² Finally, Gubu et. al. designed intramolecularly circularized anti-miR21 and anti-miR122 using circle oligodeoxynucleotides (c-ODNs) and CuAAC chemistry and determined reduced off-targeting and immunostimulatory effects in cellular-based assays.⁹³

1.4 Chemically modified oligonucleotides targeting Adenosine Deaminase Acting on RNA (ADAR)

RNA editing can be generally defined as the insertion, deletion, or modification of RNA that results in a change in coding properties.^{94,95} The most prevalent form of RNA editing is adenosine-to-inosine (A-to-I) editing of dsRNA that is catalyzed by ADAR. The human ADAR family comprises of ADAR1, ADAR2, and ADAR3, where all share a C-terminal deaminase domain as well as double-stranded RNA binding domains (dsRBDs) (**Figure 1.6A**). ADAR1 has two isoforms that are produced by two different promoters: a longer, interferon-inducible p150 isoform that has a Z α -DNA-binding domain with a nuclear export signal (NES), and a shorter p110 isoform.⁹⁶ Both ADAR1 isoforms contain a third dsRBD that ADAR2 and ADAR3 do not possess. ADAR3 differs from ADAR2 by the presence of an arginine-rich domain (R-domain), allowing it to bind to single-stranded RNA (ssRNA).⁹⁷ To date, ADAR1 and ADAR2 are reported to be catalytically active, whereas ADAR3 activity remains unknown. ADAR performs A-to-I editing by coordinating with a zinc ion to catalyze the hydrolytic deamination of adenosine, converting it into inosine (**Figure 1.6B**).⁹⁸ Inosine can base pair with cytosine, thus can be read as a guanosine by translational machinery and result in A-to-G substitutions that can potentially change a protein's amino acid sequence and function (**Figure 1.6C**).

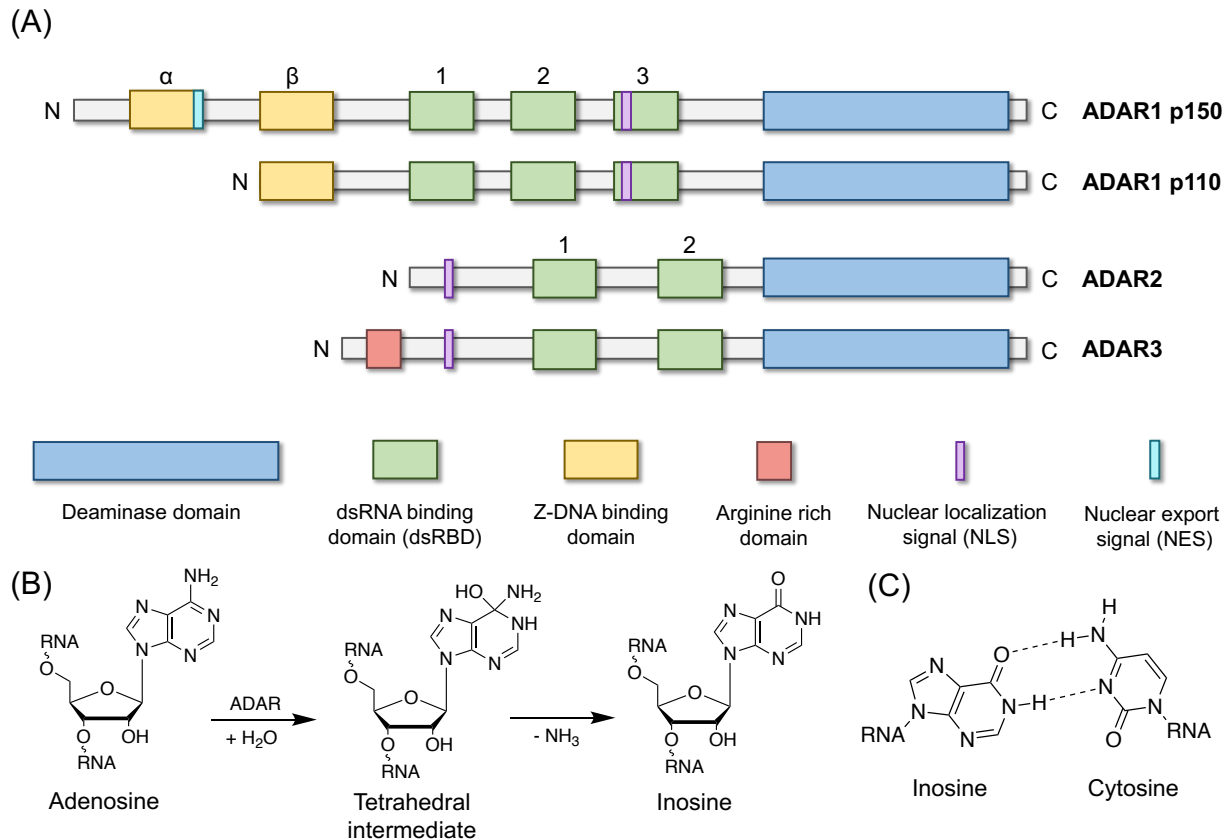


Figure 1.6 The human ADAR family and A-to-I editing reaction scheme. (A) Domain maps of human ADAR1 p150 and p110 isoforms, ADAR2, and ADAR3. (B) Reaction scheme of ADAR-catalyzed hydrolytic deamination of adenosine to inosine. (C) Base pairing of inosine with cytosine.

A-to-I editing of transcripts has an important role in numerous cellular functions (Figure 1.7).⁹⁹ ADAR can edit intronic or exonic sites, resulting in exon inclusion/skipping or altered splicing events.¹⁰⁰ Editing of dsRNA can result in secondary structure changes that cannot therefore be recognized by RNA-binding proteins for downstream cellular processes.¹⁰¹ Alternatively, ADAR1 can edit dsRNA to prevent recognition as pathogenic “non-self” by dsRNA sensors MDA5 or PKR and bypass innate immune responses. This is an important mechanism that cancer cells take advantage of to promote cell proliferation and mitigate tumor suppression.^{102,103} A-

to-I editing can also result in a variety of recoding events where an edited transcript can alter the amino acid sequence of a protein, resulting in dysfunction, truncation, or a new phenotype.¹⁰⁴ Lastly, ADAR can modulate miRNA biogenesis or gene silencing specificity by editing pre-microRNA (pre-miRNA) prior to processing by the Dicer/TRBP complex or miRNA recognition sites at the 3'-UTR of a transcript.¹⁰⁵

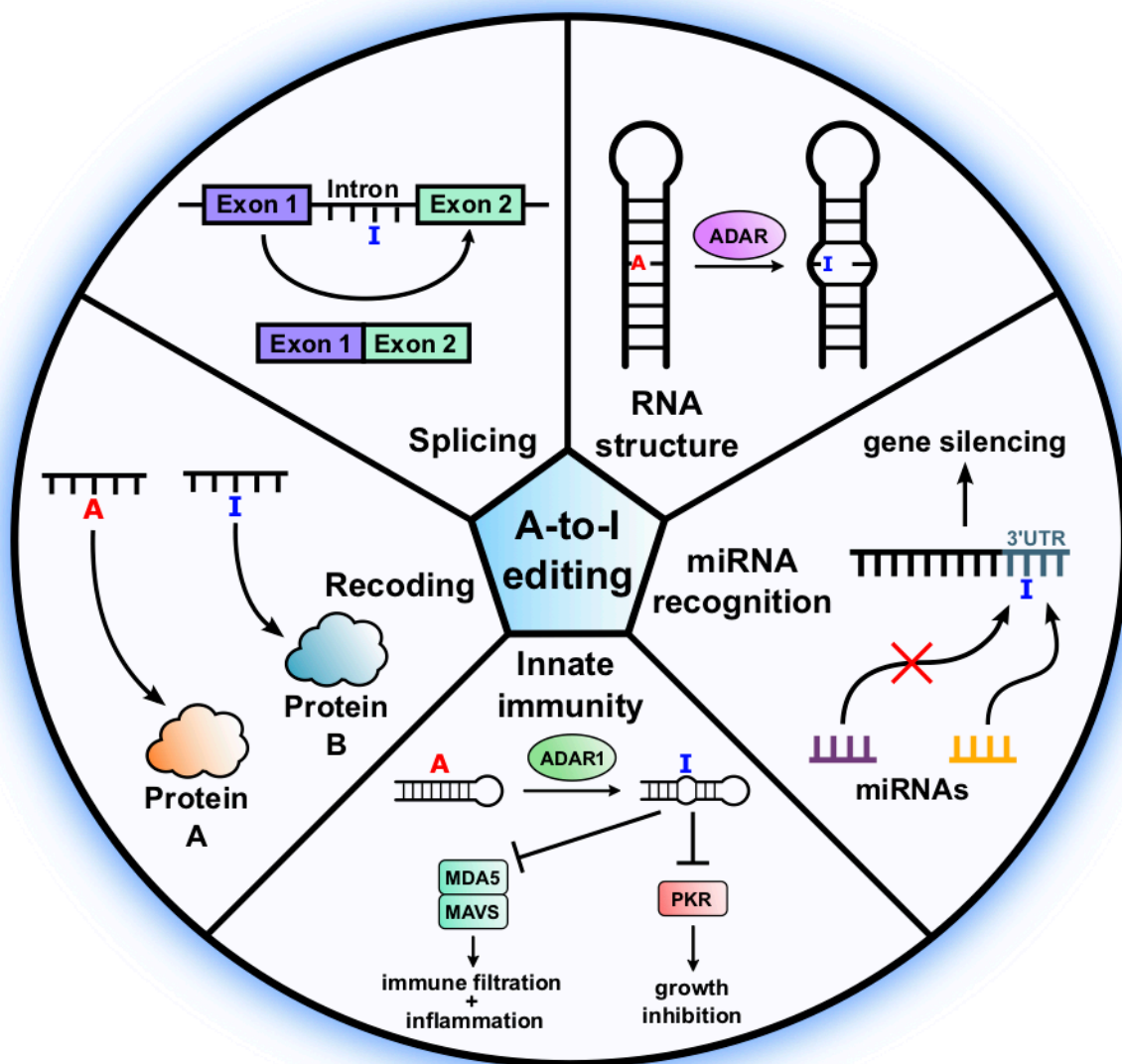


Figure 1.7 Functional roles of post-transcriptional A-to-I editing by ADAR.

In the A-to-I editing field, oligonucleotides are used for applications such as site-directed RNA editing (SDRE), crystallography, or inhibition. To date, site-directed editing strategies such as RESTORE (recruiting endogenous ADAR to specific transcripts for oligonucleotide-mediated RNA editing) and LEAPER (leveraging endogenous ADAR for programmable editing of RNA) make use of oligonucleotides to recruit endogenous ADARs to perform RNA editing at disease-related sites genes without the need to overexpress any exogenous protein, a common obstacle in RNA editing therapy applications.^{106,107} RESTORE, developed by Billy Li and Thorsten Stafforst's labs, uses ASOs that can target the 5' UAG site at the 3'-UTR of editing sites. The ASOs contain a self-complementary, fully unmodified ribonucleotide ADAR-recruiting domain that can be recognized by ADAR dsRBDs, and a 2'-OMe, LNA, and PS-linkage modified 18-mer specificity domain that can be recognized by the deaminase domain for site-specific editing activity.¹⁰⁷ On the other hand, LEAPER, developed by numerous researchers at Peking University and EdiGene Inc., takes a different approach by genetically-encoding or transfecting approximately ~70-100 nt long oligonucleotides called ADAR-recruiting RNAs (arRNAs) with minimal chemical modifications to direct endogenous ADAR to edit at specific sites. The only chemical modifications applied onto the arRNAs are three PS-linked 2'-OMe nucleotides on both termini of the ASO.

Recently, our lab has made great progress in designing chemically-modified oligonucleotides for SDRE-based applications. In 2019, previous graduate student Dr. Leanna Monteleone used a bump-hole approach to promote site-directed editing on transcripts.¹⁰⁸ In cell-based assays, she showed that transfecting guide RNA oligonucleotides containing two PS linkages on both terminal ends and an abasic

nucleotide at the nucleotide opposite the edited adenosine, also known as the “orphan base”, reduces off-target editing in the presence of overexpressed bulky ADAR2 E488 mutants when compared to wildtype ADAR2. More recently, in 2021, fellow colleague Erin Doherty synthesized cytidine analogs and incorporated them at the orphan base position onto guide editing oligonucleotides to greatly improve endogenous ADAR editing efficiency.¹⁰⁹ In collaboration with ProQR Therapeutics, Erin Doherty heavily modified the orphan cytidine analog-containing oligonucleotides with specific positioning of 2'-OMe, RNA, DNA, and PS linkages and found significantly improved endogenous ADAR editing activity of *Idua* mRNA in primary mouse liver fibroblasts. It is important to note that our lab's SDRE oligonucleotide designs are generally shorter in length to avoid any off-targeting or RNAi-like effects.¹¹⁰

Furthermore, we have been able to use dsRNA substrates where one strand is an oligonucleotide containing a high-affinity 8-azanebularine analog (**Figure 1.8A**) to solve crystal structures of ADAR2 deaminase domain and asymmetrically-dimerized ADAR2 deaminase domain with dsRBD2 (**Figure 1.8B and C**).^{111,112} In addition, Erin Doherty generated a homology model of ADAR1 using Rosetta based on the crystal structure of ADAR2d to supplement Dr. SeHee Park's discovery of a second zinc metal-binding site in ADAR1 (**Figure 1.8D**).¹¹³ These structures have provided us with a wealth of information for rational and structure-guided designs of chemically modified nucleic acids that can interact with ADAR.

Lastly, our group is currently working on ADAR1-based inhibitors using chemically modified 8-azanebularine-containing oligonucleotides that will be discussed further in Chapter 4.

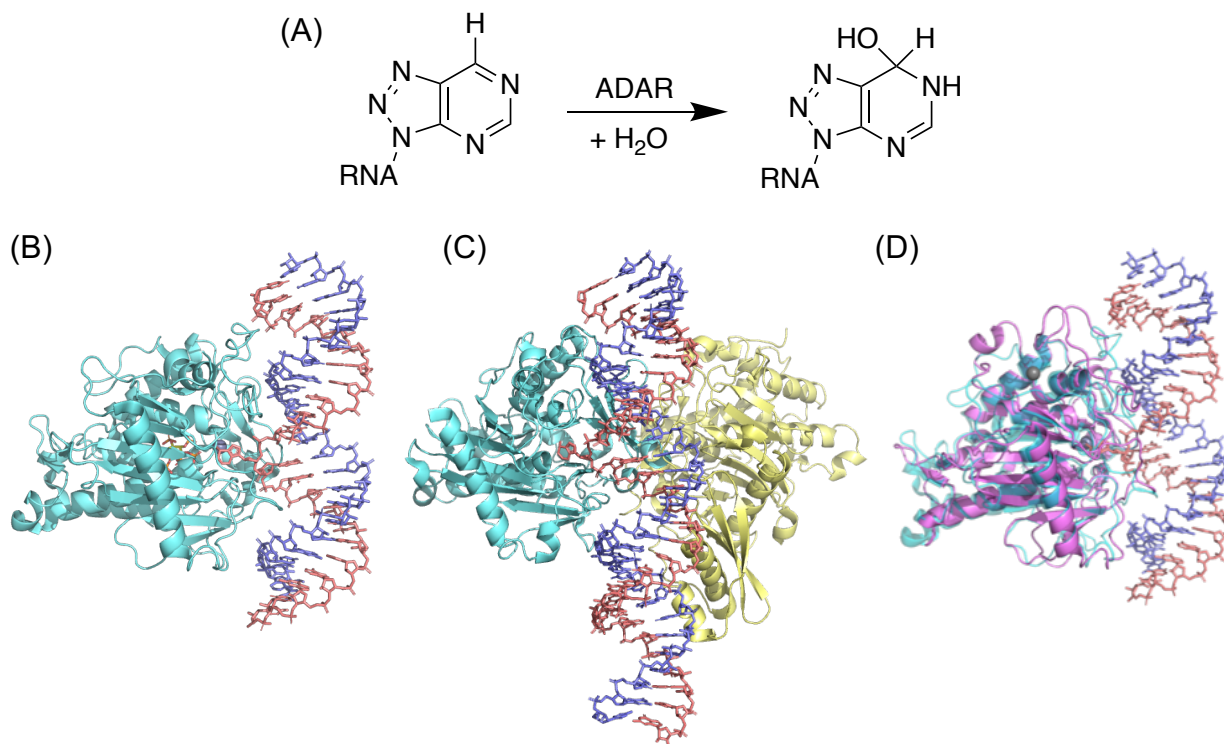


Figure 1.8 Crystal structures or models of ADAR protein bound to dsRNA substrate. (A) The 8-azanebularine analog has high affinity to the active site of ADAR2 and can trap ADAR for crystallography when 8-azanebularine is converted into a hydrated intermediate. (B) Crystal structure of hADAR2d E488Q mutant bound to *Bdf2-C* RNA duplex at 2.75 Å resolution (PDB: 5ED1).¹¹¹ The 8-azanebularine-containing RNA strand is colored deep salmon and the complementary strand is colored blue. (B) Crystal structure of hADAR2-R2d E488Q bound to *Gli1* 32 bp RNA at 2.8 Å resolution (PDB: 6VFF).¹¹² Monomer B of hADAR2-R2d E488Q is colored pale yellow. (C) Homology model of hADAR1d (light magenta) overlaying hADAR2d E488Q structure bound (transparent light blue) to *Bdf2-C* RNA duplex (PDB: 5ED1).¹¹³

1.5 References

- (1) Pham, K. M.; Suter, S. R.; Lu, S. S.; Beal, P. A. Ester Modification at the 3' End of Anti-MicroRNA Oligonucleotides Increases Potency of MicroRNA Inhibition. *Bioorganic Med. Chem.* **2021**, *29* (October 2020), 115894. <https://doi.org/10.1016/j.bmc.2020.115894>.
- (2) Roberts, T. C.; Langer, R.; Wood, M. J. A. Advances in Oligonucleotide Drug Delivery. *Nat. Rev. Drug Discov.* **2020**, *19* (10), 673–694. <https://doi.org/10.1038/s41573-020-0075-7>.
- (3) Ochoa, S.; Milam, V. T. Modified Nucleic Acids: Expanding the Capabilities of Functional Oligonucleotides. *Molecules* **2020**, *25* (20), 1–23. <https://doi.org/10.3390/molecules25204659>.
- (4) Burnett, J. C.; Rossi, J. J. RNA-Based Therapeutics: Current Progress and Future Prospects. *Chem. Biol.* **2012**, *19* (1), 60–71. <https://doi.org/10.1016/j.chembiol.2011.12.008>.
- (5) Lindow, M.; Kauppinen, S. Discovering the First MicroRNA-Targeted Drug. *J. Cell Biol.* **2012**, *199* (3), 407–412. <https://doi.org/10.1083/jcb.201208082>.
- (6) Keefe, A. D.; Pai, S.; Ellington, A. Aptamers as Therapeutics. *Nat. Rev. Drug Discov.* **2010**, *9* (7), 537–550. <https://doi.org/10.1038/nrd3141>.
- (7) Gagliardi, M.; Ashizawa, A. T. The Challenges and Strategies of Antisense Oligonucleotide Drug Delivery. *Biomedicines* **2021**, *9* (4). <https://doi.org/10.3390/biomedicines9040433>.
- (8) Khvorova, A.; Watts, J. K. The Chemical Evolution of Oligonucleotide Therapies of Clinical Utility. *Nat. Biotechnol.* **2017**, *35* (3), 238–248. <https://doi.org/10.1038/nbt.3765>.
- (9) Lundin, K. E.; Gissberg, O.; Smith, C. I. E. Oligonucleotide Therapies: The Past and the Present. *Hum. Gene Ther.* **2015**, *26* (8), 475–485. <https://doi.org/10.1089/hum.2015.070>.
- (10) Eckstein, F. Phosphorothioates, Essential Components of Therapeutic Oligonucleotides. *Nucleic Acid Ther.* **2014**, *24* (6), 374–387. <https://doi.org/10.1089/nat.2014.0506>.
- (11) Eckstein, F. Phosphorothioate Nucleotides. *Acc. Chem. Res.* **1979**, *12*, 204–210.
- (12) Geary, R. S.; Norris, D.; Yu, R.; Bennett, C. F. Pharmacokinetics, Biodistribution and Cell Uptake of Antisense Oligonucleotides. *Adv. Drug Deliv. Rev.* **2015**, *87*, 46–51. <https://doi.org/10.1016/j.addr.2015.01.008>.
- (13) Koller, E.; Vincent, T. M.; Chappell, A.; De, S.; Manoharan, M.; Bennett, C. F. Mechanisms of Single-Stranded Phosphorothioate Modified Antisense Oligonucleotide Accumulation in Hepatocytes. *Nucleic Acids Res.* **2011**, *39* (11), 4795–4807. <https://doi.org/10.1093/nar/gkr089>.
- (14) Iwamoto, N.; Butler, D. C. D.; Svrzikapa, N.; Mohapatra, S.; Zlatev, I.; Sah, Di. W. Y.; Meena; Standley, S. M.; Lu, G.; Apponi, L. H.; et al. Control of Phosphorothioate Stereochemistry Substantially Increases the Efficacy of Antisense Oligonucleotides. *Nat. Biotechnol.* **2017**, *35* (9), 845–851. <https://doi.org/10.1038/nbt.3948>.
- (15) Østergaard, M. E.; De Hoyos, C. L.; Wan, W. B.; Shen, W.; Low, A.; Berdeja, A.; Vasquez, G.; Murray, S.; Migawa, M. T.; Liang, X. H.; et al. Understanding the

- Effect of Controlling Phosphorothioate Chirality in the DNA Gap on the Potency and Safety of Gapmer Antisense Oligonucleotides. *Nucleic Acids Res.* **2020**, *48* (4), 1691–1700. <https://doi.org/10.1093/nar/gkaa031>.
- (16) Monia, B. P.; Johnston, J. F.; Sasmor, H.; Cummins, L. L. Nuclease Resistance and Antisense Activity of Modified Oligonucleotides Targeted to Ha-Ras. *J. Biol. Chem.* **1996**, *271* (24), 14533–14540. <https://doi.org/10.1074/jbc.271.24.14533>.
- (17) Choung, S.; Kim, Y. J.; Kim, S.; Park, H. O.; Choi, Y. C. Chemical Modification of SiRNAs to Improve Serum Stability without Loss of Efficacy. *Biochem. Biophys. Res. Commun.* **2006**, *342* (3), 919–927. <https://doi.org/10.1016/j.bbrc.2006.02.049>.
- (18) Ruckman, J.; Green, L. S.; Beeson, J.; Waugh, S.; Gillette, W. L.; Henninger, D. D.; Claesson-Welsh, L.; Janjić, N. 2'-Fluoropyrimidine RNA-Based Aptamers to the 165-Amino Acid Form of Vascular Endothelial Growth Factor (VEGF165): Inhibition of Receptor Binding and VEGF-Induced Vascular Permeability through Interactions Requiring the Exon 7-Encoded Domain. *J. Biol. Chem.* **1998**, *273* (32), 20556–20567. <https://doi.org/10.1074/jbc.273.32.20556>.
- (19) Allerson, C. R.; Sioufi, N.; Jarres, R.; Prakash, T. P.; Naik, N.; Berdeja, A.; Wanders, L.; Griffey, R. H.; Swayze, E. E.; Bhat, B. Fully 2'-Modified Oligonucleotide Duplexes with Improved in Vitro Potency and Stability Compared to Unmodified Small Interfering RNA. *J. Med. Chem.* **2005**, *48* (4), 901–904. <https://doi.org/10.1021/jm049167j>.
- (20) Malek-Adamian, E.; Guenther, D. C.; Matsuda, S.; Martínez-Montero, S.; Zlatev, I.; Harp, J.; Burai Patrascu, M.; Foster, D. J.; Fakhoury, J.; Perkins, L.; et al. 4'-C-Methoxy-2'-Deoxy-2'-Fluoro Modified Ribonucleotides Improve Metabolic Stability and Elicit Efficient RNAi-Mediated Gene Silencing. *J. Am. Chem. Soc.* **2017**, *139* (41), 14542–14555. <https://doi.org/10.1021/jacs.7b07582>.
- (21) Mangos, M. M.; Min, K. L.; Viazovkina, E.; Galarneau, A.; Elzagheid, M. I.; Parniak, M. A.; Damha, M. J. Efficient RNase H-Directed Cleavage of RNA Promoted by Antisense DNA or 2'-F-ANA Constructs Containing Acyclic Nucleotide Inserts. *J. Am. Chem. Soc.* **2003**, *125* (3), 654–661. <https://doi.org/10.1021/ja025557o>.
- (22) Min, K. L.; Viazovkina, E.; Galarneau, A.; Parniak, M. A.; Damha, M. J. Oligonucleotides Comprised of Alternating 2'-Deoxy-2'-Fluoro-β-D-Arabinonucleosides and D-2'-Deoxyribonucleosides (2'-F-ANA/DNA 'Altimers') Induce Efficient RNA Cleavage Mediated by RNase H. *Bioorganic Med. Chem. Lett.* **2002**, *12* (18), 2651–2654. [https://doi.org/10.1016/S0960-894X\(02\)00439-0](https://doi.org/10.1016/S0960-894X(02)00439-0).
- (23) Martin, V. P.; Ag, Z. F. D. C.; Basel, C. H. A New Access to 2'-O-Alkylated Ribonucleosides and Properties of 2'-O-Alkylated Oligoribonucleotides. *Helv. Chim. Acta* **1995**, *78*, 486–504.
- (24) Raal, F. J.; Santos, R. D.; Blom, D. J.; Marais, A. D.; Charng, M. J.; Cromwell, W. C.; Lachmann, R. H.; Gaudet, D.; Tan, J. L.; Chasan-Taber, S.; et al. Mipomersen, an Apolipoprotein B Synthesis Inhibitor, for Lowering of LDL Cholesterol Concentrations in Patients with Homozygous Familial Hypercholesterolaemia: A Randomised, Double-Blind, Placebo-Controlled Trial. *Lancet* **2010**, *375* (9719), 998–1006. [https://doi.org/10.1016/S0140-6736\(10\)60284-X](https://doi.org/10.1016/S0140-6736(10)60284-X).

- (25) Veedu, R. N.; Wengel, J. Locked Nucleic Acid as a Novel Class of Therapeutic Agents. *RNA Biol.* **2009**, *6* (3), 321–323. <https://doi.org/10.4161/rna.6.3.8807>.
- (26) Vester, B.; Wengel, J. LNA (Locked Nucleic Acid): High-Affinity Targeting of Complementary RNA and DNA. *Biochemistry* **2004**, *43* (42), 13233–13241. <https://doi.org/10.1021/bi0485732>.
- (27) Morita, K.; Hasegawa, C.; Kaneko, M.; Tsutsumi, S.; Sone, J.; Ishikawa, T.; Imanishi, T.; Koizumi, M. 2'-O,4'-C-Ethylene-Bridged Nucleic Acids (ENA): Highly Nuclease-Resistant and Thermodynamically Stable Oligonucleotides for Antisense Drug. *Bioorganic Med. Chem. Lett.* **2002**, *12* (1), 73–76. [https://doi.org/10.1016/S0960-894X\(01\)00683-7](https://doi.org/10.1016/S0960-894X(01)00683-7).
- (28) Kurreck, J.; Wyszko, E.; Gillen, C.; Erdmann, V. A. Design of Antisense Oligonucleotides Stabilized by Locked Nucleic Acids. *Nucleic Acids Res.* **2002**, *30* (9), 1911–1918. <https://doi.org/10.1093/nar/30.9.1911>.
- (29) Obad, S.; Dos Santos, C. O.; Petri, A.; Heidenblad, M.; Broom, O.; Ruse, C.; Fu, C.; Lindow, M.; Stenvang, J.; Straarup, E. M.; et al. Silencing of MicroRNA Families by Seed-Targeting Tiny LNAs. *Nat. Genet.* **2011**, *43* (4), 371–380. <https://doi.org/10.1038/ng.786>.
- (30) Owczarzy, R.; You, Y.; Groth, C. L.; Tataurov, A. V. Stability and Mismatch Discrimination of Locked Nucleic Acid-DNA Duplexes. *Biochemistry* **2011**, *50* (2), 9352–9367.
- (31) Straarup, E. M.; Fisker, N.; Hedtjörn, M.; Lindholm, M. W.; Rosenbohm, C.; Aarup, V.; Hansen, H. F.; Ørum, H.; Hansen, J. B. R.; Koch, T. Short Locked Nucleic Acid Antisense Oligonucleotides Potently Reduce Apolipoprotein B mRNA and Serum Cholesterol in Mice and Non-Human Primates. *Nucleic Acids Res.* **2010**, *38* (20), 7100–7111. <https://doi.org/10.1093/nar/gkq457>.
- (32) Swayze, E. E.; Siwkowski, A. M.; Wancewicz, E. V.; Migawa, M. T.; Wyrzykiewicz, T. K.; Hung, G.; Monia, B. P.; Bennett, C. F. Antisense Oligonucleotides Containing Locked Nucleic Acid Improve Potency but Cause Significant Hepatotoxicity in Animals. *Nucleic Acids Res.* **2007**, *35* (2), 687–700. <https://doi.org/10.1093/nar/gkl1071>.
- (33) Edvard Smith, C. I.; Zain, R. Therapeutic Oligonucleotides: State of the Art. *Annu. Rev. Pharmacol. Toxicol.* **2019**, *59*, 605–630. <https://doi.org/10.1146/annurev-pharmtox-010818-021050>.
- (34) Kumar, S.; Chinnusamy, V.; Mohapatra, T. Epigenetics of Modified DNA Bases: 5-Methylcytosine and Beyond. *Front. Genet.* **2018**, *9* (December), 1–14. <https://doi.org/10.3389/fgene.2018.00640>.
- (35) Terrazas, M.; Kool, E. T. RNA Major Groove Modifications Improve siRNA Stability and Biological Activity. *Nucleic Acids Res.* **2009**, *37* (2), 346–353. <https://doi.org/10.1093/nar/gkn958>.
- (36) Vaught, J. D.; Bock, C.; Carter, J.; Fitzwater, T.; Otis, M.; Schneider, D.; Rolando, J.; Waugh, S.; Wilcox, S. K.; Eaton, B. E. Expanding the Chemistry of DNA for in Vitro Selection. *J. Am. Chem. Soc.* **2010**, *132* (12), 4141–4151. <https://doi.org/10.1021/ja908035g>.
- (37) Tolle, F.; Brändle, G. M.; Matzner, D.; Mayer, G. A Versatile Approach Towards Nucleobase-Modified Aptamers. *Angew. Chemie - Int. Ed.* **2015**, *54* (37), 10971–10974. <https://doi.org/10.1002/anie.201503652>.

- (38) Østergaard, M. E.; Southwell, A. L.; Kordasiewicz, H.; Watt, A. T.; Skotte, N. H.; Doty, C. N.; Vaid, K.; Villanueva, E. B.; Swayze, E. E.; Bennett, C. F.; et al. Rational Design of Antisense Oligonucleotides Targeting Single Nucleotide Polymorphisms for Potent and Allele Selective Suppression of Mutant Huntingtin in the CNS. *Nucleic Acids Res.* **2013**, *41* (21), 9634–9650. <https://doi.org/10.1093/nar/gkt725>.
- (39) Østergaard, M. E.; Kumar, P.; Nichols, J.; Watt, A.; Sharma, P. K.; Nielsen, P.; Seth, P. P. Allele-Selective Inhibition of Mutant Huntingtin with 2-Thio- and C5-Triazolylphenyl-Deoxythymidine-Modified Antisense Oligonucleotides. *Nucleic Acid Ther.* **2015**, *25* (5), 266–274. <https://doi.org/10.1089/nat.2015.0547>.
- (40) Bartosik, K.; Debiec, K.; Czarnecka, A.; Sochacka, E.; Leszczynska, G. Synthesis of Nucleobase-Modified RNA Oligonucleotides by Post-Synthetic Approach. *Molecules* **2020**, *25* (15). <https://doi.org/10.3390/molecules25153344>.
- (41) Brad Wan, W.; Seth, P. P. The Medicinal Chemistry of Therapeutic Oligonucleotides. *Journal of Medicinal Chemistry*. 2016, pp 9645–9667. <https://doi.org/10.1021/acs.jmedchem.6b00551>.
- (42) Hammond, S. M.; Aartsma-Rus, A.; Alves, S.; Borgos, S. E.; Buijsen, R. A. M.; Collin, R. W. J.; Covello, G.; Denti, M. A.; Desviat, L. R.; Echevarría, L.; et al. Delivery of Oligonucleotide-based Therapeutics: Challenges and Opportunities. *EMBO Mol. Med.* **2021**, *13* (4), 1–23. <https://doi.org/10.15252/emmm.202013243>.
- (43) Perry, C. M.; Barman Balfour, J. A. Fomivirsen. *Drugs* **1999**, *57* (3), 375–380. <https://doi.org/10.1201/9781315152110>.
- (44) Xiong, H.; Veedu, R. N.; Diermeier, S. D. Recent Advances in Oligonucleotide Therapeutics in Oncology. *Int. J. Mol. Sci.* **2021**, *22* (7). <https://doi.org/10.3390/ijms22073295>.
- (45) Dolgin, E. The Tangled History of mRNA Vaccines. *Nature* **2021**, *597* (7876), 318–324. <https://doi.org/10.1038/d41586-021-02483-w>.
- (46) Karikó, K.; Muramatsu, H.; Welsh, F. A.; Ludwig, J.; Kato, H.; Akira, S.; Weissman, D. Incorporation of Pseudouridine into mRNA Yields Superior Nonimmunogenic Vector with Increased Translational Capacity and Biological Stability. *Mol. Ther.* **2008**, *16* (11), 1833–1840. <https://doi.org/10.1038/mt.2008.200>.
- (47) Song, B.; Tang, Y.; Wei, Z.; Liu, G.; Su, J.; Meng, J.; Chen, K. PIANO: A Web Server for Pseudouridine-Site (Ψ) Identification and Functional Annotation. *Front. Genet.* **2020**, *11* (March), 1–8. <https://doi.org/10.3389/fgene.2020.00088>.
- (48) Morais, P.; Adachi, H.; Yu, Y. T. The Critical Contribution of Pseudouridine to mRNA COVID-19 Vaccines. *Front. Cell Dev. Biol.* **2021**, *9* (November), 1–9. <https://doi.org/10.3389/fcell.2021.789427>.
- (49) Fire, A.; Xu, S.; Montgomery, M. K.; Kostas, S. A.; Driver, S. E.; Mello, C. C. Potent and Specific Genetic Interference by Double-Stranded RNA in *Caenorhabditis Elegans*. *Nature* **1998**, *391*, 806.
- (50) Zamore, P. D. RNA Interference: Big Applause for Silencing in Stockholm. *Cell* **2006**, *127* (6), 1083–1086. <https://doi.org/10.1016/j.cell.2006.12.001>.
- (51) Deng, Y.; Wang, C. C.; Choy, K. W.; Du, Q.; Chen, J.; Wang, Q.; Li, L.; Chung, T. K. H.; Tang, T. Therapeutic Potentials of Gene Silencing by RNA Interference:

- Principles, Challenges, and New Strategies. *Gene* **2014**, 538 (2), 217–227. <https://doi.org/10.1016/j.gene.2013.12.019>.
- (52) Bartel, D. P. MicroRNAs: Genomics, Biogenesis, Mechanism, and Function. *Cell* **2004**, 116, 281–297. <https://doi.org/10.1016/j.bios.2017.04.001>.
- (53) Wilson, R. C.; Doudna, J. A. Molecular Mechanisms of RNA Interference. *Annu. Rev. Biophys.* **2013**, 42 (1), 217–239. <https://doi.org/10.1146/annurev-biophys-083012-130404>.
- (54) Carthew, R. W.; Sontheimer, E. J. Origins and Mechanisms of MiRNAs and SiRNAs. *Cell* **2009**, 136 (4), 642–655. <https://doi.org/10.1016/j.cell.2009.01.035>.
- (55) Schirle, N. T.; MacRae, I. J. The Crystal Structure of Human Argonaute2. *Science (80-.)*. **2012**, 336 (6084), 1037–1040. <https://doi.org/10.1126/science.1221551>.
- (56) Schirle, N. T.; Sheu-Gruttadauria, J.; MacRae, I. J. Structural Basis for MicroRNA Targeting. *Science (80-.)*. **2014**, 346 (6209), 608–613. <https://doi.org/10.1126/science.1258040>.
- (57) Schirle, N. T.; Sheu-Gruttadauria, J.; Chandradoss, S. D.; Joo, C.; MacRae, I. J. Water-Mediated Recognition of T1-Adenosine Anchors Argonaute2 to MicroRNA Targets. *Elife* **2015**, 4 (September), 1–16. <https://doi.org/10.7554/eLife.07646>.
- (58) Lingel, A.; Simon, B.; Izaurrealde, E.; Sattler, M. Nucleic Acid 3'-End Recognition by the Argonaute2 PAZ Domain. *Nat. Struct. Mol. Biol.* **2004**, 11 (6), 576–577. <https://doi.org/10.1038/nsmb777>.
- (59) Frank, F.; Sonenberg, N.; Nagar, B. Structural Basis for 5'-Nucleotide Base-Specific Recognition of Guide RNA by Human AGO2. *Nature* **2010**, 465 (7299), 818–822. <https://doi.org/10.1038/nature09039>.
- (60) Song, J. J.; Smith, S. K.; Hannon, G. J.; Joshua-Tor, L. Crystal Structure of Argonaute and Its Implications for RISC Slicer Activity. *Science (80-.)*. **2004**, 305 (5689), 1434–1437. <https://doi.org/10.1126/science.1102514>.
- (61) Egli, M.; Manoharan, M. Re-Engineering RNA Molecules into Therapeutic Agents. *Acc. Chem. Res.* **2019**, 52 (4), 1036–1047. <https://doi.org/10.1021/acs.accounts.8b00650>.
- (62) Lima, W. F.; Prakash, T. P.; Murray, H. M.; Kinberger, G. A.; Li, W.; Chappell, A. E.; Li, C. S.; Murray, S. F.; Gaus, H.; Seth, P. P.; et al. Single-Stranded SiRNAs Activate RNAi in Animals. *Cell* **2012**, 150 (5), 883–894. <https://doi.org/10.1016/j.cell.2012.08.014>.
- (63) Prakash, T. P.; Lima, W. F.; Murray, H. M.; Li, W.; Kinberger, G. A.; Chappell, A. E.; Gaus, H.; Seth, P. P.; Bhat, B.; Crooke, S. T.; et al. Identification of Metabolically Stable 5'-Phosphate Analogs That Support Single-Stranded SiRNA Activity. *Nucleic Acids Res.* **2015**, 43 (6), 2993–3011. <https://doi.org/10.1093/nar/gkv162>.
- (64) Elkayam, E.; Parmar, R.; Brown, C. R.; Willoughby, J. L.; Theile, C. S.; Manoharan, M.; Joshua-Tor, L. SiRNA Carrying an (E)-Vinylphosphonate Moiety at the 5' End of the Guide Strand Augments Gene Silencing by Enhanced Binding to Human Argonaute-2. *Nucleic Acids Res.* **2017**, 45 (6), 3528–3536. <https://doi.org/10.1093/nar/gkw1171>.
- (65) Elkayam, E.; Kuhn, C. D.; Tocilj, A.; Haase, A. D.; Greene, E. M.; Hannon, G. J.; Joshua-Tor, L. The Structure of Human Argonaute-2 in Complex with MiR-20a.

- Cell* **2012**, *150* (1), 100–110. <https://doi.org/10.1016/j.cell.2012.05.017>.
- (66) Hu, B.; Zhong, L.; Weng, Y.; Peng, L.; Huang, Y.; Zhao, Y.; Liang, X. J. Therapeutic SiRNA: State of the Art. *Signal Transduct. Target. Ther.* **2020**, *5* (1). <https://doi.org/10.1038/s41392-020-0207-x>.
- (67) Khorev, O.; Stokmaier, D.; Schwardt, O.; Cutting, B.; Ernst, B. Trivalent, Gal/GalNAc-Containing Ligands Designed for the Asialoglycoprotein Receptor. *Bioorganic Med. Chem.* **2008**, *16* (9), 5216–5231. <https://doi.org/10.1016/j.bmc.2008.03.017>.
- (68) Balwani, M.; Sardh, E.; Ventura, P.; Peiró, P. A.; Rees, D. C.; Stölzel, U.; Bissell, D. M.; Bonkovsky, H. L.; Windyga, J.; Anderson, K. E.; et al. Phase 3 Trial of RNAi Therapeutic Givosiran for Acute Intermittent Porphyria. *N. Engl. J. Med.* **2020**, *382* (24), 2289–2301. <https://doi.org/10.1056/nejmoa1913147>.
- (69) Fitzgerald, K.; White, S.; Borodovsky, A.; Bettencourt, B. R.; Strahs, A.; Clausen, V.; Wijngaard, P.; Horton, J. D.; Taubel, J.; Brooks, A.; et al. A Highly Durable RNAi Therapeutic Inhibitor of PCSK9. *N. Engl. J. Med.* **2017**, *376* (1), 41–51. <https://doi.org/10.1056/nejmoa1609243>.
- (70) Pasi, K. J.; Rangarajan, S.; Georgiev, P.; Mant, T.; Creagh, M. D.; Lissitchkov, T.; Bevan, D.; Austin, S.; Hay, C. R.; Hegemann, I.; et al. Targeting of Antithrombin in Hemophilia A or B with RNAi Therapy. *N. Engl. J. Med.* **2017**, *377* (9), 819–828. <https://doi.org/10.1056/nejmoa1616569>.
- (71) Ibarra-Soza, J. M.; Morris, A. A.; Jayalath, P.; Peacock, H.; Conrad, W. E.; Donald, M. B.; Kurth, M. J.; Beal, P. A. 7-Substituted 8-Aza-7-Deazaadenosines for Modification of the SiRNA Major Groove. *Org. Biomol. Chem.* **2012**, *10* (32), 6491–6497. <https://doi.org/10.1039/c2ob25647a>.
- (72) Phelps, K. J.; Ibarra-soza, J. M.; Tran, K.; Fisher, A. J.; Beal, P. A. Click Modification of RNA at Adenosine: Structure and Reactivity of 7-Ethynyl- and 7-Triazolyl-8-Aza-7-Deazaadenosine in RNA. *ACS Chem. Biol.* **2014**, No. 9, 1780–1787.
- (73) Onizuka, K.; Harrison, J. G.; Ball-Jones, A. A.; Ibarra-Soza, J. M.; Zheng, Y.; Ly, D.; Lam, W.; Mac, S.; Tantillo, D. J.; Beal, P. A. Short Interfering RNA Guide Strand Modifiers from Computational Screening. *J. Am. Chem. Soc.* **2013**, *135* (45), 17069–17077. <https://doi.org/10.1021/ja4079754>.
- (74) Valenzuela, R. A. P.; Onizuka, K.; Ball-Jones, A. A.; Hu, T.; Suter, S. R.; Beal, P. A. Guide Strand 3'-End Modifications Regulate SiRNA Specificity. *ChemBioChem* **2016**, *17* (24), 2340–2345. <https://doi.org/10.1002/cbic.201600453>.
- (75) Peacock, H.; Fostvedt, E.; Beal, P. A. Minor-Groove-Modulating Adenosine Replacements Control Protein Binding and RNAi Activity in SiRNAs. *ACS Chem. Biol.* **2010**, *5* (12), 1115–1124. <https://doi.org/10.1021/cb100245u>.
- (76) Suter, S. R.; Sheu-Gruttadauria, J.; Schirle, N. T.; Valenzuela, R.; Ball-Jones, A. A.; Onizuka, K.; Macrae, I. J.; Beal, P. A. Structure-Guided Control of SiRNA Off-Target Effects. *J. Am. Chem. Soc.* **2016**, *138* (28), 8667–8669. <https://doi.org/10.1021/jacs.6b06137>.
- (77) Suter, S. R.; Ball-Jones, A.; Mumbleau, M. M.; Valenzuela, R.; Ibarra-Soza, J.; Owens, H.; Fisher, A. J.; Beal, P. A. Controlling MiRNA-like off-Target Effects of an SiRNA with Nucleobase Modifications. *Org. Biomol. Chem.* **2017**, *15* (47),

- 10029–10036. <https://doi.org/10.1039/c7ob02654d>.
- (78) Peacock, H.; Maydanovych, O.; Beal, P. A. N2-Modified 2-Aminopurine Ribonucleosides as Minor-Groove-Modulating Adenosine Replacements in Duplex RNA. *Org. Lett.* **2010**, *12* (5), 1044–1047. <https://doi.org/10.1021/ol100019r>.
- (79) Kannan, A.; Fostvedt, E.; Beal, P. A.; Burrows, C. J. 8-Oxoguanosine Switches Modulate the Activity of Alkylated SiRNAs by Controlling Steric Effects in the Major versus Minor Grooves. *J. Am. Chem. Soc.* **2011**, *133* (16), 6343–6351. <https://doi.org/10.1021/ja2003878>.
- (80) Ghanty, U.; Fostvedt, E.; Valenzuela, R.; Beal, P. A.; Burrows, C. J. Promiscuous 8-Alkoxyadenosines in the Guide Strand of an SiRNA: Modulation of Silencing Efficacy and off-Pathway Protein Binding. *J. Am. Chem. Soc.* **2012**, *134* (42), 17643–17652. <https://doi.org/10.1021/ja307102g>.
- (81) Rooij, E.; Kauppinen, S. Development of Micro RNA Therapeutics Is Coming of Age. *EMBO Mol. Med.* **2014**, *6* (7), 851–864. <https://doi.org/10.15252/emmm.201100899>.
- (82) Zhang, S.; Cheng, Z.; Wang, Y.; Han, T. The Risks of Mirna Therapeutics: In a Drug Target Perspective. *Drug Des. Devel. Ther.* **2021**, *15*, 721–733. <https://doi.org/10.2147/DDDT.S288859>.
- (83) Gallant-Behm, C. L.; Piper, J.; Dickinson, B. A.; Dalby, C. M.; Pestano, L. A.; Jackson, A. L. A Synthetic MicroRNA-92a Inhibitor (MRG-110) Accelerates Angiogenesis and Wound Healing in Diabetic and Nondiabetic Wounds. *Wound Repair Regen.* **2018**, *26* (4), 311–323. <https://doi.org/10.1111/wrr.12660>.
- (84) Seto, A. G.; Beatty, X.; Lynch, J. M.; Hermreck, M.; Tetzlaff, M.; Duvic, M.; Jackson, A. L. Cobomarsen, an Oligonucleotide Inhibitor of MiR-155, Coordinately Regulates Multiple Survival Pathways to Reduce Cellular Proliferation and Survival in Cutaneous T-Cell Lymphoma. *Br. J. Haematol.* **2018**, *183* (3), 428–444. <https://doi.org/10.1111/bjh.15547>.
- (85) Schmidt, M. F. RNA Interference in Drug Development. In *Chemical Biology: and Drug Discovery*; Springer Berlin Heidelberg: Berlin, Heidelberg, 2022; pp 81–87. https://doi.org/10.1007/978-3-662-64412-6_9.
- (86) Lee, E. C.; Valencia, T.; Allerson, C.; Schairer, A.; Flaten, A.; Yheskel, M.; Kersjes, K.; Li, J.; Gatto, S.; Takhar, M.; et al. Discovery and Preclinical Evaluation of Anti-MiR-17 Oligonucleotide RGLS4326 for the Treatment of Polycystic Kidney Disease. *Nat. Commun.* **2019**, *10* (1), 1–14. <https://doi.org/10.1038/s41467-019-11918-y>.
- (87) Gallant-Behm, C. L.; Piper, J.; Lynch, J. M.; Seto, A. G.; Hong, S. J.; Mustoe, T. A.; Maari, C.; Pestano, L. A.; Dalby, C. M.; Jackson, A. L.; et al. A MicroRNA-29 Mimic (Replarsen) Represses Extracellular Matrix Expression and Fibroplasia in the Skin. *J. Invest. Dermatol.* **2019**, *139* (5), 1073–1081. <https://doi.org/10.1016/j.jid.2018.11.007>.
- (88) Montgomery, R. L.; Yu, G.; Latimer, P. A.; Stack, C.; Robinson, K.; Dalby, C. M.; Kaminski, N.; Rooij, E. Micro RNA Mimicry Blocks Pulmonary Fibrosis. *EMBO Mol. Med.* **2014**, *6* (10), 1347–1356. <https://doi.org/10.15252/emmm.201303604>.
- (89) Wang, P.; Zhou, Y.; Richards, A. M. Effective Tools for RNA-Derived Therapeutics: SiRNA Interference or MiRNA Mimicry. *Theranostics* **2021**, *11*

- (18), 8771–8796. <https://doi.org/10.7150/thno.62642>.
- (90) Peacock, H.; Fucini, R. V.; Jayalath, P.; Ibarra-Soza, J. M.; Haringsma, H. J.; Flanagan, W. M.; Willingham, A.; Beal, P. A. Nucleobase and Ribose Modifications Control Immunostimulation by a MicroRNA-122-Mimetic RNA. *J. Am. Chem. Soc.* **2011**, *133* (24), 9200–9203. <https://doi.org/10.1021/ja202492e>.
- (91) Lennox, K. A.; Owczarzy, R.; Thomas, D. M.; Walder, J. A.; Behlke, M. A. Improved Performance of Anti-MiRNA Oligonucleotides Using a Novel Non-Nucleotide Modifier. *Mol. Ther. - Nucleic Acids* **2013**, *2* (AUG), e117. <https://doi.org/10.1038/mtna.2013.46>.
- (92) Ariyoshi, J.; Momokawa, D.; Eimori, N.; Kobori, A.; Murakami, A.; Yamayoshi, A. Development of Novel Antisense Oligonucleotides for the Functional Regulation of RNA-Induced Silencing Complex (RISC) by Promoting the Release of MicroRNA from RISC. *Bioconjug. Chem.* **2015**, *26* (12), 2454–2460. <https://doi.org/10.1021/acs.bioconjchem.5b00501>.
- (93) Gubu, A.; Su, W.; Zhao, X.; Zhang, X.; Fan, X.; Wang, J.; Wang, Q.; Tang, X. Circular Antisense Oligonucleotides for Specific RNase-H-Mediated MicroRNA Inhibition with Reduced Off-Target Effects and Nonspecific Immunostimulation. *J. Med. Chem.* **2021**, *64* (21), 16046–16055. <https://doi.org/10.1021/acs.jmedchem.1c01421>.
- (94) Gott, J. M.; Emeson, R. B. Functions and Mechanisms of RNA Editing. *Annu. Rev. Genet.* **2000**, *34*, 499–531.
- (95) Nishikura, K. Functions and Regulation of RNA Editing by ADAR Deaminases. *Annu. Rev. Biochem.* **2010**, *79*, 321–349. <https://doi.org/10.1146/annurev-biochem-060208-105251>.
- (96) George, C. X.; Samuel, C. E. Human RNA-Specific Adenosine Deaminase ADAR1 Transcripts Possess Alternative Exon 1 Structures That Initiate from Different Promoters, One Constitutively Active and the Other Interferon Inducible. *Proc. Natl. Acad. Sci. U. S. A.* **1999**, *96* (8), 4621–4626. <https://doi.org/10.1073/pnas.96.8.4621>.
- (97) Chen, C. X.; Cho, D. S. C.; Wang, Q.; Lai, F.; Carter, K. C.; Nishikura, K. A Third Member of the RNA-Specific Adenosine Deaminase Gene Family, ADAR3, Contains Both Single- and Double-Stranded RNA Binding Domains. *RNA* **2000**, *6* (5), 755–767. <https://doi.org/10.1017/S1355838200000170>.
- (98) Haudenschild, B. L.; Maydanovych, O.; Véliz, E. A.; Macbeth, M. R.; Bass, B. L.; Beal, P. A. A Transition State Analogue for an RNA-Editing Reaction. *J. Am. Chem. Soc.* **2004**, *126* (36), 11213–11219. <https://doi.org/10.1021/ja0472073>.
- (99) Christofi, T.; Zaravinos, A. RNA Editing in the Forefront of Epitranscriptomics and Human Health. *J. Transl. Med.* **2019**, *17* (1), 1–15. <https://doi.org/10.1186/s12967-019-2071-4>.
- (100) Rueter, S. M.; Dawson, T. R.; Emeson, R. B. Regulation of Alternative Splicing by RNA Editing. *Nature* **1999**, *399* (6731), 75–80. <https://doi.org/10.1038/19992>.
- (101) Wang, I. X.; So, E.; Devlin, J. L.; Zhao, Y.; Wu, M.; Cheung, V. G. ADAR Regulates RNA Editing, Transcript Stability, and Gene Expression. *Cell Rep.* **2013**, *5* (3), 849–860. <https://doi.org/10.1016/j.celrep.2013.10.002>.
- (102) Bhate, A.; Sun, T.; Li, J. B. ADAR1: A New Target for Immuno-Oncology Therapy. *Mol. Cell* **2019**, *73* (5), 866–868.

- <https://doi.org/10.1016/j.molcel.2019.02.021>.
- (103) Ishizuka, J. J.; Manguso, R. T.; Cheruiyot, C. K.; Bi, K.; Panda, A.; Iracheta-Vellve, A.; Miller, B. C.; Du, P. P.; Yates, K. B.; Dubrot, J.; et al. Loss of ADAR1 in Tumours Overcomes Resistance to Immune Checkpoint Blockade. *Nature* **2019**, *565* (7737), 43–48. <https://doi.org/10.1038/s41586-018-0768-9>.
- (104) Eisenberg, E.; Levanon, E. Y. A-to-I RNA Editing - Immune Protector and Transcriptome Diversifier. *Nat. Rev. Genet.* **2018**, *19* (8), 473–490. <https://doi.org/10.1038/s41576-018-0006-1>.
- (105) Nishikura, K. Editor Meets Silencer: Crosstalk between RNA Editing and RNA Interference. *Nat. Rev. Mol. Cell Biol.* **2006**, *7* (12), 919–931. <https://doi.org/10.1038/nrm2061>.
- (106) Merkle, T.; Merz, S.; Reautschnig, P.; Blaha, A.; Li, Q.; Vogel, P.; Wettengel, J.; Li, J. B.; Stafforst, T. Precise RNA Editing by Recruiting Endogenous ADARs with Antisense Oligonucleotides. *Nat. Biotechnol.* **2019**, *37* (2), 133–138. <https://doi.org/10.1038/s41587-019-0013-6>.
- (107) Qu, L.; Yi, Z.; Zhu, S.; Wang, C.; Cao, Z.; Zhou, Z.; Yuan, P.; Yu, Y.; Tian, F.; Liu, Z.; et al. Programmable RNA Editing by Recruiting Endogenous ADAR Using Engineered RNAs. *Nat. Biotechnol.* **2019**, *37* (9), 1059–1069. <https://doi.org/10.1038/s41587-019-0178-z>.
- (108) Monteleone, L. R.; Matthews, M. M.; Palumbo, C. M.; Thomas, J. M.; Zheng, Y.; Chiang, Y.; Fisher, A. J.; Beal, P. A. A Bump-Hole Approach for Directed RNA Editing. *Cell Chem. Biol.* **2019**, *26* (2), 269–277.e5. <https://doi.org/10.1016/j.chembiol.2018.10.025>.
- (109) Doherty, E. E.; Wilcox, X. E.; Van Sint Fiet, L.; Kemmel, C.; Turunen, J. J.; Klein, B.; Tantillo, D. J.; Fisher, A. J.; Beal, P. A. Rational Design of RNA Editing Guide Strands: Cytidine Analogs at the Orphan Position. *J. Am. Chem. Soc.* **2021**, *143* (18), 6865–6876. <https://doi.org/10.1021/jacs.0c13319>.
- (110) Chen, G.; Katrekar, D.; Mali, P. RNA-Guided Adenosine Deaminases: Advances and Challenges for Therapeutic RNA Editing. *Biochemistry* **2019**, *58* (15), 1947–1957. <https://doi.org/10.1021/acs.biochem.9b00046>.
- (111) Matthews, M. M.; Thomas, J. M.; Zheng, Y.; Tran, K.; Phelps, K. J.; Scott, A. I.; Havel, J.; Fisher, A. J.; Beal, P. A. Structures of Human ADAR2 Bound to DsRNA Reveal Base-Flipping Mechanism and Basis for Site Selectivity. *Nat. Struct. Mol. Biol.* **2016**, *23* (5), 426–433. <https://doi.org/10.1038/nsmb.3203>.
- (112) Thuy-Boun, A. S.; Thomas, J. M.; Grajo, H. L.; Palumbo, C. M.; Park, S.; Nguyen, L. T.; Fisher, A. J.; Beal, P. A. Asymmetric Dimerization of Adenosine Deaminase Acting on RNA Facilitates Substrate Recognition. *Nucleic Acids Res.* **2020**, *48* (14), 7958–7972. <https://doi.org/10.1093/nar/gkaa532>.
- (113) Park, S. H.; Doherty, E. E.; Xie, Y.; Padyana, A. K.; Fang, F.; Zhang, Y.; Karki, A.; Lebrilla, C. B.; Siegel, J. B.; Beal, P. A. High-Throughput Mutagenesis Reveals Unique Structural Features of Human ADAR1. *Nat. Commun.* **2020**, *11* (1), 1–13. <https://doi.org/10.1038/s41467-020-18862-2>.

Chapter 2

Identification of a precursor anti-microRNA for computationally-screened 3'-end chemical modifications and potency screening in cellular based assays

2.1 Introduction

MicroRNAs (miRNAs) are short, ~22 nucleotide (nt) endogenous RNA molecules that control gene regulation at the post-transcriptional level via the RNA interference (RNAi) pathway.¹ MiRNAs are transcribed from the genome to form primary miRNA (pri-miRNA), usually kilobases in length, which are then processed by the Drosha/DGCR8 complex into ~70 nt pre-miRNAs.² Pre-miRNA molecules are exported from the nucleus into the cytoplasm by Exportin-5 and are cleaved into a mature miRNA duplex where one strand of the duplex serves as a guide strand and the other a passenger strand.^{3,4} The mature miRNA duplex is loaded into endonuclease Ago2 and promotes passenger strand release from the guide strand.⁵ The guide miRNA-Ago2 complex, also known as the RNA-induced silencing complex (RISC), can then target mRNA transcripts at the 3'-untranslated region (3'-UTR) by base pairing with the guide miRNA seed region (nt 2-8), causing translational repression and mRNA degradation.⁶

Aberrant expression of miRNA is strongly correlated with a variety of diseases, including cancer, thus promoting incentives to generate miRNA-based therapeutics.⁷ Antisense oligonucleotides targeting microRNAs (anti-microRNAs or anti-miRs) have been shown to elicit therapeutic effects by hybridizing and inhibiting upregulated disease-associated miRNAs.⁸ To date, chemical modifications of anti-miRs have been primarily focused on the sugar-phosphate backbone to improve nuclease resistance and binding affinity towards a miRNA target.⁹ Additionally, there are other reported modification strategies to improve anti-miR potency, including ZEN modifiers, crosslinked anti-miR

duplexes, circularization, and peptide conjugation.^{10–13} No anti-miR-based therapeutics have yet reached FDA-approval, but some designs are currently in clinical trials in hopes of achieving this goal.^{14,15}

The active fraction of miRNA is that associated with an Argonaute protein; therefore, a potentially valuable approach to anti-miR modification is through a structure-guided approach where a chemically modified anti-miR binds to the miRNA-Ago2 complex and improves potency and selectivity. The crystal structure of human Argonaute2 (hAgo2) was solved in 2012 which expanded our understanding about the molecular mechanisms underlying miRNA targeting (**Figure 2.1A**).^{16,17} An intriguing structural feature of the guide-target-hAgo2 ternary complex is a small solvated pocket between the L2 and MID domains that has binding specificity towards an adenosine nucleotide at position 1 of a target RNA strand, also known as the t1A-binding pocket (**Figure 2.1B**). Anti-miRs can bind to miRNAs in a similar manner to target RNAs, thus the t1 nucleotide corresponds to the 3'-end of a typical anti-miR. The specificity for adenosine in the t1A pocket is likely due to hydrogen bonding interactions with the neighboring Ser561 residue and an ordered network of water molecules within the pocket (**Figure 2.1B**). Crystallographic, *in vitro* binding, and FRET assays confirmed the binding specificity of adenosine over other canonical or modified bases.¹⁸

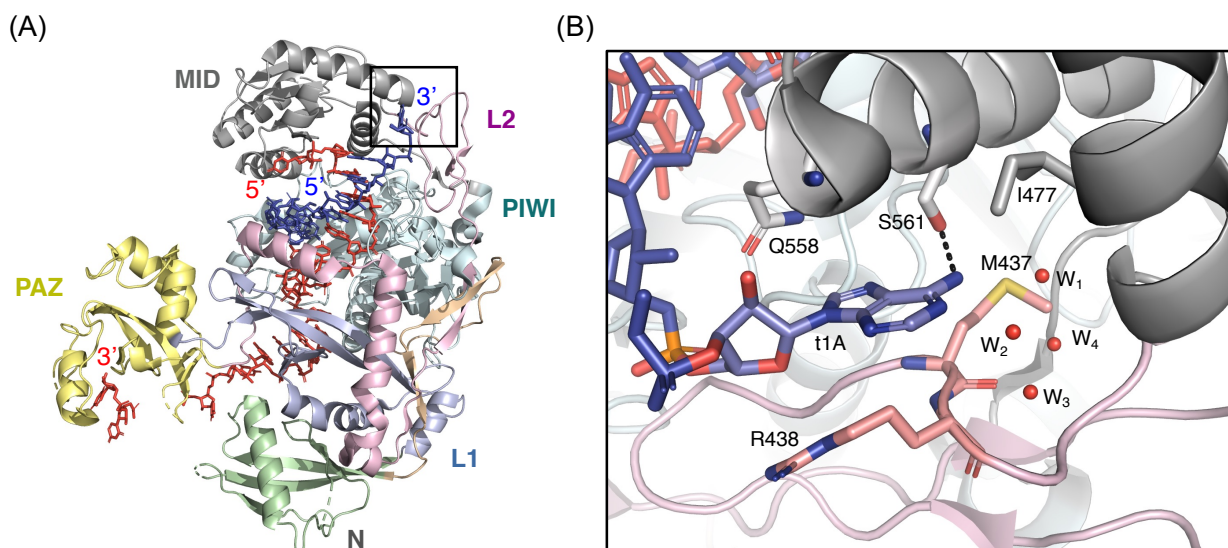


Figure 2.1 The t1-adenosine (t1A) nucleotide-binding pocket in human Argonaute2 (hAgo2). (A) The crystal structure of hAgo2 with bound guide (red) and target (blue) RNA duplex.¹⁸ The t1A-binding pocket is encased in a black box. (B) Close up of the t1A-binding pocket. Four ordered water molecules within the pocket are labeled as “W#”. A hydrogen bonding interaction between the Ser561 residue and the N6 exocyclic amine of t1A is shown with black dashed lines.

We previously used the hAgo2 crystal structure to design and computationally screen chemical modifications on the 5'-end of an siRNA guide strand using copper(I)-catalyzed azide/alkyne cycloaddition (CuAAC) chemistry to improve gene-silencing potency and reduce miRNA-like off targeting effects.¹⁹ Herein, we used this strategy to modify the 3'-end of anti-miRs that could potentially bind to a miRNA-loaded hAgo2 complex and improve interactions within the t1A-binding pocket, thus improve potency and selectivity.²⁰ This chapter describes the early to middle stages of this study, including the establishment of a cellular based anti-miR potency screening assay, computational screening of 1'-triazole-modified nucleotides docked into the t1A-pocket hAgo2 receptor, and identification of an alkynyl-precursor anti-miR for triazole modifications.

2.2 Methods

2.2.1 MiR-21 reporter plasmid generation

The miR-21 reporter plasmid was generated by inserting the miR-21 (5'-TCAACATCAGTCTGATAAGCTA-3') target sequence into the 3'-untranslated region (3'-UTR) of the renilla luciferase gene (*hRluc*) in dual luciferase reporter plasmid psiCHECK-2 (Promega). Forward and reverse primers containing the miR-21 sequence (**Table S2**) was amplified with psiCHECK-2 template using the Phusion Hot Start II DNA Polymerase kit (Thermo Scientific) to generate PCR product with overlapping regions for Gibson assembly. The PCR product was combined with Gibson Assembly Master Mix (New England Biolabs) and incubated at 50 °C for 15 minutes then transformed into XL10-Gold® Ultracompetent Cells (Agilent Technologies) according to the manufacturer's instructions. XL10-Gold cells harboring miR-21 reporter plasmid was inoculated in 100 µg/mL ampicillin-containing LB media for antibiotic resistance selection. Finally, miR-21 plasmid was harvested from XL10-Gold cells using the PureYield™ Plasmid Miniprep System (Promega) and Sanger sequenced by the UC DNA Sequencing Facility at UC Davis for sequence verification.

2.2.2 Cell culture

HeLa (ATCC CCL-2) cells were cultured in Dulbecco's modified Eagle medium (DMEM, Gibco 11995065) supplemented with 10% fetal bovine serum (FBS, Gibco) and 100X antibiotic-antimycotic solution (Anti-Anti, Gibco 15240062) to a final concentration of 10% and 1X, respectively, at 37 °C + 5% CO₂. All cells were passaged regularly to maintain exponential growth and routinely checked for mycoplasma contamination using a Universal Mycoplasma Detection Kit (ATCC, 30-1012K).

2.2.3 Transfection and dual luciferase assay

HeLa were plated onto a 96-well plate at 1×10^4 cells per well in DMEM supplemented with 10% FBS and 1X Anti-Anti solution 24 h before transfection. The following day, the cells were co-transfected in triplicate with varying concentrations of anti-miR oligonucleotide and 100 ng of miR-21 reporter plasmid using Lipofectamine 2000 (Invitrogen) according to the manufacturer's instructions in 100 μ L reduced serum media (OPTI-MEM, Gibco) per well. After 6 h incubation post-transfection, the reduced serum media was replaced with DMEM supplemented with 10% FBS. After an additional 18 h post-transfection, 24 h total, the cells were lysed and luciferase luminescent counts were measured using the Dual Luciferase Assay System (Promega). The transfected cells were washed with phosphate buffer saline (PBS, Gibco) followed by addition of 20 μ L 1X Passive Lysis Buffer (Promega) and gentle shaking on an orbital shaker for 15 minutes. Next, 100 μ L of luciferase assay reagent II (LARII, Promega) was added to each well of lysed cells to measure firefly luciferase luminescent counts on a CLARIOstar Plus microplate reader (BMG Labtech). Stop & Glo Reagent (100 μ L) (S&G, Promega) was subsequently added to quench firefly luciferase activity and measure renilla luciferase luminescent counts. For each luminescent count reading, there is a 2 s pre-measurement delay, followed by a 10 s measurement period. Finally, the renilla luciferase luminescent counts were normalized against firefly luciferase luminescent counts and plotted as a fold change in the ratio of Renilla/Firefly (RL/FF) counts relative to cells transfected with reporter plasmid, but without anti-miR oligonucleotide as a control.

2.2.4 Oligonucleotide synthesis and purification

Unless noted, all anti-miR21 oligonucleotides were ordered through the DNA/Peptide Core Research Facility at University of Utah (Salt Lake City, Utah, USA), Dharmacon (Lafayette, CO, USA), or TriLink BioTechnologies (San Diego, CA, USA). The 15mer anti-miR21 oligonucleotide with t1 nucleotide as 1'-ethynyl-2'-deoxyribose and C3 spacer (1-EdR C3) was synthesized in the laboratory using an Applied Biosystems (ABI) 394 DNA/RNA Synthesizer. Phosphoramidite, controlled pore glass (CPG), and ancillary reagents for the ABI synthesizer were purchased from Glen Research. After synthesis, the 15mer 1-EdR C3 anti-miR21 oligonucleotide on CPG support was removed from the synthesizer and dried overnight at high vacuum. The following day, the oligonucleotide was cleaved from 3'-Spacer C3 CPG using a 2:1 volume ratio of 30% NH₄OH:EtOH at room temperature overnight. The cleaved oligonucleotide solution was transferred away from CPG and concentrated to dryness using a SpeedVac concentrator, then resuspended in nuclease free water and desalted using an Illustra™ Nap™-10 Sephadex™ G-25 column (Cytiva 17085401). Next, the oligonucleotide was electrophoresed in a 19% polyacrylamide gel and visualized by UV shadowing, followed by excision from the gel and purification by crushing and soaking overnight at 4 °C in buffer containing 0.5 M NH₄OAc and 0.1 mM EDTA. Finally, the oligonucleotide was filtered using 0.22 µm cellulose acetate membrane filter (Costar® Spin-X® Centrifuge Tube Filter, Corning 8160) and ethanol precipitated or purified using silica-based octadecyl bonded phase SepPak C18 columns (Waters) in 1:1 acetonitrile:water elution. All oligonucleotides described in this chapter were characterized by MALDI-TOF mass

spectrometric analysis. Observed MALDI-TOF masses (m/z) for the oligonucleotides are provided in **Table 2.2.6**.

2.2.5 Computational screening of triazole-modified nucleotides docked into the t1A-binding pocket of hAgo2

T1-triazole modified nucleotides were docked into the t1A-binding pocket of hAgo2 using OpenEye Suite Scientific Software (New Mexico, USA).^{19,21} The general procedure for docking is as follows:

1) **Library generation:** A library of 190 3',5'-bisphosphate 2'-deoxyribose ligands with a triazole moiety at the 1' position were drawn using ChemDraw (PerkinElmer) then converted into SMILES (simplified molecular-input line-entry system) format. SMILES were uploaded onto VIDA to generate molecular models of the ligands. The triazoles designed were from a variety of azides that were commercially available through Sigma Aldrich or Enamine LLC for convenient and rapid potency screening in the laboratory once triazole-modified anti-miRs were generated. Potency screening results from triazole-modified anti-miRs are described in Chapter 3.

2) **Conformer generation:** Conformers of the triazole ligands were generated using OMEGA. A maximum of 5,000 conformers per ligand were applied to allow a wide selection of conformers for each ligand to be docked into the receptor.

3) **Receptor generation:** The t1A-binding pocket of hAgo2 receptor was generated using the MakeReceptor program from OpenEye. Using the published crystal structure of hAgo2 with bound guide and target RNA (4W5O)¹⁷, an approximate 5,000 Å³ box was encased around the t1A-binding pocket to create heavy atom contours.

Constraints were applied to the reference t1-adenosine ligand (**Figure 2.6**) to force the triazole 3',5'-bisphosphate ligand to be positioned in the pocket.

4) **Fast rigid exhaustive docking (FRED)**: Once the conformers of the triazole ligands and t1A-binding pocket receptor were made, all conformers of the triazoles were docked into the binding pocket using Fast Rigid Exhaustive Docking (FRED), available in OpenEye. The conformers were computationally scored by ChemGauss4 when docked into the receptor based on shape complementarity from ligand to receptor, hydrogen bonding between ligand and protein, and hydrogen bonding interactions with implicit solvent. A more negative score indicated a more favorable docking score. Each ligand had 25 poses assigned in the docking run.

5) **Analysis of FRED poses and scoring**: The docked poses were sorted from lowest (more favorable) to highest (least favorable) ChemGauss4 score and 17 triazoles from the top ~50 scoring ligands were chosen to determine their activity via the dual luciferase assay (described in Chapter 3), based on availability of the azides and how consistent the 25 poses from each ligand were oriented towards the t1A-binding pocket receptor and overlapped with the t1-adenosine reference ligand.

2.2.6 Table of mass spectra for anti-miR21 oligonucleotides

Bold = locked nucleic acid (LNA)

Underlined = 2'-O-methyl

d = 2'-deoxyribose

DAP = 2,6-diaminopurine

1-EdR = 1'-ethynyl-2'-deoxyribose

C3 = C3 spacer

Oligonucleotide ID	Sequence (5'-3')	Calculated Mass (m/z)	Observed Mass [M-H] ⁻ (m/z)
Anti-miR21 9mer LNA	GATAAGCTA	3013.0	3013.4
Anti-miR21 9mer 2'-OMe	<u>GAUAAGCUA</u>	2989.0	2989.9
Anti-miR21 9mer 2'-OMe/LNA	<u>GAUAAGCTA</u>	2995.0	2994.3
Anti-miR21 15mer 2'-OMe	<u>CAGUCUGAUAAGCUA</u>	4970.3	4969.6
Anti-miR21 22mer 2'-OMe	<u>UCAACAUCAGUCUGAUAAGCUA</u>	7276.8	7279.6
Anti-miR21 15mer dA	<u>CAGUCUGAUAAGCU</u> dA	4940.3	4940.1
Anti-miR21 15mer dUdA	<u>CAGUCUGAUAAGC</u> dUdA	4910.3	4909.9
Anti-miR21 15mer dDAP	<u>CAGUCUGAUAAGCU</u> dDAP	4955.3	4955.0
Anti-miR21 15mer dG	<u>CAGUCUGAUAAGCU</u> dG	4956.3	4956.2
Anti-miR21 15mer dA C3	<u>CAGUCUGAUAAGCU</u> dA(C3)	5078.4	5084.6
Anti-miR21 1-EdR C3	<u>CAGUCUGAUAAGCU</u> (1-EdR)(C3)	4980.9	4979.9

2.3 Results

2.3.1 MiR-21 dual luciferase reporter system for anti-miR potency studies in cells

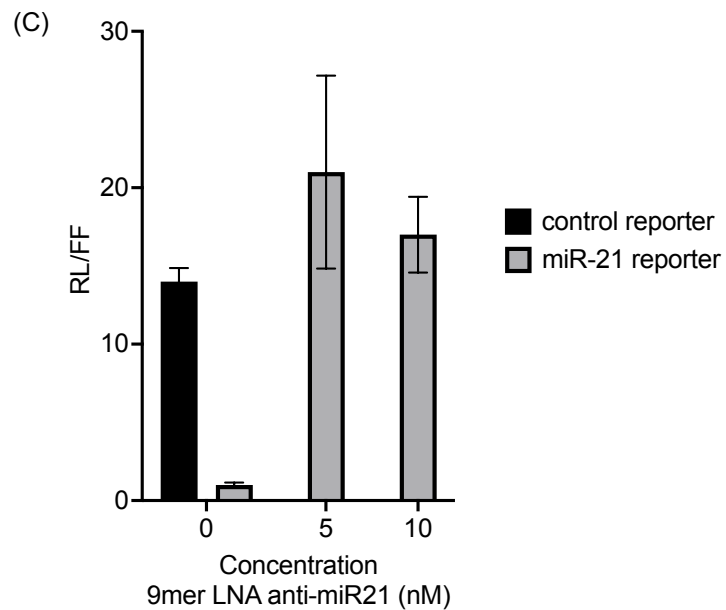
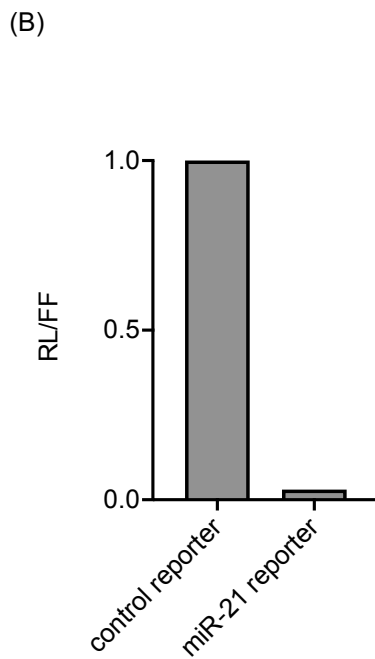
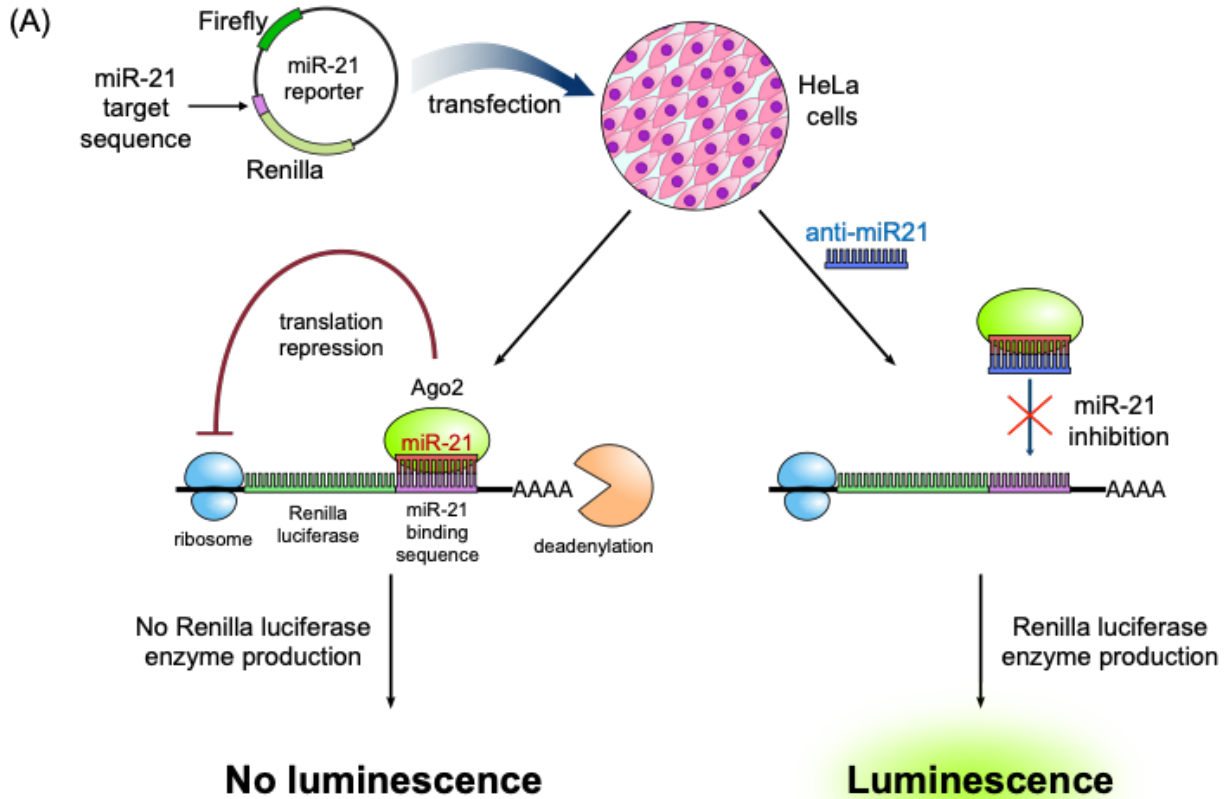


Figure 2.2 Anti-miR potency screening using miR-21 dual luciferase reporter assay in HeLa cells. (A) Basic diagram of miR-21 reporter dual luciferase reporter assay. HeLa cells transfected with a miR-21 dual luciferase reporter plasmid can be recognized by endogenous miR-21 and perform RNAi silencing of Renilla luciferase transcripts, therefore lowering luminescence detection. However, if an anti-miR21 is co-transfected with the miR-21 reporter plasmid, miR-21 can be inhibited and Renilla luciferase production is restored, resulting in higher luminescent counts. (B) Validated knockdown of Renilla luciferase expression from miR-21 reporter plasmid transfected in HeLa cells compared to control plasmid. RL/FF = Renilla/firefly luciferase activity ratio. RL/FF from miR-21 reporter bar plot was normalized to control reporter RL/FF. (C) Potency of fully locked nucleic acid- (LNA) modified 9mer anti-miR21 oligonucleotide at 5 and 10 nM in HeLa cells co-transfected with miR-21 reporter plasmid. Error represents the standard error of the mean (s.e.m.) from three dual luciferase assay replicates.

MiR-21, an abundant miRNA in HeLa cells, was chosen to evaluate the potency of anti-miR modifications using a previously reported dual luciferase assay.^{22,23} In this assay, Renilla luciferase protein expression is under the control of miR-21 since the miR-21 target sequence has been inserted into the 3'-UTR of the Renilla transcript. Functional anti-miRs can therefore inhibit miR-21 activity and increase Renilla luciferase signal (**Figure 2.2A**).

To start, the miR-21 reporter plasmid was generated in the lab and transfected into HeLa cells. When compared against control reporter plasmid that contains a control sequence in the 3'-UTR of Renilla luciferase, there is a substantial reduction of Renilla/firefly (RL/FF) ratio from miR-21 reporter plasmid-transfected cells, thus confirming miR-21 target sequence recognition by endogenous miR-21 and knockdown of Renilla luciferase expression (**Figure 2.2B**). Next, a fully LNA-modified 9mer anti-miR21 with a complementary sequence to the seed region of miR-21 and a 3'-end nucleotide adenosine base was used as a positive control for anti-miR activity.²³ At 5 and 10 nM, the LNA 9mer anti-miR21 resulted in nearly 20-fold higher activity over samples that do not contain anti-miR (**Figure 2.2C**), indicating activity and successful transfection of anti-miR into cells.

2.3.2 Potency screening of 2'-O-methylated 9mer anti-miR21

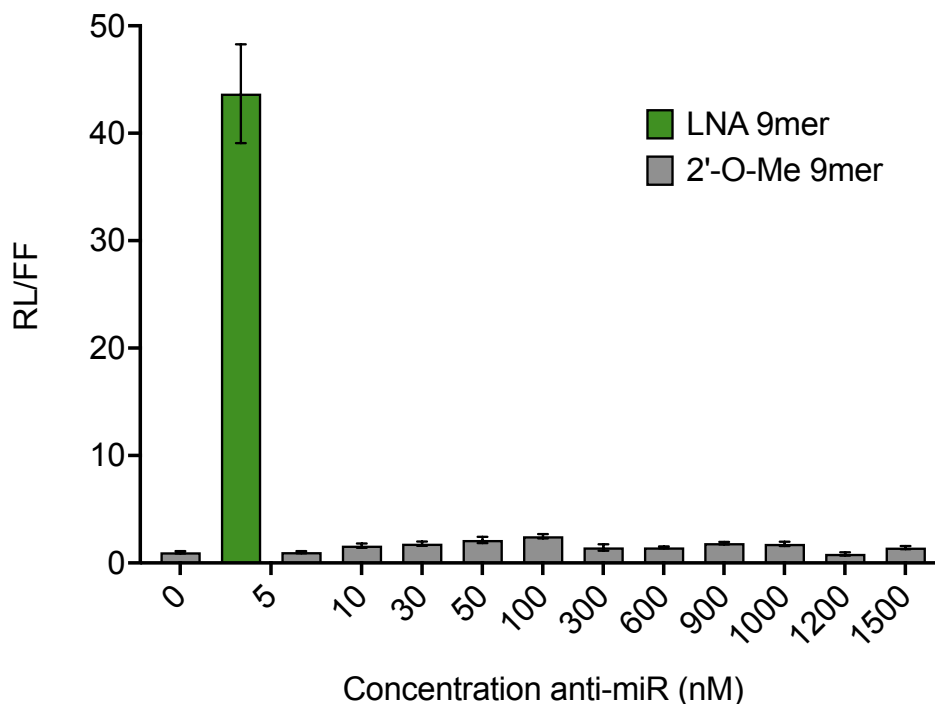


Figure 2.39 Potency profile of 2'-O-methylated 9mer anti-miR21 in HeLa cells. Error bars represent the s.e.m from three dual luciferase assay replicates.

Improvement of anti-miR activity by chemical modification at the t1 nucleotide may not be as easily detectable when the 9mer anti-miR21 is substantially potent from LNA modifications. Furthermore, too high of binding affinity by LNA modification can lead to off-targeting binding to other miRNA targets.²⁴ Therefore, the potency of 2'-O-methylated (2'-OMe) 9mer anti-miR21 was evaluated. From a wide concentration range of 5 to 1500 nM, the 2'-OMe 9mer anti-miR21 showed only minor improvements of anti-miR activity over no anti-miR control samples (**Figure 2.3**). At micromolar concentrations, there are potential cytotoxic effects occurring, as seen by slightly lower anti-miR activity at 1200 nM (**Figure 2.2**).

2.3.3 Potency screening of 2'-O-methylated anti-miR21 at varying sequence lengths

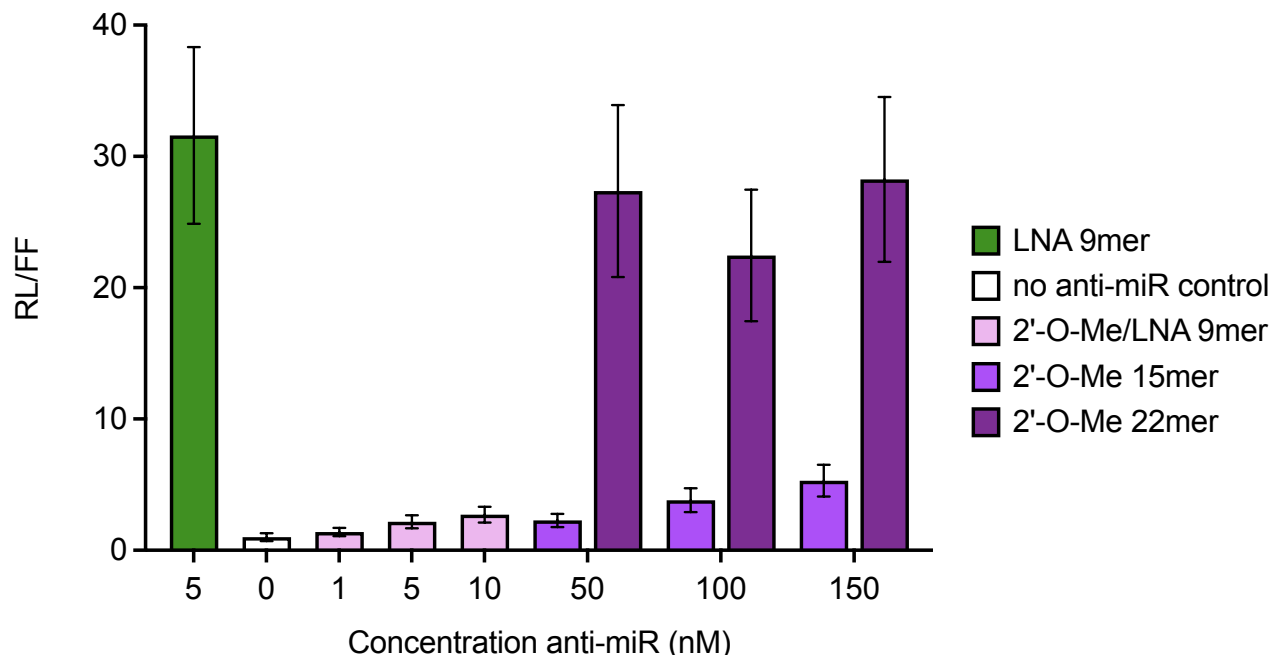


Figure 2.4 Potency profile of anti-miR21 at varying lengths. Error bars represent the s.e.m. from three dual luciferase assay replicates.

Next, potencies of anti-miR21 at varying sequence lengths were determined to improve activity over 2'-OMe 9mer anti-miR21. Reports indicate that increasing the length of chemically-modified anti-miRs with sequences that are complementary to more bases than the seed region of a miRNA guide strand can result in an increase in activity, particularly at 15 or 21 nt with full complementarity.^{25,26} Indeed, transfecting 50 to 150 nM of 2'-OMe 15mer anti-miR21 resulted in a modest ~2.5- to 5-fold increase in activity over no anti-miR control. On the other hand, a 2'-OMe 22mer anti-miR21 that is fully complementary to a mature miR-21 guide strand dramatically increased activity by 20- to 30-fold, which was comparable to the fully LNA 9mer (**Figure 2.4**). On top of this, a 9mer

2'-OMe/LNA mixmer anti-miR21 was tested and showed an improvement in activity at low, 1 to 10 nM concentrations (**Figure 2.4**).

Although the activity of the 22mer anti-miR21 was markedly high, we hypothesized that this design would, similar to the LNA-modified 9mer anti-miR21, likely encounter difficulties of detecting improvements in activity upon t1 nucleotide modifications. In addition, the full complementary nature of the 22mer would potentially promote guide miRNA strand release from hAgo2, thus removing the desired interactions between the t1 anti-miR nucleotide and the t1A-binding pocket of hAgo2.^{26,27} The 9mer 2'-OMe/LNA anti-miR21 had sufficient activity at low concentrations, but avoiding any potential off-target binding due to high affinity LNA-modifications was desired. Thus, we pursued further studies using the 2'-O-methylated 15mer sequence.

2.3.4 Potency screening of 15mer anti-miR21 with 3'-end nucleotide substitutions

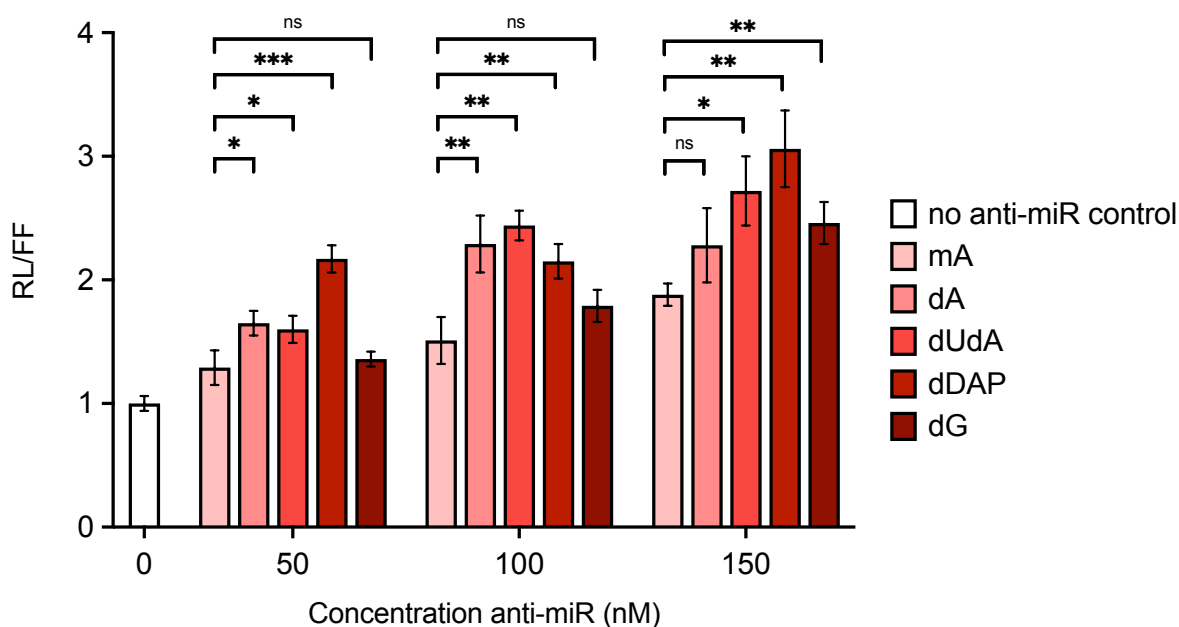


Figure 2.5 Potency profile of 15mer anti-miR21 with nucleobase substitutions or modifications at the 3'-end. Statistical significance between groups was determined using an

unpaired, one-tailed *t*-test with Welch's correction: **P* ≤ 0.05; ***P* ≤ 0.01; ****P* ≤ 0.001; ns = not significant. Error bars represent the standard error of the mean (s.e.m.) from three dual luciferase assay replicates.

Nucleobase or sugar substitutions at the 3'-end nucleotides t1 and t2 were employed on 2'-OMe 15mer anti-miR21 to screen for any relative changes in activity compared to t1 nucleotide as 2'-OMe adenosine (mA). The goal from this experiment was to verify if potencies derived from the cell-based luciferase assay could have a relative correlation in binding affinities of t1 nucleobase-substituted target RNAs towards the hAgo2 t1A-pocket, as determined by Schirle and colleagues.¹⁸ Additionally, analyzing the hAgo2 crystal structure with bound guide-target RNA duplex revealed a 2'-endo ribose sugar conformation at both the t1 and t2 nucleotides, indicating that 2'-deoxyribose nucleotides could potentially be tolerated at these positions on anti-miRs and allow convenient incorporation of nucleobase-modified 2'-deoxyribose phosphoramidite monomers by solid phase oligonucleotide synthesis. Thus, t1 2'-deoxyriboses containing adenosine (dA), 2,6-diaminopurine (dDAP), and guanosine (dG) were incorporated onto 15mer anti-miR21s and potencies were evaluated at 50 to 150 nM. A 15mer anti-miR21 with t1 and t2 as 2'-deoxyuridine and 2'-deoxyadenosine (dUdA), respectively, was also tested.

On average, all t1 2'-deoxyribose nucleotide-substituted anti-miR21, except for dG, performed better than anti-miR21 with t1 as mA, suggesting that the 2'-deoxyribose substitution at the t1 nucleotide is tolerated in the dual luciferase assay (**Figure 2.5**). Furthermore, 2'-deoxyribose substitution at the t2 nucleotide is also tolerated, as shown by the increase in activity by dUdA anti-miR21 relative to mA. Substituting adenosine at t1 with 2,6-diaminopurine (dDAP) generally resulted in the highest fold increase of activity

over the other t1 nucleotides tested, whereas dG substitution did not improve activity over dA. The activity from dDAP anti-miR21 generally reflects the binding affinity analyses by Schirle and colleagues, but the dG anti-miR21 activities do not. Nonetheless, we were encouraged by the tolerated dA substitution at the t1 nucleotide of 2'-OMe 15mer anti-miR21 and proceeded with generating a precursor for click modifications after computational screening.

2.3.5 Computational screening of t1 triazole-modified nucleotide library using Fast Rigid Exhaustive Docking (FRED)

The program suite from *OpenEye* was used to computationally screen a library of 1'-triazole nucleotide ligands bearing a variety of different substituents for complementarity with the t1A-binding pocket of hAgo2. The structures of each ligand in the library can be found in **Appendix A**. The triazole library was designed for incorporation at the t1 position of anti-miR21 using readily available azides. Conformers were then generated from the library and docked into a rigid receptor that defines the t1A-binding pocket from the published crystal structure of hAgo2 with bound guide and target RNA duplex (PDB file 4W5O) using FRED.¹⁷ A detailed description of the docking procedure can be found in **2.2.5**. It is important to note that constraints were only applied to the t1-adenosine reference ligand for FRED as any constraints applied to residues at the hAgo2 receptor resulted in a failed docking run (**Figure 2.6**). Additionally, the 2'-hydroxyl group that is present on the adenosine reference ligand was removed for each triazole ligand in the library to better reflect the t1 triazole nucleotide to be used for potency studies.

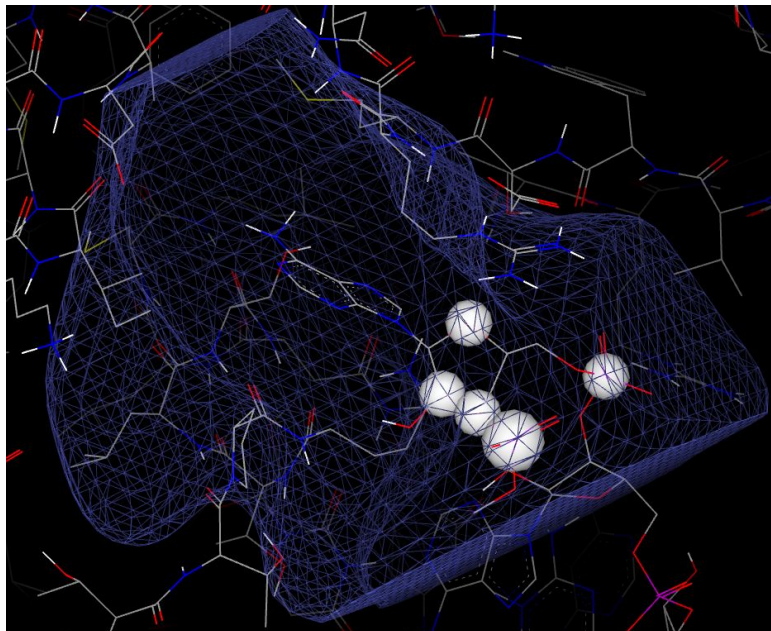


Figure 2.6 Constraints imposed on t1-adenosine reference ligand in the hAgo2 t1A-binding pocket receptor. The receptor is contoured in light blue. The 2'-carbon, 3'-carbon, 3'-phosphorous, 4'-oxygen, and 5'-phosphorous are encased in a white constraint sphere. This image was visualized using VIDA from the OpenEye suite of programs (Santa Fe, NM).

A table of the docked triazole library (**Appendix B**) ranked from lowest to highest ChemGauss4 score (most to least favorable interactions toward hAgo2 receptor) was generated from the most successful docking run after optimizing docking parameters such as the constraints described above and number of poses and conformers docked per ligand. In general, very large docked ligands that could not adequately fit into the small t1A-binding pocket receptor tended to point towards the solvent or away from the pocket to avoid clashing with receptor residues, resulting in poorer scores. Ligands that docked well were heterocyclic, aromatic, or contained at least one hydrogen bonding group. However, careful scanning of each pose was essential as a number of docked ligands contained poses that scored well, but were not reasonable in terms of the ligand's orientation towards the pocket receptor. For example, the highest-scoring pose (1 out of

25) for a 1'-triazole ligand with an ethoxybenzenyl substituent had a moderate ChemGauss4 score of -2.4816 but was flipped entirely away from the pocket, whereas the second pose (2 out of 25) had a reasonable orientation with a score of -1.0813, nearly 1.5-fold higher than the score of the first pose (**Figure 2.7A and B**).

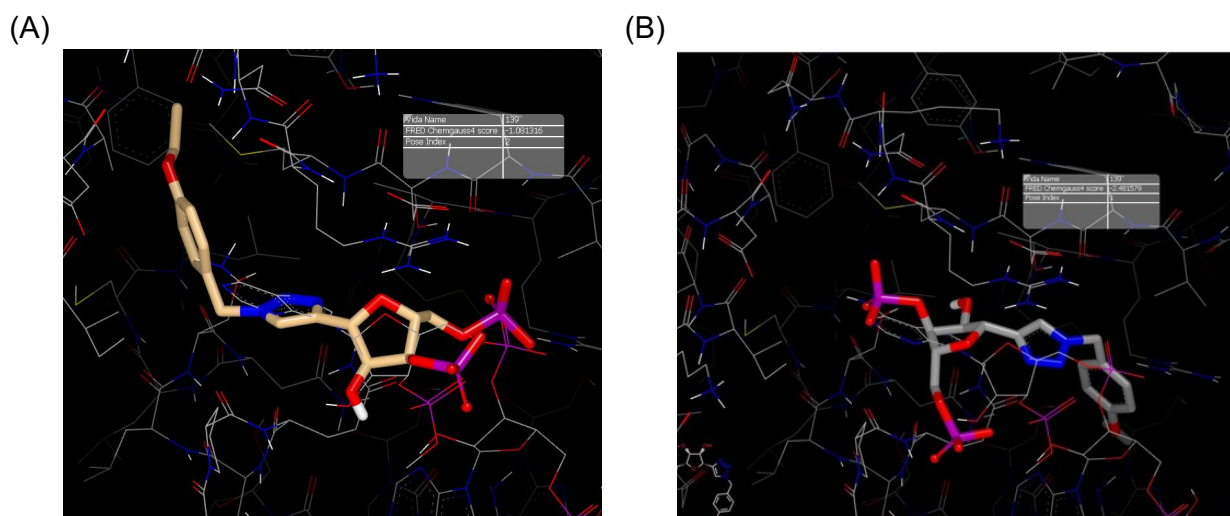


Figure 2.7 Poses of a docked 1'-triazole nucleotide ligand into the t1A hAgo2 receptor. (A) Representative pose (2 out of 25) of a triazole ligand (ethoxybenzene triazole, compound # 139) properly oriented into the t1A-binding hAgo2 receptor with a Chemgauss4 score of -1.0813. (B) Representative pose (1 out of 25) of compound #139 with the triazole modification orientated away from the receptor and generating a Chemgauss4 score of -2.4816.

Control ligands 2'-deoxyadenosine (dA), 2'-deoxycytidine (dC), 2'-deoxyguanosine (dG), 2'-deoxyuridine (dU), 2'-deoxy-2,6-diaminopurine (dDAP), and 1'-ethynyl-2'-deoxyribose (dER) bisphosphate ligands were included in the docking study (**Appendices A and B**).¹⁸ All control ligands were successfully docked into the hAgo2 receptor and generated ChemGauss4 scores with dG being the highest (-1.2471) and dU being the lowest (-0.1175). Much like the triazole ligands, the 25 poses generated for each control ligand were also inconsistently oriented towards or away from the receptor pocket, thus careful examination of each pose was necessary. The dG ligand ranked 132

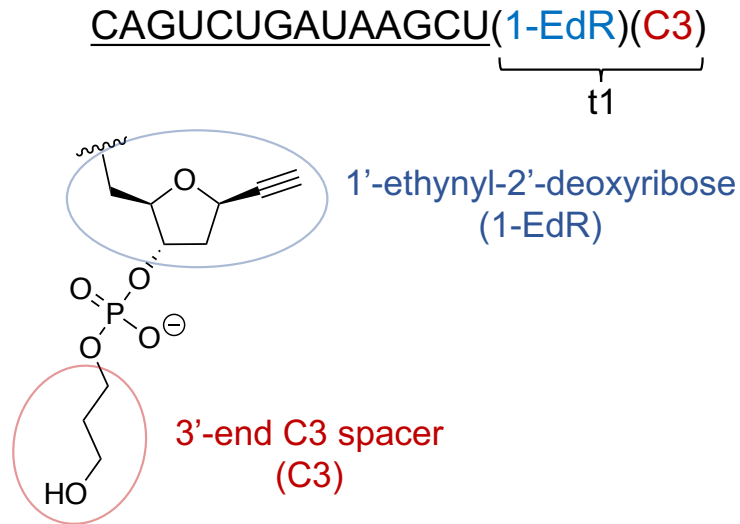
out of 196, indicating that many triazole ligands with better scores could be chosen for modifying anti-miRs in the lab to determine if potency would therefore improve.

Ultimately, we chose 17 triazole candidates from the top 50 scoring ligands docked by FRED whose scores ranged from 10- to 20-fold higher than the control 2'-deoxyadenosine ligand, contained substituents derived from azides that could be readily available from commercial sources, and generated poses that predominantly oriented the ligand towards the receptor in a reasonable manner. The docking scores and potencies of the 17 triazole-modified anti-miRs used in this study are described in Chapter 3.

2.3.6 Design and synthesis of 15mer anti-miR precursor for 3'-end triazole modifications

Finally, given the computational and potency screening results described above, a t1 alkynyl-modified 15mer anti-miR21 was synthesized and tested for potency to confirm if the modification is tolerated for subsequent triazole modifications with substituents originating from designs in the docked library (**Figure 2.8A**). A C3 spacer controlled pore glass reagent and 1'-ethynyl-2'-deoxyribose phosphoramidite were used to incorporate the alkyne at the t1 position by solid phase oligonucleotide synthesis. Overall, at a range of 37 to 150 nM transfected in HeLa cells, the t1 1'-ethynyl-2'-deoxyribose plus C3 spacer- (1-EdR C3) modified anti-miR21 had near equivalent potencies to anti-miR21 with t1 nucleotide as dA or dA plus C3 spacer, indicating that the 1-EdR nor C3 modifications do not affect anti-miR activity and could be used for triazole modifications (**Figure 2.8B**).

(A)



(B)

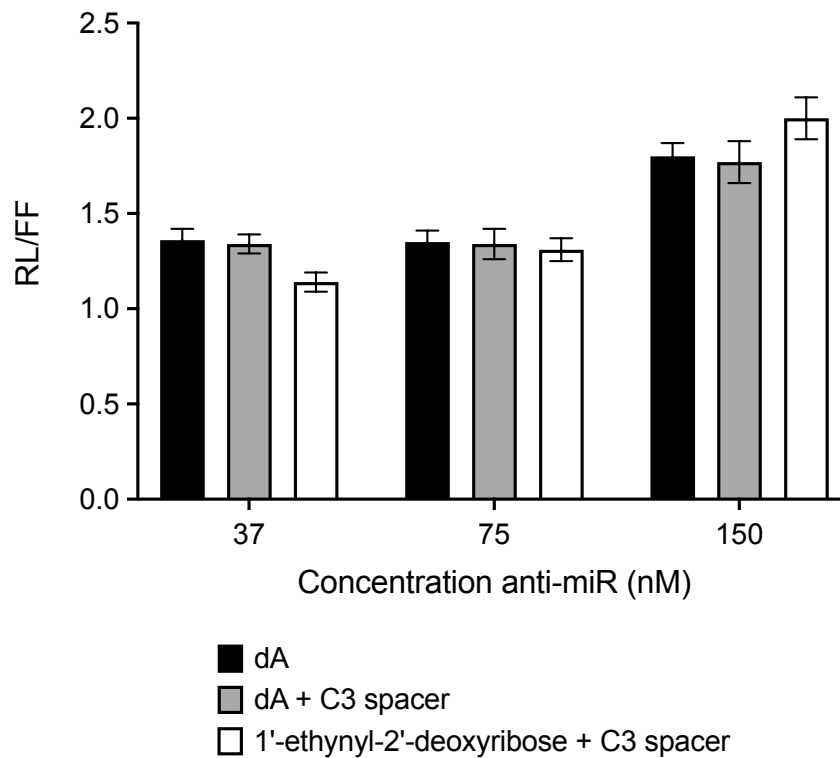


Figure 2.8 Design and potency profile of 15mer anti-miR21 with 3'-end 2'-deoxy-1'-ethynyl-ribose and C3 spacer modification. (A) Sequence of 15mer anti-miR21 with 1-EdR C3 modification at t1 nucleotide. Underlined = 2'-O-methyl; 1-EdR = 1'-ethynyl-2'-deoxyribose; C3 = C3 spacer. (B) Potency profile of 15mer anti-miR21 with t1 nucleotide as 2'-deoxyadenosine (dA), dA with a 3'-end C3 spacer, or 1'-ethynyl-2'-deoxyribose with C3 spacer modification. Error bars represent the s.e.m. from three dual luciferase assay replicates.

2.4 Discussion

Chemically modifying anti-miRs can be a valuable strategy to improve therapeutic activity by inhibiting dysregulated miRNAs that are correlated with disease.⁸ Our research group has done numerous studies on the effects of chemically modified siRNAs using a structure-guided approach by analyzing the interactions of RNA with hAgo2.^{19,28–30} In particular, we wished to see how our computational screening strategy that was used to modify the 5'-end of guide siRNA strands could be applicable to the 3'-end nucleotide of anti-miRs that would interact with the t1A-binding pocket of hAgo2 when bound to miRNA-hAgo2 as a ternary complex.^{18,19} Ultimately, we were successful in using the FRED program from *OpenEye* to dock a moderately large library of 1'-triazole-modified nucleotides into the t1A hAgo2 pocket receptor, albeit with some discrepancies that will be discussed below. In addition, a cellular-based anti-miR activity assay was established and was used to identify a precursor alkynyl-modified anti-miR that could be used to generate desired triazole modifications with potentially improved potency, as guided by the docking results.

This project is an extension from the work that former lab member Dr. Scott Suter did in collaboration with Dr. Nicole Schirle during her doctoral studies at Scripps. As described in his dissertation, Dr. Suter used FRED to dock triazole-modified nucleotides into the t1A hAgo2 pocket receptor using very similar conditions to what is mentioned in this chapter. He found two triazoles, furan and coumaran, to have a relatively more favorable ChemGauss4 score (-2.8 and -2.7, respectively) than the control adenine nucleotide ligand (-1.7) and generated a majority of poses that properly aligned with the adenine reference nucleotide ligand (**Table 2.1**). These modifications were made at the

corresponding t1 nucleotide (8th position from the 5'-end) of an 11mer target RNA that could be used by Dr. Nicole Schirle for binding affinity and crystallographic analyses when bound to hAgo2 loaded with guide miR-122. Although the docking results were encouraging, the binding affinities determined for the furan and coumaran triazole oligonucleotides were unfortunately not higher than control oligonucleotide with t1A. Furthermore, electron density of the furan triazole modification could not be detected after crystallization and X-ray diffraction of triazole modified target-guide-hAgo2 complex, suggesting that higher binding affinity of the triazole-modified nucleotide to the t1A-binding pocket is necessary.

Under the guidance of Dr. Suter and as follow up to his work, a few changes were made to the docking parameters that resulted in more encouraging results. First, a second phosphate group was added in place of the 3'-hydroxyl group from the nucleotide ligand, thus making a 5',3'-bisphosphate nucleotide that better reflects the t1 adenosine from the hAgo2 crystal structure with bound RNA duplex.¹⁸ We believe that the second phosphate group, in combination with constraints added at the 3'-phosphorous, reduced the degrees of freedom around the 3'-carbon of the ligand and allowed more reasonably oriented poses to be created when docked into the receptor. Second, we increased the number of poses from 10 to 25 per ligand to allow us to analyze more poses and improve our confidence in ligand docking performance. Third, the number of conformers generated per ligand was increased to the maximum 5,000 to reduce the likelihood of missing conformers that would have docked well. Lastly, a 2'-deoxyribose at the t1 nucleotide was determined to be tolerated in the luciferase activity assay, thus was removed from the ligands for the docking run.

Changing the docking parameters resulted in a substantial difference between the docked scores of the triazole and control ligands (**Tables 2.1 and 2.2**). Strikingly, the difference in ChemGauss4 scores between both the furan and coumaran triazole ligands with 2'-deoxyadenosine was nearly 10-fold or higher compared to about 1.5-fold previously. The ranking for the other control ligands, however, is not entirely consistent with Dr. Suter's previous docking results. The newer coumaran ChemGauss4 score is moderately lower than furan, and the dG ligand gave a score that was more than five times higher than dA and was equivalent to dDAP. Also, the dC ligand scored more than twice as high compared to dA.

Table 2.1 Former docking scores and dissociation constants of t1 nucleotide triazole-modified and control target RNA oligonucleotides (from Dr. Scott Suter's dissertation).

Nucleobase	ChemGauss4 score	Dissociation Constant (nM)
Furan	-2.8	2.0 ± 0.1
Coumaran	-2.7	3.0 ± 0.2
Adenine	-1.7	1.1 ± 0.1
Guanine	-1.5	5.2 ± 0.1
Uracil	0.65	5.9 ± 0.1
Cytosine	0.83	5.6 ± 0.1

Table 2.2 Updated docking scores and luciferase activity ratios of t1 triazole-modified and control nucleotides on 15mer anti-miR21.

Nucleobase	ChemGauss4 score	Normalized RL/FF ratio at 150 nM in HeLa cells
Furan	-2.7	3.17 ± 0.07
Coumaran	-2.1	1.98 ± 0.22
2'-deoxyguanosine (dG)	-1.2	2.46 ± 0.17
2'-deoxy-2,6-diaminopurine (dDAP)	-1.2	3.06 ± 0.31
1'-ethynyl-2'-deoxyribose (1EdR)	-0.57	2.00 ± 0.11
2'-deoxycytidine (dC)	-0.52	N/A
2'-deoxyadenosine (dA)	-0.22	1.77 ± 0.11
2'-deoxyuridine (dU)	-0.12	N/A

Nevertheless, the anti-miR potencies for some of the modifications when applied to the t1 nucleotide of a 15mer anti-miR21 reflected, to some degree, the new docking scores in hand and were encouraging enough to suggest that we could proceed with further potency screening. The RL/FF activity ratio for furan triazole was ~1.4-fold higher than dA at 150 nM, whereas the coumaran triazole had comparable activity. Indeed, these activity values are not in parallel to the dissociation constants obtained previously. Furthermore, both dG and dDAP scored nearly 6-fold more favorably than dA and had ~0.7 and ~1.3 higher luciferase activity, respectively. In addition to the furan triazole and sixteen other modifications tested for activity on anti-miRs, as described in Chapter 3, guanine and 2,6-diaminopurine base analogs could also be analyzed after organic synthesis in the lab. For example, it may be interesting to design guanine analogs derived from 7-ethynyl-8-aza-7-deazaguanosine (7-EAG), a molecule that was under development in our group, and incorporate that onto anti-miRs to then evaluate potencies after triazole modifications.

Overall, using FRED from *OpenEye* was fairly informative in guiding triazole modifications onto the 3'-end of anti-miRs to be tested in the lab. However, it would be valuable to expand our computational screening analysis and approach in future experiments to improve the rigor of our work. As reported in *Journal of American Chemical Society*, former postdoctoral researcher Dr. Kazumitsu Onizuka and colleagues from Prof. Dean Tantillo's group supplemented their ChemGauss4 scores from their docked library with the slightly older ChemGauss3 scoring system as well as scoring derived from the Consensus method.¹⁹ Using these two other scoring systems may provide us with more information about the relative trends observed by the ChemGauss4-

derived scores from the docked library. AutoDock4 is another molecular docking software suite that, unlike FRED from *OpenEye*, can allow flexibility at the receptor by treating specific side chains as explicit and can interact with the ligand without limiting any rotation around torsional degrees of freedom.³¹ In addition, as Dr. Suter mentions in his dissertation, DOCKKovalent could be used to screen for interactions of nucleophilic residues such as Ser561 and Lys476 within the t1A hAgo2 pocket with any electrophilic triazoles from the library.³² Indeed, it would be particularly interesting to see how DOCKKovalent could be used to identify any interactions of the nucleophilic residues with the highly potent ester triazoles, as described in Chapter 3. Lastly, a computational method called Rosetta-Vienna RNP- $\Delta\Delta G$ combines protein modeling from Rosetta, RNA modeling by Vienna, and free energy calculations by Rosetta to predict relative binding affinities of RNA-protein complexes.³³ Such a method may be useful to predict the binding affinity of t1-modified anti-miR with miRNA-loaded hAgo2. Combining the computational screening methods above may improve our understanding of the interactions between chemically modified anti-miR and hAgo2 and could further supplement our rationale to proceed with more cellular and biochemical experiments.

2.5 References

- (1) Gebert, L. F. R.; MacRae, I. J. Regulation of MicroRNA Function in Animals. *Nat. Rev. Mol. Cell Biol.* **2019**, *20* (1), 21–37. <https://doi.org/10.1038/s41580-018-0045-7>.
- (2) Lee, Y.; Kim, M.; Han, J.; Yeom, K. H.; Lee, S.; Baek, S. H.; Kim, V. N. MicroRNA Genes Are Transcribed by RNA Polymerase II. *EMBO J.* **2004**, *23* (20), 4051–4060. <https://doi.org/10.1038/sj.emboj.7600385>.
- (3) Bohnsack, M. T.; Czapinski, K.; Görlich, D. Exportin 5 Is a RanGTP-Dependent DsRNA-Binding Protein That Mediates Nuclear Export of Pre-MiRNAs. *Rna* **2004**, *10* (2), 185–191. <https://doi.org/10.1261/rna.5167604>.
- (4) Grishok, A.; Pasquinelli, A. E.; Conte, D.; Li, N.; Parrish, S.; Ha, I.; Baillie, D. L.; Fire, A.; Ruvkun, G.; Mello, C. C. Genes and Mechanisms Related to RNA Interference Regulate Expression of the Small Temporal RNAs That Control *C. Elegans* Developmental Timing. *Cell* **2001**, *106* (1), 23–34. [https://doi.org/10.1016/S0092-8674\(01\)00431-7](https://doi.org/10.1016/S0092-8674(01)00431-7).
- (5) Carthew, R. W.; Sontheimer, E. J. Origins and Mechanisms of MiRNAs and SiRNAs. *Cell* **2009**, *136* (4), 642–655. <https://doi.org/10.1016/j.cell.2009.01.035>.
- (6) Wilson, R. C.; Doudna, J. A. Molecular Mechanisms of RNA Interference. *Annu. Rev. Biophys.* **2013**, *42* (1), 217–239. <https://doi.org/10.1146/annurev-biophys-083012-130404>.
- (7) Rooij, E.; Kauppinen, S. Development of Micro RNA Therapeutics Is Coming of Age. *EMBO Mol. Med.* **2014**, *6* (7), 851–864. <https://doi.org/10.15252/emmm.201100899>.
- (8) Stenvang, J.; Petri, A.; Lindow, M.; Obad, S.; Kauppinen, S. Inhibition of MicroRNA Function by AntimiR Oligonucleotides. *Silence* **2012**, *3* (1), 1. <https://doi.org/10.1186/1758-907X-3-1>.
- (9) Lennox, K. A.; Behlke, M. A. Chemical Modification and Design of Anti-MiRNA Oligonucleotides. *Gene Ther.* **2011**, *18* (12), 1111–1120. <https://doi.org/10.1038/gt.2011.100>.
- (10) Lennox, K. A.; Owczarzy, R.; Thomas, D. M.; Walder, J. A.; Behlke, M. A. Improved Performance of Anti-MiRNA Oligonucleotides Using a Novel Non-Nucleotide Modifier. *Mol. Ther. - Nucleic Acids* **2013**, *2* (AUG), e117. <https://doi.org/10.1038/mtna.2013.46>.
- (11) Mie, Y.; Hirano, Y.; Kowata, K.; Nakamura, A.; Yasunaga, M.; Nakajima, Y.; Komatsu, Y. Function Control of Anti-MicroRNA Oligonucleotides Using Interstrand Cross-Linked Duplexes. *Mol. Ther. - Nucleic Acids* **2018**, *10* (March), 64–74. <https://doi.org/10.1016/j.omtn.2017.11.003>.
- (12) Gubu, A.; Su, W.; Zhao, X.; Zhang, X.; Fan, X.; Wang, J.; Wang, Q.; Tang, X. Circular Antisense Oligonucleotides for Specific RNase-H-Mediated MicroRNA Inhibition with Reduced Off-Target Effects and Nonspecific Immunostimulation. *J. Med. Chem.* **2021**, *64* (21), 16046–16055. <https://doi.org/10.1021/acs.jmedchem.1c01421>.
- (13) Ariyoshi, J.; Momokawa, D.; Eimori, N.; Kobori, A.; Murakami, A.; Yamayoshi, A. Development of Novel Antisense Oligonucleotides for the Functional Regulation

- of RNA-Induced Silencing Complex (RISC) by Promoting the Release of MicroRNA from RISC. *Bioconjug. Chem.* **2015**, *26* (12), 2454–2460. <https://doi.org/10.1021/acs.bioconjchem.5b00501>.
- (14) Winkle, M.; El-Daly, S. M.; Fabbri, M.; Calin, G. A. Noncoding RNA Therapeutics — Challenges and Potential Solutions. *Nat. Rev. Drug Discov.* **2021**, *20* (8), 629–651. <https://doi.org/10.1038/s41573-021-00219-z>.
- (15) Zhang, S.; Cheng, Z.; Wang, Y.; Han, T. The Risks of Mirna Therapeutics: In a Drug Target Perspective. *Drug Des. Devel. Ther.* **2021**, *15*, 721–733. <https://doi.org/10.2147/DDDT.S288859>.
- (16) Schirle, N. T.; MacRae, I. J. The Crystal Structure of Human Argonaute2. *Science* (80-.). **2012**, *336* (6084), 1037–1040. <https://doi.org/10.1126/science.1221551>.
- (17) Schirle, N. T.; Sheu-Gruttadauria, J.; MacRae, I. J. Structural Basis for MicroRNA Targeting. *Science* (80-.). **2014**, *346* (6209), 608–613. <https://doi.org/10.1126/science.1258040>.
- (18) Schirle, N. T.; Sheu-Gruttadauria, J.; Chandradoss, S. D.; Joo, C.; MacRae, I. J. Water-Mediated Recognition of T1-Adenosine Anchors Argonaute2 to MicroRNA Targets. *Elife* **2015**, *4* (September), 1–16. <https://doi.org/10.7554/eLife.07646>.
- (19) Onizuka, K.; Harrison, J. G.; Ball-Jones, A. A.; Ibarra-Soza, J. M.; Zheng, Y.; Ly, D.; Lam, W.; Mac, S.; Tantillo, D. J.; Beal, P. A. Short Interfering RNA Guide Strand Modifiers from Computational Screening. *J. Am. Chem. Soc.* **2013**, *135* (45), 17069–17077. <https://doi.org/10.1021/ja4079754>.
- (20) Pham, K. M.; Suter, S. R.; Lu, S. S.; Beal, P. A. Ester Modification at the 3' End of Anti-MicroRNA Oligonucleotides Increases Potency of MicroRNA Inhibition. *Bioorganic Med. Chem.* **2021**, *29* (October 2020), 115894. <https://doi.org/10.1016/j.bmc.2020.115894>.
- (21) McGann, M. FRED Pose Prediction and Virtual Screening Accuracy. *J. Chem. Inf. Model.* **2011**, *51* (3), 578–596. <https://doi.org/10.1021/ci100436p>.
- (22) Lui, W. O.; Pourmand, N.; Patterson, B. K.; Fire, A. Patterns of Known and Novel Small RNAs in Human Cervical Cancer. *Cancer Res.* **2007**, *67* (13), 6031–6043. <https://doi.org/10.1158/0008-5472.CAN-06-0561>.
- (23) Obad, S.; Dos Santos, C. O.; Petri, A.; Heidenblad, M.; Broom, O.; Ruse, C.; Fu, C.; Lindow, M.; Stenvang, J.; Straarup, E. M.; et al. Silencing of MicroRNA Families by Seed-Targeting Tiny LNAs. *Nat. Genet.* **2011**, *43* (4), 371–380. <https://doi.org/10.1038/ng.786>.
- (24) Burel, S. A.; Hart, C. E.; Cauntay, P.; Hsiao, J.; Machemer, T.; Katz, M.; Watt, A.; Bui, H. H.; Younis, H.; Sabripour, M.; et al. Hepatotoxicity of High Affinity Gapmer Antisense Oligonucleotides Is Mediated by RNase H1 Dependent Promiscuous Reduction of Very Long Pre-mRNA Transcripts. *Nucleic Acids Res.* **2015**, *44* (5), 2093–2109. <https://doi.org/10.1093/nar/gkv1210>.
- (25) Hogan, D. J.; Vincent, T. M.; Fish, S.; Marcusson, E. G.; Bhat, B.; Nelson Chau, B.; Zisoulis, D. G. Anti-MiRs Competitively Inhibit MicroRNAs in Argonaute Complexes. *PLoS One* **2014**, *9* (7). <https://doi.org/10.1371/journal.pone.0100951>.
- (26) De, N.; Young, L.; Lau, P. W.; Meisner, N. C.; Morrissey, D. V.; MacRae, I. J. Highly Complementary Target RNAs Promote Release of Guide RNAs from Human Argonaute2. *Mol. Cell* **2013**, *50* (3), 344–355. <https://doi.org/10.1016/j.molcel.2013.04.001>.

- (27) Ariyoshi, J.; Matsuyama, Y.; Kobori, A.; Murakami, A.; Sugiyama, H.; Yamayoshi, A. Effective Anti-MiRNA Oligonucleotides Show High Releasing Rate of MicroRNA from RNA-Induced Silencing Complex. *Nucleic Acid Ther.* **2017**, *27* (5), 303–308. <https://doi.org/10.1089/nat.2017.0663>.
- (28) Suter, S. R.; Sheu-Gruttadauria, J.; Schirle, N. T.; Valenzuela, R.; Ball-Jones, A. A.; Onizuka, K.; Macrae, I. J.; Beal, P. A. Structure-Guided Control of SiRNA Off-Target Effects. *J. Am. Chem. Soc.* **2016**, *138* (28), 8667–8669. <https://doi.org/10.1021/jacs.6b06137>.
- (29) Suter, S. R.; Ball-Jones, A.; Mumbleau, M. M.; Valenzuela, R.; Ibarra-Soza, J.; Owens, H.; Fisher, A. J.; Beal, P. A. Controlling MiRNA-like off-Target Effects of an SiRNA with Nucleobase Modifications. *Org. Biomol. Chem.* **2017**, *15* (47), 10029–10036. <https://doi.org/10.1039/c7ob02654d>.
- (30) Valenzuela, R. A. P.; Onizuka, K.; Ball-Jones, A. A.; Hu, T.; Suter, S. R.; Beal, P. A. Guide Strand 3'-End Modifications Regulate SiRNA Specificity. *ChemBioChem* **2016**, *17* (24), 2340–2345. <https://doi.org/10.1002/cbic.201600453>.
- (31) Morris, G. M.; Huey, R.; Lindstrom, W.; Sanner, M. F.; Belew, R. K.; Goodsell, D. S.; Olson, A. J. AutoDock4 and AutoDockTools4: Automated Docking with Selective Receptor Flexibility. *J. Comput. Chem.* **2009**, *30* (16), 2785–2791. <https://doi.org/10.1002/jcc>.
- (32) London, N.; Miller, R. M.; Krishnan, S.; Uchida, K.; Irwin, J. J.; Eidam, O.; Gibold, L.; Cimermančič, P.; Bonnet, R.; Shoichet, B. K.; et al. Covalent Docking of Large Libraries for the Discovery of Chemical Probes. *Nat. Chem. Biol.* **2014**, *10* (12), 1066–1072. <https://doi.org/10.1038/nchembio.1666>.
- (33) Kappel, K.; Jarmoskaite, I.; Vaidyanathan, P. P.; Greenleaf, W. J.; Herschlag, D.; Das, R. Blind Tests of RNA–Protein Binding Affinity Prediction. *Proc. Natl. Acad. Sci. U. S. A.* **2019**, *116* (17), 8336–8341. <https://doi.org/10.1073/pnas.1819047116>.

2.6 Table of primer sequences

Name	Sequence (5' to 3')
miR21 target F	TCAACATCAGTCTGATAAGCTAGGCCGCTGGCCGCAATAAAA
miR21 target R	TAGCTTATCAGACTGATGTTGATCGAGCGATCGCCTAGAATTACTGC

Chapter 3

Potency and characterization of 3'-end ester-modified anti-microRNA oligonucleotides

3.1 Introduction

This chapter continues to describe our study of computationally screened, structure-guided 3'-end chemical modifications on anti-miRNA in cellular based assays.¹ Previously, our group used OpenEye molecular docking software to screen for chemical modifications at the 5'-end of siRNA guide strands using copper(I)-catalyzed azide/alkyne cycloaddition (CuAAC) reactions.² Briefly, we found that 1'-ethynyl-ribose-derived triazole modifications at the 5'-end of PIK3CB siRNA was well-tolerated and need only fit the general shape of the siRNA guide 5'-end nucleotide-binding site located in the MID/PIWI domains of hAgo2. Fortunately, this strategy proved to be successful in the work described here. In particular, we found that a 2'-deoxy-1'-ethynyl-ribose-derived triazole bearing an ester substituent at the 3'-end nucleotide (t1) of anti-miR21 and anti-miR122 imparted a 9-fold and 6-fold higher activity at 300 nM and 5 nM, respectively, in cultured human cells compared to anti-miR containing a canonical t1 adenosine. Further investigative experiments were then conducted to identify the possible mechanism for the substantial increase in 3'-end ester-modified anti-miR activity.

3.2 Methods

3.2.1 MiR-122 dual luciferase reporter plasmid generation

The miR-122 target sequence (5' – ACAAACACCATTGTCACACTCCA – 3') was cloned into the psiCHECK-2 dual luciferase reporter plasmid (Promega) using the same

methods to generate miR-21 reporter plasmid described in the Methods section of Chapter 2. Primer sequences are listed in **Table 3.6**.

3.2.2 Cell culture

Culturing conditions for HuH-7 (Japanese Collection of Research Bioresources, JCRB0403) and HEK293T (ATCC, CTRL-3216) cells are the same as for HeLa cells described in the Methods section of Chapter 2.

3.2.3 Transfection and dual luciferase assay

Cells were transfected with anti-miR oligonucleotides at the indicated concentrations in the Results section (**3.3**) and potencies were determined by the dual luciferase assay following the same procedure described in the Methods section of Chapter 2.

For the hAgo2 pulldown assay, HEK293T cells were plated onto a 24-well plate at 1.5×10^4 cells per well in DMEM supplemented with 10% FBS and 1X Anti-Anti solution 24 h before transfection. The cells were co-transfected with 10 pmol of miR-21 mimic duplex and 200 ng of hAgo2 overexpression vector using Lipofectamine 2000 (Invitrogen) according to the manufacturer's instructions in 100 μ L reduced serum media (OPTI-MEM) per well. The cells were replaced with 500 μ L DMEM supplemented with 10% FBS without antibiotic prior to adding the 100 μ L nucleic acid/lipid transfection complex. After 48 h transfection, the cell media was removed and the cells were scraped into 50 μ L of lysis buffer containing Pierce IP Lysis Buffer (Thermo Scientific) and 100X Halt Protease Inhibitor Cocktail (Thermo Scientific) diluted to 1X per well. The cells in lysis buffer were shaken on an orbital shaker at ~ 75 rpm 4 $^{\circ}$ C for 30 min for lysis. The resulting cell lysate

was then cleared of cell debris by centrifugation at 16,000 x g for 20 min at 4 °C. Finally, the supernatant was transferred to a new tube for lysate protein concentration determination by the Quick Start™ Bradford Protein Assay kit (BIO-RAD) according to the manufacturer's instructions.

For fluorescence microscopy, HeLa cells were plated at 5×10^4 per well in 450 μ L DMEM with 10% FBS over a cover slip treated with 1M HCl in a 24-well plate. After 24 h, the cells were transfected with Cy3™ Dye-Labeled Anti-miR™ Negative Control #1 (Invitrogen, AM17011) to a final concentration of 25, 50, or 100 nM using OPTI-MEM and 3 μ L Lipofectamine RNAiMAX (Invitrogen) to 50 μ L total volume per well for 24 h at 37 °C + 5% CO₂ before immunostaining (see **3.2.12**).

3.2.4 Oligonucleotide preparation

All anti-miR21 and anti-miR122 oligonucleotides were either purchased from GE Healthcare Dharmacon (Horizon Discovery) or synthesized in the lab using an Applied Biosystems (ABI) 394 DNA/RNA Synthesizer. Primers for cloning were purchased from Integrated DNA Technologies (IDT). All phosphoramidite, controlled pore glass (CPG), and ancillary reagents were purchased from Glen Research. Oligonucleotides synthesized in the laboratory were cleaved from CPG solid support using 2:1 of 30% NH₄OH and EtOH overnight. The cleaved oligonucleotide solution was transferred away from the CPG beads and concentrated to dryness using a SpeedVac concentrator then resuspended in nuclease free water and desalted using an illustra™ Nap™-10 Sephadex™ G-25 columns (Cytiva 17085401). All oligonucleotides were electrophoresed in a 19% polyacrylamide gel and extracted from the gel after UV shadowing. The oligonucleotide was then purified from the gel by crushing and soaking

at 4 °C overnight in buffer containing 0.5 M NH₄OAc and 0.1 mM EDTA and filtered using 0.22 µm cellulose acetate membrane filter (Costar® Spin-X® Centrifuge Tube Filter, Corning 8160). Finally, the oligonucleotides were ethanol precipitated or purified by silica-based octadecyl bonded phase SepPak C18 columns (Waters) in 1:1 acetonitrile/water elution and characterized by MALDI-TOF mass spectrometric analysis. All oligonucleotide sequences and masses are reported in **Table 3.2.14**.

3.2.5 Generation of t1-triazole modified anti-miR via copper(I)-catalyzed azide/alkyne cycloaddition (CuAAC) reaction

The procedure to generate triazole-modified anti-miRs is an adaptation from a report by Dr. Kazumitsu Onizuka and colleagues.² In a 1.5 mL microcentrifuge tube, 0.88 µL of 100 mM CuSO₄ (88 nmol) dissolved in nuclease free water, was combined with 1.75 µL of 100 mM Tris(3-hydroxypropyltriazolylmethyl)amine (THPTA, 175 nmol), also dissolved in nuclease free water, and incubated for 5 min at room temperature. (+)-Sodium L-ascorbate (1.75 µL of 100 mM, 175 nmol), in nuclease free water, was then added to the solution for reduction of Cu²⁺ to Cu⁺, where a blue-to-clear solution color change is observed. Next, 1.05 µL of 100 mM azide (105 nmol), dissolved in DMSO, was added to the solution and mixed well by pipetting. DMSO (6 µL) of was added to the solution to facilitate miscibility and reduce precipitation of azide in the reaction tube. HEPES pH 7 buffer (6.07 µL of 100 mM) was used to dissolve 3.5 nmol of dried-down alkyne-modified anti-miR oligonucleotide and transferred to the reaction tube, resulting in a total reaction volume of 17.5 µL. The solution was incubated for ~2.5 h at room temperature then quenched using 17.5 µL of 80% formamide loading buffer (80% formamide, 10 mM EDTA, 0.05% xylene cyanol FF, and 0.05% bromophenol blue in MilliQ®-purified water). To purify the CuAAC oligonucleotide product, the quenched

reaction was loaded into a denaturing (8 M urea) 19% PAGE gel and electrophoresed for ~3 h at 20W. After electrophoresis, the oligonucleotide bands were crushed and soaked as described above. The oligonucleotides were either ethanol precipitated or purified using a SepPak C18 cartridge and characterized by MALDI-TOF mass spectrometry. CuAAC reactions were scaled 1.5- or 3-fold greater to generate more oligonucleotide product per reaction, as needed.

3.2.6 Snake venom phosphodiesterase (SVPD) assay

Anti-miR21 oligonucleotides were diluted to 8 μ M final concentration in 0.01 U/mL SVPD diluted in buffer (50 mM Tris pH 7.2 and 10 mM MgCl₂ in nuclease-free water) and incubated at 37 °C. Aliquots of 5 μ L were taken at 12, 24, and 48 h timepoints and combined with equal volume of 80% formamide loading buffer (80% formamide, 10 mM EDTA, 0.05% xylene cyanol FF, and 0.05% bromophenol blue in MilliQ[®]-purified water) then heated at 95 °C for 2 min. The samples were stored at -20 °C until all samples were ready for electrophoresis. For each sample, 40 pmol of the oligonucleotide subjected to SVPD was electrophoresed in a 19% denaturing (8 M urea) polyacrylamide gel for 3 h at 90 V. The gel was stained in SYBR[™] Gold Nucleic Acid Gel Stain (Invitrogen) diluted in 1X TBE for 20 min with gentle shaking and imaged on a Typhoon Trio Variable Mode Imager (GE Healthcare). The oligonucleotide gel bands were quantified using ImageQuant software (Molecular Dynamics). Percent intact oligonucleotide at each time point (**Figure 3.7**) was determined as a percentage of band intensity over the respective zero time point band intensity.

3.2.7 hAgo2 mammalian and yeast expression vector generation

The mammalian hAgo2 overexpression vector for the 5'-biotin anti-miR21

pulldown assay was generated by PCR-amplifying the hAgo2 gene from pIRES-neo-FLAG-HA-N-Ago2 vector (gift from Tuschl lab³ through Addgene) using “hAgo2 GA F” and “hAgo2 GA R” primers (sequences listed in **Table 3.6**) and cloning into BamHI/NotI double restriction-digested pcDNA3.1 vector by Gibson Assembly. The hAgo2 gene insert, pcDNA3.1 vector, and Gibson Assembly Master Mix (New England Biolabs) were combined and incubated at 50 °C for 30 min, then transformed into XL10-Gold[®] Ultracompetent cells (Agilent Technologies) using the manufacturer’s instructions. pcDNA hAgo2 plasmids from XL10-Gold cells were harvested using a PureYield Plasmid Miniprep System (Promega).

The yeast expression vector containing poly-Histidine-tagged (10xHis) full-length hAgo2 (termed yeAgo2 vector) was generated by first PCR-amplifying the hAgo2 gene from the pcDNA hAgo2 vector described above using forward primer “GA yeAgo2 F” containing a TEV protease cleavage site sequence and “GA yeAgo2 R” reverse primer. Next, the pSc yeast expression vector containing 10xHis-tagged full-length ADAR2 (gift from fellow colleague Alexander Thuy-Boun) was double-digested with BamHI and XhoI restriction enzymes to remove the ADAR2 gene. The TEV-tagged hAgo2 gene insert was then PCR-amplified again using a 78mer forward primer “BamHI His tag primer F” to add the 10xHis-tag and BamHI restriction site back onto the hAgo2 gene and “GA yeAgo2 R” reverse primer. Another round of PCR was performed on the hAgo2 gene using a 52mer forward primer “GA BamHI F” to add Gibson assembly overlapping region sequences to the vector and “GA yeAgo2 R” reverse primer. Finally, the 10xHis, TEV-tagged hAgo2 gene insert and digested pSc vector were Gibson assembled using Gibson Assembly Master Mix at 50 °C incubation for 1 h before XL-10 Gold[®] Ultracompetent Cell

transformation. XL-10 Gold *Escherichia coli* cells were harvested of yeAgo2 plasmid using PureYield™ Plasmid MiniPrep System.

All PCR amplifications were performed using a 2-step protocol with Phusion Hot Start II DNA Polymerase (Thermo Scientific). Primer annealing temperatures were determined using the T_m calculator from Thermo Fisher Scientific.

3.2.8 MiR-21 mimic duplex generation

Equimolar amounts of dry microRNA-21 guide (5' -p-UAGCUUAUCAGACUGAUGUUGA -3') and passenger (5' -AACAUCAUCAGUCUGAUAAAGCUAAU - 3') ssRNA were dissolved in IDT™ Nuclease-Free Duplex Buffer (100 mM potassium acetate, 30 mM HEPES, pH 7.5) and combined in a thermal cycler PCR tube. The tube was heated in a thermal cycler at 94 °C for 5 min, followed by gradual cooling to room temperature at a rate of 1 °C/min to allow annealing. The resulting miR-21 duplex was stored at -20 °C prior to transfection in HEK293T cells for subsequent hAgo2 pulldown assays.

3.2.9 hAgo2 pulldown assay

The procedure for the biotin pulldown of miR21-loaded hAgo2 was adapted from previous reports.^{4,5} The 5'-biotinylated anti-miR21 pulldown reactions were prepared by combining 300 µg HEK293T cell lysate, 375 µL 2X TENT (20 mM Tris-HCl pH 8.0, 2 mM EDTA, 500 mM NaCl, and 1% (v/v) Triton X-100) buffer, 7.5 µL of 100X Halt™ Protease Inhibitor Cocktail (Thermo Scientific), 7.5 µL of 40 U/µL RiboLock RNase Inhibitor (Thermo Scientific), 100 pmol of 5'-biotinylated anti-miR21 oligonucleotide, and brought to a final reaction volume of 750 µL using Pierce™ IP Lysis Buffer (Thermo Scientific) in

a 1.5 mL microcentrifuge tube. The samples were incubated for 30 min at room temperature on a rotating mixer. Next, 75 μ L (1.5 mg) of DynabeadsTM M-280 Streptavidin beads (Invitrogen) were separated using a BDTM IMagnet magnetic stand (BD Biosciences) for 3 min at a time and washed three times in 1X TENT buffer. The beads were then added to each sample, mixed by pipetting, and allowed to mix on a rotating mixer for an additional 30 min. Next, the beads were separated using the magnetic stand and washed three times using 750 μ L of ice-cold 1X TENT buffer. The beads were resuspended in 40 μ L 1X Laemmli Buffer supplemented with DTT, boiled for 5 min at 95 °C to elute captured proteins, then separated on the magnetic stand. The eluted proteins in 1X Laemmli buffer were transferred to a new microcentrifuge tube and stored at -80 °C before SDS-PAGE and western blotting.

3.2.10 Western blotting

For pulled down hAgo2, 10 μ L of each pulldown sample elution was loaded into a BOLTTM 4-12% Bis-Tris Plus SDS-PAGE gel (Invitrogen) alongside 15 μ L PageRulerTM Prestained Protein Ladder (Thermo Scientific) and electrophoresed at 200 V for 40 min. The proteins were transferred onto Immobilon-P PVDF membrane (Millipore Sigma) for 30 min at 10 V using a Trans-Blot[®] SD Semi-Dry Transfer Cell (Bio-Rad). The membrane was washed in TBST buffer three times then blocked for 1 h in TBST supplemented with 5% Blotting-Grade Blocker (nonfat dry milk, Bio-Rad) at room temperature. The membrane was washed again in TBST three times then incubated in TBST supplemented with 2.5% Blotting-Grade Blocker and a 1:1,000 dilution of anti-Ago2 primary antibody (Wako, 4G8) at 4 °C overnight. The following day, the membrane was washed three times in TBST and incubated in TBST supplemented with 2.5% Blotting-Grade Blocker

and a 1:2,000 dilution of anti-mouse IgG alkaline phosphatase conjugate secondary antibody (SC-2008, Santa Cruz Biotechnologies) for 1 h at room temperature. After the PVDF membrane was washed an additional three times in TBST, the membrane was incubated in ECF substrate (GE Healthcare) for 5 min at room temperature and imaged on a GelDoc Go imaging system (Bio-Rad) under SYBR Gold settings on a UV/Stain-free tray.

For PDCD4 and 10xHis-tagged ADAR2 or hAgo2 western blotting detection, respective 20 µg of HeLa cell lysate or 10 to 30 µg lysate from BCY123 cells was used for SDS-PAGE, followed by the same western blotting procedures as described above. PDCD4 monoclonal primary antibody (Santa Cruz Biotechnologies, k4C1) was used at a 1:200 dilution for detection of PDCD4. Primary 6xHis-Tag Monoclonal Antibody (Invitrogen, MA1-21315) was used at a 1:1,000 dilution for detection of 10xHis-tagged ADAR2 or Ago2. Secondary antibody goat anti-mouse IgG alkaline phosphatase conjugate (Invitrogen 31320) was used at a 1:30,000 dilution.

3.2.11 RT-qPCR

HeLa cells transfected with modified anti-miR21 and control oligonucleotides were lysed and total RNA was isolated using an RNeasy Plus Mini Kit (Qiagen). Up to 1 µg of total RNA template was used for reverse transcription using the High Capacity cDNA Reverse Transcription Kit (Applied Biosystems). Reverse transcriptase control (RTC) samples containing RNA and no reverse transcriptase were performed in parallel to samples prepared for generating cDNA to check for genomic DNA contamination. The cDNA template was then used with the following TaqMan[®] Gene Expression Assays (Applied Biosystems) containing 20X FAM-dye labeled TaqMan[®] probes according to the

manufacturer's instructions: PDCD4 (Hs00377253_m1), TNF α (Hs00174128_m1), and GAPDH (Hs99999905_m1). Quantitative PCR (qPCR) runs were performed using a CFX Connect Real-Time PCR System (BioRad) and data was analyzed using CFX Maestro software. Relative gene expression of PDCD4 and TNF α was normalized to GAPDH control and quantified using the $2^{-\Delta\Delta C_t}$ method.⁶

3.2.12 Immunofluorescence and fluorescence microscopy

HeLa cells transfected with Cy3TM Dye-Labeled Anti-miRTM Negative Control #1 for 24 h (see **3.2.3** for transfection conditions) were aspirated of media from each well and fixed with 0.5 mL Image-iT Fixative Solution (4% formaldehyde in PBS, pH 7.3, methanol-free, Invitrogen, FB002) for 15 min at room temperature. Fixative solution was then removed and washed three times for 5 min each using Dulbecco's phosphate-buffered saline (DPBS, Gibco, 14190144). DPBS was removed and cells were permeabilized using 0.5 mL permeabilization solution (0.5% Triton X-100 in PBS) in each well for 15 min at room temperature. The cells were washed again three times for 5 minutes using DPBS after aspirating permeabilization solution, then 0.5 mL blocking buffer (3% BSA in PBS, diluted from Thermo Scientific Blocker, PI37525) was added and incubated for 1 h at room temperature. After another three washes with PBS for 5 min, HeLa cells were stained overnight at 4 °C with mouse IgG alpha tubulin monoclonal primary antibody (Invitrogen, A11126) diluted to 1 μ g/mL in 0.5 mL PBS with 1% BSA (diluted from Thermo Scientific Blocker, PI37525).

The following day, primary antibody staining solution was removed and the cells were washed three times for 5 min using DPBS then stained for 1 h at room temperature, covered from light, with 0.5 mL secondary antibody solution containing

rabbit anti-mouse IgG (H+L) cross-adsorbed Alexa-Fluor 488 conjugate (Invitrogen, A11059) diluted to 1 µg/mL using PBS with 1% BSA. The secondary antibody staining solution was removed and cells were washed three times for 5 min using DPBS. One to two drops of NucBlue™ Live ReadyProbes™ Reagent (Hoechst 33342, Invitrogen, R37605) was added to each well of cells in 0.5 mL DPBS and incubated for 20 min at room temperature. Finally, the cover slip containing fixed cells was mounted onto a microscope slide and imaged under DAPI, GFP, and/or RFP fluorescent cube settings at 20X magnification using an EVOS M7000 Imaging System (Invitrogen), courtesy of Prof. Marie Heffern lab.

3.2.13 Expression of poly-Histidine-tagged full-length hAgo2 protein

Poly-Histidine-tagged full length hAgo2 was expressed in *Saccharomyces cerevisiae* BCY123 cells using protocols described in previous reports.⁷⁻⁹ *yeAgo2* vector (see **3.2.7**) was transformed into BCY123 cells by a lithium acetate protocol and streaked onto plates containing yeast minimal media minus uracil (CM - Ura) and incubated at 30 °C for 2-3 days. A single colony from the plate was picked and used to inoculate a 15 mL starter culture of CM - Ura + 2% glucose for overnight incubation at 30 °C. Next, 300 µL of start culture was used to inoculate 30 mL of CM – Ura + 3% glycerol + 2% lactate media and incubated for 20 – 24 h at 30 °C, until the culture OD₆₀₀ reached 1.5 – 2.0. Once the appropriate OD₆₀₀ was reached, a galactose solution was added to the culture to reach a final concentration of 3% to induce protein expression for approximately 6 h. After induction, the yeast cells were pelleted down by centrifugation, supernatant was removed, and stored at -80 °C until ready for lysis.

The yeast cell lysis procedure described was modified from a protocol written by DeCaprio and Kohl.¹⁰ The yeast cells were resuspended in three volumes of ice-cold lysis buffer¹¹ [50 mM NaH₂PO₄, pH 8.0; 0.3 M NaCl; 0.5 mM Tris(2-carboxyethyl) phosphine hydrochloride (TCEP)] supplemented with Halt™ Protease Inhibitor Cocktail (Thermo Scientific, 78430) to 1X concentration then combined with one volume of pre-acid-washed 500 µm glass beads in ice-cold lysis buffer. The sample was vortexed for 30 s and allowed to cool in an ice water bath for 1 to 2 min for a total of three times. Lysate supernatant was cleared away from the beads by centrifugation at 10,000 x g for 5 min at 4 °C, transferred to a new tube, then centrifuged again at 10,000 x g for 30 min at 4 °C to remove any aggregated proteins and reduce any background from western blotting. Finally, the supernatant was transferred to another tube and stored at -80 °C or kept on ice for western blotting.

3.2.14 Tables of mass spectra and sequences for anti-miR oligonucleotides

Antisense oligonucleotides targeting microRNA (Anti-miR) and MALDI-TOF MS data:

Underlined = 2'-O-Methyl (2'-O-Me)

Bold = Locked nucleic acid (LNA)

d = 2'-deoxyribose

(1-EdR) = 1'-ethynyl-2'-deoxyribose

(Bi) = Biotin

(C3) = C3 spacer

Oligonucleotide ID	Sequence (5'-3')	Calculated Mass (m/z)	Observed Mass [M-H] ⁻ (m/z)
Anti-miR21 9mer LNA	GATAAGCTA	3013.0	3013.4
Anti-miR21 15mer	<u>CAGUCUGAUAAGCUA</u>	4968.9	4969.6
Anti-miR21 22mer	<u>UCAACAUCAGUCUGAUAAGCU</u> <u>A</u>	7276.8	7279.6

Anti-miR21 dA	<u>CAGUCUGAUUAAGCU</u> dA	4940.3	4940.1
Anti-miR21 dA C3	<u>CAGUCUGAUUAAGCU</u> dA(C3)	5090.0	5090.6
Anti-miR21 1-EdR C3	<u>CAGUCUGAUUAAGCU</u> (1-EdR)(C3)	4980.9	4979.9
Anti-miR21 5'-1-EdR C3	(1-EdR) <u>CAGUCUGAUUAAGCU</u> (C3)	4980.9	4984.0
Anti-miR122 15mer	<u>CAUUGUCACACUCCA</u>	4878.9	4875.0
Anti-miR122 LNA/2'-O-Me mixmer, 1-EdR C3	<u>CATTGTCACACTCC</u> (1-EdR)(C3)	4925.9	4925.6

MALDI-TOF MS data of Anti-miR21 with t1 or t15 triazole modification bearing various substituents:

Anti-miR21 triazole sequence:		
5' – <u>CAGUCUGAUUAAGCU</u> (triazole)(C3) -3' or 5' – (triazole) <u>CAGUCUGAUUAAGCU</u> (C3) – 3'		
Substituent on anti-miR21 triazole	Calculated Mass (m/z)	Observed Mass [M-H]⁻ (m/z)
quinoline	5166.0	5164.1
chlorobenzene	5134.9	5135.0
1,4-difluorobenzene	5137.0	5136.4
piperidine amide	5149.0	5154.1
pentanoic acid	5125.0	5123.3
benzene	5099.5	5099.3
oxazolidine	5122.5	5123.5
pyridine	5102.0	5101.7
butanol	5097.0	5097.3
methyl furan	5118.0	5121.0
thiophene	5119.5	5120.0
fluorobenzene	5119.0	5117.0
methyl acetate	5096.0	5095.9
furan	5105.0	5104.8
bromothiophene	5198.9	5197.0
nitrobenzene	5146.0	5143.9
1,2-difluorobenzene	5137.0	5138.4
ethyl acetate	5109.9	5111.3
N-ethylacetamide	5108.9	5109.3
acetic acid	5069.0	5072.0

5' methyl acetate	5091.4	5096.0
5' ethyl acetate	5109.9	5109.7
5' N-ethylacetamide	5110.5	5108.9

MALDI-TOF MS data of Anti-miR122 2'-O-Me/LNA mixmer with t1 triazole bearing various substituents:

Anti-miR122 triazole sequence: 5' - <u>CATTGTCACACTCC</u> (triazole)(C3) – 3'		
Substituent on anti-miR122 triazole	Calculated Mass (m/z)	Observed Mass [M-H] ⁻ (m/z)
ethyl acetate	5055.0	5053.4
methyl furan	5063.0	5064.6
N-ethylacetamide	5054.0	5054.9

5'-biotinylated anti-miR21 sequences and MALDI-TOF MS data:

Oligonucleotide ID	Sequence (5'-3')	Calculated Mass (m/z)	Observed Mass [M-H] ⁻ (m/z)
5'-biotin anti-miR21 t1 dA C3	(Bi) <u>CAGUCUGAU AAGCU</u> dA(C3)	5388.4	5389.0
5'-biotin scramble sequence	(Bi) <u>ACCAUAUUCGGAU</u> dG(C3)	5496.5	5496.8
5'-biotin anti-miR21 triazole, t1 ethyl acetate	(Bi) <u>CAGUCUGAU AAGCU</u> (triazole)(C3)	5517.5	5515.1
5'-biotin anti-miR21 triazole, t1 N-ethylacetamide	(Bi) <u>CAGUCUGAU AAGCU</u> (triazole)(C3)	5516.5	5512.4
5'-biotin anti-miR21 triazole, t1 fluorobenzene	(Bi) <u>CAGUCUGAU AAGCU</u> (triazole)(C3)	5525.5	5525.3

3.3 Results

3.3.1 Improved potency of anti-miR21 by 3'-end triazole modifications in HeLa cells

Based on the computational screening results described in Chapter 2, seventeen 3'-end triazole-modified 15mer anti-miR21 oligonucleotides with different substituents were chosen out of fifty of the top-scoring docked ligands to be synthesized in the lab by copper(I)-catalyzed azide/alkyne cycloaddition (CuAAC) chemistry (**Figure 3.1A and B**). The ChemGauss4 scores (**Table 3.1**) for all seventeen triazoles selected were approximately 10- to 20-fold lower (more favorable docking) than 2'-deoxyadenosine (-0.2178) and had docked poses that were reasonably oriented towards the hAgo2 t1A-binding receptor. All the triazoles were generated at quantitative yields, as determined by PAGE, using commercially available azides and reagents with the precursor 15mer anti-miR21 with t1 1-EdR C3 modification (see **3.2.5** for CuAAC reaction procedure). After purification and characterization, the triazole-modified anti-miR21 oligonucleotides were then transfected into HeLa cells at a concentration range of 25 to 300 nM and potency was determined by the dual luciferase assay.

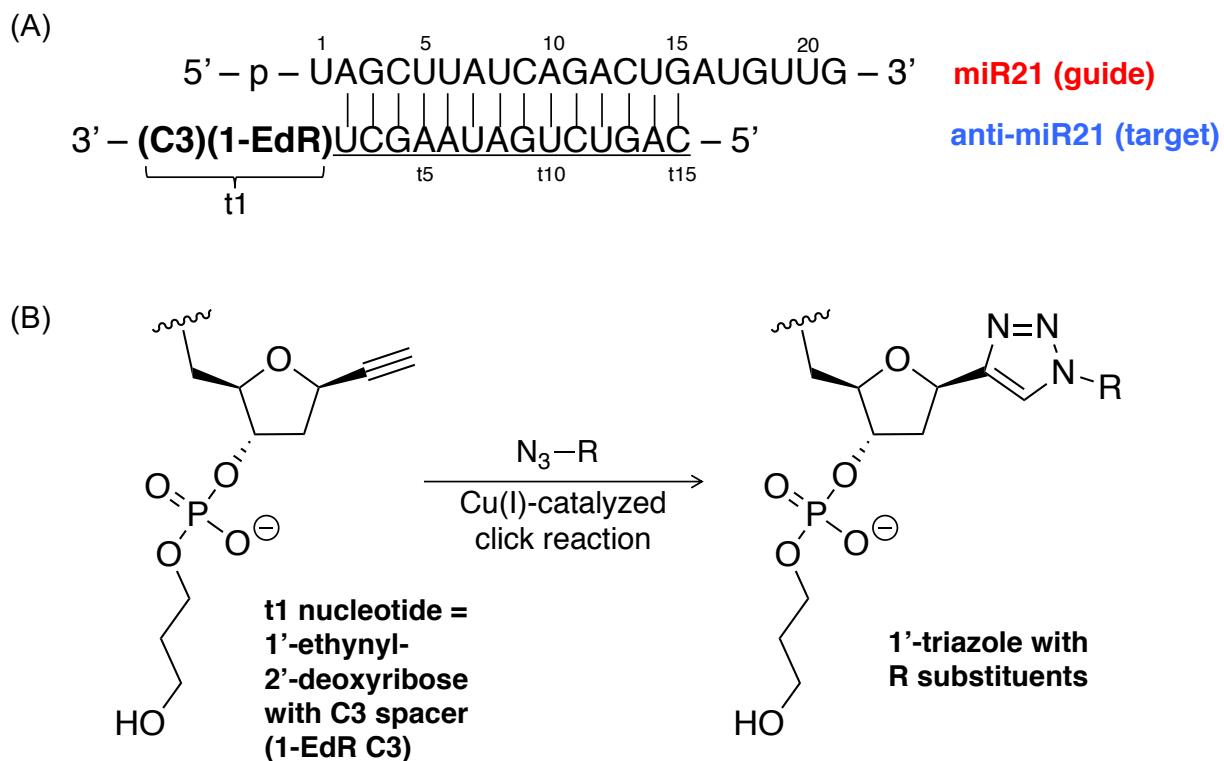
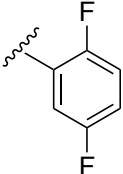
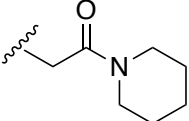
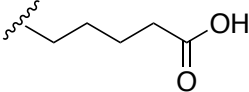
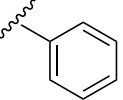
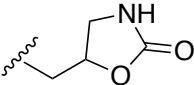
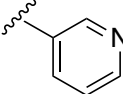
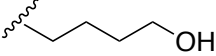
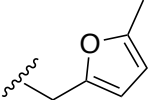
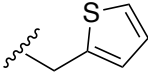
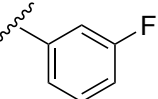
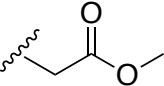
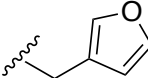
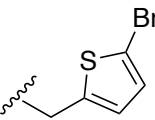
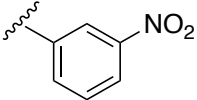
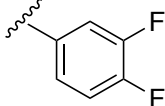
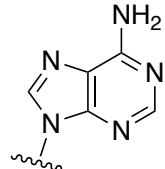


Figure 3.1 Design of 3'-end triazole-modified 15mer anti-miR21. (A) Sequence of miR21 guide and anti-miR21 sequences. Underlined = 2'-O-methylated; 1-EdR = 1'-ethynyl-2'-deoxyribose; C3 = C3 spacer. (B) Copper(I)-catalyzed azide/alkyne cycloaddition (CuAAC) reaction scheme on the t1 1-EdR C3 moiety to generate triazoles bearing R substituents.

Table 3.1 Triazoles tested for potency on 3'-end of 15mer anti-miR21.

Number	Triazole substituent name	Structure of triazole substituent	ChemGauss4 docking score
1	quinoline		-4.8338
2	chlorobenzene		-3.4750

3	1,4-difluorobenzene		-3.2672
4	piperidine amide		-3.0777
5	pentanoic acid		-2.9892
6	benzene		-2.8743
7	oxazolidine		-2.8354
8	pyridine		-2.8075
9	butanol		-2.8021
10	methyl furan		-2.7051
11	thiophene		-2.6758
12	fluorobenzene		-2.6706
13	methyl acetate		-2.6650
14	furan		-2.6633
15	bromothiophene		-2.5260
16	nitrobenzene		-2.3583

17	1,2-difluorobenzene		-2.3280
	2'-deoxyadenosine		-0.2178

At 150 and 300 nM, four anti-miR21 triazoles: thiophene, methyl furan, furan, and methyl acetate, showed an increase in miR-21 inhibitory activity in comparison to control anti-miR21 where the t1 nucleotide is 2'-deoxyadenosine (**Figure 3.2**). The thiophene, methyl furan, and furan triazole anti-miR21 showed a ~2.5- to 3-fold higher Renilla/firefly (RL/FF) luciferase ratio than adenine control at 150 and 300 nM. However, most strikingly, the triazole anti-miR21 bearing a methyl ester substituent was about 6- to 9-fold more potent at these concentrations. Structure activity relationships of the ester-modified anti-miR21 were therefore carried out to further explore the cause for its substantial increase in potency.

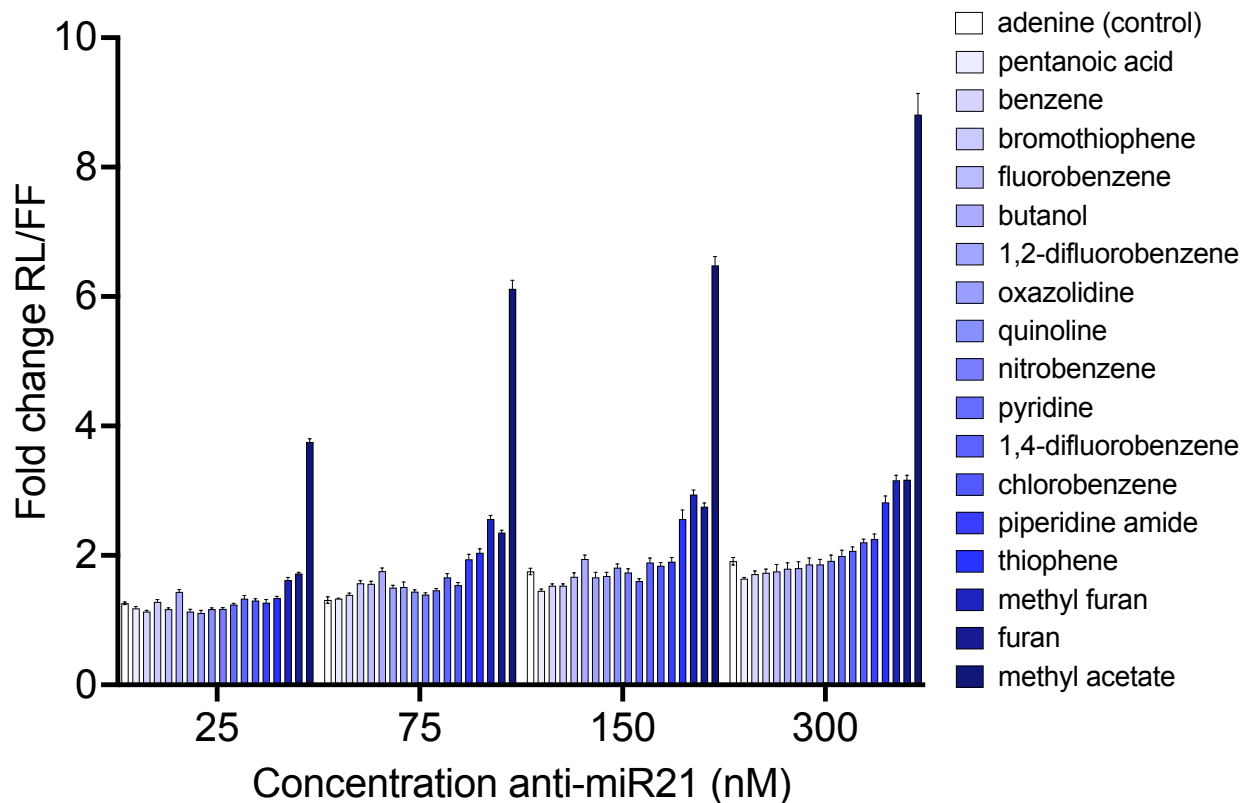


Figure 3.2 Potency profile of 3'-end triazole-modified anti-miR21 in HeLa cells. All bar plots, except for adenine control, are arranged in ascending fold change in Renilla/firefly (RL/FF) luciferase activity ratio at 300 nM anti-miR21 concentration and are normalized to no anti-miR21 control. Error bars are represented as a standard error of the mean (s.e.m.) from at least three biological replicates.

3.3.2 Structure activity relationships of ester functional group on 3'-end modified anti-miR21

Two approaches to explore the structure activity relationship of the 3'-end ester-modified anti-miR21 were employed (**Figure 3.3A**). One approach was to replace the methyl ester triazole substituent with other similar functional groups such as an ethyl ester, N-ethylacetamide, or acetic acid. The other approach was to determine the modification position dependence by instead modifying the 5'-end with the ester triazole and similar functional groups. From 25 to 300 nM, the ethyl acetate substituent, which extends the alkyl chain from the methyl acetate group by one carbon, increased the fold

change of RL/FF by 1- to 2-fold over the methyl acetate modification when applied at the 3'-end (**Figure 3.3B**). However, substituting the ester with an amide (N-ethylacetamide) or carboxylic acid (acetic acid) resulted in little to no improvement of activity over 3'-end 2'-deoxyadenine control (**Figure 3.3B**). Modifying the 5'-end of anti-miR21 with methyl and ethyl ester triazole resulted in a nearly 3- to 4-fold improvement in activity over 3'-end adenine control from 25 to 300 nM, respectively, whereas the N-ethylacetamide modification had equivalent activity (**Figure 3.3B**).

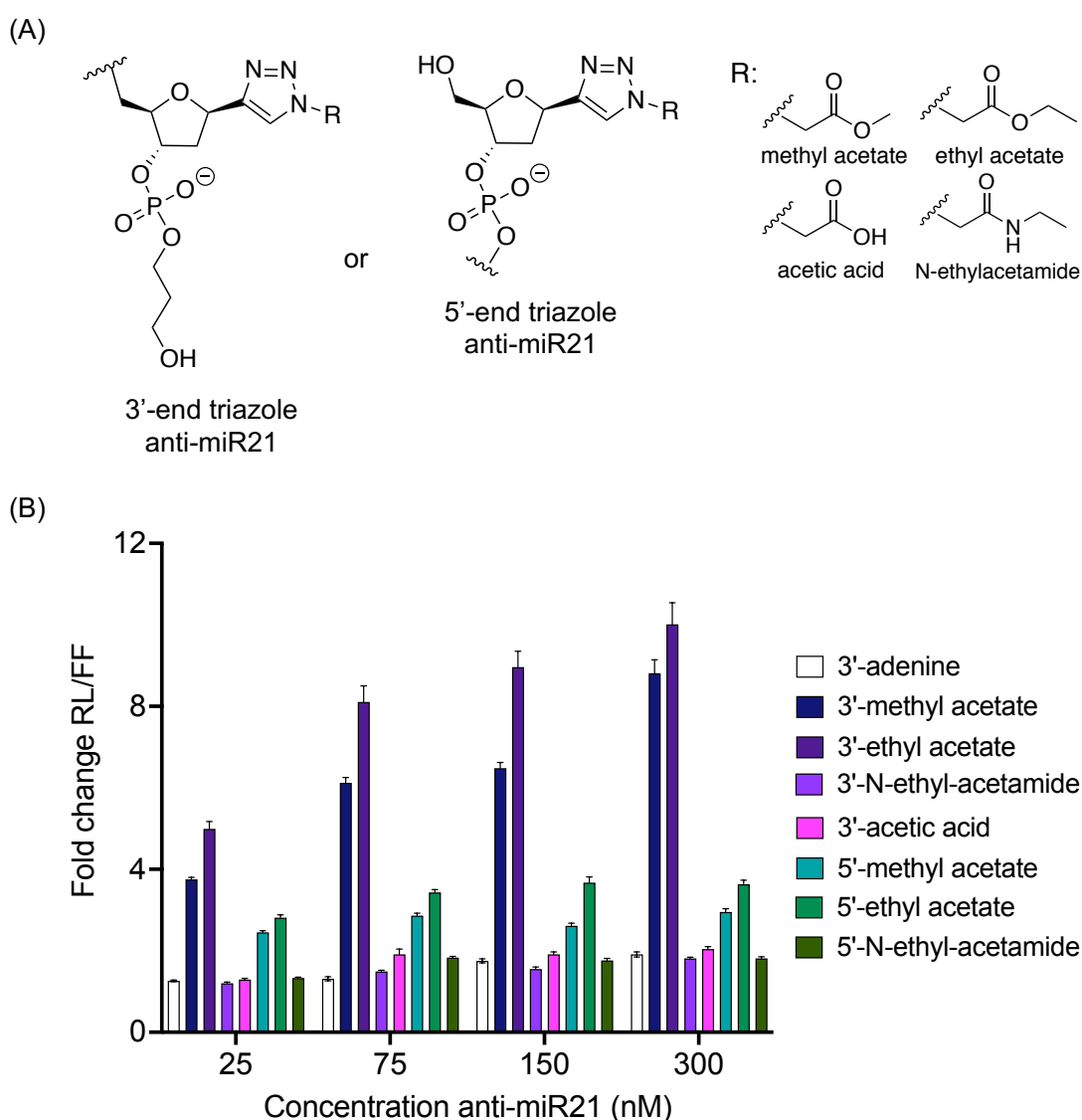


Figure 3.3 Structure activity relationship of 3'-end ester-modification on anti-miR21 in HeLa cells. (A) Potency profile of 3'- or 5'-end triazole modified anti-miR21. Bar plots are represented

as fold change in RL/FF ratio normalized to no anti-miR21 control. Error bars are represented as s.e.m. from at three biological replicates. (B) Structure of 3'- (t1) or 5'-end (t15) triazole modification bearing R substituents on anti-miR21.

3.3.3 Improved potency of anti-miR122 by 3'-end triazole modification in HuH-7 cells

Next, we wanted to determine the generalizability of 3'-end triazole modifications when applied onto other anti-miRs that would target different miRNAs. Thus, we pursued modifications on anti-miR122 that would be capable of de-repressing miR-122 targets in hepatocarcinoma HuH-7 cells.¹²⁻¹⁴ To start, fully 2'-O-methylated 15mer anti-miR122 was co-transfected with a miR-122 reporter plasmid in HuH-7 cells and was compared against transfected 15mer anti-miR21 with t1 2'-deoxyadenosine. No apparent improvement of activity was observed with either oligonucleotide from 25 to 300 nM (**Figure 3.4B**), indicating that the anti-miR122 may require more chemical modifications to improve metabolic stability and that anti-miR21 has specificity towards only a miR-21 target sequence.

(A) 5' – CAGUCUGAUAAGCdA – 3' anti-miR21
 5' – CAUUGUCACACUCCA – 3' anti-miR122

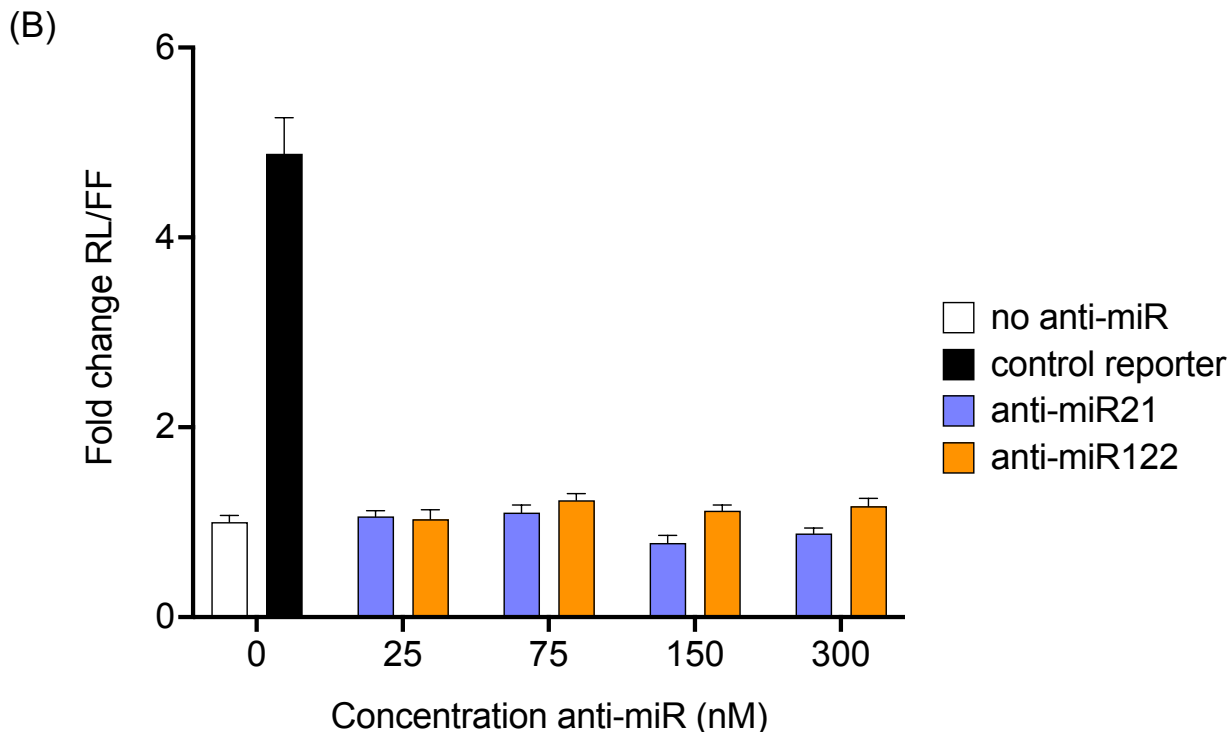


Figure 3.4 Potency of 2'-O-methylated anti-miR122 oligonucleotide in HuH-7 cells. (A) Sequence of anti-miR21 and anti-miR122 oligonucleotides. Underlined = 2'-O-methylated; dA = 2'-deoxyadenosine. (B) Potency profile of anti-miR122 in HuH-7 cells co-transfected with miR-122 reporter plasmid. Psi-CHECK2 plasmid without miR-122 target sequence (control reporter) in the Renilla luciferase 3'-UTR was transfected into HuH-7 cells as a control. Bar plots are represented as fold change in RL/FF activity ratio normalized to no anti-miR control with a ratio of 1. Error bars are represented as s.e.m. from three biological replicates.

The 2'-O-methyl uridine nucleotides in anti-miR122 were replaced with locked nucleic acid thymidine (LNA T) modifications to improve potency and metabolic stability (**Figure 3.5A**). LNA modifications are reported to improve anti-miR potency.¹⁵ Indeed, modifying anti-miR122 with LNA T and an ethyl ester or methyl furan triazole modification at the 3'-end resulted in a dose-dependent increase in potency from 0.25 to 5 nM concentration (**Figure 3.5B**). Furthermore, anti-miR122 with the 1'-ethynyl-2'-

deoxyribose plus C3 spacer modification at the t1 nucleotide (labeled as “ethyne” in **Figure 3.5**) or a triazole modification bearing an N-ethylacetamide substituent did not significantly increase potency. These results are in agreement with what was observed with 3'-end triazole-modified anti-miR21 in HeLa cells.

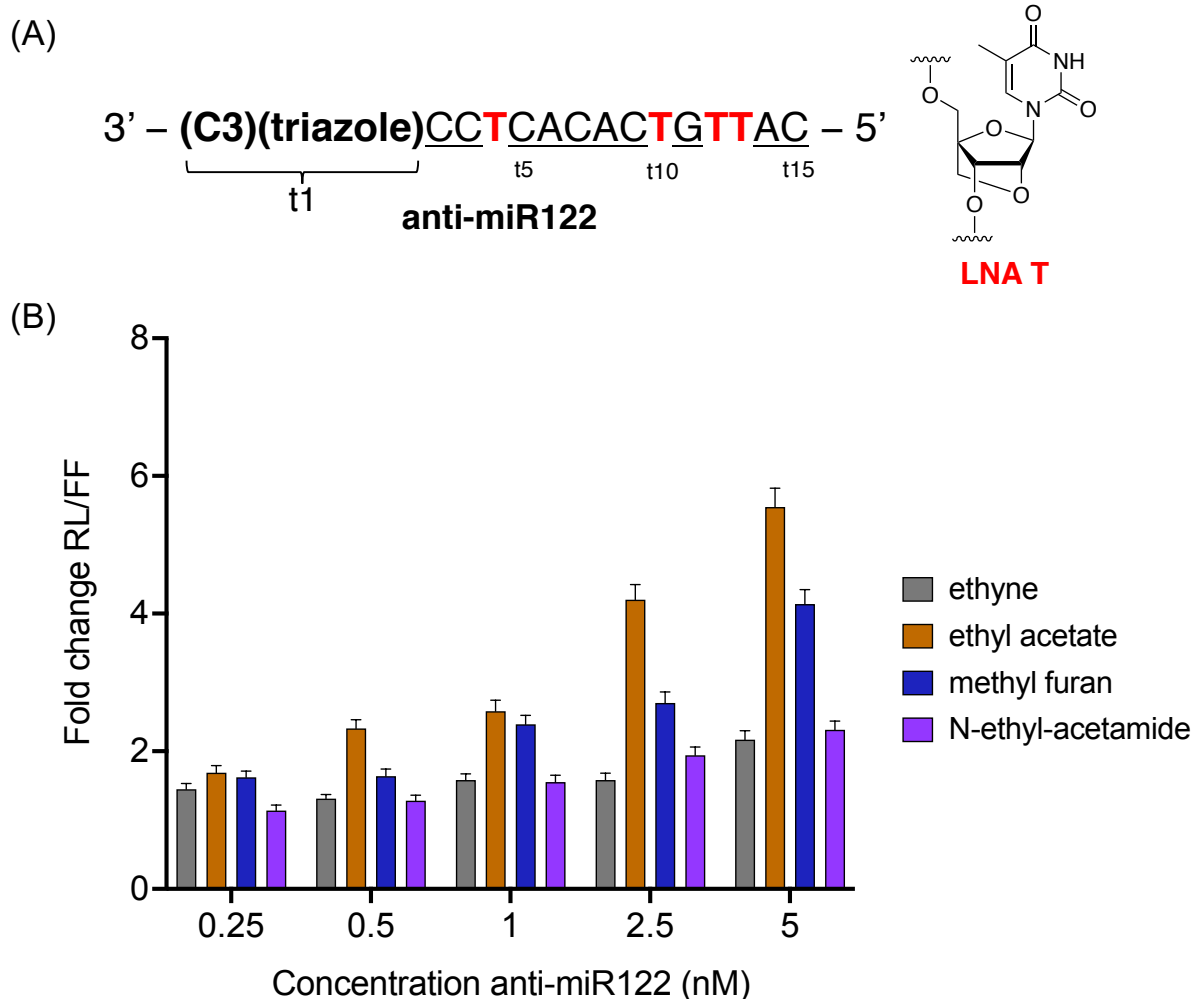


Figure 3.5 Potency profile of 3'-end triazole-modified anti-miR122 in HuH-7 cells. (A) Sequence of anti-miR122 oligonucleotide. 2'-O-methyl and locked nucleic acid thymidine (LNA T, structure on right) modified nucleotides are underlined and in bold red, respectively. (B) Potency profile of t1 triazole-modified anti-miR122 oligonucleotides in HuH-7 cells. Bar plots are represented as a fold RL/FF change normalized to no anti-miR122 control. Error bars are represented as s.e.m. from three biological replicates.

As follow-up, a control experiment was performed to evaluate the sequence specificity of ethyl ester triazole-modified anti-miR122 in HeLa cells transfected with miR-21 reporter plasmid. No increase in activity was observed from 6.25 to 30 nM anti-miR122, whereas anti-miR21 with the ethyl ester modification had a 2- to 4.5-fold increase in activity over no anti-miR control within this concentration range (**Figure 3.6B**), indicating that the highly-potent ethyl ester modification on anti-miR122 is specific towards a miR-122 target sequence. This result supplements what was observed in the contrary experiment in determining sequence specificity of anti-miR21 in HuH-7 cells with miR-122 reporter (**Figure 3.4**).

(A) 5' – CAGUCUGAUAAGCU(e.a.)(C3) – 3' anti-miR21 ethyl acetate
 5' – CATTGTCACACTCCA(e.a.)(C3) – 3' anti-miR122 ethyl acetate

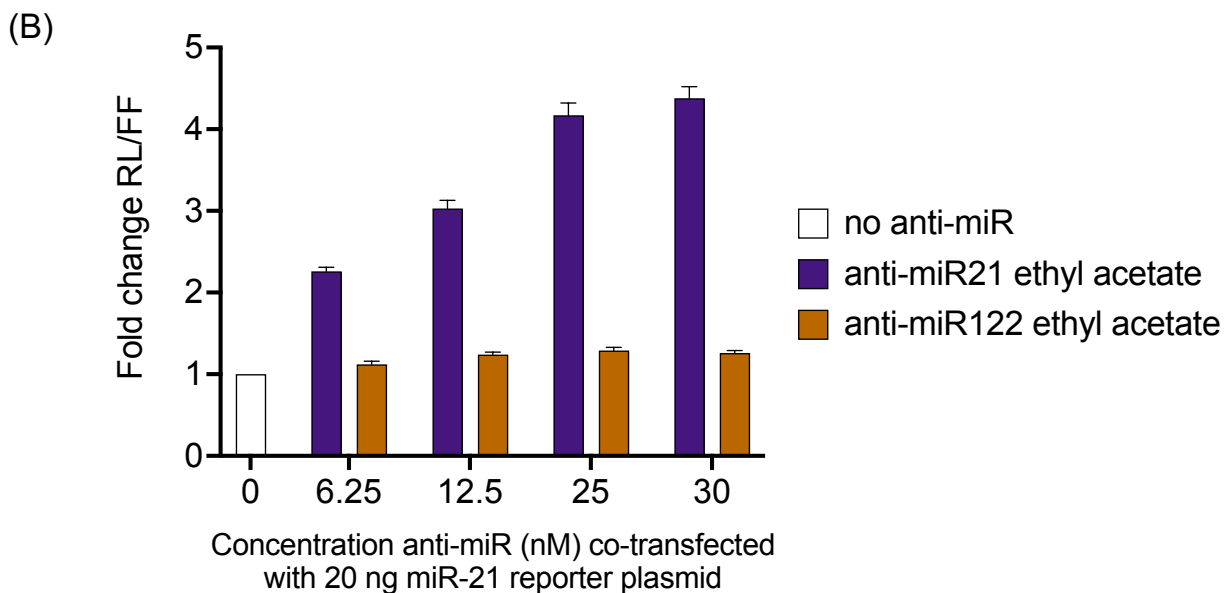


Figure 3.6 Potency selectivity comparison of anti-miR21 to anti-miR122 in HeLa cells. (A) Sequence of ethyl acetate-modified anti-miR21 and anti-miR122 oligonucleotides. Underlined = 2'-O-methylated; e.a. = ethyl acetate triazole modification; C3 = C3 spacer; Bold = locked nucleic acid. (B) Potency profile of ethyl acetate-modified anti-miR21 and anti-miR122 in HeLa cells co-transfected with 20 ng miR-21 reporter plasmid.

3.3.4 Exonuclease resistance assay of 3'-end triazole-modified anti-miR21

Next, snake venom phosphodiesterase (SVPD) assays were carried out to evaluate the effect of 3'-end triazole-modified anti-miR21 oligonucleotides on nuclease resistance. After 37 °C incubation in 0.01 U/mL SVPD for up to 48 h, the control 15mer 2'-O-methylated anti-miR21 with t1 2'-deoxyadenosine and C3 spacer was completely degraded to shorter products (**Figure 3.7**). Interestingly, all the other oligonucleotides in the assay showed a substantial degree of SVPD resistance, including anti-miR21 bearing the precursor 1'-ethynyl modification and 1'-triazole with chlorobenzene or N-ethylacetamide substituents that did not improve anti-miR potency (**Figure 3.7**). An explanation to this result could be that the C-nucleoside nature at the t1 nucleotide of these modified anti-miR21 may reduce recognition by 3'-exonuclease, thus improve metabolic stability.¹⁶

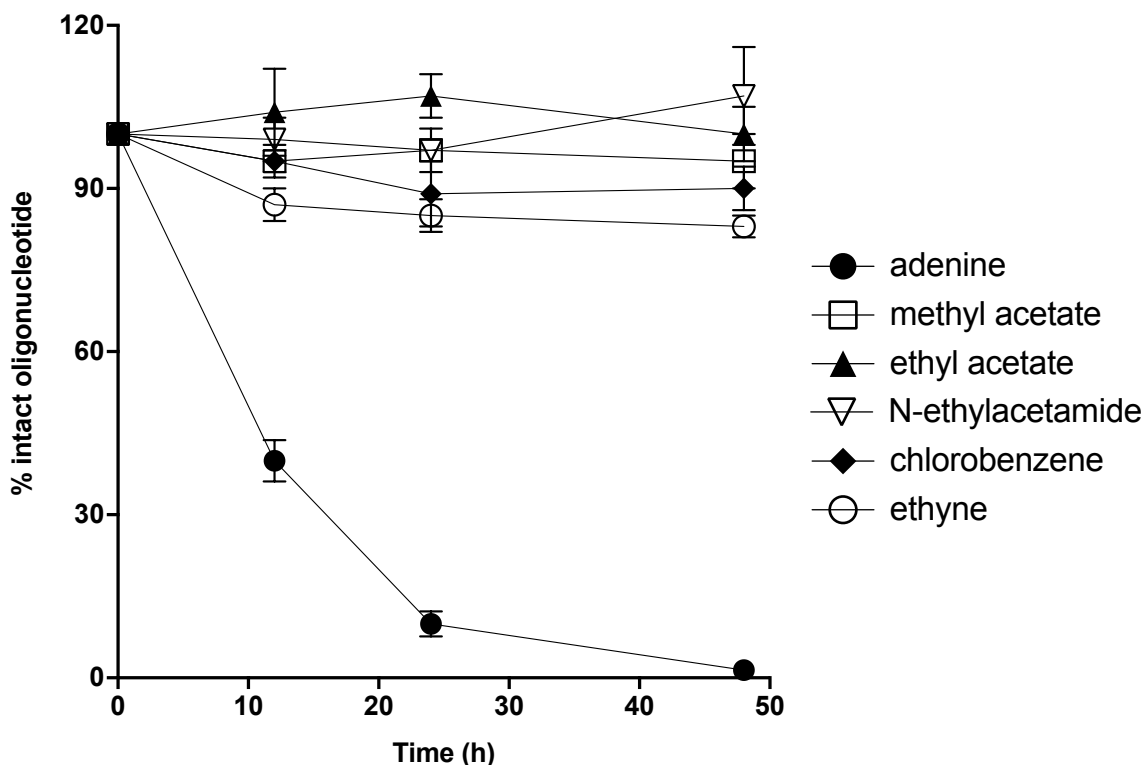


Figure 3.7 Decay curve of 3'-end triazole-modified anti-miR21 in snake venom phosphodiesterase (SVPD). Error bars represent as a standard deviation from three SVPD assay replicates.

3.3.5 Biotin pulldown of miR-21-loaded hAgo2 using 3'-end modified anti-miR21 to assess binding affinity

Pulldown assays of hAgo2 loaded with miR-21 using 5'-biotinylated anti-miR21 were then conducted to evaluate the correlation of improved activity of 3'-end ester-modified anti-miR21 with increased binding affinity to the t1A-binding pocket of hAgo2. hAgo2 was overexpressed in HEK293T cells transfected with miR-21 mimic duplex and captured with 5'-biotinylated anti-miR21 containing 3'-end modifications and streptavidin-coated magnetic beads, then eluted to detect hAgo2 protein levels by western blotting (**Figure 3.8A**). Anti-miR sequence specificity of this assay was confirmed by quantifying a lower amount of hAgo2 pulled down by scramble sequence 5'-biotin anti-miR21 in comparison to t1 adenine anti-miR21 (**Figure 3.8B and C**). However, inconsistent levels

of hAgo2 were pulled down by anti-miR21 bearing the potent ethyl ester triazole modification and ineffective N-ethylacetamide and fluorobenzene substituents (**Figure 3.8B and C**), suggesting that this assay may be too insensitive for adequately quantifying changes in binding affinity to hAgo2 or requires further optimization.

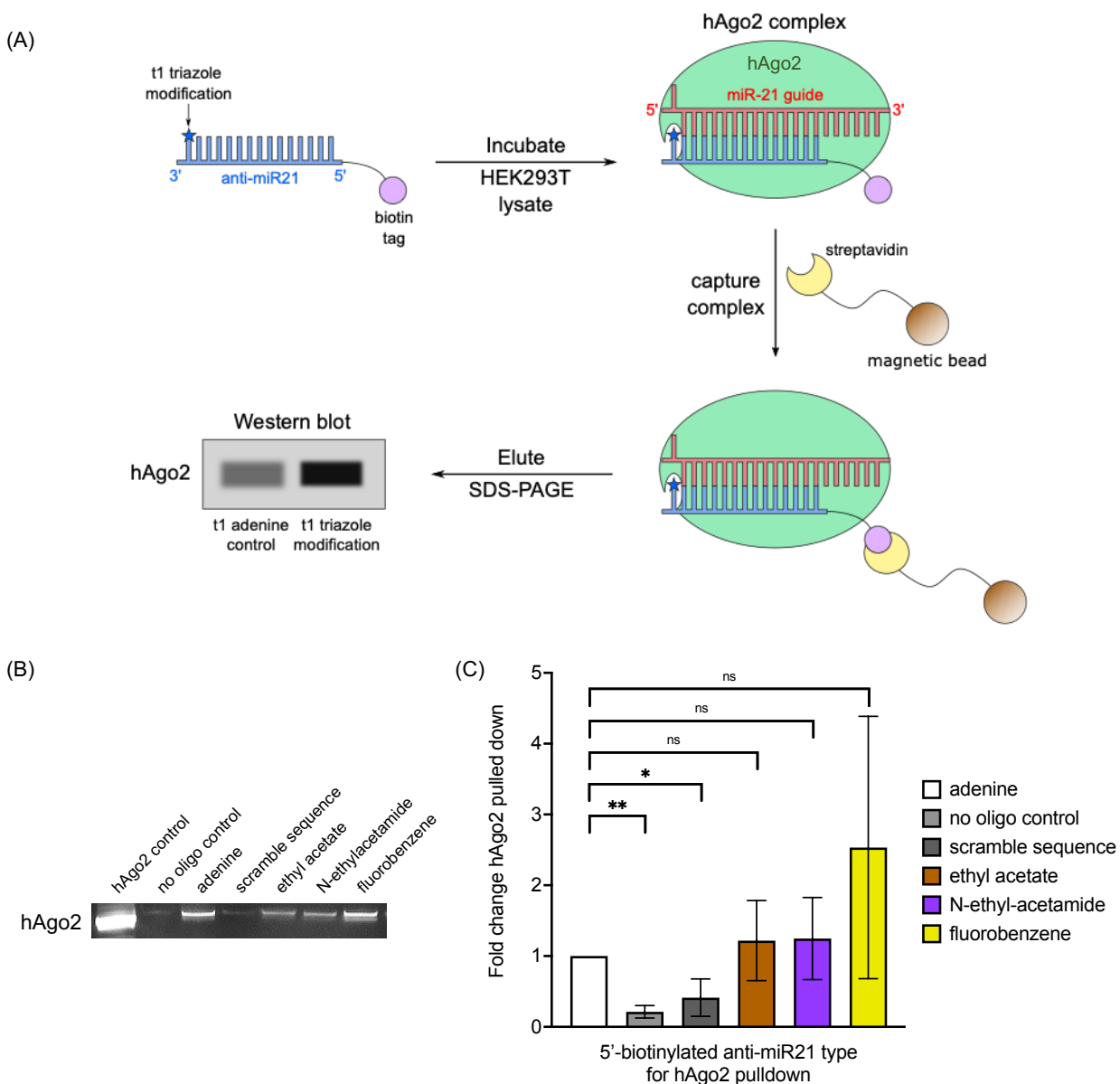


Figure 3.8 5'-biotin anti-miR21 pulldown of miR-21 guide-loaded hAgo2. (A) Workflow schematic of 5'-biotinylated anti-miR21 pulldown of hAgo2 from HEK293T lysate. (B) Representative western blot of hAgo2 protein from pulldown assay. hAgo2 control is from 10 μ g HEK293T lysate overexpressed with hAgo2. (C) Bar plot of fold change pulled down hAgo2 protein detected by western blotting. Statistical significance between groups was determined using an unpaired, one-tailed *t*-test with Welch's correction: * $P \leq 0.05$; ** $P \leq 0.01$; ns, not

significant. Error bars represent the standard deviation of fold change hAgo2 from three biological replicates.

3.3.6 Analyses of 3'-end modified anti-miR21-induced changes in endogenous miR-21 target gene regulation

Two endogenous miR-21 target transcripts, Programmed Cell Death 4 (PDCD4) and tumor necrosis factor α (TNF α), were evaluated for changes in regulation in the presence of 3'-end modified anti-miR21 in HeLa cells (**Table 3.2**).^{17,18} PDCD4 is reported to be downregulated by upregulated levels of miR-21 in HeLa cells whereas TNF α is upregulated. Anti-miR21 treatment is therefore expected to increase and decrease levels of PDCD4 and TNF α , respectively (**Table 3.2**).¹⁷⁻¹⁹

To detect changes in PDCD4 protein expression, HeLa cells were treated with 150 or 300 nM of 3'-end triazole-modified 15mer anti-miR21 with ethyl acetate or fluorobenzene substituents alongside controls that include t1 adenine, a fully 2'-O-methylated 22mer anti-miR21 (used in experiments described in Chapter 2), and a 2'-O-methylated 15mer scramble sequence oligonucleotide (**Figure 3.9A and B**). Surprisingly, at 150 nM, both 22mer anti-miR21 and scramble sequence controls seemed to increase PDCD4 expression by 0.5-fold, while the ethyl ester triazole-modified anti-miR21 decreased expression by about 0.25-fold (**Figure 3.9C**). Adenine and fluorobenzene anti-miR21-transfected samples had nearly equal levels of PDCD4 expression to no anti-miR control. On the other hand, the ethyl ester triazole-modified anti-miR21 seemed to increase PDCD4 expression at an equivalent level to 22mer control at 300 nM. Additionally, fluorobenzene anti-miR21-treated samples increased expression slightly and scramble sequence control reduced expression to near equivalent levels of no anti-miR control samples (**Figure 3.9C**). Similar to the results determined with the hAgo2

pulldown assay, PDCD4 protein expression changes in HeLa cells upon treatment with 3'-end modified anti-miR21 were overall minimal.

Table 3.2 Endogenous miR-21 targets in HeLa cells for analyses upon anti-miR21 treatment.

Target gene	Function	Regulation by miR-21	Expected change upon anti-miR21 treatment
PDCD4	Tumor suppressor; inhibits cell growth, tumor invasion, metastasis, and inducing apoptosis	Downregulated	Increase
TNF α	Pro-inflammatory cytokine (cell signaling); cell survival, proliferation, differentiation, and death	Upregulated	Decrease

(A) 5' – CAGUCUGAUAAAGCUdX(C3) – 3' 15mer anti-miR21
 5' – UCAACAUCAGUCUGAUAAAGCUA – 3' 22mer anti-miR21

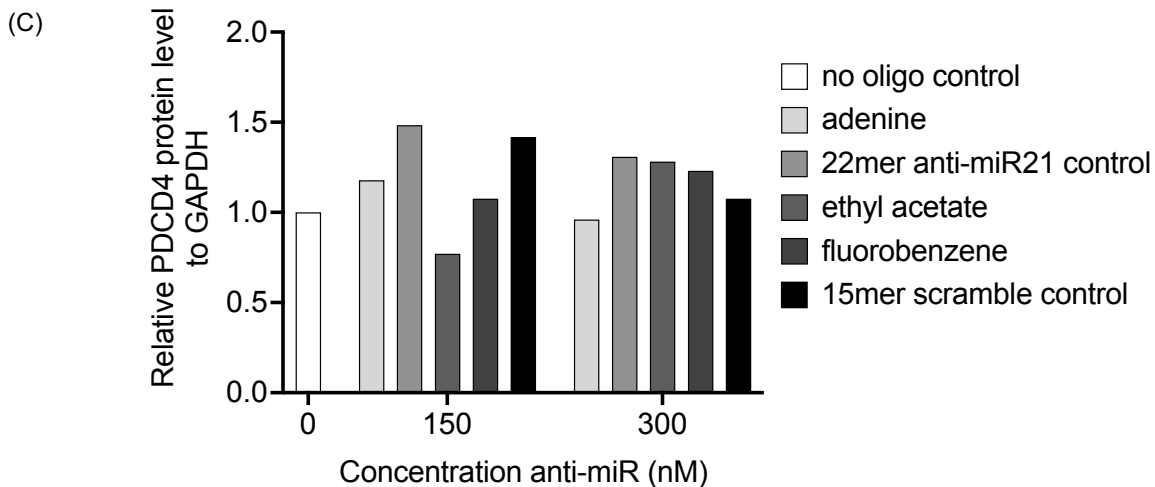
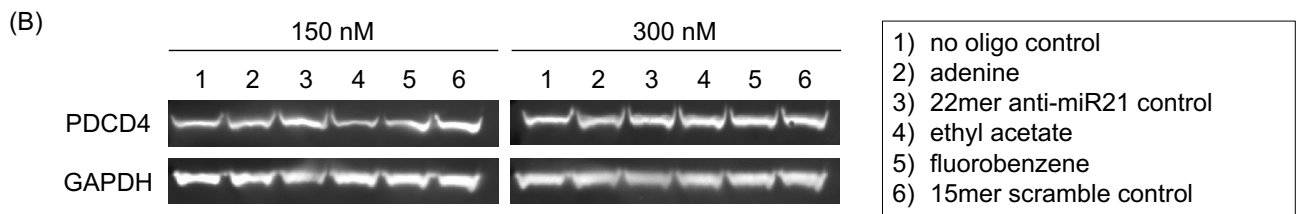


Figure 3.9 Protein expression analysis of PDCD4 from HeLa cells treated with 3'-end modified anti-miR21. (A) Sequence of 15mer and 22mer anti-miR21 oligonucleotides. Underlined = 2'-O-methyl ribose; d = 2'-deoxy; Bold X = adenosine, ethyl acetate triazole, or fluorobenzene triazole modification; C3 = C3 spacer. (B) Western blot of PDCD4 from HeLa cell lysate transfected with anti-miR21. (C) Bar plot of relative PDCD4 protein level to GAPDH from HeLa cells transfected with anti-miR21 oligonucleotides.

Furthermore, PDCD4 mRNA levels generally did not change when HeLa cells were treated with 3'-end modified anti-miR21 (**Figure 3.10A**). A fully LNA-modified, highly potent 9mer anti-miR21 oligonucleotide (used in experiments described in Chapter 2), however, increased relative PDCD4 mRNA expression by up to about 1.5-fold at 100 nM (**Figure 3.10B**). Interestingly, all oligonucleotides tested reduced TNF α mRNA at 300 nM, where the ethyl ester and fluorobenzene triazole-modified anti-miR21 decreased TNF α mRNA by nearly 0.5-fold (**Figure 3.10C**). Yet, when the concentration was doubled to 600 nM, TNF α levels returned to base level relative to scramble sequence control (**Figure 3.10C**).

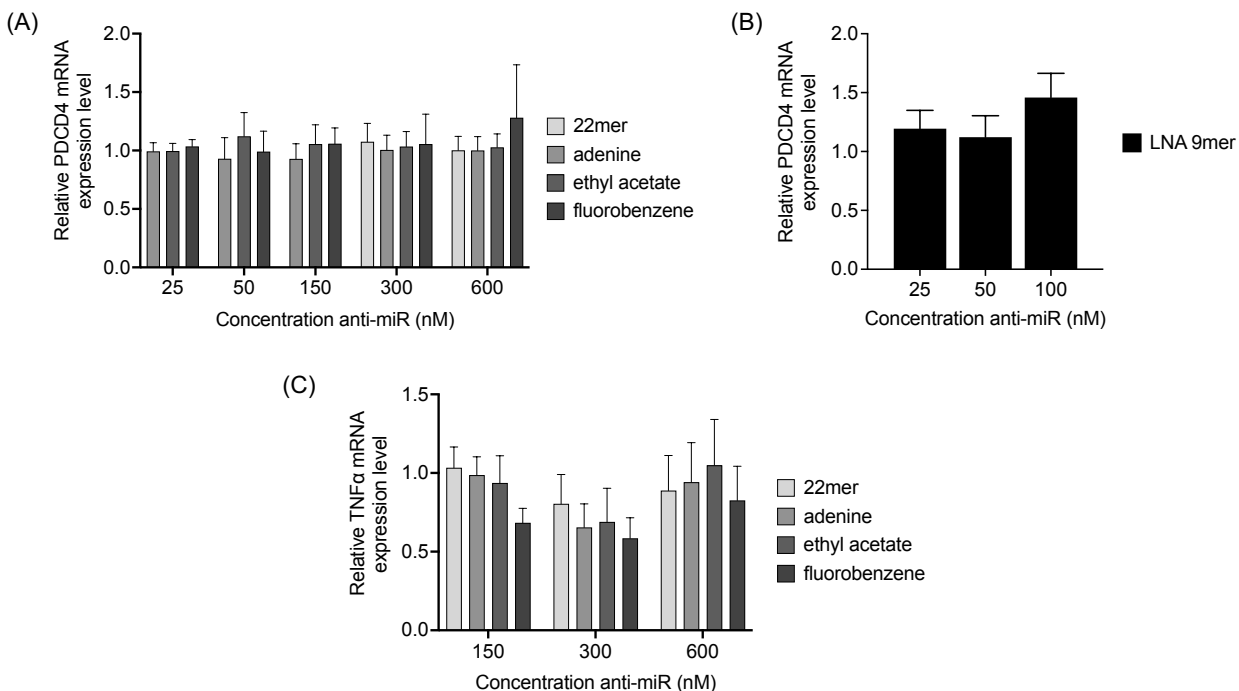


Figure 3.10 RT-qPCR analysis of endogenous miR-21 targets in HeLa cells treated with anti-miR21. (A) Bar plot of relative expression level of PDCD4 mRNA to GAPDH from samples treated with 22mer or 15mer anti-miR21. (B) Bar plot of relative expression level of PDCD4 mRNA to GAPDH from samples treated with a fully LNA-modified 9mer anti-miR21. (C) Bar plot of relative expression of TNF α mRNA to GAPDH from samples treated with 22mer or 15mer anti-miR21. All bar plots are normalized to a 15mer scrambled sequence oligonucleotide control. Errors are represented as a standard deviation from triplicate RT-qPCR runs.

3.3.7 Transfection efficiency of anti-miR oligonucleotide by fluorescence microscopy

In response to the inconsistent results of miR-21 target gene repression or de-repression observed above, anti-miR transfection efficiency was qualitatively assessed by transfecting HeLa cells with cyanine 3 (Cy3) conjugated anti-miR scramble sequence control. It is apparent that the abundance of Cy3-conjugated anti-miR transfected into HeLa cells increases as the concentration is raised from 25 to 100 nM, as seen in the “Cy3” column of fluorescent cell microscope images (**Figure 3.11**). When the DAPI (nuclei-stained), Alexa Fluor 488, and Cy3 images are merged together, it can be seen that the Cy3-conjugated anti-miR predominantly overlaps with the Alexa Fluor 488-stained regions of HeLa cells (**Figure 3.11**). This result indicates that transfection was highly efficient and transfected anti-miR by lipid nanoparticle reagents is localized in the cytoplasm.

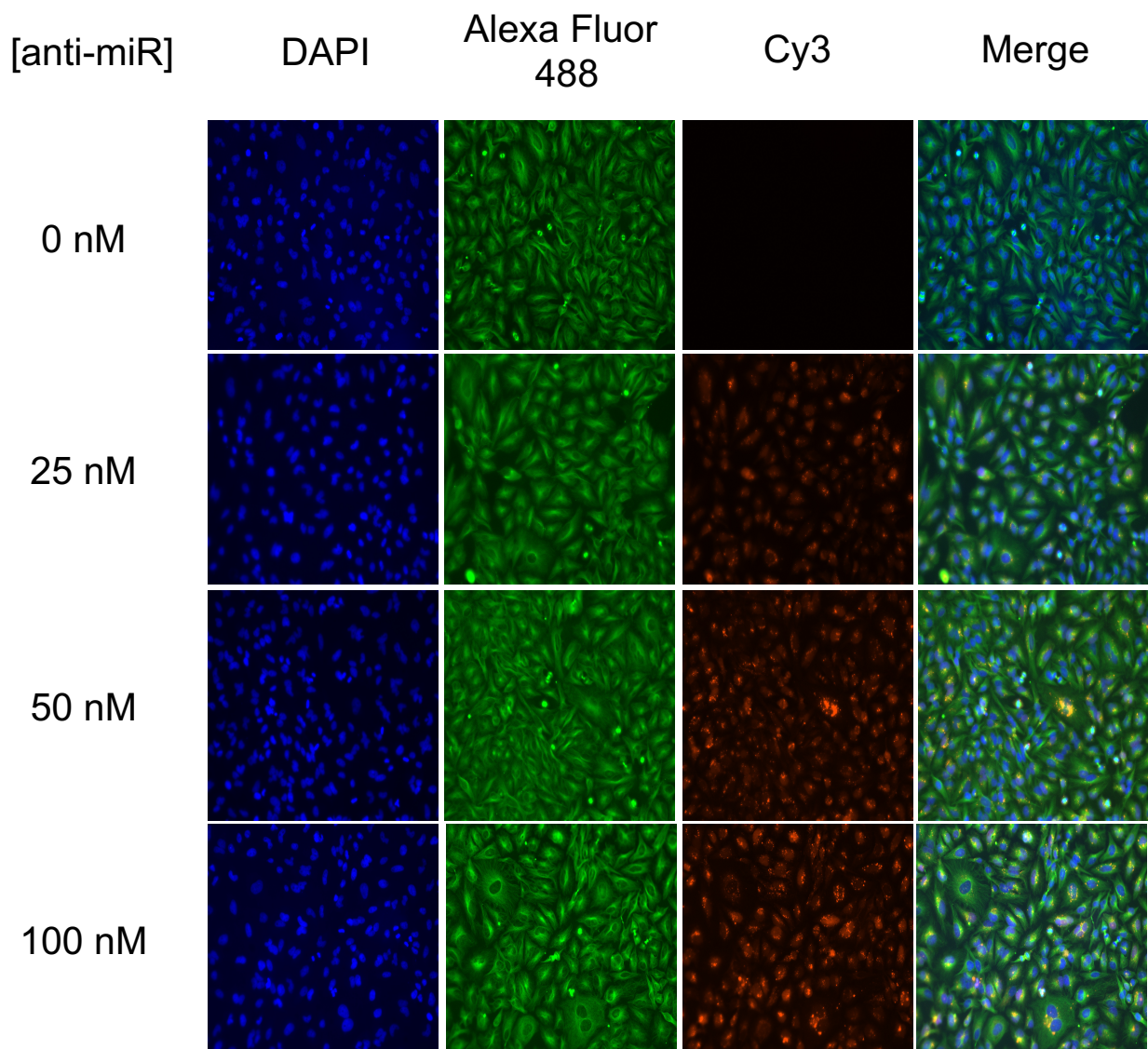


Figure 3.11 Fluorescence microscopy of HeLa cells transfected with Cy3-conjugated anti-miR. DAPI (4',6-diamino-2-phenylindole) fluorescent cube setting was used to detect nuclei staining. Alexa Fluor 488 fluorescent dye, conjugated to alpha tubulin antibody cytosolic marker, was detected by GFP (Green Fluorescent Protein) fluorescent cube setting. Cyanine 3 (Cy3) dye was detected by RFP (Red Fluorescent Protein) fluorescent cube setting. All three images at each respective concentration were merged in the right column.

3.3.8 Protein expression of poly-Histidine-tagged full-length hAgo2 in *Saccharomyces cerevisiae* BCY123 cells

Lastly, recombinant, poly-Histidine-tagged full-length human Ago2 was expressed in *Saccharomyces cerevisiae* BCY123 strain cells to be used for future hAgo2 filter binding assays, as done by Schirle and colleagues.^{11,20,21} Our research group

established a robust method, based on methodology written by Macbeth and Bass, in expressing and purifying ADAR protein in *S. cerevisiae* cells for biochemical and crystallographic studies.^{8,22–25} A poly-Histidine (10xHis), TEV (tobacco etch virus) protease-tagged hAgo2 gene was cloned in the pSc expression vector then transformed into BCY123 cells (see 3.2.7). The BCY123 cells were grown, induced by galactose, then lysed by glass beads to detect expression of hAgo2 by western blotting (see 3.2.13). Although not as abundant as full-length 10xHis-tagged ADAR2 protein, expression of hAgo2 was moderate in 10 to 30 µg of yeast cell lysates (**Figure 3.12**).

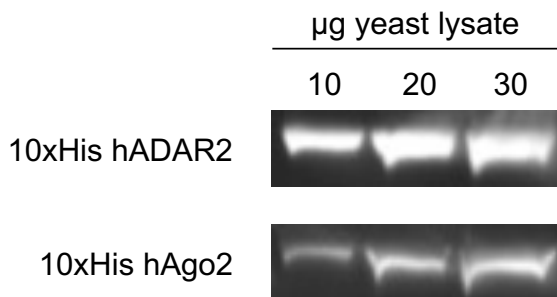


Figure 3.12 Western blotting detection of polyhistidine-tagged human ADAR2 and Ago2.

3.4 Discussion

Chemical modifications on anti-miRs are typically applied on the sugar and phosphate backbone to improve metabolic stability, binding affinity to a miRNA strand, and to minimize off-target effects.^{26,27} Aside from our publication in *Bioorganic and Medicinal Chemistry Letters*, no other reports suggest designing hAgo2 structure-guided chemical modifications in place of or at the nucleobase of anti-miRs. We designed triazole modifications at the 3'-end of two anti-miRs using copper(I)-click chemistry that were guided by a computational screening approach of docking triazole-modified nucleotides into the t1A-binding pocket of hAgo2, as described in Chapter 2. Using cell-based dual luciferase assays, three 1'-triazoles bearing structurally similar heterocyclic substituents (furan, methyl furan, and thiophene) imparted a modest, ~3-fold increase in activity at 300 nM when applied at the t1 nucleotide of anti-miR21 and compared against anti-miR21 with t1 adenine control (**Figure 3.2**). Surprisingly, however, a methyl ester-substituted triazole anti-miR21 at the t1 nucleotide resulted in a substantial, upwards of 9-fold higher anti-miR activity when transfected into HeLa cells at 300 nM (**Figure 3.2**). Thus, multiple experiments and analyses addressing different parameters were conducted to elucidate the mechanism behind the highly active ester triazole-modified anti-miR.

To start, it is important to note that although we were successful in identifying a highly active anti-miR21 using our chemical modification strategy, we could not clearly demonstrate that better molecular docking scoring was directly correlated with higher potency, based on the implication that the docked ligand has improved non-covalent interactions towards the t1A hAgo2 pocket receptor (**Table 3.1**). The methyl ester triazole

ligand gave a ChemGauss4 score of -2.6650, which was actually lower than methyl furan and thiophene with scores of -2.7051 and -2.6758, respectively. Nonetheless, this computational screening approach allowed us to identify some patterns that could be used for future 3'-end triazole modification strategies. For one, it is apparent that smaller, heterocyclic triazole substituents such as thiophene and furan are favorable to improving anti-miR activity at the 3'-end. Interestingly, a methylated furan (methyl furan) substituent is tolerated and exhibited nearly equivalent activity as furan, whereas a brominated thiophene (bromothiophene) substituent scored decently, but did not improve activity comparatively to thiophene. These results suggest that alkylation on these compounds are tolerated while halogenation is not. A methylated thiophene and brominated furan azide were not commercially available, therefore was omitted from computational and potency screening. The second pattern identified from the screening approach is the highly improved activity by particularly small esters. No other large esters that were docked in this study (e.g. ligands 17, 94, or 186) scored well and would presumably not have shown improvement in anti-miR activity. The ethyl acetate ligand did not rank in the top 50 compounds from the computational screening approach, unlike methyl acetate, but nonetheless scored far better than the larger esters docked and was even more potent than methyl acetate. A closer examination of the scores and ranking of the docked triazole ligands can be found in the Appendix section of this dissertation.

Structure activity relationship analyses were then conducted to determine the specificity of the ester substituent by either replacing the methyl ester with other similar functional groups or testing activity at the 5'-end of anti-miR21 (**Figure 3.3A**). An ethyl ester triazole-modified anti-miR21 slightly improved activity over methyl ester, while an

N-ethylacetamide substituent showed no improvement (**Figure 3.3B**). Additionally, we hypothesized that the methyl ester could be hydrolyzed after endosomal uptake into HeLa cells, resulting in a free acid that could introduce electrostatic interactions with the t1A-binding hAgo2 pocket.²⁸ A 3'-acetic acid triazole anti-miR21 however, did not improve activity from 25 to 300 nM (**Figure 3.3B**). Further testing, such as using a propyl ester triazole modification, would need to be conducted to better understand the small enhancement of activity by the ethyl ester substituent.

Modifying the 5'-end of anti-miR21 with methyl and ethyl ester triazoles resulted in an improved activity that had a similar trend to what was seen with 3'-end modified anti-miR21 but at a lower magnitude (**Figure 3.3B**). It is still unclear how the activity can be improved when ester-modified at the 5'-end. Upon structural analysis of the t16 nucleotide in the crystal structure of hAgo2 with bound duplex guide and seed-plus-supplementary target RNA extending beyond the seed region, we noticed that the amino group from the Lys65 residue may provide hydrogen bonding interactions towards the carbonyl oxygen group of cytosine (**Figure 3.13**).²⁹ The 5.8 Å distance of this hydrogen bond is quite distant, however. Nonetheless, a similar interaction could perhaps be occurring at this site if a carbonyl oxygen from a methyl or ethyl ester 1'-triazole modified t16 nucleotide can hydrogen bond with Lys65, therefore contributing to improved anti-miR activity. Note that inserting a nitrogen atom between the carbonyl and the alkyl group to generate the N-ethylacetamide modification at either end of anti-miR did not increase activity, suggesting that atom placement can shift the positioning of the alkyl group and dramatically interfere with potential interactions towards hAgo2. Another possibility is the

ester functional group is susceptible to reaction by a nucleophilic residue whereas an amide is not.

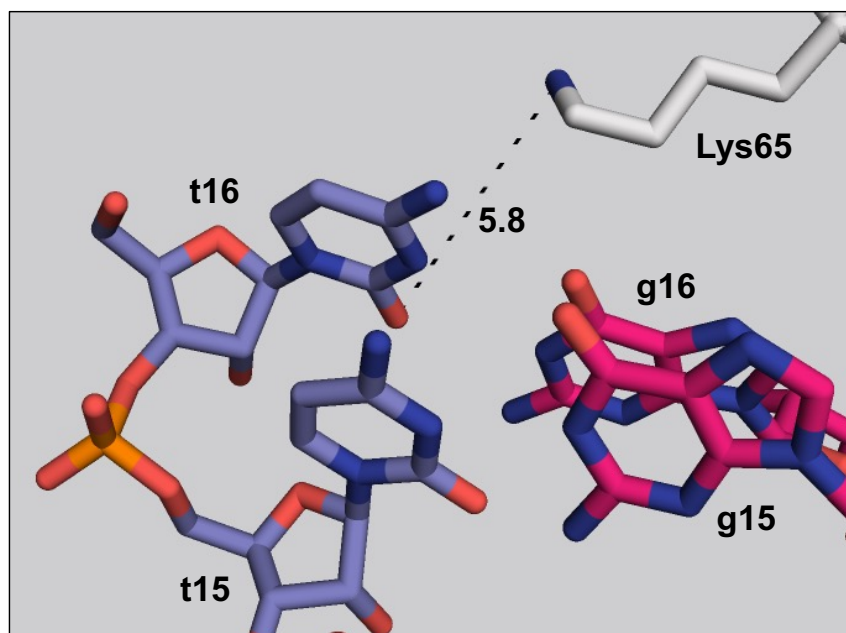


Figure 3.13 Close up of target RNA nucleotide 16 (t16) interaction in hAgo2 crystal structure complexed with guide-target RNA duplex (PDB: 6N4O). A possible hydrogen bonding interaction between the side chain of Lys65 and cytosine base on t16 nucleotide is shown as a dashed black line with a measured distance of 5.8 Å.

Next, we successfully established that the potent 3'-end ester modification can be reproducible and generalizable when applied to an anti-miR122 sequence. Interestingly, adding LNA modifications was necessary to improve potency to a degree where a dose-dependent increase of activity by an ethyl ester modification could be observed (**Figure 3.5A and B**). Furthermore, we found that methyl furan triazole-modified anti-miR122 had slightly higher activity than when modified on anti-miR21 (**Figures 3.2 and 3.5B**). Differences in miR-122 abundance in HuH-7 cells compared to miR-21 in HeLa cells as well as duplex stability of anti-miR122 towards a miR-122 target strand could account for this slight variation in methyl furan activity. Sequence specificity experiments in either HeLa or HuH-7 cells with miR-21 or miR-122 reporter plasmids, respectively, furthermore

confirmed that improvement of triazole-modified activity was not limited to anti-miR21 sequences (**Figures 3.4A-B, and 3.6A-B**).

Snake venom phosphodiesterase (SVPD) assays were conducted to rule out if the high potency of 3'-end ester-modified anti-miR21 oligonucleotide was solely due to improved nuclease resistance. Indeed, all modifications tested, including 1'-ethynyl precursor and fluorobenzene and N-ethylacetamide triazole anti-miR21 that did not improve activity, demonstrated a significant increase in 3'-exonuclease resistance over 48 hours in comparison to t1 adenine anti-miR21 control (**Figure 3.7**). As mentioned above, the C-nucleoside structure of the 1'-ethynyl or 1'-triazole modification in combination with a 3'-end C3 spacer at the t1 nucleotide is likely not recognized by 3'-exonucleases. This nuclease-resistant chemical modification pattern could be beneficial for designing oligonucleotides intended for other areas of research in our laboratory – RNA editing oligonucleotides, for example.^{25,30} Supplementary SVPD assays for 3'-end modified anti-miR122 sequences could further confirm the validity of using 3'-end ester triazole modifications as well.

A pulldown assay with 5'-biotinylated anti-miR21 bearing different 3' end modifications and human cell lysates containing miR21-loaded hAgo2 (**Figure 3.8A**) was then used with the goal of determining if improved potency was correlated with increased binding towards miRNA-loaded hAgo2. However, while the assay results clearly indicated that the modified anti-mR21 oligonucleotides bound miR21-loaded hAgo2 (i.e. a scrambled sequence control showed less hAgo2 pulled down), no differences were observed between the anti-miRs with different 3' end modifications (**Figure 3.8B and C**). Thus, we still have not unequivocally established that the novel 3' end modifications

described here increase hAgo2 binding affinity. It is possible that the hAgo2 affinity differences for the differently modified anti-miRs are too small to be observed with this assay system or the differences in anti-miR activity observed here arise from effects other than changes in binding affinity to hAgo2. The improved activity could come from a variety of other sources including improved binding to other human Argonaute proteins with structurally similar t1-binding pockets (e.g. hAgo1).³¹

Anti-miR transfection efficiency could be another source of variability when observing improved anti-miR activity by 3'-end modification. However, we determined that control Cy3-conjugated anti-miRs were efficiently transfected in a dose-dependent manner in HeLa cells (**Figure 3.11**). Given this, it is unclear to what degree 3'-end modified anti-miR21 can inhibit endogenous miR-21 in cells, based on our work in quantifying regulatory changes of miR-21 target genes such as PDCD4 and TNF α (**Figure 3.9 and 3.10**). Another target, PTEN (phosphatase and tensin homolog), as well as a control HMGA2 (high mobility group AT-hook 2) gene assay by Thermo Fisher, was also evaluated for changes upon HeLa cell treatment with anti-miR21 or control let-7 anti-miR, but was unsuccessful.³² Some reports suggest that changes in miR-21 gene target regulation in cells treated with anti-miR21 are subtle.^{19,33} Indeed, a 9mer LNA-modified anti-miR21 that we determined to be highly potent in dual luciferase assays (described in Chapter 2) only increased PDCD4 mRNA levels by 0.5-fold in HeLa cells at 100 nM (**Figure 3.10 B**).

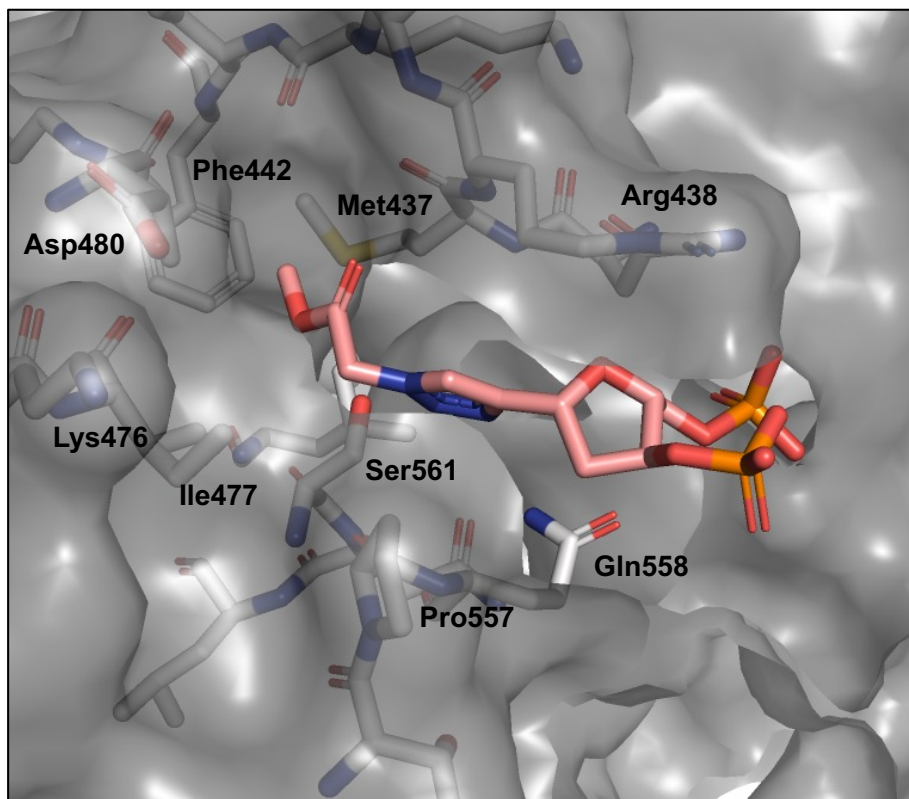


Figure 3.14 Highest-scored pose of methyl acetate triazole ligand docked into the t1A-binding hAgo2 receptor. hAgo2 amino acid residues in close proximity to the ligand are labeled.

Overall, we successfully computationally screened and experimentally identified a highly potent 3'-end ester triazole anti-miR modification that was reproducible in multiple luciferase assays, generalizable in two different anti-miR sequences, and was highly metabolically stable. This study expands the repertoire of anti-miR chemical modification strategies to improve potency of miRNA inhibition. However, further work is necessary to confirm our hypothesis that improved binding interactions of t1 ester-modified anti-miR towards the nucleotide-binding pocket of hAgo2 is the primary contributor to improved anti-miR activity. The highest-scoring docked pose of methyl ester triazole ligand with t1A hAgo2 receptor suggests that nearby polar residues Ser561, Asp480, and Lys476, or non-polar Met437 and Phe442 could provide hydrogen bonding and/or van der Waals-

type interactions towards the methyl ester substituent that are more substantial than when the t1 nucleotide is adenine (**Figure 3.14**).

Given that the hAgo2 pulldown experiments using 5'-biotinylated anti-miR21 were overall inconclusive, we decided to pursue expression and purification of full-length hAgo2 using methodologies established in our lab and Prof. Ian MacRae's lab at Scripps Research Institute.^{8,11,20,21,23,24,34,35} To date, we were successful in expressing poly-Histidine, TEV-tagged full-length hAgo2 in *S. cerevisiae* BCY123 strain yeast cells (**Figure 3.12**). The next steps are to increase the scale of hAgo2 expression and purify miR-21-loaded hAgo2 complex using methodologies described by Schirle and colleagues, perform hAgo2 cleavage assays to confirm hAgo2 activity, then do filter binding assays with radiolabeled, 3'-end triazole-modified anti-miR21 to obtain binding affinity data (K_D).^{11,21} Additionally, making mutations at t1A-pocket residues described above can allow us to proceed with structure activity relationship binding studies of 3'-end modified anti-miR with miRNA-loaded hAgo2 (**Figure 3.14**). One caveat to consider with the filter binding assay is that Schirle and colleagues found a small, ~0.5-fold reduction in K_D when substituting a short target RNA t1 nucleotide adenosine with modified bases 2,6'-diaminopurine (DAP).²¹ Thus, larger fold reduction in K_D values determined by t1 ester-modified anti-miR would be desirable and could provide us with the last piece of evidence needed to fully address our hypothesis.

3.5 References

- (1) Pham, K. M.; Suter, S. R.; Lu, S. S.; Beal, P. A. Ester Modification at the 3' End of Anti-MicroRNA Oligonucleotides Increases Potency of MicroRNA Inhibition. *Bioorganic Med. Chem.* **2021**, *29* (October 2020), 115894. <https://doi.org/10.1016/j.bmc.2020.115894>.
- (2) Onizuka, K.; Harrison, J. G.; Ball-Jones, A. A.; Ibarra-Soza, J. M.; Zheng, Y.; Ly, D.; Lam, W.; Mac, S.; Tantillo, D. J.; Beal, P. A. Short Interfering RNA Guide Strand Modifiers from Computational Screening. *J. Am. Chem. Soc.* **2013**, *135* (45), 17069–17077. <https://doi.org/10.1021/ja4079754>.
- (3) Meister, G.; Landthaler, M.; Patkaniowska, A.; Dorsett, Y.; Teng, G.; Tuschl, T. Human Argonaute2 Mediates RNA Cleavage Targeted by MiRNAs and SiRNAs. *Mol. Cell* **2004**, *15* (2), 185–197. <https://doi.org/10.1016/j.molcel.2004.07.007>.
- (4) Panda, A.; Martindale, J.; Gorospe, M. Affinity Pulldown of Biotinylated RNA for Detection of Protein-RNA Complexes. *Bio-Protocol* **2016**, *6* (24). <https://doi.org/10.21769/bioprotoc.2062>.
- (5) Palumbo, C. M.; Gutierrez-Bujari, J. M.; O'Geen, H.; Segal, D. J.; Beal, P. A. Versatile 3' Functionalization of CRISPR Single Guide RNA. *ChemBioChem* **2020**, *95616*, 1–9. <https://doi.org/10.1002/cbic.201900736>.
- (6) Livak, K. J.; Schmittgen, T. D. Analysis of Relative Gene Expression Data Using Real-Time Quantitative PCR and the 2- $\Delta\Delta$ CT Method. *Methods* **2001**, *25* (4), 402–408. <https://doi.org/10.1006/meth.2001.1262>.
- (7) Goodman, R. A.; Macbeth, M. R.; Beal, P. A. ADAR Proteins: Structure and Catalytic Mechanism. In *Current Topics in Microbiology and Immunology*; 2012; Vol. 353, pp 1–33. <https://doi.org/10.1007/82>.
- (8) Thuy-Boun, A. S.; Thomas, J. M.; Grajo, H. L.; Palumbo, C. M.; Park, S.; Nguyen, L. T.; Fisher, A. J.; Beal, P. A. Asymmetric Dimerization of Adenosine Deaminase Acting on RNA Facilitates Substrate Recognition. *Nucleic Acids Res.* **2020**, *48* (14), 7958–7972. <https://doi.org/10.1093/nar/gkaa532>.
- (9) Wang, Y.; Havel, J.; Beal, P. A. A Phenotypic Screen for Functional Mutants of Human Adenosine Deaminase Acting on RNA 1. *ACS Chem. Biol.* **2015**, *10* (11), 2512–2519. <https://doi.org/10.1021/acscchembio.5b00711>.
- (10) DeCaprio, J.; Kohl, T. O. Lysing Yeast Cells with Glass Beads for Immunoprecipitation. *Cold Spring Harb. Protoc.* **2020**, *2020* (11), 477–481. <https://doi.org/10.1101/pdb.prot098590>.
- (11) Schirle, N. T.; Sheu-Gruttadauria, J.; MacRae, I. J. Structural Basis for MicroRNA Targeting. *Science (80-.)*. **2014**, *346* (6209), 608–613. <https://doi.org/10.1126/science.1258040>.
- (12) Fukuhara, T.; Kambara, H.; Shiokawa, M.; Ono, C.; Kato, H.; Morita, E.; Okuzaki, D.; Maehara, Y.; Koike, K.; Matsuura, Y. Expression of MicroRNA MiR-122 Facilitates an Efficient Replication in Nonhepatic Cells upon Infection with Hepatitis C Virus. *J. Virol.* **2012**, *86* (15), 7918–7933. <https://doi.org/10.1128/jvi.00567-12>.
- (13) Chang, J.; Nicolas, E.; Marks, D.; Sander, C.; Lerro, A.; Buendia, M. A.; Xu, C.; Mason, W. S.; Moloshok, T.; Bort, R.; et al. MiR-122, a Mammalian Liver-Specific MicroRNA, Is Processed from Hcr MRNA and May Downregulate the High Affinity

- Cationic Amino Acid Transporter CAT-1. *RNA Biol.* **2004**, *1* (2), 106–113. <https://doi.org/10.4161/rna.1.2.1066>.
- (14) Takahashi, M.; Yamada, N.; Hatakeyama, H.; Murata, M.; Sato, Y.; Minakawa, N.; Harashima, H.; Matsuda, A. In Vitro Optimization of 2'-OMe-4'-Thioribonucleoside-Modified Anti-MicroRNA Oligonucleotides and Its Targeting Delivery to Mouse Liver Using a Liposomal Nanoparticle. *Nucleic Acids Res.* **2013**, *41* (22), 10659–10667. <https://doi.org/10.1093/nar/gkt823>.
- (15) Fabani, M. M.; Gait, M. J. MiR-122 Targeting with LNA/2'-O-Methyl Oligonucleotide Mixmers, Peptide Nucleic Acids (PNA), and PNA-Peptide Conjugates. *Rna* **2008**, *14* (2), 336–346. <https://doi.org/10.1261/rna.844108>.
- (16) Hatano, A.; Makita, S.; Kirihara, M. Synthesis and Redox-Active Base-Pairing Properties of DNA Incorporating Mercapto C-Nucleosides. *Tetrahedron* **2005**, *61* (7), 1723–1730. <https://doi.org/10.1016/j.tet.2004.12.038>.
- (17) Yao, Q.; Xu, H.; Zhang, Q. Q.; Zhou, H.; Qu, L. H. MicroRNA-21 Promotes Cell Proliferation and down-Regulates the Expression of Programmed Cell Death 4 (PDCD4) in HeLa Cervical Carcinoma Cells. *Biochem. Biophys. Res. Commun.* **2009**, *388* (3), 539–542. <https://doi.org/10.1016/j.bbrc.2009.08.044>.
- (18) Xu, L.; Xu, Q.; Li, X.; Zhang, X. MicroRNA-21 Regulates the Proliferation and Apoptosis of Cervical Cancer Cells via Tumor Necrosis Factor- α . *Mol. Med. Rep.* **2017**, *16* (4), 4659–4663. <https://doi.org/10.3892/mmr.2017.7143>.
- (19) Gubu, A.; Su, W.; Zhao, X.; Zhang, X.; Fan, X.; Wang, J.; Wang, Q.; Tang, X. Circular Antisense Oligonucleotides for Specific RNase-H-Mediated MicroRNA Inhibition with Reduced Off-Target Effects and Nonspecific Immunostimulation. *J. Med. Chem.* **2021**, *64* (21), 16046–16055. <https://doi.org/10.1021/acs.jmedchem.1c01421>.
- (20) Schirle, N. T.; MacRae, I. J. The Crystal Structure of Human Argonaute2. *Science* (80-.). **2012**, *336* (6084), 1037–1040. <https://doi.org/10.1126/science.1221551>.
- (21) Schirle, N. T.; Sheu-Gruttadauria, J.; Chandradoss, S. D.; Joo, C.; MacRae, I. J. Water-Mediated Recognition of T1-Adenosine Anchors Argonaute2 to MicroRNA Targets. *Elife* **2015**, *4* (September), 1–16. <https://doi.org/10.7554/eLife.07646>.
- (22) Macbeth, M. R.; Bass, B. L. Large-Scale Overexpression and Purification of ADARs from *Saccharomyces Cerevisiae* for Biophysical and Biochemical Studies. *Methods Enzymol.* **2007**, *424* (07), 319–331. [https://doi.org/10.1016/S0076-6879\(07\)24015-7](https://doi.org/10.1016/S0076-6879(07)24015-7).
- (23) Matthews, M. M.; Thomas, J. M.; Zheng, Y.; Tran, K.; Phelps, K. J.; Scott, A. I.; Havel, J.; Fisher, A. J.; Beal, P. A. Structures of Human ADAR2 Bound to DsRNA Reveal Base-Flipping Mechanism and Basis for Site Selectivity. *Nat. Struct. Mol. Biol.* **2016**, *23* (5), 426–433. <https://doi.org/10.1038/nsmb.3203>.
- (24) Monteleone, L. R.; Matthews, M. M.; Palumbo, C. M.; Thomas, J. M.; Zheng, Y.; Chiang, Y.; Fisher, A. J.; Beal, P. A. A Bump-Hole Approach for Directed RNA Editing. *Cell Chem. Biol.* **2019**, *26* (2), 269-277.e5. <https://doi.org/10.1016/j.chembiol.2018.10.025>.
- (25) Doherty, E. E.; Wilcox, X. E.; Van Sint Fiet, L.; Kemmel, C.; Turunen, J. J.; Klein, B.; Tantillo, D. J.; Fisher, A. J.; Beal, P. A. Rational Design of RNA Editing Guide Strands: Cytidine Analogs at the Orphan Position. *J. Am. Chem. Soc.* **2021**, *143* (18), 6865–6876. <https://doi.org/10.1021/jacs.0c13319>.

- (26) Lima, J. F.; Cerqueira, L.; Figueiredo, C.; Oliveira, C.; Azevedo, N. F. Anti-MiRNA Oligonucleotides: A Comprehensive Guide for Design. *RNA Biol.* **2018**, *15* (3), 338–352. <https://doi.org/10.1080/15476286.2018.1445959>.
- (27) Stenvang, J.; Petri, A.; Lindow, M.; Obad, S.; Kauppinen, S. Inhibition of MicroRNA Function by AntimiR Oligonucleotides. *Silence* **2012**, *3* (1), 1. <https://doi.org/10.1186/1758-907X-3-1>.
- (28) Geisow, M. J.; Evans, W. H. PH in the Endosome. Measurements during Pinocytosis and Receptor-Mediated Endocytosis. *Exp. Cell Res.* **1984**, *150* (1), 36–46. [https://doi.org/10.1016/0014-4827\(84\)90699-2](https://doi.org/10.1016/0014-4827(84)90699-2).
- (29) Sheu-Gruttadauria, J.; Xiao, Y.; Gebert, L. F.; MacRae, I. J. Beyond the Seed: Structural Basis for Supplementary Micro RNA Targeting by Human Argonaute2. *EMBO J.* **2019**, *38* (13), 1–14. <https://doi.org/10.15252/embj.2018101153>.
- (30) Mizrahi, R. A.; Schirle, N. T.; Beal, P. A. Potent and Selective Inhibition of A-to-I RNA Editing with 2'-O-Methyl/Locked Nucleic Acid-Containing Antisense Oligoribonucleotides. *ACS Chem. Biol.* **2013**, *8* (4), 832–839. <https://doi.org/10.1021/cb300692k>.
- (31) Faehnle, C. R.; Elkayam, E.; Haase, A. D.; Hannon, G. J.; Joshua-Tor, L. The Making of a Slicer: Activation of Human Argonaute-1. *Cell Rep.* **2013**, *3* (6), 1901–1909. <https://doi.org/10.1016/j.celrep.2013.05.033>.
- (32) Xu, J.; Zhang, W.; Lv, Q.; Zhu, D. Overexpression of MiR-21 Promotes the Proliferation and Migration of Cervical Cancer Cells via the Inhibition of PTEN. *Oncol. Rep.* **2015**, *33* (6), 3108–3116. <https://doi.org/10.3892/or.2015.3931>.
- (33) Androsavich, J. R.; Chau, B. N.; Bhat, B.; Linsley, P. S.; Walter, N. G. Disease-Linked MicroRNA-21 Exhibits Drastically Reduced mRNA Binding and Silencing Activity in Healthy Mouse Liver. *Rna* **2012**, *18* (8), 1510–1526. <https://doi.org/10.1261/rna.033308.112>.
- (34) Park, S. H.; Doherty, E. E.; Xie, Y.; Padyana, A. K.; Fang, F.; Zhang, Y.; Karki, A.; Lebrilla, C. B.; Siegel, J. B.; Beal, P. A. High-Throughput Mutagenesis Reveals Unique Structural Features of Human ADAR1. *Nat. Commun.* **2020**, *11* (1), 1–13. <https://doi.org/10.1038/s41467-020-18862-2>.
- (35) Suter, S. R.; Sheu-Gruttadauria, J.; Schirle, N. T.; Valenzuela, R.; Ball-Jones, A. A.; Onizuka, K.; Macrae, I. J.; Beal, P. A. Structure-Guided Control of SiRNA Off-Target Effects. *J. Am. Chem. Soc.* **2016**, *138* (28), 8667–8669. <https://doi.org/10.1021/jacs.6b06137>.

3.6 Table of primer sequences

Name	Sequence (5' to 3')
miR122_target_forward	ACAAACACCATTGTCACACTCCAGGCCGCTGGCCGCA ATAAAA
miR122_target_reverse	TGGAGTGTGACAATGGTGTGGTTGTTTCGAGCGATCGCCTA GAATTACTGC
hAgo2 GA F	CGACTACGCCGGATCCATGTACTCGGGAGCCGGC
hAgo2 GA R	GCATGCTCGAGCGGCCGCTCAAGCAAAGTACATGGTG CGCA
GA yeAgo2 F	GAGAACCTCTATTTCCAGGGAATGTACTCGGGAGCCG GCC
GA yeAgo2 R	ATCTAGTCATTACGATCCTCGAGTCAAGCAAAGTACAT GGTGCGCAG
BamHI His tag primer F	GGATCCGTAACCATGTCACACCATCACCATCACCATCA CCATCACCATGAGAACCTCTATTTCCAGGGAATGTACT CG
GA BamHI F	AACGTCAAGGAGAAAAACCCCGGATCCGTAACCATG TCACACCATCACCAT

Chapter 4

Cellular-based ADAR inhibition assays using 8-azanebularine-containing HER1 oligonucleotides and ADAR deaminase domain mutants

4.1 Introduction

It is becoming increasingly known that ADAR is strongly associated with cancer and immune stimulatory processes.¹⁻⁵ For example, downregulated expression of ADAR2 is reported to correlate with brain cancer cell development due to under-edited levels of glutamate receptor GluR-B mRNA, known to influence cell apoptosis.⁶ In other cancer cells, interferon-stimulated genes (ISGs) and type I interferon (IFN) production is upregulated, resulting in higher expression of ADAR1 that can perform A-to-I editing on dsRNAs and evade recognition by dsRNA sensors MDA5 and PKR which are responsible for immune filtration, inflammation, translation inhibition, and cell growth arrest.⁷ Furthermore, mutations in ADAR1 are associated with autoimmune disorder Aicardi-Goutières syndrome (AGS) and rare genetic pigmental disorder dyschromatosis symmetrica hereditaria 1 (DSH).⁸ Developing therapeutics that target ADAR is therefore desirable.

To date, there are no FDA-approved ADAR-targeting therapeutics. In particular, molecules targeting ADAR1 for inhibition are currently being studied and developed in academic and industrial settings to treat cancer. Our research group, as well as others, has worked on screening and testing small molecule inhibitors targeting ADAR1.⁹⁻¹³ There is recent dispute over the validity of using nucleoside analogs 8-azaadenosine and 8-chloroadenosine as small molecule inhibitors of ADAR1, thus indicating that careful, continued exploration of ADAR inhibitor design and testing is required.¹⁴ Additionally, to our knowledge, there are no reports of inhibiting ADAR1 using

chemically-modified oligonucleotides that contain 8-azanebularine (8-azaN), a well-studied nucleoside analog in our lab for ADAR structural and biochemical studies.^{15–20} In this chapter, numerous preliminary, cellular-based experiments using HER1 RNA oligonucleotide containing 8-azanebularine with the goal of inhibiting ADAR1 are presented. Preliminary data from ADAR deaminase domain (ADARd) protein inhibitors of ADAR in cells are also described.

4.2 Methods

4.2.1 Oligonucleotide synthesis and purification

All strands of HER1 RNA containing the 8-azanabularine modification (top) and the complementary (bottom) strand for the second generation HER1 16bp duplex were synthesized on an Applied Biosystems (ABI) 394 RNA/DNA Synthesizer. Otherwise, all 2'-O-methylated complementary strands for the other HER1 16bp duplexes were ordered from Integrated DNA Technologies (IDT). All phosphoramidite, controlled pore glass (CPG), and ancillary reagents for the ABI synthesizer were purchased from Glen Research, except for 8-azanebularine (BA0425) and 2'-deoxy-Benner's base (dZ, product number dZ-PA-101), which were purchased from Berry and Associates and Firebird Biomolecular Sciences, LLC, respectively.

Synthesized oligonucleotides on controlled pore glass (CPG) solid support were removed from the synthesizer and dried overnight under high vacuum. Next, the oligonucleotides were deprotected and cleaved from the CPG support in 3:1 volume ratio of 30% NH₄OH:EtOH at 55 °C overnight. The cleaved oligonucleotide solution was transferred away from the CPG and dried down to a pellet using a SpeedVac concentrator. HER1 oligonucleotides containing 8-azanebularine base were treated with

55% (v/v) Et₃N•3HF for ribose 2'-deprotection overnight at room temperature then precipitated using 75 mM sodium acetate in 65% butanol with freezing at -80 °C for at least 2 h. The supernatant containing deprotected oligonucleotide was then concentrated to dryness using the SpeedVac concentrator, resuspended in nuclease free water, and desalted in Illustra™ Nap™-10 Sephadex™ G-25 columns (Cytiva 17085401).

For the “generation 2” HER1 16mer complementary strand, the dZ base was deprotected by treating the oligonucleotide on CPG support with 1 M DBU (1,8-diazabicyclo[5.4.0]undec-7-ene) in acetonitrile at room temperature overnight. The dZ-deprotected oligonucleotide was then removed of supernatant and dried under high vacuum again before CPG solid support cleavage as mentioned above. After cleavage from CPG support, the oligonucleotide was treated with 1 M tetrabutylammonium fluoride solution in THF dried over 3 Å molecular sieves for 24-hour 2'-deprotection at room temperature, followed by 65% butanol precipitation as mentioned above.

All oligonucleotides were electrophoresed by denaturing PAGE and visualized by UV shadowing. The gel bands were excised and gel-purified by crushing and soaking in buffer containing 0.5 M ammonium acetate and 0.1 mM EDTA at 4 °C overnight, followed by filtering in 0.22 µm cellulose acetate membrane filter (Costar® Spin-X® Centrifuge Tube Filter, Corning 8160). The filtrate containing oligonucleotide was ethanol precipitated or purified by silica-based octadecyl bonded phase SepPak C18 cartridges (Waters) in 1:1 acetonitrile:water elution and characterized by MALDI-TOF mass spectrometric analysis. The MALDI-TOF mass spectra for the HER1 oligonucleotides are provided in **Table 4.2.9**.

4.2.2 Human serum stability assay of 8-azaN-containing HER1 RNAs

HER1 RNAs with 8-azaN were hybridized in IDT Nuclease-Free Duplex Buffer (30 mM HEPES, pH 7.5; 100 mM potassium acetate) by heating at 95 °C for 5 minutes, followed by a slow cooling of -1 °C/min to room temperature. The 8-azaN-containing and complementary strands of the 16 bp duplex were hybridized in a 1:1 molar ratio. In a 50 µL reaction volume, the HER1 8-azaN RNA was diluted to a final concentration of 8 µM with Dulbecco's Phosphate Buffer Saline (DPBS, Gibco 14190144) and 5 µL of human serum (Millipore Sigma H4522) to 10% final concentration. Each reaction was incubated at 37 °C and 5 µL aliquots were taken out at 0, 15, 30, 60, 120, 240, and 480 min and combined with 5 µL of 10% glycerol in 1X TBE buffer and immediately stored at -80 °C. Each aliquoted time point containing 40 pmol of HER1 8-azaN RNA was loaded into either 10% or 20% non-denaturing Novex™ TBE Gels (Invitrogen, EC62752BOX or EC63152BOX) for the larger or 16bp HER1 8-azaN RNAs, respectively, and electrophoresed at 200 V for 30 min. The gel was then stained in SYBR™ Gold Nucleic Acid Gel Stain (Invitrogen S11494) for 20 min and imaged on the GelDoc Go Imaging System (Bio-Rad) under SYBR™ Gold settings on a UV/Stain-free tray.

4.2.3 Cell culture

HeLa (CCL-2), HEK293T (CRL-3216), and U87 (HTB-14) cells were purchased from ATCC and cultured in Dulbecco's modified Eagle medium (DMEM, Gibco 11995065) supplemented with fetal bovine serum (FBS, Gibco) and 100X antibiotic-antimycotic solution (Anti-Anti, Gibco 15240062) to a final concentration of 10% and 1X, respectively.

All cells were passaged at exponential phase and routinely tested for mycoplasma contamination using LookOut[®] Mycoplasma Detection PCR kit (Sigma Aldrich, MP0035).

4.2.4 Transfection of cells with HER1 8-azaebularine-containing RNA inhibitors

HeLa cells were plated at 3×10^4 cells per well in a 24-well plate and transfected with 50 nM siRNA targeting ADAR1 (siADAR1 L + S)²¹ with sense strand sequence 5' – CCAGCACAGCGGAGUGGUUU – 3' and antisense strand sequence 5' – UACCACUCCGCUGUGCUGGUU – 3', scramble siRNA negative control with sense strand sequence 5' – GGCGAGGUAGCUCCUAACUGA – 3' and antisense strand sequence 5' – UCAGUUAGGAGCUACCUCGCC – 3', both purchased from Dharmacon, or 31.25 – 500 nM HER1 RNA duplex using 1.5 Lipofectamine RNAiMAX for 48 h.

HEK293T cells were transfected either by co-transfection or a two-step transfection method when overexpressing ADAR1 alongside treatment with HER1 8-azaN-containing RNA. For the co-transfection method, HEK293T cells were plated at 7.5×10^4 in a 24-well plate and transfected with 500 ng of pcDNA ADAR1 p110, full-length ADAR2, or pcDNA3.1 empty vector control plasmid and 25-500 nM HER1 8-azaN 16bp RNA duplex using 5 μ L Lipofectamine 2000 per well for 48 h at 37 °C + 5% CO₂. For the two-step transfection method, HEK293T cells were plated at 7.5×10^4 in a 24-well plate and transfected with 500 ng of plasmid for 24 hours using 5 μ L Lipofectamine 2000, then subsequently transfected with 25-500 nM HER1 8-azaN for 24 hours using 1.5 μ L Lipofectamine RNAiMAX per well.

For endogenous NUP43 editing inhibition studies, HEK293T cells were plated at 4×10^5 cells in 6-well plate format and transfected with 100 nM siADAR1 (Silencer[®] Select siRNA, Ambion, s1008) or Stealth[™] RNAi Negative Control, Medium GC duplex

(Invitrogen, 12935-300) and HER1 16bp 8-azaN RNA duplexes at a concentration range of 125-500 nM using 7.5 μ L Lipofectamine RNAiMAX for 48 h at 37 °C + 5% CO₂.

U87 cells were also plated at 4 x 10⁵ cells per well in a 6-well plate and transfected under the same conditions described above with HEK293T cells for endogenous NUP43 editing inhibition.

4.2.5 Electroporation of cells with HER1 8-azaN inhibitors

HEK293T and U87 cells were electroporated at 5 x 10⁶ final cell density at 250 V pulse in a 0.4 cm cuvette with a final concentration of 250 nM siADAR1 (s1008), Stealth™ RNAi Negative Control, Medium GC duplex, or HER1 16bp RNA duplex using the Ingenio® EZporator® Electroporation System (MIR51000) and plated at 4 x 10⁵ cells in 6-well plate format for 72 h at 37 °C + 5% CO₂.

4.2.6 Transfection of cells with ADAR deaminase inhibitor plasmid constructs

HeLa cells were plated at 5 x 10⁵ cells per well in a 6-well plate and transfected with 2500 ng pcDNA.3.1 overexpression vector containing ADAR1 deaminase (ADAR1d) gene with E912A, E912A/D1023A, or E912/D1023K mutations or pcDNA3.1 empty vector control using 12.5 μ L Lipofectamine 2000 (Invitrogen) for 48 h at 37 °C + 5% CO₂.

HEK293T cells were plated at 1 x 10⁵ cells per well in 24-well plate format and co-transfected with a constant 500 ng pcDNA3.1 ADAR2 full-length and 250, 500, or 750 ng of ADAR2 deaminase (ADAR2d) gene with E396A, E396A/D503A, or E396/D503K mutations using 5 μ L Lipofectamine 2000 for 48 h at 37 °C + 5% CO₂. pcDNA3.1 empty vector plasmid was transfected along with the ADAR2d vector to keep the amount of plasmid equal in each well.

4.2.7 RNA editing analysis from cultured cells

Transfected HeLa or HEK293T cells were lysed in 1 mL TRIzol reagent per duplicate of wells in a 24-well plate or per single well in a 6-well plate and purified of total RNA using the TRIzol Plus RNA Purification Kit (Invitrogen, 12183555) followed by DNaseI treatment using Turbo DNA-free kit (Invitrogen, AM1907) to remove any genomic DNA contaminants. Total RNA was reverse transcribed into single-stranded cDNA using High Capacity Reverse Transcription Kit (Applied Biosystems, 4368813) according to the manufacturer's instructions. The total cDNA was then amplified into amplicons using PCR primers covering a specific ADAR RNA editing target of interest and Phusion Green Hot Start II High-Fidelity PCR Master Mix (Thermo Scientific, F566). Annealing temperatures for each set of primers were determined by the T_m Calculator website from Thermo Fisher Scientific. A list of editing target primer sequences and annealing temperatures are provided in **4.6 Table of Oligonucleotides**.

Total RNA from U87 cells were also isolated using the TRIzol PureLink RNA Mini Kit then subsequently treated with DynabeadsTM mRNA Purification Kit (Invitrogen, 61006) to acquire purified mRNA, according to the manufacturer's instructions. Next, U87 mRNA was used as the template for RT-PCR using Access RT-PCR System (Promega, A1250) and forward and reverse primers for NEIL1 (NEIL1 out F and NEIL1 out R) or 5-HT_cR (5HT2cR Xbs F and 5HT2cR HiA R)²² to generate cDNA. The thermal cycler conditions for RT-PCR were set as follows: 1) reverse transcription at 45 °C for 45 min; 2) AMV Reverse Transcriptase and RNA/cDNA/primer denaturation at 94 °C for 2 min; 3) second strand cDNA synthesis and PCR amplification at 94 °C for 30 s, 60 °C for 1 min, and 68 °C for 2 min; repeat 3) for 24 cycles total; 4) final extension at 68 °C for 7 min; 5)

Hold at 4 °C. After RT-PCR, the resulting cDNA was further amplified by nested PCR for 20 cycles under two-step protocol using Phusion Green Hot Start II High-Fidelity PCR Master Mix and primers “NEIL1 in F” and “NEIL1 in R” for NEIL1 and “5-HT_{2C}R S16 in F” and “5-HT_{2C}R A11 in R” for 5-HT_{2C}R, respectively. The nested RT-PCR primer sequences can be found in **4.6 Table of Oligonucleotides**.

After PCR, all amplicons were run on 1.3% agarose gel and purified using QIAquick Gel Extraction Kit (Qiagen, 28706). The gel extracted amplicons were then submitted to GeneWiz for Sanger sequencing. The “A” and “G” (inosine read as guanosine) peaks at a given edit site from the amplicon were quantified to determine % editing by the following calculation: % editing = [(peak value of G)/(peak of value A + peak of G)] x 100

4.2.8 Western blotting

Transfected cells were lysed in Pierce™ IP Lysis Buffer (Thermo Scientific™ 87787) and protein concentration was determined using Pierce™ BCA Protein Assay Kit (Thermo Scientific™ 23225). Bolt Plus Bis-Tris 4-12% gels were loaded with 10, 20, or 40 µg lysate and electrophoresed at 200 V for 40 min in a Mini Gel Tank (A25997) then transferred onto PVDF membrane using an iBlot™ 2 Gel Transfer Device (IB21001). The PVDF membrane was blocked in 5% blocking solution for 1 h at room temperature using Tris-buffered saline with 0.1% Tween® 20 detergent (TBST) and Blotting-Grade Blocker nonfat dry milk (BioRad 1706404). The membrane was washed three times for 5 min with TBST on an orbital shaker then incubated in anti-HA tag monoclonal antibody (Invitrogen MA1-21315, 1:1,000 dilution) in 2.5% blocking solution at 4 °C overnight with

shaking. The following day, the PVDF membrane was washed three times for 5 min with TBST then incubated with goat anti-mouse IgG secondary antibody (Invitrogen, 31320, 1:30,000 dilution) in 2.5% blocking solution for 1 h at room temperature. The membrane was washed three times for 5 min again then stained with ECF Western Blotting substrate (Cytiva Lifesciences, RPN5785) for 5 min and imaged for fluorescence on the GelDoc Go Imaging System (Bio-Rad) under SYBR™ Gold settings on a UV/Stain-free tray.

4.2.9 Table of mass spectra for HER1 oligonucleotides

Name	Sequence (5' – 3')	Calculated Mass	Observed Mass
HER1 8-azaN 16mer, top strand	GAGAAUUNGCGGGUCG	5186.2	5186.9
HER1 16mer, bottom strand	CGACCCGCCAAUUCUC	4976.0	4975.9
HER1 16mer GC ctrl, top strand	GAGAAUUGGCGGGUCG	5216.2	5218.8
HER1 16mer, bottom strand, 3'-end 2'-OMe	CGACCCGCCAAU <u>UCUC</u>	5032.2	5031.4
HER1 16mer, bottom strand, 5'-end 2'-OMe	<u>CGACCCGCCAAUUCUC</u>	5046.2	5046.0
HER1 8-azaN 16mer, top strand, 2'OMe both ends	<u>GAGAAUUNGCGGGUCG</u>	5312.4	5313.5
HER1 16mer, bottom strand, 2'OMe both ends	<u>CGACCCGCCAAUUCUC</u>	5102.3	5098.9
HER1 8-azaN 16mer, generation 2, top strand	<u>G</u> *A*GAAUUNGCGG+G+T*+C*G	5356.6	5359.1
HER1 16mer, generation 2, bottom strand	C*G* <u>ACCCGCdZdNAUUC</u> *U*C	5121.4	5112.4
HER1 8-azaN 33mer	CGACCCGCCAAUUCUUCGAGAAUUNGCGG GUCG	10530.4	10527.5
HER1 8-azaN 33mer, PS linked	C*G*ACCCGCCAAUUCUUCGAGAAUUNGCG GGU*C*G	10594.6	10608.5
HER1 8-azaN 34mer, 3'-end 1-EdR C3	CGACCCGCCAAUUCUUCGAGAAUUNGCGG GUCG(1-EdR)(C3)	10872.5	10869.6

<p>N = 8-azanebularine + = LNA <u>Underlined</u> = 2'-OMe dN = 2'-deoxynebularine dZ = 2'-deoxy Benner's Base * = phosphorothioate (PS) linkage 1-EdR C3 = 2'-deoxy-1'-ethynyl-ribose with C3 spacer</p>

4.3 Results

4.3.1 Human serum stability of HER1 RNA oligonucleotides containing 8-azanebularine.

The nuclease resistance of seven HER1 RNAs containing 8-azanebularine that vary in length and backbone modifications (**Figure 4.1A**) was determined by incubation in 10% human serum at 37 °C for 0, 5, 15, 30, 60, 120, 240, and 480 min. Four of the seven RNAs are short 16bp duplexes with or without phosphate or ribose sugar modifications to improve duplex stability and metabolic stability. The other three RNAs were longer, 33 and 34mer sequences that contain a small hairpin structure on the 5' end based on previous reports in our lab when determining ADAR1 or ADAR2 substrate selectivity via biochemical assays and Sats-FACS-Seq methodology.^{23,24}

(C)

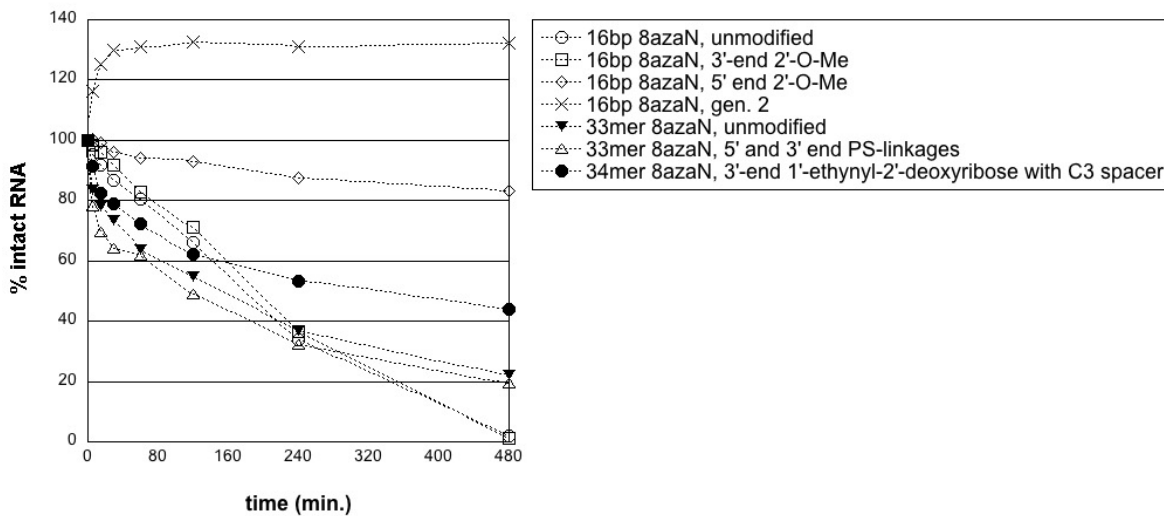
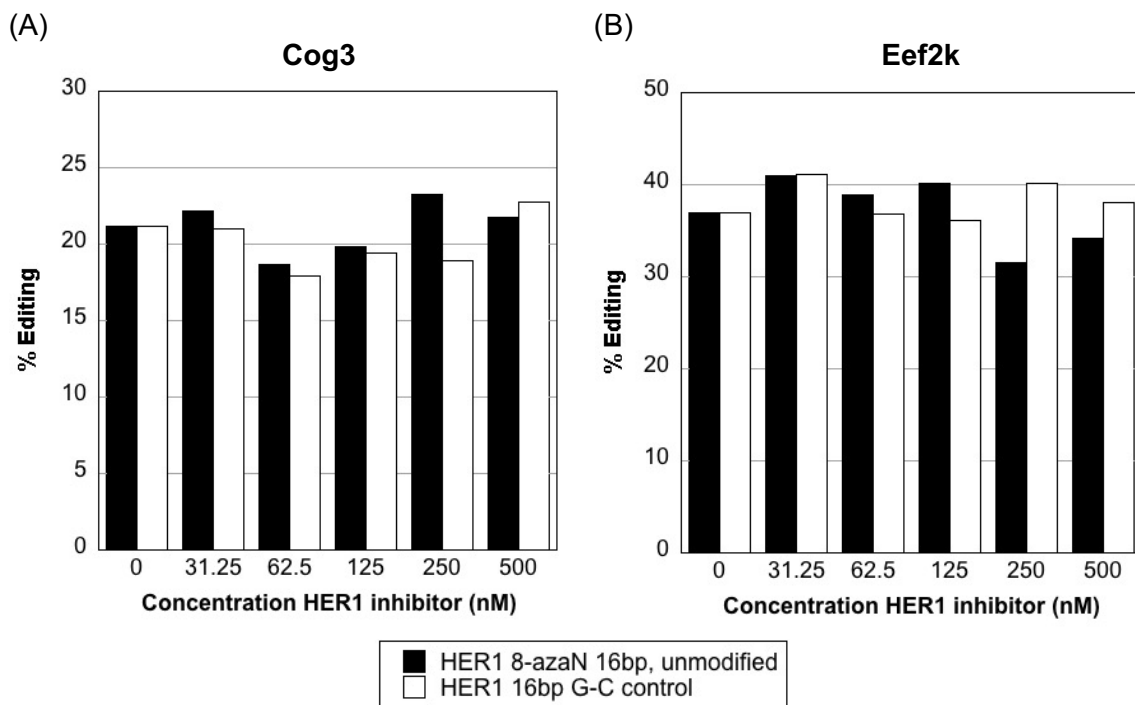


Figure 4.1 Serum stability of 8-azanebularine- (8-azaN) containing HER1 RNAs. (A) Sequence and chemical modification structures of the HER1 8-azaN RNAs tested in serum stability assay. (B) Non-denaturing PAGE of HER1 8-azaN RNA at indicated timepoints in 10% human serum. (C) Plot of % intact HER1 8-azaN RNA over time in presence of 10% human serum.

In 10% human serum, all HER1 8-azaN RNAs are nuclease resistant at up to 240 min. At 480 min, however, there is reduction or complete loss of an RNA band, indicating nuclease degradation (**Figure 4.1B**). Surprisingly, complete retention of RNA at 480 min was observed for the 16 bp duplex where its bottom strand is 2'-O-methylated at the 5'-end (16 bp 8N, 5'-2'OMe) and the generation 2 duplex (16bp 8N, gen. 2) where both the 8-azaN-containing and bottom strands are heavily modified with nuclease resistant and thermally stable modifications, in addition to modified bases nebularine and Benner's base based on work by colleagues Erin Doherty, Hannah Brinkman, and Dr. Leanna Monteleone.²⁵ Also, duplex stability for the generation 2 duplex seemed to improve at increasing incubation time at 37 °C with 10% human serum, as seen by the converging of diffused gel band at 0 min to a clear, distinct band from 60 min onward. For the longer RNAs, there is complete loss of RNA at 480 min for the unmodified RNA and a modest

reduction in gel band intensity for the 33mer RNA containing phosphorothioate (PS) linkages on either end. Only a minor reduction in RNA band intensity is seen at 480 min for the 34mer RNA containing a 1'-ethynyl-2'-deoxyribose, C3-spacer (1-EdR C3) modification at the 3'-end. The improved nuclease resistance of HER1 8-azaN RNA by modification with 1-EdR C3 on the 3'-end is in agreement with what we observed in the snake venom phosphodiesterase (SVPD) stability assay of the anti-miR21 with 3'-end 1-EdR C3 modification, as was discussed in Chapter 3.

4.3.2 Inhibition profile of endogenous ADAR1 targets in HeLa cells by HER1 8-azaN duplex.



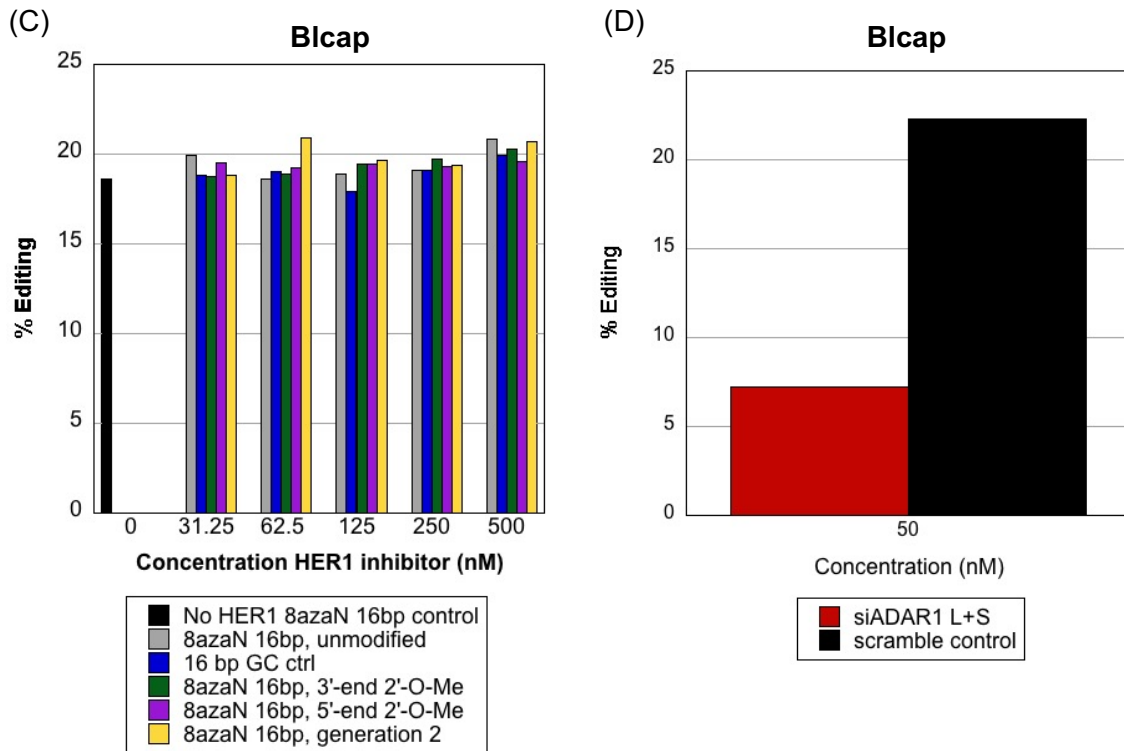


Figure 4.2 Editing of endogenous ADAR1 targets in HeLa cells upon transfection with HER1 8-azanebularine 16bp duplexes. (A) Editing percentage of Cog3 in HeLa cells with 0-500 nM 16 bp HER1 8-azaN duplex or GC base pair control. (B) Editing percentage of Eef2k in HeLa cells with 0-500 nM 16 bp HER1 8-azaN duplex or GC base pair control. (C) Editing percentage of Bicap in HeLa cells with 0-500 nM 16 bp HER1 duplexes. (D) Editing percentage of Bicap in HeLa cells with 50 nM siRNA targeting ADAR1 p110 and p150 (L + S) or scramble duplex control.

HeLa cells were used as the starting point for inhibitory studies by HER1 RNA duplexes containing 8-azaN based on data from our lab's collaboration with the Emeson lab at Vanderbilt University, where a sufficiently detectable level of percent A-to-I editing of endogenous transcripts Cog3 and Eef2k in HeLa cells was determined.²⁶ Cog3 was to serve as a HER1 RNA inhibitor negative control as Cog3 is preferentially edited by ADAR2, whereas Eef2k target is preferentially edited by ADAR1.²⁷⁻³⁰ If the HER1 duplexes containing 8-azaN successfully inhibited ADAR in cells, there would be an expected reduction in editing towards a given transcript that can be determined through

Sanger sequencing cDNA derived from cellular RNA isolates (see 'RNA editing analysis from cultured cells' in Methods section). However, at 31.25 to 500 nM concentrations of 8-azaN-containing HER1 16 bp unmodified RNA duplex, both Cog3 and Eef2k targets did not show any significant reduction in percent editing relative to 16bp RNA duplex containing a G-C base pair in place of 8-azaN across from C base. (**Figure 4.2A and 4.2B**).

Blcap was another transcript determined by Malik and colleagues to be a more-preferred editing target by ADAR1 over ADAR2 where its mRNA expression levels were not affected upon media acidification.²⁶ Again, at 31.25 to 500 nM concentrations unmodified HER1 8-azaN 16bp RNA duplex, there was no percent editing reduction at the Blcap edit site (**Figure 4.2C**). Additionally, HER1 8-azaN RNA duplexes bearing varying degrees of backbone modifications (3'-end 2'-OMe, 5'-end 2'-OMe, and generation 2) tested in 10% human serum stability assays described above also did not reduce Blcap percent editing. However, transfecting HeLa cells with 50 nM of siRNA targeting ADAR1 p110 and p150 isoforms (siADAR1 L+S)²¹ resulted in an approximate two-third fold reduction in % editing of Blcap compared to scramble sequence duplex control, indicating that RNA transfection was efficient (**Figure 4.2D**).

4.3.3 Editing profile of endogenous ADAR1 targets in HEK293T cells treated with HER1 8-azaN 16 bp duplex.

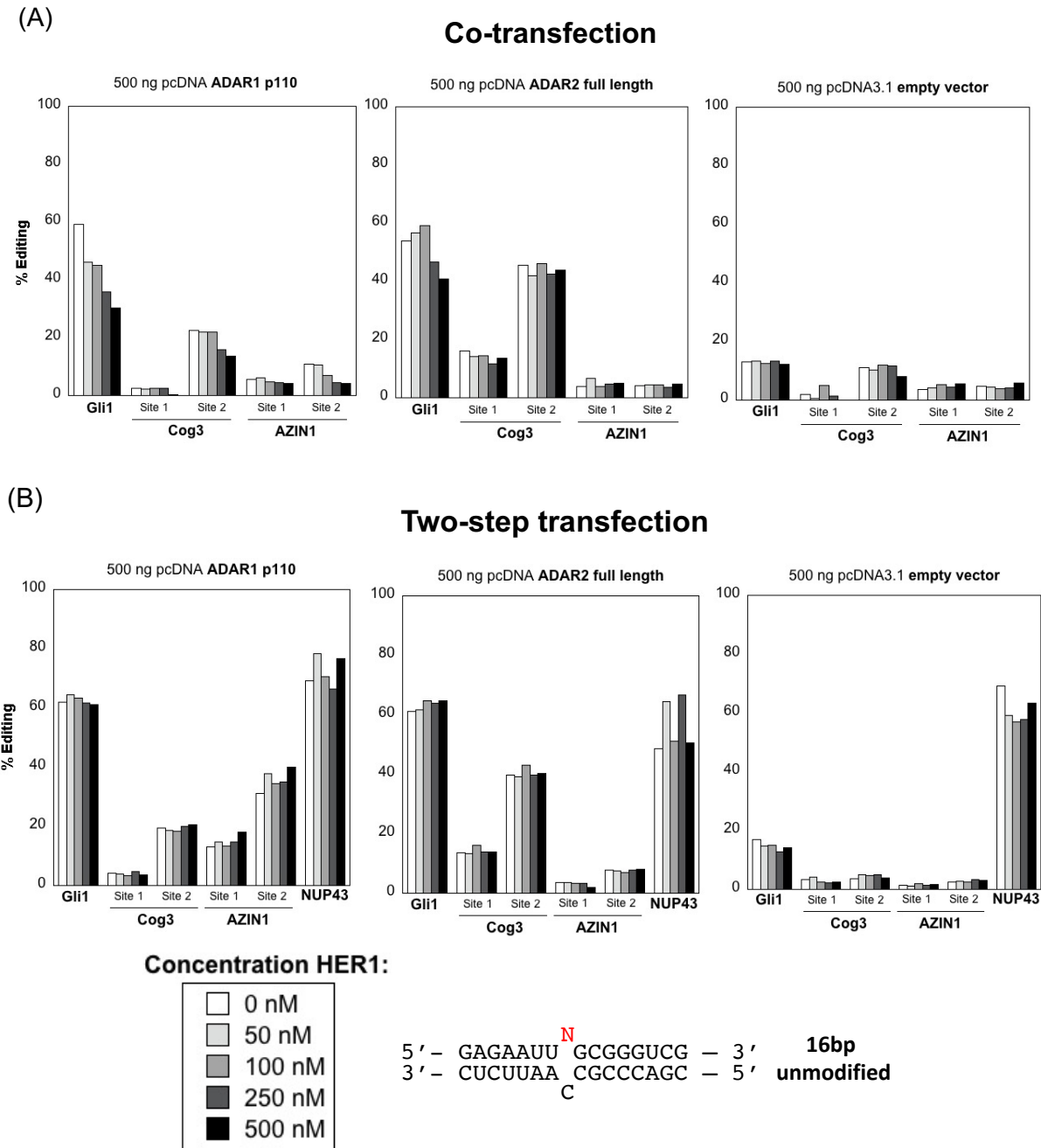


Figure 4.3 Percent editing profile of ADAR targets in HEK293T cells. (A) Panel of editing from co-transfection of ADAR overexpression plasmid and HER1 8-azaN duplex or (B) two-step transfection.

Next, editing inhibition of overexpressed ADAR1 p110 targeting endogenous transcripts Gli1, Cog3, AZIN1, and NUP43 by HER1 8-azaN RNA duplexes in HEK293T cells was determined. Full-length ADAR2 (ADAR2 FL) was overexpressed in HEK293T cells with empty vector used as a control for editing inhibition by HER1 RNA duplex. These experiments followed previous graduate student Dr. Leanna Monteleone's work to check for ADAR1 editing activity inhibition by the same targets but with 33mer HER1 8-azaN-containing RNA with PS linkages on both 5' and 3' ends (**Figure 4.1A**).

A dose-dependent reduction of percent editing, from 60% to 30%, of Gli1 can be seen in HEK293T cells co-transfected with 500 ng ADAR1 p110 overexpression vector and 0 to 500 nM unmodified HER1 16bp RNA duplex containing 8-azanebularine at the edited adenosine position (**Figure 4.3A and B**). At edit site 2 of Cog3 and AZIN1, there is an editing reduction from 20% to 15% and 10% to 5%, respectively, in the presence of up to 500 nM HER1 8-azaN 16bp RNA duplex. Editing percentages remained generally the same for the remaining edit sites in ADAR1 p110-overexpressed HEK293T cells. In the case of ADAR2 FL-overexpressed cells, both Cog3 edit sites doubled in percent editing, thus showing that Cog3 is more sensitive to A-to-I editing by ADAR2 over ADAR1 (**Figure 4.3A**). Editing percentages for all transcripts were minor, ranging from ~2% to ~10%, when HEK293T cells were co-transfected with 500 ng pcDNA3.1 empty vector control and HER1 8-azaN 16bp RNA duplex, suggesting that both ADAR1 p110 and ADAR2 FL were successfully transfected and overexpressed to increase editing activity (**Figure 4.3A**).

To check for potential transfection interference by co-transfection of vector and HER1 duplex, HEK293T cells were also transfected by a "two-step" transfection method

where the ADAR overexpression vector was transfected first for 24 hours, then the HER1 8-azaN 16bp RNA duplex was subsequently transfected for an additional 24 hours before lysis and processing for RNA editing analysis. Indeed, differences in editing for all endogenous transcripts was observed using this transfection method (**Figure 4.3B**). In particular, percent editing increased by nearly two-fold at site 1 and ~five- to eight-fold at site 2 in the AZIN1 transcript (**Figure 4.3B**) with ADAR1 p110 overexpression, which is in agreement with reports stating the correlation between AZIN1 editing and ADAR1 overexpression.³¹ Also, the editing levels remained relatively equal from 0 to 500 nM of transfected HER1 8-azaN 16bp RNA for all transcripts in the presence of overexpressed ADAR1 p110, ADAR2 FL, or empty vector control, suggesting that the HER1 duplex did not elicit any inhibition.

After optimization of primer design, the amplicons corresponding to transcript NUP43 was successfully generated and editing was analyzed from HEK293T cells transfected with the two-step method. Interestingly, NUP43 had a high degree of ~60% editing at all concentrations of HER1 8-azaN 16bp RNA duplex and overexpression of ADAR1 p110 and ADAR2 FL or empty vector control (**Figure 4.3B**). This result indicated that NUP43 is a highly-preferred editing transcript by endogenous ADAR in HEK293T cells and would not require ADAR overexpression for inhibitory analysis using modified HER1 8-azaN RNA duplex. This hypothesis was explored further and is described in **Result 4.3.5**.

4.3.4 Quantification of overexpressed ADAR protein at varying concentration of HER1 8-azaN 16 bp duplex in HEK293T cells.

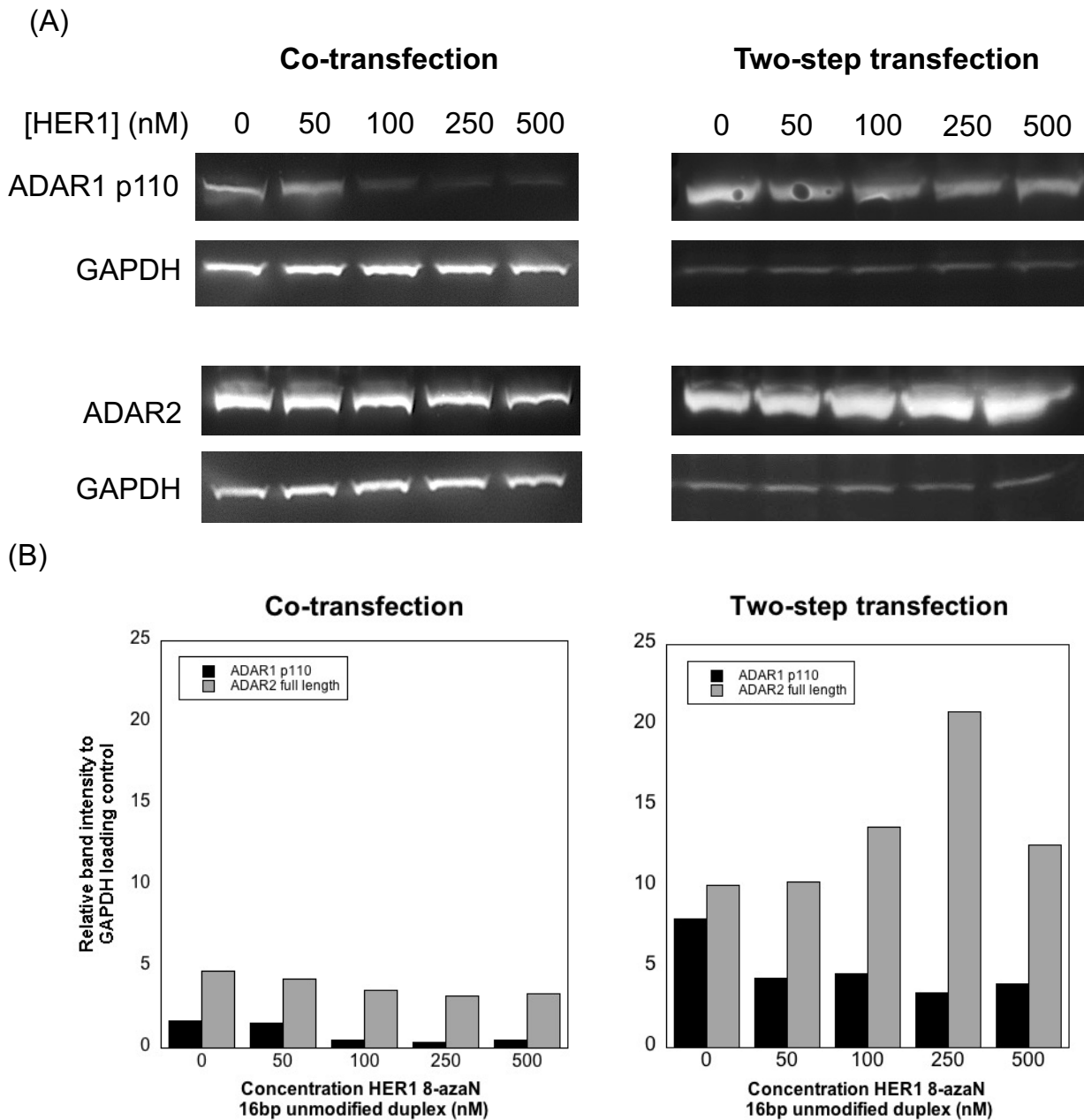


Figure 4.4 Overexpression of HA-tagged ADAR1 p110 isoform or ADAR2 full length protein in cells with respect to HER1 RNA inhibitor. (A) Western blotting detection of overexpressed ADAR1 p110 and full-length ADAR2 (ADAR2 FL) in HEK293T cells transfected with HER1 8-azanebularine-containing 16bp RNA duplex. (B) Bar plot of relative protein expression of ADAR1 p110 and ADAR2 FL to GAPDH control.

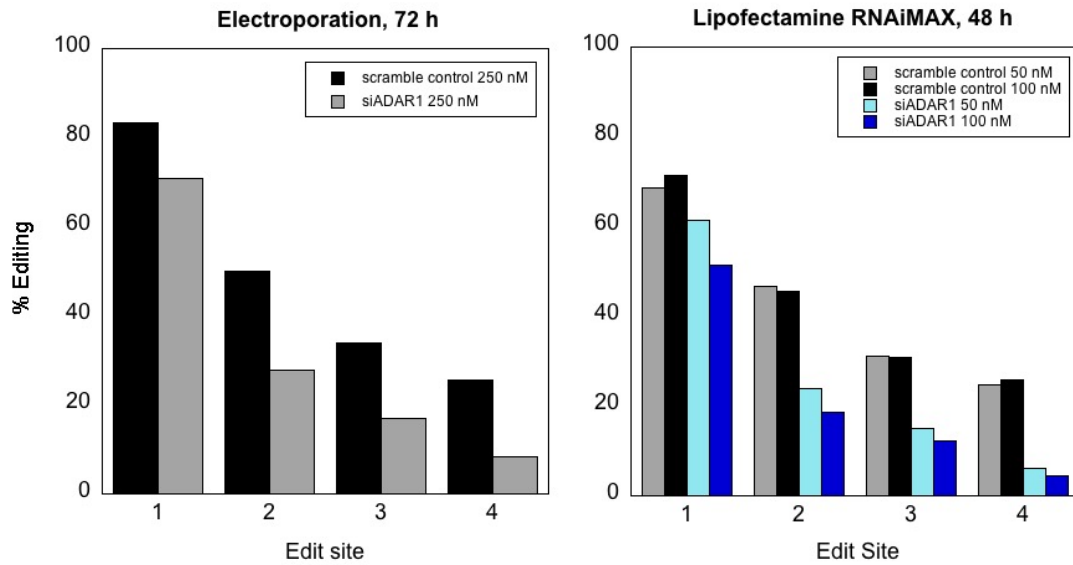
Western blotting analysis was then performed to quantify expression of ADAR1 p110 and ADAR2 FL protein in HEK293T lysate treated with HER1 8-azaN 16bp RNA duplex. In HEK293T lysate co-transfected with overexpression vector and HER1 duplex, the relative expression of both ADAR1 p110 and ADAR2 FL proteins are significantly lower than cells transfected with vector and HER1 duplex by the two-step transfection method (**Figure 4.4A and B**). ADAR1 p110 protein is expressed at a range of three- to five-fold higher amounts from the two-step transfection method compared to co-transfection, whereas ADAR2 FL is expressed two- to four-fold higher. In both transfection methods, ADAR1 p110 expression decreases as the concentration of HER1 8-azaN 16bp RNA duplex is transfected into HEK293T cells; ADAR2 FL expression remains generally equal across all concentrations of HER1 duplex, with some error. Additionally, ADAR2 FL expression is relatively higher than ADAR p110 in both transfection methods, suggesting that ADAR2 can, in general, express more readily than ADAR1 in cells.

Overall, ADAR1 p110 expression seems to be sensitive to HER1 8-azaN RNA duplex treatment in HEK293T cells while ADAR2 FL remains unaffected. Co-transfecting ADAR overexpression vector and increasing concentrations of HER1 8-azaN duplex results in a decrease in both ADAR1 p110 protein expression as well as editing percentages for endogenous transcripts in HEK293T cells (**Figure 4.3A**). On the other hand, decreases in ADAR p110 expression from cells treated with the two-step transfection method did not decrease editing percentages from increasing amounts of HER1 8-azaN duplex (**Figure 4.3B**).

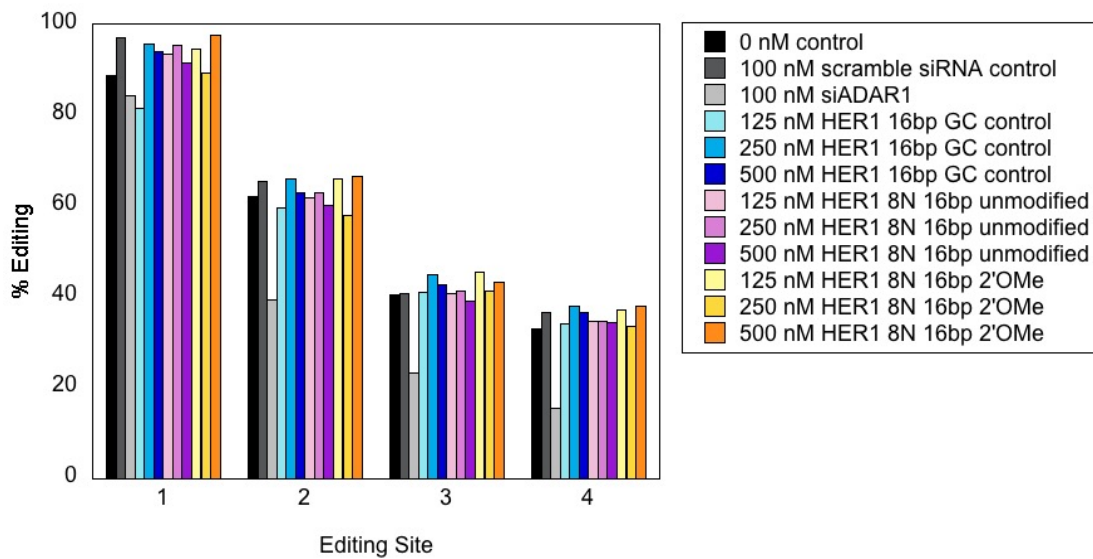
4.3.5 Endogenous transcript editing profile in cells treated with HER1 8-azaN RNA duplexes.

Based on the results from **4.3.3.**, HER1 8-azaN-containing duplexes were introduced into HEK293T cells by either electroporation or lipid nanoparticle-mediated transfection to investigate if endogenous ADAR would be inhibited and therefore reduce editing of transcript NUP43. In both electroporation and transfection methods, editing of NUP43 at four different edit sites (chr6:150046736, chr6:150046673, chr6:150046643, and chr6:150046642, identified through REDportal)³² was identified (**Figure 4.5A and B**). Furthermore, treating HEK293T cells with siRNA targeting ADAR1 (siADAR1) resulted in a decrease in percent editing at all edit sites, indicating that siADAR1 was successfully being introduced into the cells and performing knockdown of endogenous ADAR1 transcripts to reduce editing activity. Interestingly, editing at NUP43 edit site 4 was most sensitive to siADAR1 treatment by both electroporation and transfection, approximately two- to three-fold lower than scramble siRNA control samples. Thus, editing at NUP43 site 4 served as a potentially valuable and sensitive ADAR1-editing target to compare with HER1 8-azaN duplex.

(A) **NUP43 % Editing in HEK293T cells**



(B)



(C)

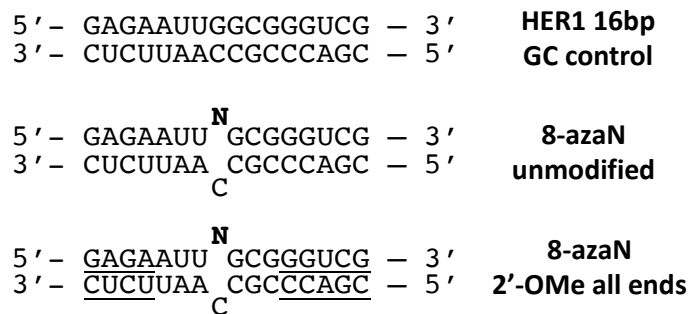
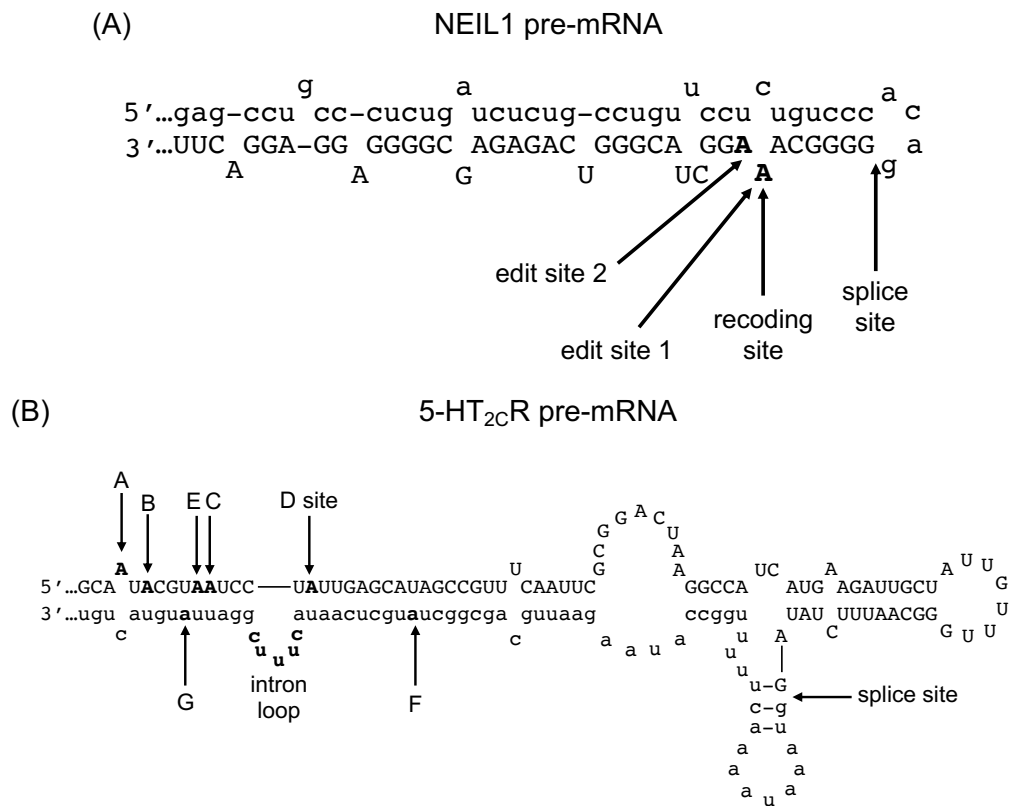


Figure 4.5 Editing profile of endogenous NUP43 editing target at various edit sites in HEK293T cells transfected with siRNA control or HER1 8-azaN inhibitor duplexes. (A) Editing profile of NUP43 at edit sites 1-4 with electroporated (left plot) or transfected (right plot) siADAR1 or scramble control at indicated concentrations. (B) Editing profile of NUP43 at edit sites 1-4 transfected with 100 nM siADAR1, scramble siRNA control, or 125-500 nM HER1 RNA inhibitor duplex. (C) Sequence of HER1 RNA duplexes. Bold N = 8-azanebularine base; underlined = 2'-O-methyl ribose.

Subsequently, unmodified 8-azaN-containing HER1 16bp RNA duplex, duplex containing 2'-OMe modifications on both strands (8-azaN 2'-OMe all ends), and 16bp duplex with G-C base pair in place of 8-azaN as a control (**Figure 4.5C**) were transfected into HEK293T cells at 125 to 500 nM concentration using Lipofectamine RNAiMAX. No editing reduction of NUP43 at any edit site was observed for either unmodified or 2'-O-methylated HER1 8-azaN duplexes at any concentration (**Figure 4.5 B**).



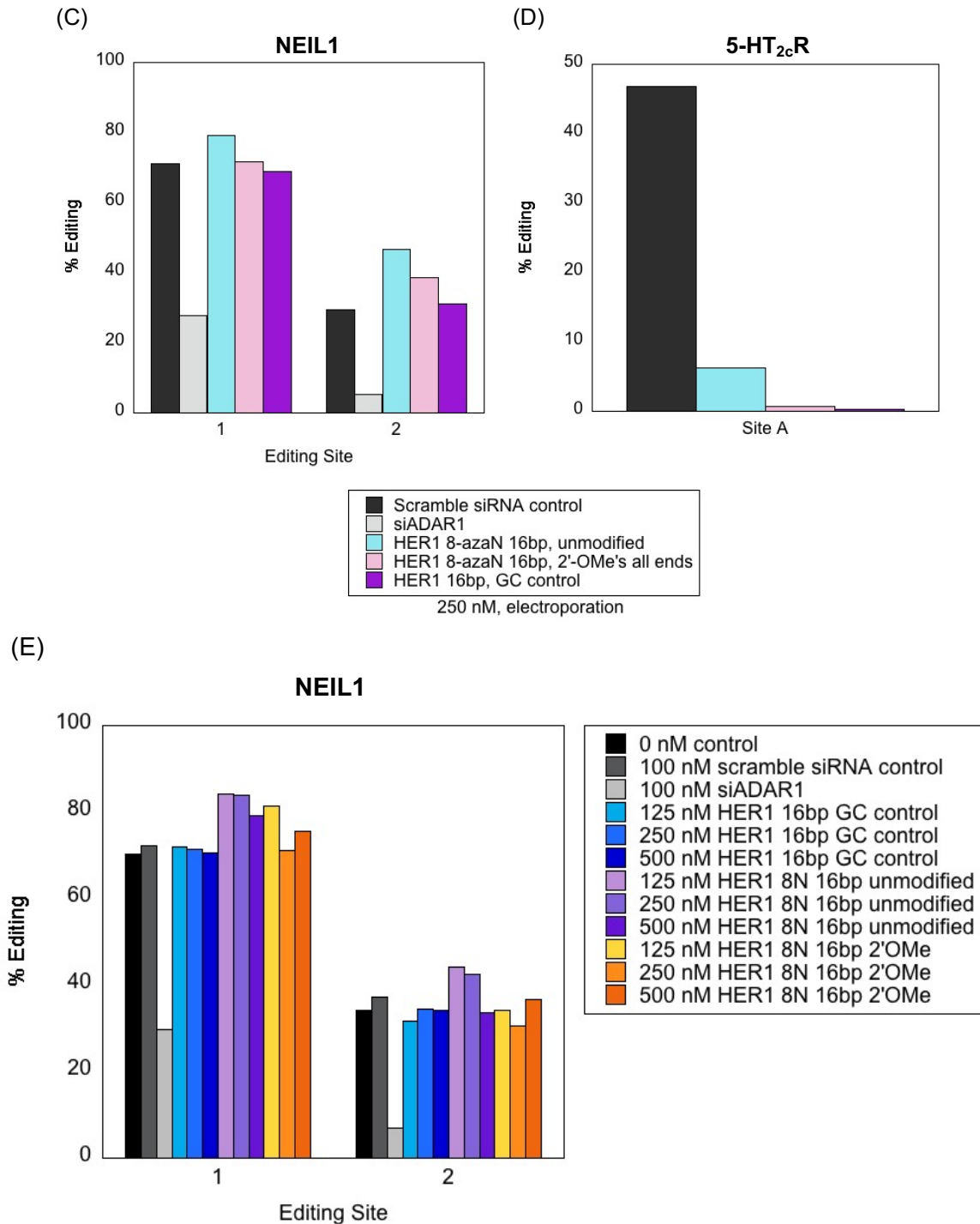


Figure 4.6 Percent editing profile of endogenous NEIL1 and 5-HT_{2c}R mRNA transcripts in U87 cells treated with HER1 8-azaN duplexes. (A) Predicted RNA sequence and secondary structure of NEIL1 pre-mRNA surrounding edit and splice sites.³³ Intronic sequences are in lowercase. (B) Predicted RNA sequence secondary structure of 5-HT_{2c}R pre-mRNA with indicated edit sites, splice site, and intronic loop.³⁴ Intronic sequences are also in lowercase. (C) Editing of NEIL1 at two sites in U87 cells electroporated with 250 nM siADAR1 (s1008), scramble siRNA negative control, or HER1 16bp RNA inhibitor duplex for 72 hours. (D) Editing of the A

site of 5-HT_{2c}R in U87 cells electroporated with scramble siRNA negative control or HER1 16bp RNA inhibitor duplex for 72 hours. (E) Editing of NEIL1 at two sites in U87 cells transfected with 100 nM siADAR1 (s1008), scramble siRNA negative control, or 125-500 nM HER1 16bp GC control, unmodified 16bp 8-azaN, or 16bp 2'-OMe 8-azaN using Lipofectamine RNAiMAX for 48 hours.

Human glioblastoma U87 cells were also treated with HER1 8-azaN duplex inhibitors to see if endogenous ADAR1 could be inhibited and reduce editing activity towards NEIL1 and 5-HT_{2c}R, two transcripts that our research group has used for A-to-I editing studies in great detail (**Figure 4.6A and B**).^{26,33-37} Electroporated U87 cells with siADAR1 resulted in greater than two-fold reduction in NEIL1 editing at site 1 and six-fold reduction at site 2 relative to scramble siRNA control (**Figure 4.6C**). Unmodified and 2'-O-methylated HER1 16bp duplexes containing 8-azanebularine at 125 to 500 nM concentration did not reduce NEIL1 editing by any degree relative to GC control duplex (**Figure 4.6C**). Surprisingly, in the case of 5-HT_{2c}R transcript, electroporation with all three HER1 16bp duplexes tested nearly abolished editing at Site A (**Figure 4.6D**). Sanger sequence traces could not be generated from amplicon samples derived from U87 cells siADAR1 electroporation, thus percent editing values were omitted from the bar plot. Nonetheless, scramble siRNA control-treated U87 samples resulted in ~45% editing at Site A. No editing was observed at any of the other exonic 5-HT_{2c}R editing sites on the pre-mRNA transcript (**Figure 4.6B**).

U87 cells were then transfected with 100 nM siADAR1 or scramble siRNA control and 125 to 500 nM HER1 16bp duplexes using Lipofectamine RNAiMAX. Editing analysis could be determined for only NEIL1 as generating amplicons for the 5-HT_{2c}R transcript was unsuccessful. Similar to the results seen by electroporation, NEIL1 editing from U87 cells transfected with HER1 8-azaN duplexes did not reduce editing to any significant

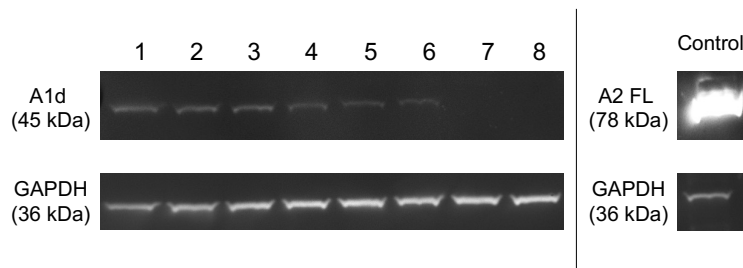
degree at any concentration (**Figure 4.6E**). siADAR1 at 100 nM reduced editing ~two-fold at site 1 and ~six-fold at site 2 from NEIL1 which is consistent with what was seen in electroporated U87 cell samples (**Figure 4.6C**).

4.3.6 Editing profile of ADAR editing targets in cells treated with ADAR deaminase domain (ADARd) protein inhibitors.

Cellular-based editing inhibition by ADAR deaminase domain (ADARd) mutants was performed to supplement fellow graduate student Herra Grajo's *in vitro* analyses (not yet published). HeLa or HEK293T cells were overexpressed with ADARd mutants that are catalytically inactive or with control ADARd double mutants that are both catalytically inactive and mutated at the dimerization interface and thus cannot asymmetrically dimerize with a monomer of ADAR to perform RNA editing.²⁰

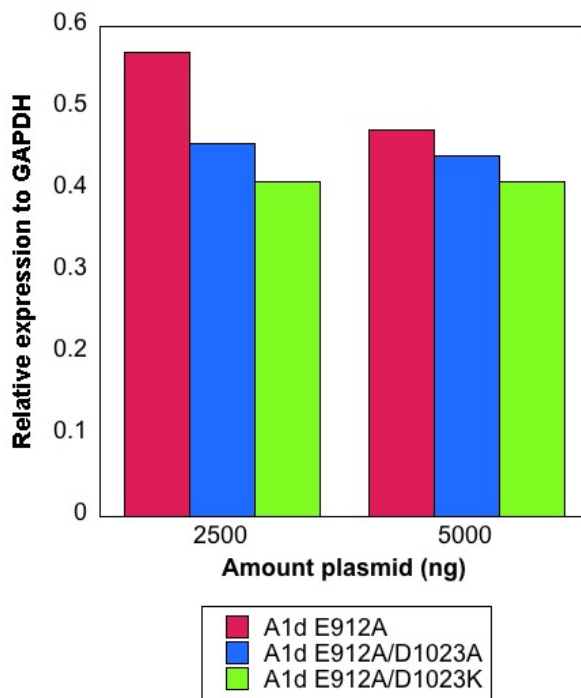
To start, ADAR1d protein was overexpressed in HeLa cells by transfection with 2500 or 5000 ng pcDNA3.1 vector containing ADAR1d E912A catalytically inactive single mutant gene or E912A/D1023A or E912A/D1023K catalytically inactive and dimerization interface-mutated double mutants then quantified by western blotting (**Figure 4.7A**).^{20,38} Although ADAR1d mutant expression was detectable, protein abundance at 5000 ng overexpression vector transfection did not seem to increase in comparison to 2500 ng (**Figure 4.7B**). Thus, 2500 ng pcDNA3.1 ADAR1d mutant vector was used to determine editing of endogenous transcripts Blcap, Eef2k, and Cog3 in HeLa cells. No reduction was observed in any of the transcripts in the presence of overexpressed ADAR1d E912A mutant relative to E912A/D1023A or E912A/D1023K double mutant controls (**Figure 4.7C**).

(A)



Lane	Protein	ng pcDNA plasmid transfected
1	A1d E912A	2500
2	A1d E912A	5000
3	A1d E912A/D1023A	2500
4	A1d E912A/D1023A	5000
5	A1d E912A/D1023K	2500
6	A1d E912A/D1023K	5000
7	Empty vector	2500
8	Empty vector	5000
Control	A2 FL (HEK293T cells)	500 (24-well plate format)

(B)



(C)

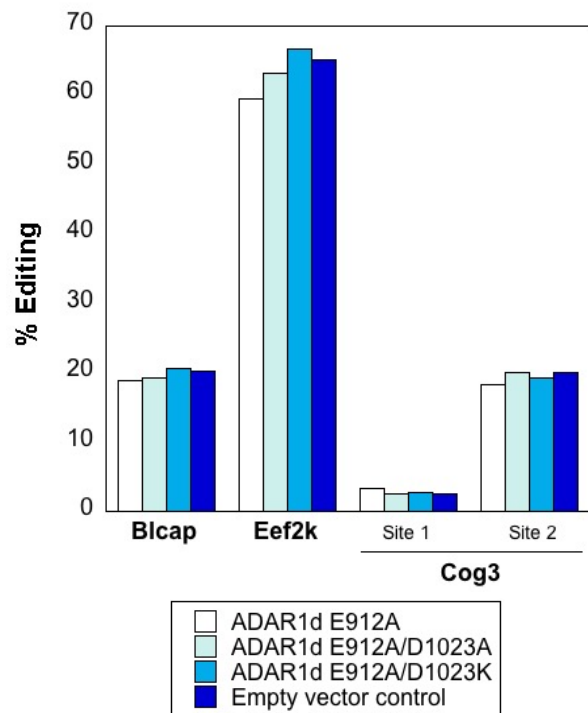
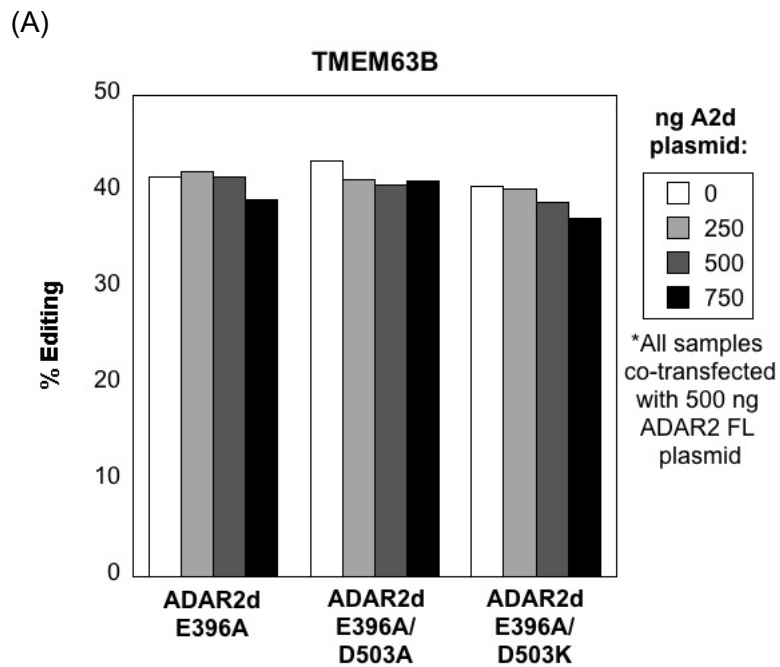


Figure 4.7 Editing of endogenous transcripts in HeLa cells treated with overexpression of ADAR1d mutant protein inhibitors. (A) Protein expression of HA-tagged ADAR1d E912A, E912A/D1023A, and E912A/D1023K mutants transfected at 2500 or 5000 ng overexpression vector in HeLa cells detected by western blotting. As a blotting detection control, lysate from HEK293T cells transfected with 500 ng HA-tagged ADAR2 full length overexpression vector was used. (B) Relative protein expression of ADAR1d mutants to GAPDH control. (C) Percent editing profile of Bicap, Eef2k, and Cog3 editing targets in HeLa cells with transfected 2500 ng pcDNA ADAR1d E912A, E912A/D1023A, and E912A/D1023K mutants.

In the case of ADAR2d mutants, HEK293T cells were co-transfected with a constant amount (500 ng) of pcDNA3.1 containing full-length ADAR2 gene and 250 to 750 ng of ADAR2 E396A catalytically inactive single mutant or E396A/D503A or E396A/D503K double mutants.^{20,39,40} pcDNA3.1 empty vector was also transfected to keep the amount of plasmid transfected equal per sample. No significant editing inhibition of ADAR2-preferred substrate TMEM63B^{19,20,41,42} was observed using any amount of overexpressed ADAR2d E396A mutant relative to ADAR2D E396A/D503A or E396A/D503K double mutants (**Figure 4.8A**).



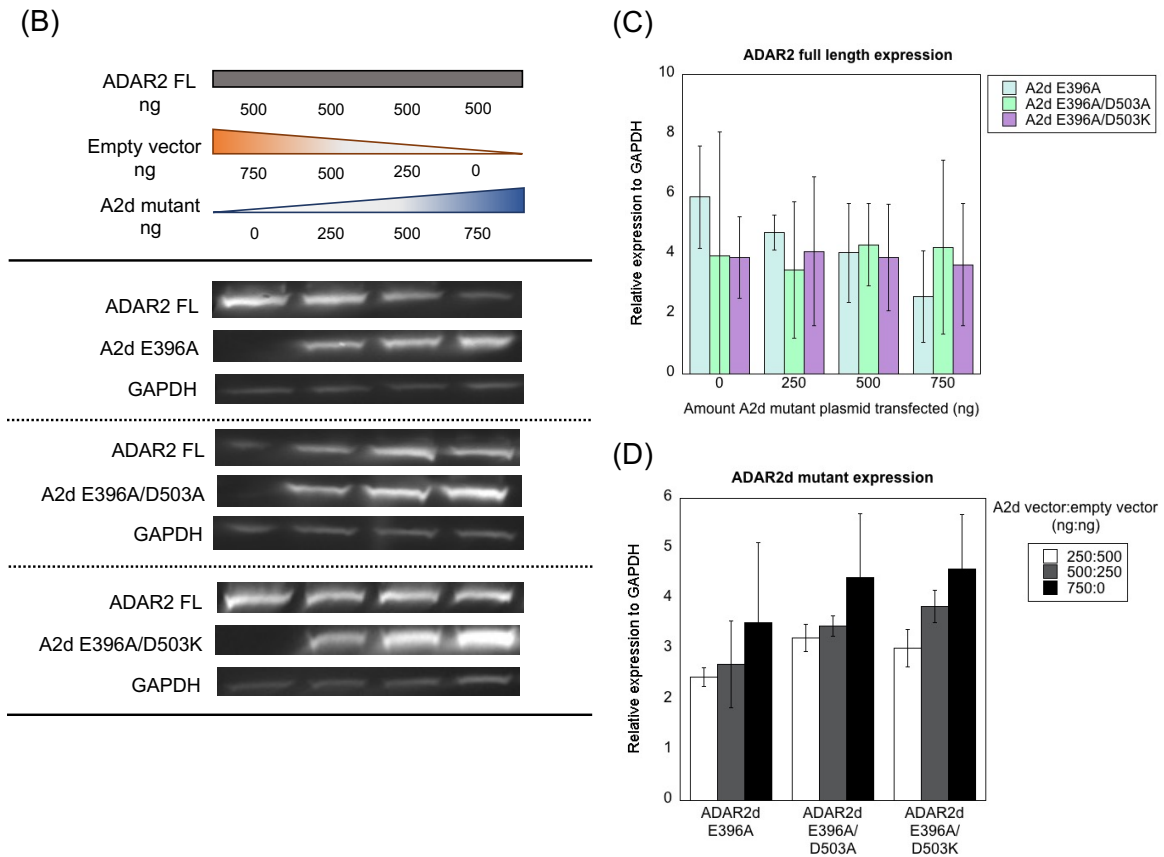


Figure 4.8 Editing of endogenous ADAR2 target in HEK293T cells co-transfected with ADAR2 full length protein and ADAR2d mutant protein inhibitors. (A) Editing profile of ADAR2 editing target TMEM63B with transfected ADAR2d mutants at 0, 250, 500, and 750 ng vector amount. (B) Representative western blot of ADAR2 full length (ADAR2 FL), ADAR2d E396A, E396A/503A, E396A/503K, and GAPDH control protein expression at varying ADAR2d mutant overexpression vector amounts. (C) Bar plot of relative ADAR2 full length protein expression to GAPDH control with respect to amount of transfected ADAR2d mutant overexpression vector. (D) Bar plot of relative ADAR2d mutant expression to GAPDH from 250-750 ng overexpression vector transfected. Error bars are represented from three western blotting experiments.

Protein expression of the ADAR2d mutants was then quantified by western blotting in order to determine if improper expression led to inefficient inhibition of endogenous ADAR2 in HEK293T cells. Although transfection of full length ADAR2 vector was kept constant, its expression was overall inconsistent when co-transfected with ADAR2d mutant vector (**Figure 4.8B and C**). Yet, expression of the ADAR2d mutants was modestly consistent with increasing amounts of vector transfected, particularly with 250

ng vector for all three mutants and 500 ng for ADAR2d E396A/503A and E396A/D503K double mutants (**Figure 4.8D**).

4.4 Discussion

There is an increasing number of reports strongly suggesting that ADAR1 editing activity can be correlated with cancer and autoimmune disorders.¹⁻⁵ Thus, the development of inhibitors targeting ADAR1 is desirable as a therapeutic. In the case of nucleoside analog inhibitors, there are disagreements over the experimental validity of some analogs purported to act as an ADAR1 inhibitor, molecules such as 8-azaadenosine and 8-chloroadenosine.¹¹⁻¹⁴ In fact, previous graduate student Dr. SeHee Park demonstrated in *in vitro* deamination assays that incubating 0.1 to 1,000 μ M 8-azaadenosine with human Gli1 RNA substrate and wild type ADAR1d or full length ADAR1 p110 did not result in inhibition, as described in her doctoral dissertation. Thus, it is clear that the development of ADAR1 inhibitors necessitates careful attention to detail in experimental design in order to be used as a therapeutic inhibitor.

Here, an array of cellular-based assays was conducted to assess the effectiveness of RNA-based and protein-based inhibitors. Unfortunately, none of the conditions from cells treated with either chemically modified HER1 RNA duplexes or ADARd mutant protein proved to be successful in terms of inhibiting ADAR1 or ADAR2. Based on the results obtained, a handful of key parameters to consider when designing cell-based experiments for ADAR inhibition will be discussed.

We were motivated to pursue the use of HER1 16bp RNA duplex containing 8-azanebularine that substitutes the edited adenosine as an inhibitor because Dr. SeHee Park found that, in her efforts to crystallize ADAR1, the duplex bound to hyperactive

ADAR1d E1008Q mutant with substantially higher affinity ($K_D = 11$ nM) than HER1 16bp duplex containing canonical adenosine at the editing site, as determined through EMSA. This result can also be found in her doctoral dissertation. Not only was the high binding affinity in parallel to what was determined with 23mer, 8-azaN-containing dsRNA for ADAR2d crystallization¹⁸, it also suggests that the 8-azaN in HER1 can act as a catalytic trap in ADAR1 and inhibit enzymatic activity.^{16,43} Indeed, fellow graduate student Herra Grajo determined via *in vitro* deamination assays that HER1 8-azaN 16bp RNA duplex can inhibit full length ADAR1 p110 in the presence of RNA substrates NEIL1 and 5-HT_{2c}R at nanomolar IC₅₀ values (data not yet published), which further stimulated efforts to determine inhibition in cells.

Prior to inhibitory analyses in cells, HER1 16bp RNA duplexes or longer (33 or 34mer) RNAs containing 8-azaN, with or without sugar and/or phosphate backbone chemical modifications, were incubated in 10% human serum at 37°C to assess metabolic stability. As anticipated, the heavily modified “generation 2” HER1 16bp duplex and 34mer RNA bearing a 3'-end 1'-ethynyl-ribose analog with C3 spacer exhibited an improvement of nuclease resistance compared to unmodified 8-azaN-containing duplex or 33mer RNA controls (**Figures 4.1A, B, and C**). On the contrary, it was surprising to observe a substantial improvement of metabolic stability by the HER1 16bp duplex where the 5'-end of the bottom strand was 2'-O-methylated compared to both the 3'-end bottom strand 2'-O-methylated and unmodified duplexes (**Figure 4.1A, B, and C**). One possibility for this result may be that the 3'-exonucleases present in human serum can generally degrade the 3'-end of 2'-O-methylated oligonucleotides at a faster rate than when 2'-O-methyl modifications are placed toward the 5'-end. Increasing the number of

2'-O-methyl groups on the 5'-end of one duplex and the 3'-end of another could be done to further explore sensitivity towards 3'-exonuclease in human serum.

Although the 16bp HER1 8-azaN-containing duplexes mentioned above were found to have high metabolic stability, none of them resulted in inhibition by any degree when determining RNA editing of endogenous transcript Bicap in HeLa cells (**Figure 4.2C**). There are a lot of possible explanations to this result, which could be narrowed down to: concentration of inhibitor, relative expression of endogenous ADAR1 in HeLa cells for editing activity, half-life of transcript, or insufficient degree of chemical modification for metabolic stability, cellular uptake, or thermal stability. To address the issue of concentration dependence of inhibitor, a wide range of 31.25 – 500 nM of HER1 16bp duplexes containing 8-azaN was transfected into HeLa cells. Using higher concentrations than 500 nM was undesirable as we did not want to reach concentrations where cell cytotoxicity may potentially be observed, which can be normally found within the micromolar range of chemically modified nucleic acids.^{44–47}

HeLa cells are known to contain a sufficient amount of endogenous ADAR1. In particular, human ADAR1 isoform p110 is predominantly found in the nucleus of HeLa cells whereas p150 is found in the cytoplasm.^{48–50} Also, the editing percentages towards transcripts Cog3, Eef2k, and Bicap from HeLa cells are in agreement with what was seen by Malik and colleagues.²⁶ Given this information, we considered HeLa cells to be an encouraging starting point to determine ADAR1 editing inhibition by 8-azaN-containing RNA duplex. However, none of the endogenous transcripts described above showed reduced editing when HeLa cells were treated with HER1 inhibitor, therefore other cell lines containing overexpressed or sufficient amounts of endogenous ADAR was pursued.

Our laboratory has made great use of HEK293T cells to overexpress ADAR1 p110 and increase editing signals of various endogenous transcripts.^{19,20,51} Former lab member Dr. Leanna Monteleone investigated the inhibitory profile of 33mer HER1 RNA containing 8-azaN in place of the edited adenosine and two PS linkages on both 5'- and 3'-ends (sequence shown in **Figure 4.1A**) in HEK293T cells overexpressed with ADAR1 p110 and full-length ADAR2 and empty vector as controls. Her preliminary data revealed a relatively dose-dependent reduction of editing towards endogenous transcript AZIN1 at two different edit sites when using 50 to 500 nM of the 33mer HER1 RNA that was not as apparent in the ADAR2 FL overexpressed or empty vector control samples (data not published). This result was encouraging as AZIN1 is an ADAR1-preferred editing substrate for regulation and led us to believe that ADAR1 was indeed being inhibited by the HER1 RNA containing 8-azaN.^{31,52,53} However, Dr. Monteleone found that the relative protein expression of ADAR1 p110 to GAPDH as increasing amounts of HER1 RNA was transfected was overall inconclusive. Thus, follow-up experiments using HER1 8-azaN 16bp RNA duplex were performed.

The transfection method seemed to have a moderate contribution to the RNA editing sensitivity and, in particular, the levels of ADAR overexpression in HEK293T cells. Although not at the same magnitude as Dr. Monteleone's result, a dose-dependent reduction of editing at AZIN1 edit site 2 was observed when HEK293T was co-transfected with 50 to 500 nM HER1 8-azaN 16bp RNA duplex and ADAR1 p110 overexpression vector (**Figure 4.3A**). However, when HEK293T cells were treated with the two-step transfection method, percent editing at both AZIN1 edit sites more than doubled and did not show a reproducible dose dependent reduction of editing at site 2 due to HER1 8-

azaN 16bp RNA duplex treatment (**Figure 4.3B**). Furthermore, the relative ectopic expression of full-length ADAR1 p110 and ADAR2 proteins were dramatically different by both transfection methods (**Figure 4.3C**). An intriguing observation that came from the western blotting analysis is a decrease in relative expression of overexpressed ADAR1 p110 to GAPDH control as transfected HER1 8-azaN duplex increased, whereas ADAR2 FL was generally unaffected (**Figure 4.4A and B**), which may indicate that ADAR1 p110 overexpression is not a desirable method to pursue further for HER1 inhibition studies. Overall, it is crucial to monitor ADAR1 expression and ensure that it remains consistent as the concentration of HER1 8-azaN RNA inhibitor treatment increases. Otherwise, false positive results of HER1 8-azaN inhibition may arise. Given this, we turned back to HER1 8-azaN RNA inhibitory assays that depend strictly on endogenous levels of ADAR and transcripts in cells.

Interestingly, we found that an NUP43 edit site⁵⁴ was highly edited at equal percentages in HEK293T overexpressing ADAR1 p110, ADAR2 FL, or transfected with empty vector control, indicating that NUP43 was a transcript that could be edited well without the need of overexpressed ADAR1 (**Figure 4.3B**). As anticipated, the NUP43 edit site, along with three others, showed moderate to high levels of editing, presumably by endogenous ADAR1 (**Figures 4.5A and B**). Indeed, electroporating or transfecting an siRNA targeting ADAR1 (siADAR1) resulted in a ~20% to 60% reduction in editing of NUP43, therefore confirming that endogenous ADAR1 in HEK293T cells highly edits NUP43 (**Figures 4.5A and B**). A similar effect was seen by an siADAR1 with a different sequence targeting ADAR1 in HeLa cells (**Figure 4.2D**). The siADAR1 control also gave some insight into how long-lived the ADAR1 mRNA is and that it can be

silenced by siRNA over the course of 48 hours. In other words, if ADAR1 transcripts had longer half-lives, evaluating inhibition of ADAR1 editing activity towards substrates by HER1 8-azaN inhibitors would have proven more difficult.

Nonetheless, even by using two different methods to introduce HER1 8-azaN duplexes into HEK293T cells, no degree of inhibition could be observed from any NUP43 edit site (**Figure 4.5B**). Note that we included a duplex containing 2'-OMe modifications on both 5'- and 3'- ends of the top and bottom strands that we thought could be another metabolically stable candidate to test, based on Herra Grajo's *in vitro* deamination assay data (not yet published) showing that this duplex was as equally potent as the unmodified duplex (**Figure 4.5A**). This result was also observed in glioblastoma U87 cells with respective NEIL1 transcript (**Figure 4.6A, C, and E**).^{33,35} Furthermore, the puzzling result of nearly abolished editing activity towards U87 transcript 5-HT_{2C}R at Site A was determined, including electroporated GC control duplex (**Figure 4.6B and D**).^{22,33} Obtaining editing data for the 5-HT_{2C}R transcript in U87 cells treated with HER1 duplexes by lipid nanoparticle-mediated transfection was unsuccessful. Future optimization will need to be performed to generate inhibitory profiles by HER1 8-azaN-containing duplexes towards NEIL1 and 5-HT_{2C}R transcripts in U87 cells that can satisfactorily align with Herra Grajo's *in vitro* inhibition data. Western blotting can then be performed to quantify endogenous ADAR1 expression with transfected HER1 8-azaN inhibitor.

As mentioned above, none of the ribose and phosphate backbone modifications applied to the HER1 8-azaN-containing duplex seemed to improve inhibition of ADAR in cells, even though some designs were found to be highly metabolically stable in 10% human serum (**Figure 4.1A, B, and C**). Thus, other chemical modification strategies are

being implemented by colleagues Herra Grajo and Victorio Jáuregui-Matos to achieve desired inhibitory effects. To date, Herra Grajo designed a longer, highly modified 32mer 8-azaN HER1 oligonucleotide bearing 2'-OMe groups, a polyethylene glycol (PEG) linker that connects the 3'-end of the 8-azaN-containing strand to the 5'-end of the complementary strand for improved nuclease resistance⁵⁵⁻⁵⁷, a cholesterol triethylene glycol (TEG) spacer conjugation at the 5'-end of the 8-azaN-containing strand to increase cellular uptake^{58,59}, and, finally, a cyanine 3 (Cy3) fluorophore conjugate at the 3'-end of the complementary strand to examine cellular localization upon transfection of the oligonucleotide by fluorescence microscopy. She found that this oligonucleotide has an IC₅₀ comparable to the unmodified 8-azaN 16bp duplex and the duplex containing 2'-O-methylation on all ends of each strand (data not yet published). Meanwhile, Victorio Jáuregui-Matos designed crosslinked HER1 8-azaN 16bp duplex based on vinyl or copper(1)-catalyzed alkyne-azide cycloaddition (CuAAC) chemistry to further diminish degradation by nucleases.⁶⁰⁻⁶² Future work will be done to evaluate nuclease resistance and inhibitory potency of these newly modified duplexes.

One final parameter to establish convincing cell-based potency analysis of the HER1 8-azaN inhibitors is to explore the use of other cell lines and transcripts. For example, ADAR-dependent HCC1806 and MDA-MB-468 and ADAR-independent SK-BR-3 and MCF-7 cells can be used to assess A-to-I editing of transcript BPNT1 in the presence of HER1 8-azaN inhibitor.¹⁴ DHFR is another transcript in MCF-7 cells that was reported to be highly edited by ADAR1 and is substantially reduced at multiple sites when treated with siADAR1.⁶³ We attempted to generate amplicons from DHFR primers to

quantify A-to-I editing in HEK293T and U87 cell lines in the presence of HER1 8-azaN inhibitor, but the outcome was unsuccessful.

Finally, cellular-based assays were performed to determine inhibitory potency of ADARd mutant proteins that take advantage of the dimerization-dependent editing mechanisms our group discovered through crystallographic and biochemical studies.^{20,51} Similar to HER1 8-azaN inhibitor treatment, HeLa and HEK293T cells transfected with respective catalytically inactive ADAR1d E912A or ADAR2d E396A, or double mutants E912A/D1023A, E912A/D1023K, E396A/D503A or E396A/D503K that are catalytically inactive and mutated at their dimerization interface, did not result in inhibition of full-length ADAR1 or ADAR2 and reduce in editing activity across several transcripts (**Figure 4.7A-C and Figure 4.8A-D**). ADAR1d mutant protein expression in HeLa cells was relatively low and did not increase when transfected overexpression vector was doubled (**Figure 4.7A and B**), suggesting that overexpression in another cell line such as HEK293T cells could be more suitable for higher expression, therefore increase the likelihood of observing inhibition. However, western blotting data of overexpressed ADAR2 FL and ADAR2d mutant from co-transfected HEK293T cells led to relatively inconsistent expression (**Figure 4.8B, C, and D**). Herra Grajo determined a low micromolar IC₅₀ for the ADAR2d E396A mutant and no inhibition of ADAR2 FL by the double mutants, indicating that increasing the expression of the ADARd mutants while decreasing full-length ADAR1 or ADAR2 may be conducive to inhibition detection. Lastly, including nuclear export and/or import signals onto the ADARd mutant constructs with fused fluorescent protein tag may prove useful to improve monitoring and control of protein localization and, therefore, inhibition of ADAR in cells.⁶⁴

In conclusion, it is apparent that inhibiting ADAR in cellular based assays by 8-azaN-containing, chemically modified RNA or ADARd mutant protein inhibitors requires a careful attention to detail in experimental design in order to reflect the encouraging results that our group has determined *in vitro*. Nevertheless, the work described in this chapter may serve as a valuable starting point for optimization.

4.5 References

- (1) Ishizuka, J. J.; Manguso, R. T.; Cheruiyot, C. K.; Bi, K.; Panda, A.; Iracheta-Vellve, A.; Miller, B. C.; Du, P. P.; Yates, K. B.; Dubrot, J.; et al. Loss of ADAR1 in Tumours Overcomes Resistance to Immune Checkpoint Blockade. *Nature* **2019**, *565* (7737), 43–48. <https://doi.org/10.1038/s41586-018-0768-9>.
- (2) Zhang, Y.; Qian, H.; Xu, J.; Gao, W. ADAR, the Carcinogenesis Mechanisms of ADAR and Related Clinical Applications. *Ann. Transl. Med.* **2019**, *7* (22), 686–686. <https://doi.org/10.21037/atm.2019.11.06>.
- (3) Wang, C.; Zou, J.; Ma, X.; Wang, E.; Peng, G. Mechanisms and Implications of ADAR-Mediated RNA Editing in Cancer. *Cancer Lett.* **2017**, *411*, 27–34. <https://doi.org/10.1016/j.canlet.2017.09.036>.
- (4) Wang, H.; Chen, S.; Wei, J.; Song, G.; Zhao, Y. A-to-I RNA Editing in Cancer: From Evaluating the Editing Level to Exploring the Editing Effects. *Front. Oncol.* **2021**, *10* (February), 1–12. <https://doi.org/10.3389/fonc.2020.632187>.
- (5) Herbert, A. ADAR and Immune Silencing in Cancer. *TRENDS in CANCER* **2019**, *5* (5), 272–282. <https://doi.org/10.1016/j.trecan.2019.03.004>.
- (6) Galeano, F.; Tomaselli, S.; Locatelli, F.; Gallo, A. A-to-I RNA Editing: The “ADAR” Side of Human Cancer. *Semin. Cell Dev. Biol.* **2012**, *23* (3), 244–250. <https://doi.org/10.1016/j.semcdb.2011.09.003>.
- (7) Bhate, A.; Sun, T.; Li, J. B. ADAR1: A New Target for Immuno-Oncology Therapy. *Mol. Cell* **2019**, *73* (5), 866–868. <https://doi.org/10.1016/j.molcel.2019.02.021>.
- (8) Rice, G. I.; Kasher, P. R.; Forte, G. M. A.; Mannion, N. M.; Greenwood, S. M.; Szykiewicz, M.; Dickerson, J. E.; Bhaskar, S. S.; Zampini, M.; Briggs, T. A.; et al. Mutations in ADAR1 Cause Aicardi-Goutières Syndrome Associated with a Type I Interferon Signature. *Nat. Genet.* **2012**, *44* (11), 1243–1248. <https://doi.org/10.1038/ng.2414>.
- (9) Choudhry, H. High-Throughput Screening to Identify Potential Inhibitors of the Zα Domain of the Adenosine Deaminase 1 (ADAR1): High-Throughput Screening to Identify Potential Inhibitors. *Saudi J. Biol. Sci.* **2021**, *28* (11), 6297–6304. <https://doi.org/10.1016/j.sjbs.2021.06.080>.
- (10) Wang, X.; Li, J.; Zhu, Y.; Zeng, T.; Ding, J. Targeting ADAR1 with a Novel Small-Molecule for the Treatment of Prostate Cancer. *Res. Sq.* **2021**, 1–16.
- (11) Ramírez-Moya, J.; Baker, A. R.; Slack, F. J.; Santisteban, P. ADAR1-Mediated RNA Editing Is a Novel Oncogenic Process in Thyroid Cancer and Regulates MiR-200 Activity. *Oncogene* **2020**, *39* (18), 3738–3753. <https://doi.org/10.1038/s41388-020-1248-x>.
- (12) Ding, H. Y.; Yang, W. Y.; Zhang, L. H.; Li, L.; Xie, F.; Li, H. Y.; Chen, X. Y.; Tu, Z.; Li, Y.; Chen, Y.; et al. 8-Chloro-Adenosine Inhibits Proliferation of MDA-MB-231 and SK-BR-3 Breast Cancer Cells by Regulating ADAR1/P53 Signaling Pathway. *Cell Transplant.* **2020**, *29*, 1–9. <https://doi.org/10.1177/0963689720958656>.
- (13) Zipeto, M. A.; Court, A. C.; Sadarangani, A.; Delos Santos, N. P.; Balaian, L.; Chun, H. J.; Pineda, G.; Morris, S. R.; Mason, C. N.; Geron, I.; et al. ADAR1 Activation Drives Leukemia Stem Cell Self-Renewal by Impairing Let-7

- Biogenesis. *Cell Stem Cell* **2016**, *19* (2), 177–191.
<https://doi.org/10.1016/j.stem.2016.05.004>.
- (14) Cottrell, K. A.; Soto-Torres, L.; Dizon, M. G.; Weber, J. D. 8-Azaadenosine and 8-Chloroadenosine Are Not Selective Inhibitors of ADAR. *Cancer Res. Commun.* **2021**, *1* (2), 56–64. <https://doi.org/10.1158/2767-9764.crc-21-0027>.
- (15) Maydanovych, O.; Beal, P. A. C6-Substituted Analogues of 8-Azanebularine: Probes of an RNA-Editing Enzyme Active Site. *Org. Lett.* **2006**, *8* (17), 3753–3756. <https://doi.org/10.1021/ol061354j>.
- (16) Haudenschild, B. L.; Maydanovych, O.; Véliz, E. A.; Macbeth, M. R.; Bass, B. L.; Beal, P. A. A Transition State Analogue for an RNA-Editing Reaction. *J. Am. Chem. Soc.* **2004**, *126* (36), 11213–11219. <https://doi.org/10.1021/ja0472073>.
- (17) Phelps, K. J.; Tran, K.; Eifler, T.; Erickson, A. I.; Fisher, A. J.; Beal, P. A. Recognition of Duplex RNA by the Deaminase Domain of the RNA Editing Enzyme ADAR2. *Nucleic Acids Res.* **2015**, *43* (2), 1123–1132. <https://doi.org/10.1093/nar/gku1345>.
- (18) Matthews, M. M.; Thomas, J. M.; Zheng, Y.; Tran, K.; Phelps, K. J.; Scott, A. I.; Havel, J.; Fisher, A. J.; Beal, P. A. Structures of Human ADAR2 Bound to DsRNA Reveal Base-Flipping Mechanism and Basis for Site Selectivity. *Nat. Struct. Mol. Biol.* **2016**, *23* (5), 426–433. <https://doi.org/10.1038/nsmb.3203>.
- (19) Monteleone, L. R.; Matthews, M. M.; Palumbo, C. M.; Thomas, J. M.; Zheng, Y.; Chiang, Y.; Fisher, A. J.; Beal, P. A. A Bump-Hole Approach for Directed RNA Editing. *Cell Chem. Biol.* **2019**, *26* (2), 269–277.e5. <https://doi.org/10.1016/j.chembiol.2018.10.025>.
- (20) Thuy-Boun, A. S.; Thomas, J. M.; Grajo, H. L.; Palumbo, C. M.; Park, S.; Nguyen, L. T.; Fisher, A. J.; Beal, P. A. Asymmetric Dimerization of Adenosine Deaminase Acting on RNA Facilitates Substrate Recognition. *Nucleic Acids Res.* **2020**, *48* (14), 7958–7972. <https://doi.org/10.1093/nar/gkaa532>.
- (21) Wong, S. K.; Lazinski, D. W. Replicating Hepatitis Delta Virus RNA Is Edited in the Nucleus by the Small Form of ADAR1. *Proc. Natl. Acad. Sci. U. S. A.* **2002**, *99* (23), 15118–15123. <https://doi.org/10.1073/pnas.232416799>.
- (22) Yang, W.; Wang, Q.; Kanes, S. J.; Murray, J. M.; Nishikura, K. Altered RNA Editing of Serotonin 5-HT_{2C} Receptor Induced by Interferon: Implications for Depression Associated with Cytokine Therapy. *Mol. Brain Res.* **2004**, *124* (1), 70–78. <https://doi.org/10.1016/j.molbrainres.2004.02.010>.
- (23) Wang, Y.; Park, S. H.; Beal, P. A. Selective Recognition of RNA Substrates by ADAR Deaminase Domains. *Biochemistry* **2018**, *57* (10), 1640–1651. <https://doi.org/10.1021/acs.biochem.7b01100>.
- (24) Wang, Y.; Beal, P. A. Probing RNA Recognition by Human ADAR2 Using a High-Throughput Mutagenesis Method. *Nucleic Acids Res.* **2016**, *44* (20), 9872–9880. <https://doi.org/10.1093/nar/gkw799>.
- (25) Doherty, E. E.; Wilcox, X. E.; Van Sint Fiet, L.; Kemmel, C.; Turunen, J. J.; Klein, B.; Tantillo, D. J.; Fisher, A. J.; Beal, P. A. Rational Design of RNA Editing Guide Strands: Cytidine Analogs at the Orphan Position. *J. Am. Chem. Soc.* **2021**, *143* (18), 6865–6876. <https://doi.org/10.1021/jacs.0c13319>.
- (26) Malik, T. N.; Doherty, E. E.; Gaded, V. M.; Hill, T. M.; Beal, P. A.; Emeson, R. B. Regulation of RNA Editing by Intracellular Acidification. *Nucleic Acids Res.* **2021**,

- 49 (7), 4020–4036. <https://doi.org/10.1093/nar/gkab157>.
- (27) Tran, S. S.; Jun, H. I.; Bahn, J. H.; Azghadi, A.; Ramaswami, G.; Van Nostrand, E. L.; Nguyen, T. B.; Hsiao, Y. H. E.; Lee, C.; Pratt, G. A.; et al. Widespread RNA Editing Dysregulation in Brains from Autistic Individuals. *Nat. Neurosci.* **2019**, *22* (1), 25–36. <https://doi.org/10.1038/s41593-018-0287-x>.
- (28) Rossetti, C.; Picardi, E.; Ye, M.; Camilli, G.; D'erchia, A. M.; Cucina, L.; Locatelli, F.; Fianchi, L.; Teofili, L.; Pesole, G.; et al. RNA Editing Signature during Myeloid Leukemia Cell Differentiation. *Leukemia* **2017**, *31* (12), 2824–2832. <https://doi.org/10.1038/leu.2017.134>.
- (29) Chen, W.; He, W.; Cai, H.; Hu, B.; Zheng, C.; Ke, X.; Xie, L.; Zheng, Z.; Wu, X.; Wang, H. A-to-I RNA Editing of BLCAP Lost the Inhibition to STAT3 Activation in Cervical Cancer. *Oncotarget* **2017**, *8* (24), 39417–39429. <https://doi.org/10.18632/oncotarget.17034>.
- (30) Silvestris, D. A.; Picardi, E.; Cesarini, V.; Fosso, B.; Mangraviti, N.; Massimi, L.; Martini, M.; Pesole, G.; Locatelli, F.; Gallo, A. Dynamic Inosinome Profiles Reveal Novel Patient Stratification and Gender-Specific Differences in Glioblastoma. *Genome Biol.* **2019**, *20* (1), 1–18. <https://doi.org/10.1186/s13059-019-1647-x>.
- (31) Okugawa, Y.; Toiyama, Y.; Shigeyasu, K.; Yamamoto, A.; Shigemori, T.; Yin, C.; Ichikawa, T.; Yasuda, H.; Fujikawa, H.; Yoshiyama, S.; et al. Enhanced AZIN1 RNA Editing and Overexpression of Its Regulatory Enzyme ADAR1 Are Important Prognostic Biomarkers in Gastric Cancer. *J. Transl. Med.* **2018**, *16* (1), 1–11. <https://doi.org/10.1186/s12967-018-1740-z>.
- (32) Picardi, E.; D'Erchia, A. M.; Giudice, C. Lo; Pesole, G. REDportal: A Comprehensive Database of A-to-I RNA Editing Events in Humans. *Nucleic Acids Res.* **2017**, *45* (D1), D750–D757. <https://doi.org/10.1093/nar/gkw767>.
- (33) Yeo, J.; Goodman, R. A.; Schirle, N. T.; David, S. S.; Beal, P. A. RNA Editing Changes the Lesion Specificity for the DNA Repair Enzyme NEIL1. *Proc. Natl. Acad. Sci. U. S. A.* **2010**, *107* (48), 20715–20719. <https://doi.org/10.1073/pnas.1009231107>.
- (34) Schirle, N. T.; Goodman, R. A.; Krishnamurthy, M.; Beal, P. A. Selective Inhibition of ADAR2-Catalyzed Editing of the Serotonin 2c Receptor Pre-mRNA by a Helix-Threading Peptide. *Org. Biomol. Chem.* **2010**, *8* (21), 4898–4904. <https://doi.org/10.1039/c0ob00309c>.
- (35) Mizrahi, R. A.; Schirle, N. T.; Beal, P. A. Potent and Selective Inhibition of A-to-I RNA Editing with 2'-O-Methyl/Locked Nucleic Acid-Containing Antisense Oligoribonucleotides. *ACS Chem. Biol.* **2013**, *8* (4), 832–839. <https://doi.org/10.1021/cb300692k>.
- (36) Onizuka, K.; Yeo, J.; David, S. S.; Beal, P. A. NEIL1 Binding to DNA Containing 2'-Fluorothymidine Glycol Stereoisomers and the Effect of Editing. *ChemBioChem* **2012**, *13* (9), 1338–1348. <https://doi.org/10.1002/cbic.201200139>.
- (37) Mizrahi, R. A.; Phelps, K. J.; Ching, A. Y.; Beal, P. A. Nucleoside Analog Studies Indicate Mechanistic Differences between RNA-Editing Adenosine Deaminases. *Nucleic Acids Res.* **2012**, *40* (19), 9825–9835. <https://doi.org/10.1093/nar/gks752>.

- (38) Heale, B. S. E.; Keegan, L. P.; McGurk, L.; Michlewski, G.; Brindle, J.; Stanton, C. M.; Caceres, J. F.; O'Connell, M. A. Editing Independent Effects of ADARs on the MiRNA/SiRNA Pathways. *EMBO J.* **2009**, *28* (20), 3145–3156. <https://doi.org/10.1038/emboj.2009.244>.
- (39) Valente, L.; Nishikura, K. RNA Binding-Independent Dimerization of Adenosine Deaminases Acting on RNA and Dominant Negative Effects of Nonfunctional Subunits on Dimer Functions. *J. Biol. Chem.* **2007**, *282* (22), 16054–16061. <https://doi.org/10.1074/jbc.M611392200>.
- (40) Singh, M.; Kesterson, R. A.; Jacobs, M. M.; Joers, J. M.; Gore, J. C.; Emeson, R. B. Hyperphagia-Mediated Obesity in Transgenic Mice Misexpressing the RNA-Editing Enzyme ADAR2. *J. Biol. Chem.* **2007**, *282* (31), 22448–22459. <https://doi.org/10.1074/jbc.M700265200>.
- (41) Wu, D.; Zang, Y. Y.; Shi, Y. Y.; Ye, C.; Cai, W. M.; Tang, X. H.; Zhao, L.; Liu, Y.; Gan, Z.; Chen, G. Q.; et al. Distant Coupling between RNA Editing and Alternative Splicing of the Osmosensitive Cation Channel Tmem63b. *J. Biol. Chem.* **2020**, *295* (52), 18199–18212. <https://doi.org/10.1074/jbc.RA120.016049>.
- (42) Costa Cruz, P. H.; Kato, Y.; Nakahama, T.; Shibuya, T.; Kawahara, Y. A Comparative Analysis of ADAR Mutant Mice Reveals Site-Specific Regulation of RNA Editing. *Rna* **2020**, *26* (4), 454–469. <https://doi.org/10.1261/rna.072728.119>.
- (43) Véliz, E. A.; Easterwood, L. H. M.; Beal, P. A. Substrate Analogues for an RNA-Editing Adenosine Deaminase: Mechanistic Investigation and Inhibitor Design. *J. Am. Chem. Soc.* **2003**, *125* (36), 10867–10876. <https://doi.org/10.1021/ja029742d>.
- (44) Juliano, R. L.; Wang, L.; Tavares, F.; Brown, E. G.; James, L.; Ariyaratna, Y.; Ming, X.; Mao, C.; Suto, M. Structure-Activity Relationships and Cellular Mechanism of Action of Small Molecules That Enhance the Delivery of Oligonucleotides. *Nucleic Acids Res.* **2018**, *46* (4), 1601–1613. <https://doi.org/10.1093/nar/gkx1320>.
- (45) Janas, M. M.; Jiang, Y.; Schlegel, M. K.; Waldron, S.; Kuchimanchi, S.; Barros, S. A. Impact of Oligonucleotide Structure, Chemistry, and Delivery Method on in Vitro Cytotoxicity. *Nucleic Acid Ther.* **2017**, *27* (1), 11–22. <https://doi.org/10.1089/nat.2016.0639>.
- (46) Papargyri, N.; Pontoppidan, M.; Andersen, M. R.; Koch, T.; Hagedorn, P. H. Chemical Diversity of Locked Nucleic Acid-Modified Antisense Oligonucleotides Allows Optimization of Pharmaceutical Properties. *Mol. Ther. - Nucleic Acids* **2020**, *19* (March), 706–717. <https://doi.org/10.1016/j.omtn.2019.12.011>.
- (47) Chen, S.; Le, B. T.; Chakravarthy, M.; Kosbar, T. R.; Veedu, R. N. Systematic Evaluation of 2'-Fluoro Modified Chimeric Antisense Oligonucleotide-Mediated Exon Skipping in Vitro. *Sci. Rep.* **2019**, *9* (1), 7–11. <https://doi.org/10.1038/s41598-019-42523-0>.
- (48) Yang, J. H.; Nie, Y.; Zhao, Q.; Su, Y.; Pypaert, M.; Su, H.; Rabinovici, R. Intracellular Localization of Differentially Regulated RNA-Specific Adenosine Deaminase Isoforms in Inflammation. *J. Biol. Chem.* **2003**, *278* (46), 45833–45842. <https://doi.org/10.1074/jbc.M308612200>.
- (49) Desterro, J. M. P.; Keegan, L. P.; Lafarga, M.; Berciano, M. T.; O'Connell, M.;

- Carmo-Fonseca, M. Dynamic Association of RNA-Editing Enzymes with the Nucleolus. *J. Cell Sci.* **2003**, *116* (9), 1805–1818. <https://doi.org/10.1242/jcs.00371>.
- (50) Qu, L.; Yi, Z.; Zhu, S.; Wang, C.; Cao, Z.; Zhou, Z.; Yuan, P.; Yu, Y.; Tian, F.; Liu, Z.; et al. Programmable RNA Editing by Recruiting Endogenous ADAR Using Engineered RNAs. *Nat. Biotechnol.* **2019**, *37* (9), 1059–1069. <https://doi.org/10.1038/s41587-019-0178-z>.
- (51) Park, S. H.; Doherty, E. E.; Xie, Y.; Padyana, A. K.; Fang, F.; Zhang, Y.; Karki, A.; Lebrilla, C. B.; Siegel, J. B.; Beal, P. A. High-Throughput Mutagenesis Reveals Unique Structural Features of Human ADAR1. *Nat. Commun.* **2020**, *11* (1), 1–13. <https://doi.org/10.1038/s41467-020-18862-2>.
- (52) Chen, L.; Li, Y.; Lin, C. H.; Chan, T. H. M.; Chow, R. K. K.; Song, Y.; Liu, M.; Yuan, Y. F.; Fu, L.; Kong, K. L.; et al. Recoding RNA Editing of AZIN1 Predisposes to Hepatocellular Carcinoma. *Nat. Med.* **2013**, *19* (2), 209–216. <https://doi.org/10.1038/nm.3043>.
- (53) Takeda, S.; Shigeyasu, K.; Okugawa, Y.; Yoshida, K.; Mori, Y.; Yano, S.; Noma, K.; Umeda, Y.; Kondo, Y.; Kishimoto, H.; et al. Activation of AZIN1 RNA Editing Is a Novel Mechanism That Promotes Invasive Potential of Cancer-Associated Fibroblasts in Colorectal Cancer. *Cancer Lett.* **2019**, *444* (October 2018), 127–135. <https://doi.org/10.1016/j.canlet.2018.12.009>.
- (54) Mellis, I. A.; Gupte, R.; Raj, A.; Rouhanifard, S. H. Visualizing Adenosine-to-Inosine RNA Editing in Single Mammalian Cells. *Nat. Methods* **2017**, *14* (8), 801–804. <https://doi.org/10.1038/nMeth.4332>.
- (55) Ikeda, Y.; Nagasaki, Y. Impacts of PEGylation on the Gene and Oligonucleotide Delivery System. *J. Appl. Polym. Sci.* **2014**, *131* (9). <https://doi.org/10.1002/app.40293>.
- (56) Lu, X.; Zhang, K. PEGylation of Therapeutic Oligonucleotides: From Linear to Highly Branched PEG Architectures. *Nano Res.* **2018**, *11* (10), 5519–5534. <https://doi.org/10.1007/s12274-018-2131-8>.
- (57) Yoshinaga, N.; Naito, M.; Tachihara, Y.; Boonstra, E.; Osada, K.; Cabral, H.; Uchida, S. PEGylation of mRNA by Hybridization of Complementary PEG-RNA Oligonucleotides Stabilizes mRNA without Using Cationic Materials. *Pharmaceutics* **2021**, *13* (6). <https://doi.org/10.3390/pharmaceutics13060800>.
- (58) Holasová, Š.; Mojžíšek, M.; Bunčák, M.; Vokurková, D.; Radilová, H.; Šafářová, M.; Červinka, M.; Haluza, R. Cholesterol Conjugated Oligonucleotide and LNA: A Comparison of Cellular and Nuclear Uptake by Hep2 Cells Enhanced by Streptolysin-O. *Mol. Cell. Biochem.* **2005**, *276* (1–2), 61–69. <https://doi.org/10.1007/s11010-005-2912-8>.
- (59) Raouane, M.; Desmaële, D.; Urbinati, G.; Massaad-Massade, L.; Couvreur, P. Lipid Conjugated Oligonucleotides: A Useful Strategy for Delivery. *Bioconjug. Chem.* **2012**, *23* (6), 1091–1104. <https://doi.org/10.1021/bc200422w>.
- (60) Mie, Y.; Hirano, Y.; Kowata, K.; Nakamura, A.; Yasunaga, M.; Nakajima, Y.; Komatsu, Y. Function Control of Anti-MicroRNA Oligonucleotides Using Interstrand Cross-Linked Duplexes. *Mol. Ther. - Nucleic Acids* **2018**, *10* (March), 64–74. <https://doi.org/10.1016/j.omtn.2017.11.003>.
- (61) Abdelhady, A. M.; Hirano, Y.; Onizuka, K.; Okamura, H.; Komatsu, Y.; Nagatsugi,

- F. Synthesis of Crosslinked 2'-OMe RNA Duplexes and Their Application for Effective Inhibition of MiRNA Function. *Bioorganic Med. Chem. Lett.* **2021**, *48* (June), 128257. <https://doi.org/10.1016/j.bmcl.2021.128257>.
- (62) Gubu, A.; Su, W.; Zhao, X.; Zhang, X.; Fan, X.; Wang, J.; Wang, Q.; Tang, X. Circular Antisense Oligonucleotides for Specific RNase-H-Mediated MicroRNA Inhibition with Reduced Off-Target Effects and Nonspecific Immunostimulation. *J. Med. Chem.* **2021**, *64* (21), 16046–16055. <https://doi.org/10.1021/acs.jmedchem.1c01421>.
- (63) Nakano, M.; Fukami, T.; Gotoh, S.; Nakajima, M. A-to-I RNA Editing up-Regulates Human Dihydrofolate Reductase in Breast Cancer. *J. Biol. Chem.* **2017**, *292* (12), 4873–4884. <https://doi.org/10.1074/jbc.M117.775684>.
- (64) Xu, T.; Johnson, C. A.; Gestwicki, J. E.; Kumar, A. Conditionally Controlling Nuclear Trafficking in Yeast by Chemical-Induced Protein Dimerization. *Nat. Protoc.* **2010**, *5* (11), 1831–1843. <https://doi.org/10.1038/nprot.2010.141>.

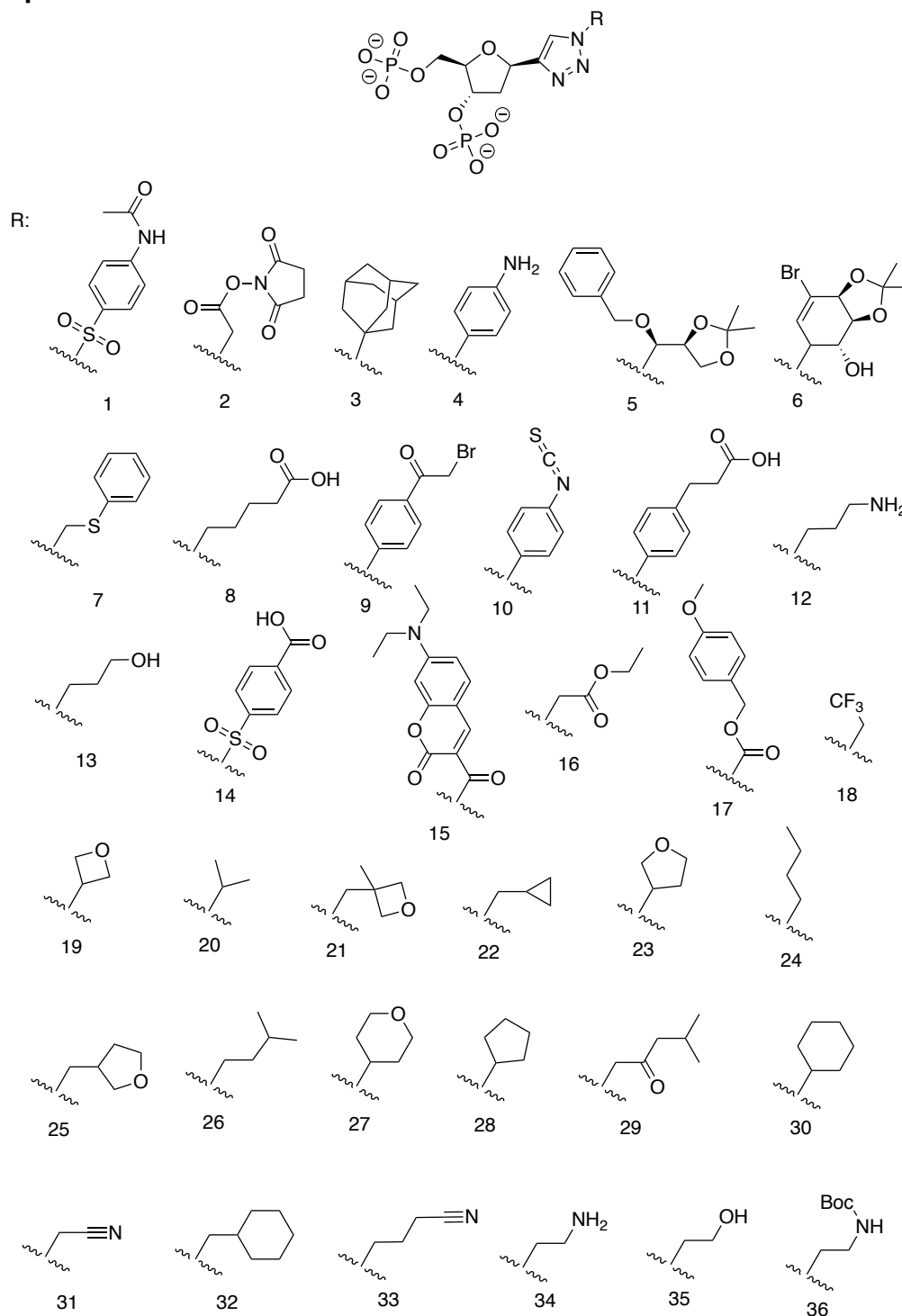
4.6 Table of Oligonucleotides

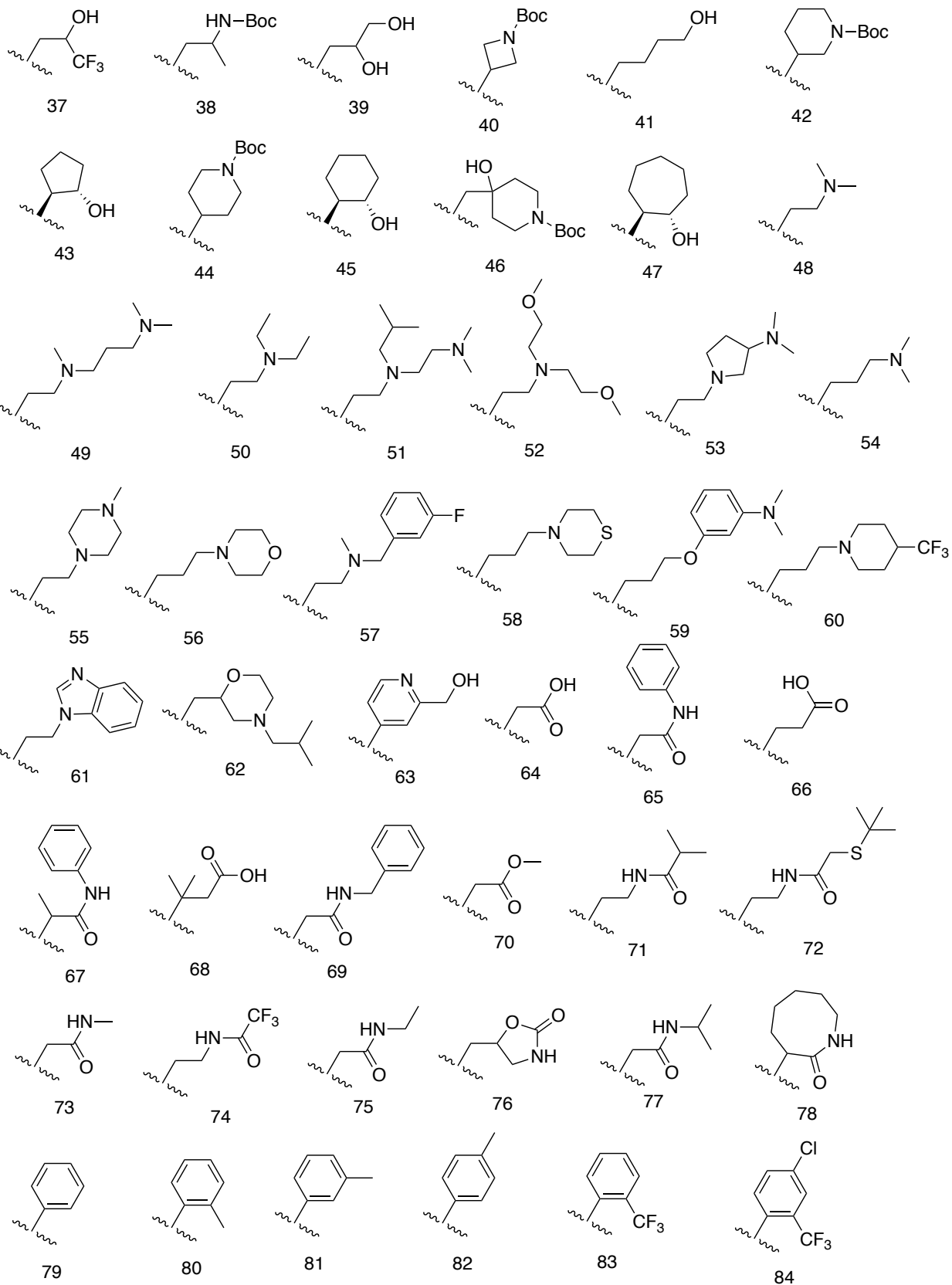
Primers for A-to-I editing in cells:

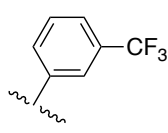
Name	Sequence (5' to 3')
Cog3 F	CAGTCCTTACTTGGAGCGTCA
Cog3 R	CTGAATAAACTGCTCACAGGCC
Eef2k F	GTAATTTACAGCAGGACGCTTTCA
Eef2k R	GTAGAGACAGGGTCTCGC
Blcap F	GACAGCCAGAGAGCACAG
Blcap R	TGAGCAGGTAGAAGCCCAT
Gli1 F	CGAGCCGAGTATCCAGGATACAAC
Gli1 R	CCCATATCCCAGAGTATCAGTAGGTGG
AZIN1 F	TGATGGTGTTTATGGTTCTTTTGCAAG
AZIN1 R	CAGCATCTTGCATCTCATACCAATC
NUP43 F	ATTGACCTGAGACCTTAATGAC
NUP43 R	ACCTGTAATCCCAGCTACTC
NEIL1 out F	TCCAGACCTGCTGGAGCTAT
NEIL1 out R	TGGCCTTGGATTTCTTTTG
NEIL1 in F	CCCAAGGAAGTGGTCCAGTTGG
NEIL1 in R	CTGGAACCAGATGGTACGGCC
5HT2cR Xba out F	GCTCTAGAGATTATGTCTGGCCACTACCTAGATAT
5HT2cR HiA out R	CCGCAAGCTTATAGGAACTGATACACCTATAGAAATTGC
5HT2cR S16 in F	TTTGTGCCCGTCTGGATTTCTTTAG
5HT2cR A11 in R	TCTTCATGATGGCCTTAGTCCGCGA
TMEM63B F	AACTACGTCATTGCCTCAGC
TMEM63B R	AGGTAGGCGTAGTAGAGATTG

Appendices

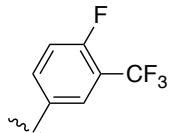
Appendix A: Library of 3',5'-bisphosphate, 1'-triazole-modified nucleotides for Fast Rigid Exhaustive Docking (FRED) into the adenosine-binding pocket of hAgo2, from Chapter 2.



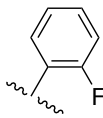




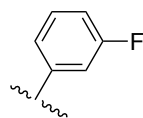
85



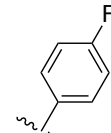
86



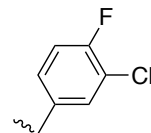
87



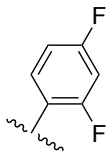
88



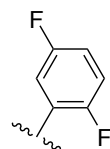
89



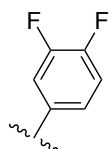
90



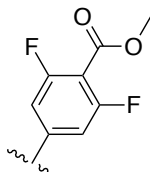
91



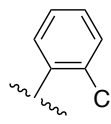
92



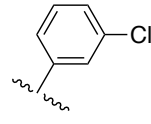
93



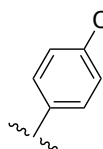
94



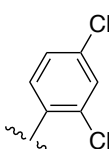
95



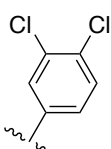
96



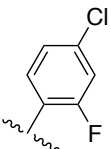
97



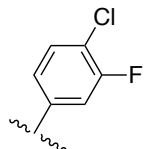
98



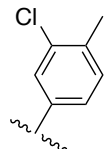
99



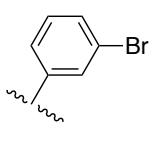
100



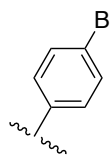
101



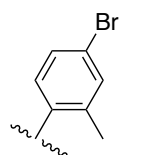
102



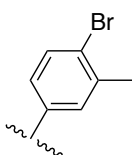
103



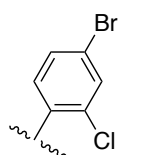
104



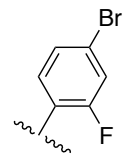
105



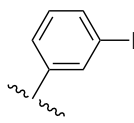
106



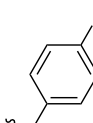
107



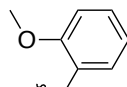
108



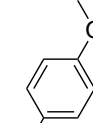
109



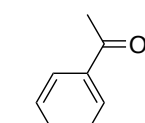
110



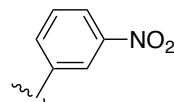
111



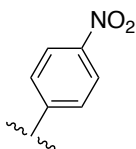
112



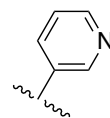
113



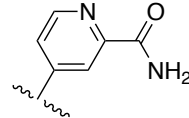
114



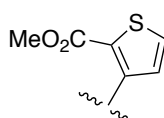
115



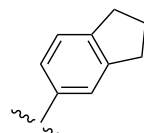
116



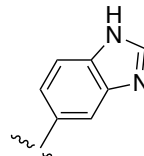
117



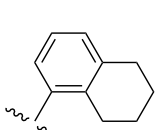
118



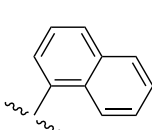
119



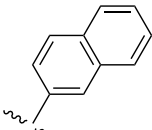
120



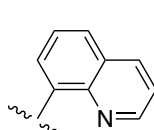
121



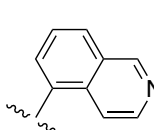
122



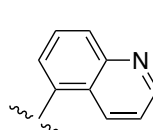
123



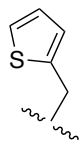
124



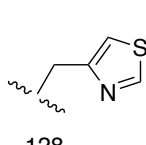
125



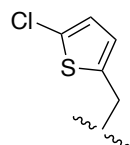
126



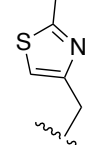
127



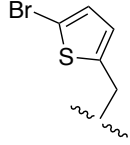
128



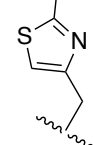
129



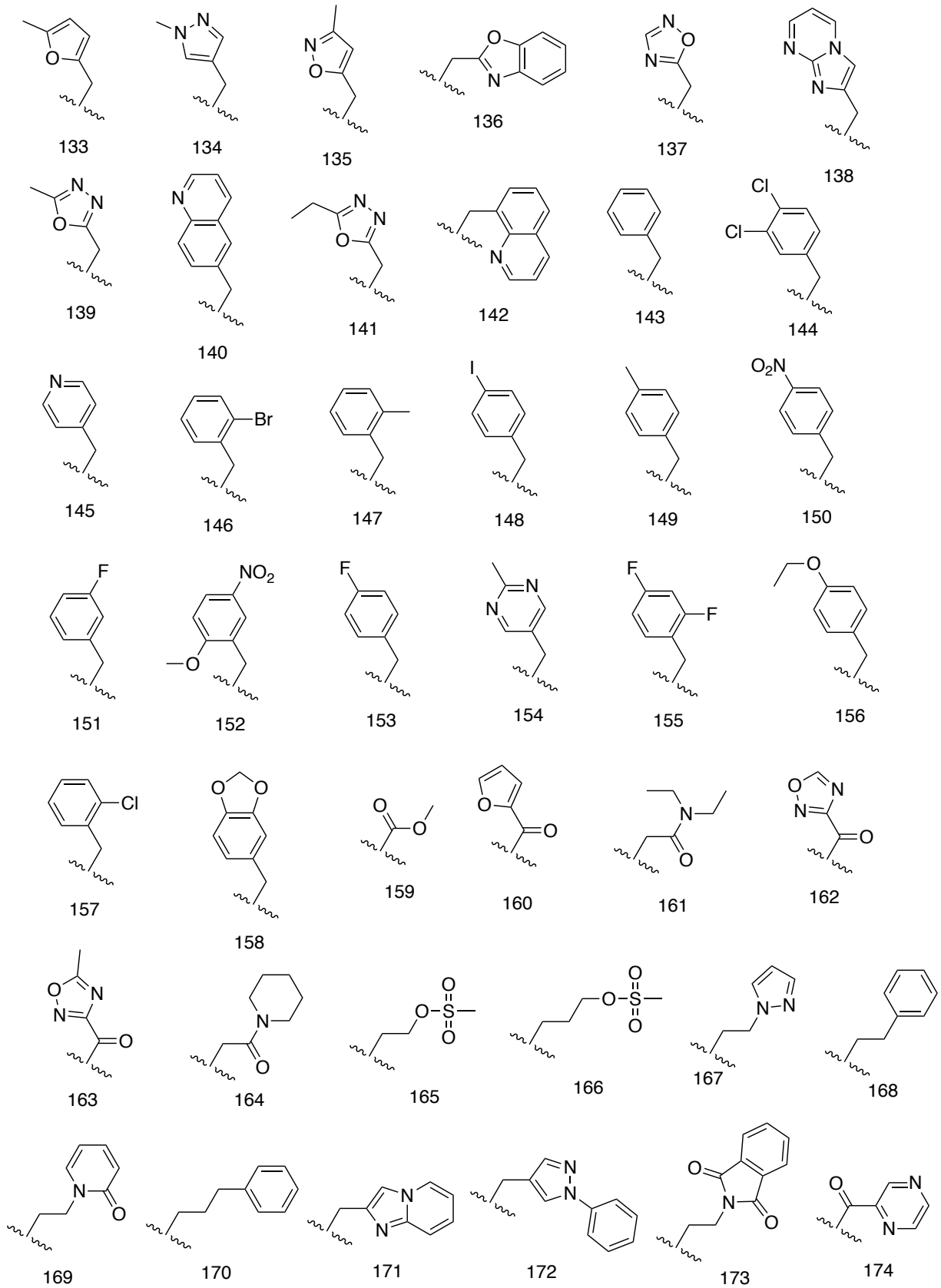
130

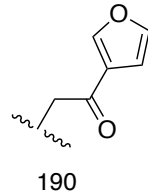
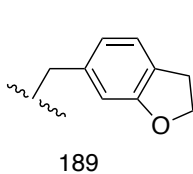
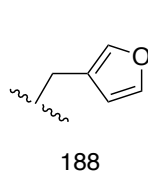
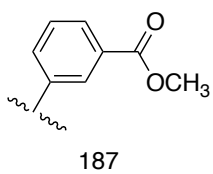
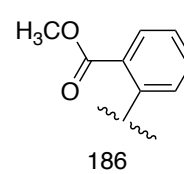
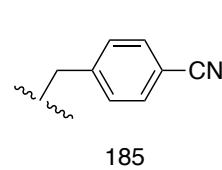
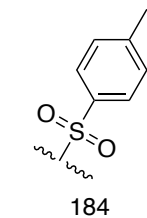
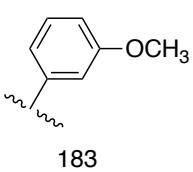
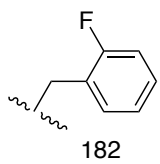
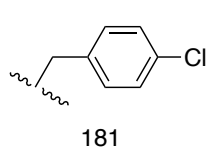
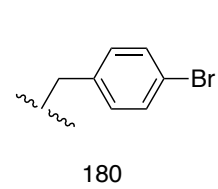
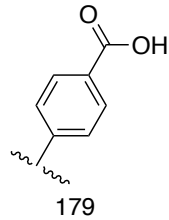
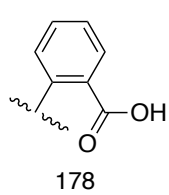
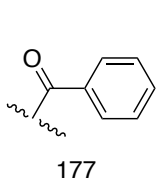
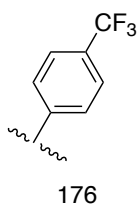
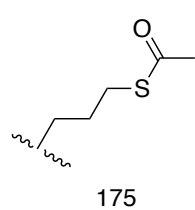


131

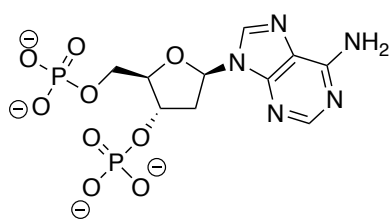


132

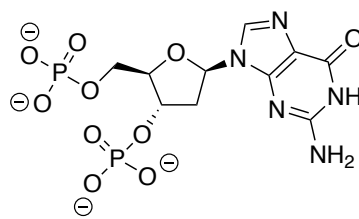




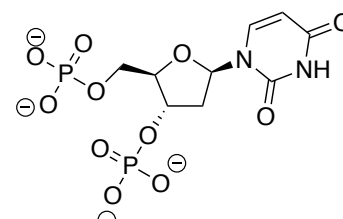
Control ligands:



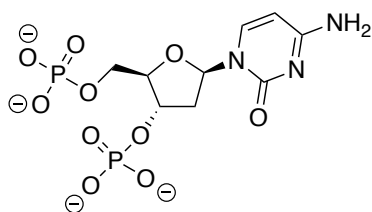
dA
(2'-deoxyadenosine)



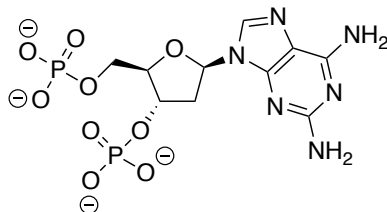
dG
(2'-deoxyguanosine)



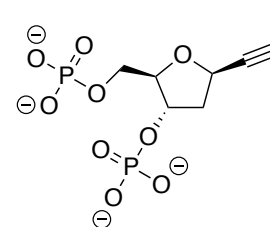
dU
(2'-deoxyuridine)



dC
(2'-deoxycytidine)



dDAP
(2'-deoxy-2,6-diaminopurine)



dER
(1'-ethynyl-2'-deoxyribose)

Appendix B: Table of ChemGauss4 scores of docked triazole nucleotide ligands, from Chapter 2.

Ranking Number	Molecule ID	FRED Chemgauss4 score
1	142	-4.8338
2	95	-3.4750
3	73	-3.4477
4	83	-3.3766
5	22	-3.3605
6	92	-3.2672
7	138	-3.2660
8	186	-3.2652
9	147	-3.2516
10	37	-3.1801
11	164	-3.0777
12	8	-2.9892
13	185	-2.9726
14	63	-2.8916
15	79	-2.8743
16	76	-2.8354
17	116	-2.8075
18	139	-2.8067
19	41	-2.8021
20	32	-2.7696
21	183	-2.7363
22	75	-2.7294
23	133	-2.7051
24	96	-2.6950
25	127	-2.6758
26	88	-2.6706
27	70	-2.6650
28	188	-2.6633
29	128	-2.6291
30	135	-2.5858
31	152	-2.5606
32	81	-2.5377
33	16	-2.5343
34	30	-2.5308
35	131	-2.5260
36	150	-2.4967

37	158	-2.4926
38	144	-2.4857
39	48	-2.4827
40	117	-2.4738
41	108	-2.4443
42	155	-2.3909
43	111	-2.3851
44	114	-2.3583
45	182	-2.3480
46	25	-2.3421
47	190	-2.3391
48	93	-2.3280
49	80	-2.3078
50	65	-2.3070
51	134	-2.2999
52	130	-2.2901
53	187	-2.2784
54	103	-2.2657
55	45	-2.2178
56	33	-2.2174
57	168	-2.2168
58	7	-2.2051
59	26	-2.2036
60	97	-2.1671
61	19	-2.1553
62	189	-2.0997
63	156	-2.0904
64	121	-2.0893
65	109	-2.0596
66	12	-2.0541
67	167	-2.0205
68	154	-2.0035
69	149	-2.0018
70	34	-1.9971
71	28	-1.9816
72	118	-1.9536
73	157	-1.9448
74	145	-1.9319
75	2	-1.9171
76	165	-1.9150
77	23	-1.9129

78	39	-1.9124
79	101	-1.9049
80	29	-1.9012
81	125	-1.8976
82	166	-1.8926
83	132	-1.8739
84	129	-1.8571
85	24	-1.8527
86	175	-1.8454
87	143	-1.8395
88	36	-1.8264
89	146	-1.8233
90	87	-1.8054
91	54	-1.8006
92	162	-1.7911
93	85	-1.7856
94	171	-1.7713
95	43	-1.7669
96	148	-1.7534
97	3	-1.7468
98	98	-1.6973
99	170	-1.6942
100	124	-1.6818
101	18	-1.6801
102	110	-1.6561
103	136	-1.6495
104	106	-1.6442
105	172	-1.6386
106	180	-1.5962
107	105	-1.5769
108	13	-1.5674
109	47	-1.5661
110	151	-1.5386
111	161	-1.5376
112	77	-1.5320
113	90	-1.5308
114	181	-1.5133
115	174	-1.5025
116	91	-1.4922
117	66	-1.4755
118	169	-1.4706

119	140	-1.4674
120	119	-1.4576
121	173	-1.4536
122	99	-1.4162
123	31	-1.4039
124	102	-1.3999
125	50	-1.3988
126	107	-1.3844
127	27	-1.3835
128	61	-1.3141
129	122	-1.3085
130	160	-1.2932
131	178	-1.2890
132	dG	-1.2471
133	20	-1.2268
134	21	-1.2151
135	dDAP	-1.1723
136	62	-1.1423
137	71	-1.1181
138	153	-1.1044
139	120	-1.0874
140	78	-1.0858
141	56	-1.0843
142	35	-1.0763
143	4	-1.0457
144	163	-1.0393
145	137	-1.0047
146	52	-0.9577
147	89	-0.9299
148	86	-0.9171
149	59	-0.8715
150	104	-0.8461
151	100	-0.8279
152	74	-0.8207
153	68	-0.7604
154	72	-0.6570
155	64	-0.6414
156	67	-0.6066
157	dER	-0.5693
158	49	-0.5646
159	141	-0.5547

160	17	-0.5430
161	84	-0.5238
162	53	-0.5220
163	dC	-0.5213
164	1	-0.4448
165	176	-0.4162
166	126	-0.4089
167	57	-0.3678
168	112	-0.2996
169	38	-0.2777
170	dA	-0.2178
171	82	-0.1711
172	58	-0.1707
173	184	-0.1383
174	dU	-0.1175
175	42	-0.0887
176	123	-0.0700
177	60	-0.0127
178	6	-0.0047
179	10	0.0151
180	69	0.0264
181	51	0.0655
182	14	0.1025
183	5	0.2634
184	179	0.3184
185	46	0.4500
186	113	0.4761
187	159	0.5030
188	55	0.6522
189	11	0.7269
190	9	0.8010
191	177	0.8286
192	115	0.9064
193	94	1.3489
194	40	1.5459
195	44	1.8495
196	15	3.0367